

## AN EVALUATION OF SENSING FAT DEPTH FOR THE AUTOMATION OF UNIFORM FAT TRIMMING OF BEEF STRIPLOIN

A Thesis submitted by

Fraser Border, BEng (Hons)

For the award of

**Doctor of Philosophy** 

## **ABSTRACT**

The trimming of excess fat from beef striploin primal is currently a manual process costing the Australian beef industry an estimated \$89 million annually due to yield losses within beef processing plants. Robotics have been successfully deployed to address efficiency and productivity issues in similar products such as pork but are yet to be adapted to red meat. Specifically, a sensing technology capable of acquiring the fat depth information required for automated trimming is yet to be developed.

The work undertaken in this dissertation investigates the characteristics of the beef striploin primal and the processing considerations to develop a sensing performance framework for the application of beef striploin fat trimming. Computed-Tomography is used to provide a means of benchmarking the error present between manual measurements and the 'gold standard' of sensing technologies for this application in the performance metrics of accuracy (described as median error), precision (described as Inter-Quartile Range of error), linearity (described as R-squared quantity of actual vs predicted measurements), reliability (described as the expected probability of acquiring 'no read' measurements across surveyed nodes), and response time (described as the time required to acquire measurements). A weighted sensor performance evaluation framework was developed based upon analyses conducted on key aspects of the striploin primal fat profile and the fat specifications and operational constraints of the fat trimming process.

Fat depth measurement systems were developed using A-Mode and B-Mode ultrasound sensing technologies to obtain results that could be assessed using the developed weighted sensor evaluation framework. In applying this framework it was identified that the A-Mode (score: 47 / 75) ultrasound system was more suitable than B-Mode (score: 29 / 75) for

implementation within a commercial automated fat trimming system. Though the majority of literature recommends the use of B-Mode ultrasound for fat depth measurements it was found that the performance metrics considered favoured simplicity and fast response typical of A-mode ultrasound technology.

Further work to validate the recommendation of A-Mode ultrasound technologies for uniform fat trimming of beef striploin is recommended by integrating this technology within an automated system for commercial use.

## **CERTIFICATION OF THESIS**

I, Fraser Border, declare that the PhD Thesis entitled An Evaluation of Sensors for the Automation of Uniform Fat Trimming of Beef Striploin is not more than 100,000 words in length including quotes and exclusive of tables, figures, appendices, bibliography, references, and footnotes. The thesis contains no material that has been submitted previously, in whole or in part, for the award of any other academic degree or diploma. Except where otherwise indicated, this thesis is my own work.

Date: 15 December 2023

Endorsed by:

Dr Derek Long Principal Supervisor

Professor Craig Baillie Associate Supervisor

Student and supervisors' signatures of endorsement are held at the University.

## **ACKNOWLEDGEMENTS**

Completing this thesis would not have been possible without the support of so many. This process has very much shown me just how much can be achieved when you surround yourself with incredible people.

Craig, you were the first person who introduced me to the field of agriculture, and I can't thank you enough for not only going out of your way to provide an opportunity for me but provide both direction and freedom for me to explore and achieve throughout this journey. Your genuine input and support have been invaluable to me growing as a researcher, and person, and I really appreciate you being such a large part of my research journey and life thus far.

Peter, you showed me how enjoyable research could be and how to appreciate the process of exploring. You have been an incredible mentor, and I am so grateful for all the wisdom you have imparted upon me. Your enthusiasm for research has been infectious, and I have learned so much from you and appreciate all the time we spent philosophising together during your last years of research. I'd hoped that I would've completed this during your time at the university, but regardless, this completion is as much yours as it is mine.

Derek, you came at such a critical time of my journey when I was starting to doubt that I would reach the end of this submission. Your practical approach and weekly support have been a constant source of motivation for me. At times I felt that you'd been thrown in the deep end to have to try to manage me as a PhD candidate but your ability to keep me going during the challenging times has been truly remarkable. Your dedication to my success has been evident, and I am so grateful for your guidance and support.

Koorosh, I appreciate the time we've spent undertaking practical research. Your ability to zoom out and see the larger picture and, at the same time, plan the finer details to ensure a project is completed is an ability I will continue to refine throughout my robotics career. Thank you for being a part of my research journey and for providing the opportunity to partake in R&D projects – particularly with uniform fat trimming since 2017. This collaboration has informed the work presented in Chapter 6.

The processor team - Justin, Chris, Patty, Wardy, and everyone else; the research I've been working on couldn't have happened without you all. I understand that you have more urgent and important things to focus on during the day-to-day operation of the plant, and I truly do appreciate that you've always made yourselves available and supported me in so many ways. When we find a solution to this issue, I hope you all can benefit from it most.

The Toowoomba Family Vets team – Louie, Dave and Ellie. I am humbled by your openness to collaborate without me having much to offer in return. This research wouldn't have been completed without you all. In the short time I spent in the veterinary clinic I've developed a respect for the prowess of your craft and the wit in your humour you have and use to perform such a difficult job. I encourage people to use your clinic often; I hope this may offset any trauma I may have caused to your pet owners carrying large volumes of meat through your waiting room.

The Australian Meat Processors Corporation (AMPC) team, particularly Stuart and Amanda, I appreciate you the discussions we've had regarding processors' needs. These discussions have shaped my perspective more than you know.

This research has been supported by the Australian Government Research Training Program Scholarship.

## **DEDICATION**

To all my family and friends who have been patient enough with me throughout this process.

## **TABLE OF CONTENTS**

ABSTRACT	i
CERTIFICATION OF THESIS	iii
ACKNOWLEDGEMENTS	iv
DEDICATION	vi
TABLE OF CONTENTS	vii
LIST OF TABLES	хi
LIST OF FIGURES	κiii
ABBREVIATIONS & TERMINOLOGYxv	√iii
CHAPTER 1: INTRODUCTION	. 1
1.1 Background	. 1
1.1.1 The Challenges of Australia's Red Meat Industry	.4
1.1.2 Limitations of Conventional Technology in Red Meat Processing	, 7
1.1.3 Automation Focus: Uniform Fat Trimming of Beef Striploin	10
1.2 Research Objectives	14
1.3 Thesis Outline	15
CHAPTER 2: LITERATURE REVIEW	18
2.1 Defining Uniform Fat Trimming of Beef Striploin	
2.1.1 Beef Striploin Primal	19
2.1.2 Uniform Fat Trimming Process	24
2.1.3 Product Fat Specifications	26
2.2 Progress Towards Automated Beef Striploin Fat Trimming	30
2.2.1 Registered Patents	30
2.2.2 Commercial Systems	34
2.2.3 Summary of Automation Progress	48
2.3 Desktop Evaluation of Sensing Technologies	48
2.3.1 X-Ray	51
2.3.2 Ultrasound	56
2.3.3 Vibrational Spectroscopy	69
2.3.4 Electrical Impedance	72

	2.3.5 Tactile	. 74
	2.3.6 Discussion	. 78
	2.4 Conclusion	. 83
СН	APTER 3: SENSING SYSTEM DEFINITION FOR BEEF STRIPLOIN FAT	
TR	IMMING	. 85
	3.1 Introduction	. 85
	3.1.1 Preliminary Work	. 85
	3.1.2 Processor-Specific Context	. 87
	3.1.3 Chapter Aims	100
	3.2 Product Variability & Processing Constraints	102
	3.2.1 Experimental Set-Up	103
	3.2.2 Experimental Analysis	104
	3.2.3 Results	105
	3.2.4 Discussion	107
	3.3 Time Motion Study of Uniform Fat Trimming	110
	3.3.1 Experimental Set-Up	110
	3.3.2 Experimental Analysis	111
	3.3.3 Results	111
	3.3.4 Discussion	113
	3.4 Subcutaneous Fat Characteristics	114
	3.4.1 Experimental Set-Up	114
	3.4.2 Experimental Analysis	122
	3.4.3 Results	128
	3.4.4 Discussion	139
	3.5 Conclusion	142
СН	APTER 4: SENSOR PERFORMANCE METRICS USING CT	
BE	NCHMARKING	146
	4.1 Introduction	146
	4.1.1 Performance Metrics	147
	4.1.2 Chapter Aims	148
	4.2 Experimental Setup	148
	4.3 Experimental Analysis	154

	4.4 Results	164
	4.5 Discussion	170
	4.6 Conclusion	182
CH	APTER 5: ANALYSIS OF B-MODE ULTRASOUND SENSING SYSTEM	183
	5.1 Introduction	183
	5.1.1 Chapter Aims	184
	5.2 Experimental Setup	185
	5.2.1 Preliminary Investigation into Sensor Feasibility	185
	5.2.2 Experimentation	195
	5.3 Experimental Analysis	198
	5.4 Results	200
	5.5 Discussion	206
	5.6 Conclusion	211
CH	APTER 6: ANALYSIS OF A-MODE ULTRASOUND SENSING SYSTEM	212
	6.1 Introduction	212
	6.1.1 Chapter Aims	213
	6.2 Experimental Setup	213
	6.2.1 Preliminary Investigation into Sensor Feasibility	213
	6.2.2 Experimentation	217
	6.3 Experimental Analysis	229
	6.4 Results	231
	6.5 Discussion	237
	6.6 Conclusion	241
CH	APTER 7: CONCLUSION	242
	7.1 Achievement Against Research Objectives	242
	7.1.1 Review of Sensing Technologies for Uniform in Fat Trimming.	242
	7.1.2 Provide insights from the analysis of striploin characteristics a	and
trin	nming task	243
	7.1.3 Establishment of sensor performance evaluation metric speci-	fic
to ι	uniform fat trimming automation	245
	7.1.4 Development of ultrasound systems to evaluate performance	for
aut	omation implementation	246

7.1.5 Evaluation of systems to conclude upon the technologies'	
appropriateness for this application	246
7.2 Recommendations for Future Work	250
7.2.1 Sensing of Subcutaneous Fat Depth Measurements	250
7.2.2 Automation of Uniform Fat Trimming of Beef Striploin	251
REFERENCES	254
APPENDICES	289
Appendix A: Product & Process Analysis	289
A.1: Cavities Created by Table Boning	289
A.2: Dataset for Product Variability of Untrimmed Striploins	294
A.3: Time-Motion Analysis of Striploin Fat Trimming	298
Appendix B: Dataset for Manual Fat Depth Measurements	299
B.1: Fat Depth Measurements (LHS & RHS)	299
B.2: Trim Cut Path for Combined (LHS & RHS) Striploin Dataset	301
B.3: Gradient of Fat Depth Measurements	302
Appendix C: Computed-Tomography Error Dataset Measurements	s. 307
Appendix D: B-Mode Ultrasound Device Datasheets	309
D.1: B-Mode Ultrasound: ReproScan Flexx	309
D.2: B-Mode Ultrasound System (Butterfly iQ+)	309

## **LIST OF TABLES**

able 1-1: Typical operating costs of global beef processors
able 1-2: Comparison of red meat species
able 1-3: Significance of striploin within carcase value
able 2-1: Fat thickness specifications of beef striploin25
able 2-2: Limitations of Frontmatec 3D Loin Trimmer
able 2-3: Comparison of feasible sensing technologies
able 3-1: Variability of physical characteristics of beef striploin86
able 3-2: Key constraints to consider for automated trimming99
able 3-3: Measurements of typical untrimmed atriploins
able 3-4: Statistical summary of measurements
able 3-5: Comparison of striploin characteristic study
able 3-6: Motion analysis of fat trimming beef striploin
able 3-7: Summary of time recordings for fat trimming
able 3-8: Summary of the striploin dataset characteristics
able 3-9: Measurement node mesh for the striploin dataset 116
able 3-10: K-S Test results for manual measurements
able 3-11: Summary of manual fat depth measurements
able 3-12: Fat depth measurements (LHS, RHS, Combined) 135
able 3-13: Summary of gradient measures for striploin dataset 139
able 4-1: Comparison of striploins with 'typical' characteristics 149
able 4-2: Summary of error dataset (ruler - CT)
able 4-3: Example of value for +6 mm (under-trimming)
able 4-4: Thresholds for ranking sensor accuracy
able 4-5: Thresholds for ranking sensor precision
able 4-6: Thresholds for ranking sensor linearity
able 4-7: Thresholds for ranking sensor reliability
able 4-8: Thresholds for ranking sensor response time
able 4-9: Sensor Performance evaluation framework
able 5-1: Summary of error dataset (ruler - B-Mode ultrasound) 20

Table 5-2: Comparison of B-Mode ultrasound and CT	209
Table 5-3: Applied performance evaluation framework: B-Mode	210
Table 6-1: Striploin dataset for A-Mode experimentation	218
Table 6-2: Summary of error dataset (ruler - A-Mode ultrasound)	231
Table 6-3: Comparison of A-Mode ultrasound and CT	239
Table 6-4: Applied performance evaluation framework: A-Mode	240
Table 7-1: Performance comparison: B-Mode vs A-Mode ultrasound	247

## **LIST OF FIGURES**

Figure 1-1: Industry turnover comparison	2
Figure 1-2: Agriculture production industry value-add	2
Figure 1-3: The supply chain of red meat industry	3
Figure 1-4: The significance of red meat export value	4
Figure 1-5: Juxtaposition: manufacturing vs meat processing	8
Figure 1-6: Beef carcass breakdown of primal/sub-primal cuts	12
Figure 2-1: Anatomical location of a striploin primal	19
Figure 2-2: Striploin-Derived Products	20
Figure 2-3: Striploin products	20
Figure 2-4: Striploin portions	21
Figure 2-5: Anatomical terms and planes of bovine	22
Figure 2-6: Carcase splitting: LHS & RHS striploins	23
Figure 2-7: Anatomical & slicer nomenclature	23
Figure 2-8: Slicer nomenclature for striploin features	24
Figure 2-9: Manual fat trimming methods	25
Figure 2-10: Ideal trimming for uniform fat trimming	26
Figure 2-11: Defining fat thickness specification	28
Figure 2-12: "Perfect" trimming cross-section examples	29
Figure 2-13: Patent: Mechanised pork trimming system	31
Figure 2-14: Patent: Forming uniform fat thickness	32
Figure 2-15: Patent: Mechanised fat trimming	33
Figure 2-16: Frontmatec's automatic loin trimmer system	35
Figure 2-17: Automatic loin trimmer: mechanism	35
Figure 2-18: Automatic loin trimmer: wheel & blade contour	36
Figure 2-19: Automatic loin trimmer: Optical probe	37
Figure 2-20: 'Finished' pork loin from Automatic loin trimmer	37
Figure 2-21: Frontmatec's 3D loin trimmer system	38
Figure 2-22: The 'planer' blade of 3D loin trimmer	39
Figure 2-23: Back View: 3D Loin Trimmer	39

Figure 2-24:	Isometric View: 3D Loin Trimmer	. 40
Figure 2-25:	The images acquired by 3D Loin Trimmer ultrasonics	. 40
Figure 2-26:	Ultrasonic measurement positions of 3D Loin Trimmer	. 41
Figure 2-27:	Locating mechanism of ultrasound probe	. 42
Figure 2-28:	The 3D model generated by 3D loin trimmer	. 42
Figure 2-29:	'Finished' pork primal using 3D loin trimmer	. 43
Figure 2-30:	Marel's 6000DHT Loin Trimmer system	. 45
Figure 2-31:	6000DHT cutting shoe profile	. 45
Figure 2-32:	The optical probe for Marel's AutoTrimmer system	. 46
Figure 2-33:	Conveyor view of AutoTrimmer System	. 47
Figure 2-34:	A typical Computed-Tomography system	. 51
Figure 2-35:	CT imaging mechanism	. 52
Figure 2-36:	Illustration of x-ray technology imaging	. 53
Figure 2-37:	Comparison of medical and RapiScan CT	. 56
Figure 2-38:	Diagram of piezoelectric ultrasound transducer	. 57
Figure 2-39:	Ultrasonic TOF calculation diagram	. 58
Figure 2-40:	Illustration of A-Mode ultrasound technology	. 60
Figure 2-41:	Comparison of A-Mode and B-Mode ultrasound	. 61
Figure 2-42:	Comparison of information (A-Mode vs B-Mode)	. 62
Figure 2-43:	Beef carcase tissues shown by B-Mode ultrasound	. 62
Figure 2-44:	A convex array of ultrasonic transducers	. 63
Figure 2-45:	Ultrasound configuration types	. 64
Figure 2-46:	Convex vs Linear vs Phased Array	. 65
Figure 2-47:	Ultrasonic transducer focal lengths	. 66
Figure 2-48:	Coordinate frame of an ultrasound probe	. 67
Figure 2-49:	Example: B-Mode Ultrasound measuring muscle depth $\dots$	. 69
Figure 2-50:	NIR Spectroscopy with PCA	. 72
Figure 2-51:	Electrical impedance measuring fat depth	. 74
Figure 2-52:	Force-torque to discriminate beef striploin tissues	. 77
Figure 2-53:	Using tactile transients to discriminate tissues	. 78
Figure 3-1: 9	Striploin dimensions: length, width and height	. 86
Figure 3-2: l	Jpward 'hide pulling' mechanism	. 88

Figure 3-3:	Downward 'hide pulling' mechanism	89
Figure 3-4:	Upward 'hide pulling' mechanism	90
Figure 3-5:	Striploins in chiller prior to grading	90
Figure 3-6:	Beef sides cut for grading	91
Figure 3-7:	Cut lines defining rib face of striploin	92
Figure 3-8:	Removal of the flank from hindquarter	93
Figure 3-9:	Removal of flank at processor's facility	94
Figure 3-10:	Removal of the striploin from the hindquarter	94
Figure 3-11:	Striploin removed at the processor's facility	95
Figure 3-12:	Chine sawing for easier removal of smaller bones	96
Figure 3-13:	: An illustration of bones under the striploin	96
Figure 3-14:	: An analysis of flat bones and button bones	97
Figure 3-15:	: Cut lines determining the dimensions of striploin 1	.03
Figure 3-16:	: Experimental set-up for striploin survey 1	.04
Figure 3-17:	: Illustration of fat tear damage 1	.07
Figure 3-18:	: A slicer performing uniform fat trimming 1	.11
Figure 3-19:	Results of fat trimming timing observations 1	.13
Figure 3-20:	: Plastic grid used for node mesh marking	.15
Figure 3-21:	: Location and positioning of measurement nodes 1	.17
Figure 3-22:	: Marking measurement nodes on the striploin 1	.18
Figure 3-23:	: Faces cut to measure fat thickness at nodes 1	.18
Figure 3-24:	: Method of acquiring manual fat depth measurements 1	.19
Figure 3-25:	: Orientation of fat depth measurements	.19
Figure 3-26:	: Unavoidable measurement misalignment 1	.20
Figure 3-27:	: Illustration of error: pre-trim vs post-trim 1	.21
Figure 3-28:	: Unit volume of measurement nodes on RHS striploin 1	.24
Figure 3-29:	: Unit volume of measurement nodes on LHS striploin 1	.24
Figure 3-30:	: An illustration of trimming gradient	.27
Figure 3-32:	: Histogram of fat depth (manual)1	.31
Figure 3-33:	: Distribution plot for fat depth across striploins 1	.31
Figure 3-34:	: Nodes requiring trimming for striploin dataset 1	.32
Figure 3-35:	: Unit volumes not requiring trimming (LHS & RHS) 1	.33

Figure 3-36: Unit volumes not requiring trimming (combined) 13	34
Figure 3-37: Unit volumes with large fat deposits (LHS & RHS) 13	36
Figure 3-38: Unit volumes with large fat deposits (combined)	37
Figure 3-39: Forward gradient of cut path along striploin length 13	38
Figure 3-40: Forward gradient of cut path along striploin width 13	38
Figure 4-1: CT laser lines used to align the striploin during imaging 1	50
Figure 4-2: Adhesive CT markers1	51
Figure 4-3: Screenshot of CT markers showing in images	51
Figure 4-4: CT markers causing artifacting within CT images 15	52
Figure 4-5: Offsetting image to avoid artifacting 15	52
Figure 4-6: Measuring fat thickness using CT images	53
Figure 4-7: Registering measurement nodes: CT and manual 15	54
Figure 4-8: CT error datasets (unfiltered vs filtered)	54
Figure 4-9: Error distribution of unfiltered data (CT)	56
Figure 4-10: CT vs manual (ruler) measurements	57
Figure 4-11: Residual error plot of CT-Ruler dataset (in mm)	58
Figure 4-12: Residual error plot of CT-Ruler dataset (%)	58
Figure 5-1: B-Mode ultrasound systems evaluated 18	36
Figure 5-2: Machine vision applied to ReproScan 18	
Figure 5-3: Difficulties using ReproScan	37
Figure 5-4: Butterfly iQ+ probe components	38
Figure 5-5: Photo of Butterfly iQ+ with standoff	39
Figure 5-6: Improvement of images using ultrasonic standoff 18	39
Figure 5-7: A screenshot of the Butterfly iQ+ user-interface	90
Figure 5-8: Creating a phantom for preliminary testing	93
Figure 5-9: Preliminary testing of Butterfly iQ+19	94
Figure 5-10: Example of preliminary experiment results	94
Figure 5-11: Experimental set-up for B-Mode ultrasound	95
Figure 5-12: Marking measurement nodes for Mode-B experiment 19	96
Figure 5-13: Illustration of using B-Mode ultrasound	97
Figure 5-14: Difficulties Encountered using B-Mode	97
Figure 5-15: Manual measurements of fat depth at each node 19	98

Figure 5-16: Example of "No read" measurements
Figure 5-17: B-Mode error datasets (unfiltered vs filtered) 201
Figure 5-18: Error distribution of unfiltered data (B-Mode) 202
Figure 5-19: B-Mode vs manual (ruler) measurements
Figure 5-20: Residual error plot of USB-Ruler Dataset (in mm) 204
Figure 5-21: Residual relative error plot of US <sub>B</sub> -Ruler Dataset (%) 205
Figure 6-1: System integration of A-Mode ultrasound probe 214
Figure 6-2: A diagram illustrating A-Mode hardware
Figure 6-3: Software interface of the A-Mode ultrasound system 215
Figure 6-4: Striploin plate supporting striploin near the robot 219
Figure 6-5: Measurement node locations on the striploin plate 220
Figure 6-6: Experimental setup in processor's facility
Figure 6-7: Marking measurement nodes using laser dot
Figure 6-8: C-Arm bracket positioning sensors at nodes
Figure 6-9: LiDAR & ultrasound sensors assembled on C-Arm 223
Figure 6-10: Twin sensing configuration
Figure 6-11: Illustration: Calculation of fat height using LiDAR 225
Figure 6-12: Illustration: Calculation of fat depth
Figure 6-13: Measurement nodes precisely taught to the robot 226
Figure 6-14: Illustration: Limitation of sensing orientation 227
Figure 6-15: Measurements displayed by robot program 228
Figure 6-16: Images of measured cross-sections
Figure 6-17: A-Mode error datasets (unfiltered vs filtered) 232
Figure 6-18: Error distribution of unfiltered data (A-Mode)
Figure 6-19: A-Mode vs manual (ruler) measurements
Figure 6-20: Residual error plot of USA-Ruler Dataset (in mm) 236
Figure 6-21: Residual relative error plot of USA-Ruler Dataset (%) 236

## **ABBREVIATIONS & TERMINOLOGY**

AMIC	Australian Meat Industry Council
AMPC	Australian Meat Processor Corporation
СТ	Computed-Tomography
cwe	Carcase Weight Equivalent
DEXA	Dual-Energy X-ray Absorptiometry
DMRI	Danish Meat Research Institute
E&Y	Ernest and Young
MLA	Meat and Livestock Australia
MSA	Meat Standards Australia
OCM	Objective Carcase Measurement
Primal/s	a large 'primary' meat product within a carcase
Processing run	similar quality carcases processed together
Processor/s	a red meat processing plant/s
RMAC	Red Meat Advisory Council
Slicer/s	a person who trims excess fat from striploins
TOF	Time-of-Flight
UFT	Uniform Fat Trimming
UNECE U	nited Nations Economic Commission for Europe

## **CHAPTER 1: INTRODUCTION**

#### 1.1 Background

Australia's agricultural sector is considered to be one of the five pillars of the economy and crucial for Australia's prosperity. This industry provides 93% of the nation's domestic food supply and supports 445,000 employees within 23,000 businesses with approximately 90% of these jobs based in regional or remote areas of Australia (Ernest & Young 2021). An industry survey conducted by the Australian Bureau of Agricultural and Resource Economics and Sciences found that from 2021 to 2022 Australia's agricultural production value totalled \$93b gross with an export value of \$71b (ABARES, 2023).

According to report by Ernest & Young (2021) the red meat and livestock industry had the 16th largest turnover of all key industries in Australia, contributing \$69.9b (1.3%) towards Australia's key industry total value (see Figure 1-1). According to report by Ernest and Young (E&Y) the red meat and livestock industry (referred to as "red meat") contributes most significantly (45%) towards the total value of Australia's total agriculture production (Ernest & Young, 2021). This is illustrated in the chart presented in Figure 1-2.

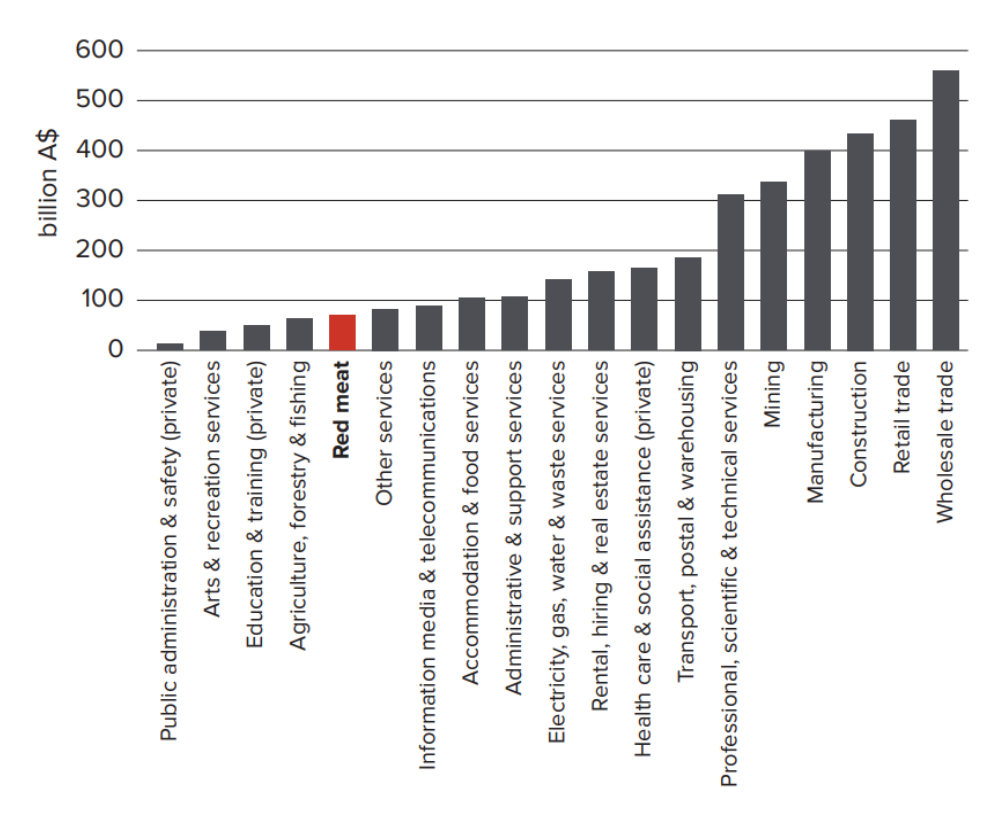


Figure 1-1: Industry turnover compared with other industries between 2019-20. Source – (Ernest & Young, 2021)

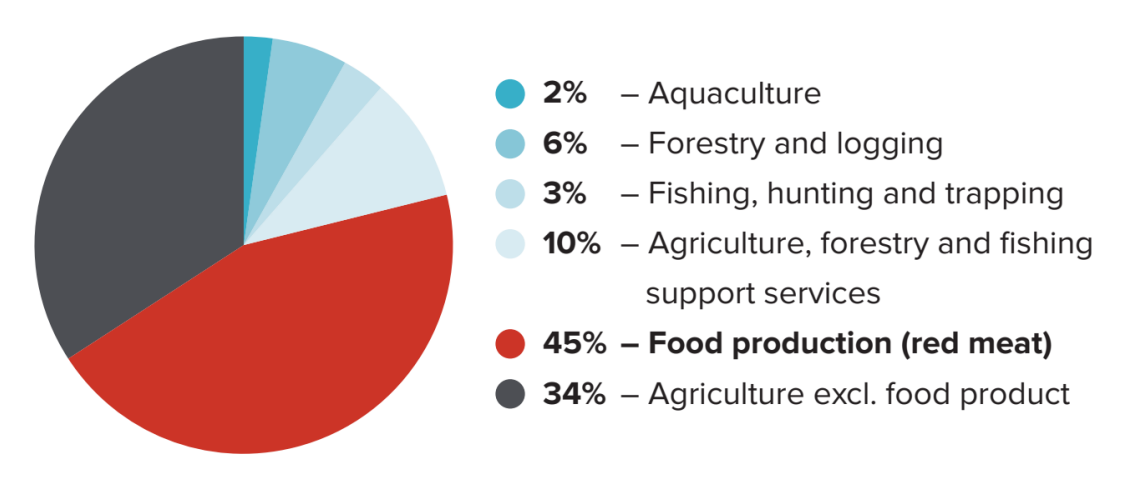


Figure 1-2: Agriculture production industry value add in 2019-20. Source – (Ernest & Young, 2021)

The red meat and livestock industry spans three species of domesticated animals: bovine, ovine and caprine, which are slaughtered to create beef (including veal and buffalo), sheepmeat (also referred to as lamb or mutton), and goatmeat products respectively. The red meat industry supply chain includes the production (farming of animals), processing (slaughter and creation of products) and retail (sale of

product) of an assortment of various meat products for domestic and export markets (see Figure 1-3). In 2020, Australia was the world's largest sheepmeat exporter, and the second largest exporter in beef products and goatmeat globally.

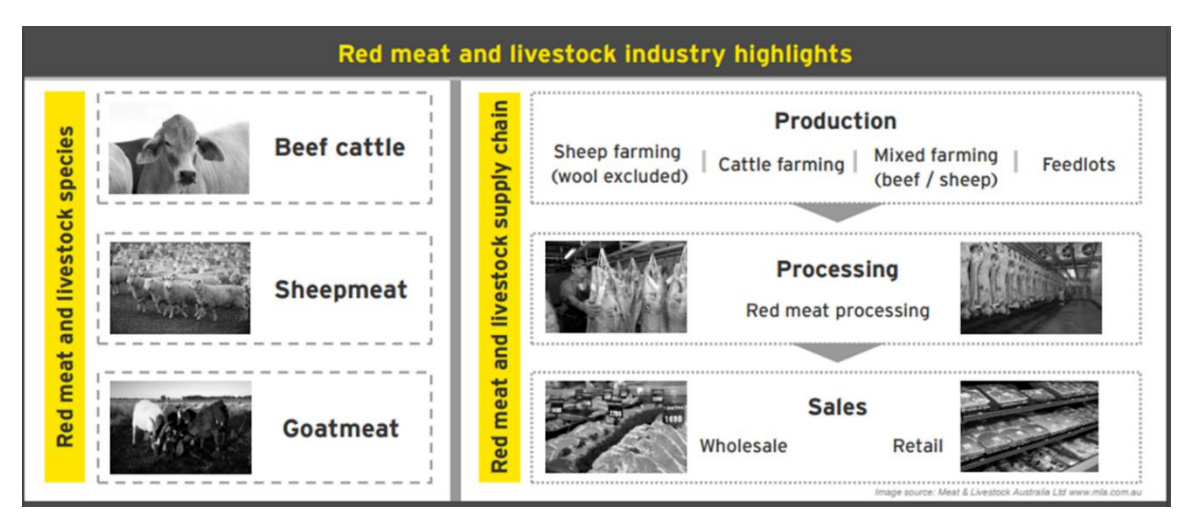


Figure 1-3: The supply chain of the red meat processing industry. Source – (Ernest & Young, 2017a)

Red meat processing is a crucial sub-sector of the red meat industry that adds value by creating meat products from livestock for sale in both the domestic and international markets. In 2020, 7.1 million head of cattle were slaughtered for processing products for domestic and international markets whilst 1.05 million head were exported as livestock (Ernest & Young, 2021). Of the red meat and livestock industry's export value of \$18.4b in 2019 - 2020, the significant majority of this value (\$15b; 82%) was derived from meat products whereas approximately \$2b (11%) was derived from livestock (Ernest & Young, 2021). The significance of the red meat processing export value is illustrated by the relative proportion of export value of "Chilled/frozen meat" as shown in Figure 1-4.

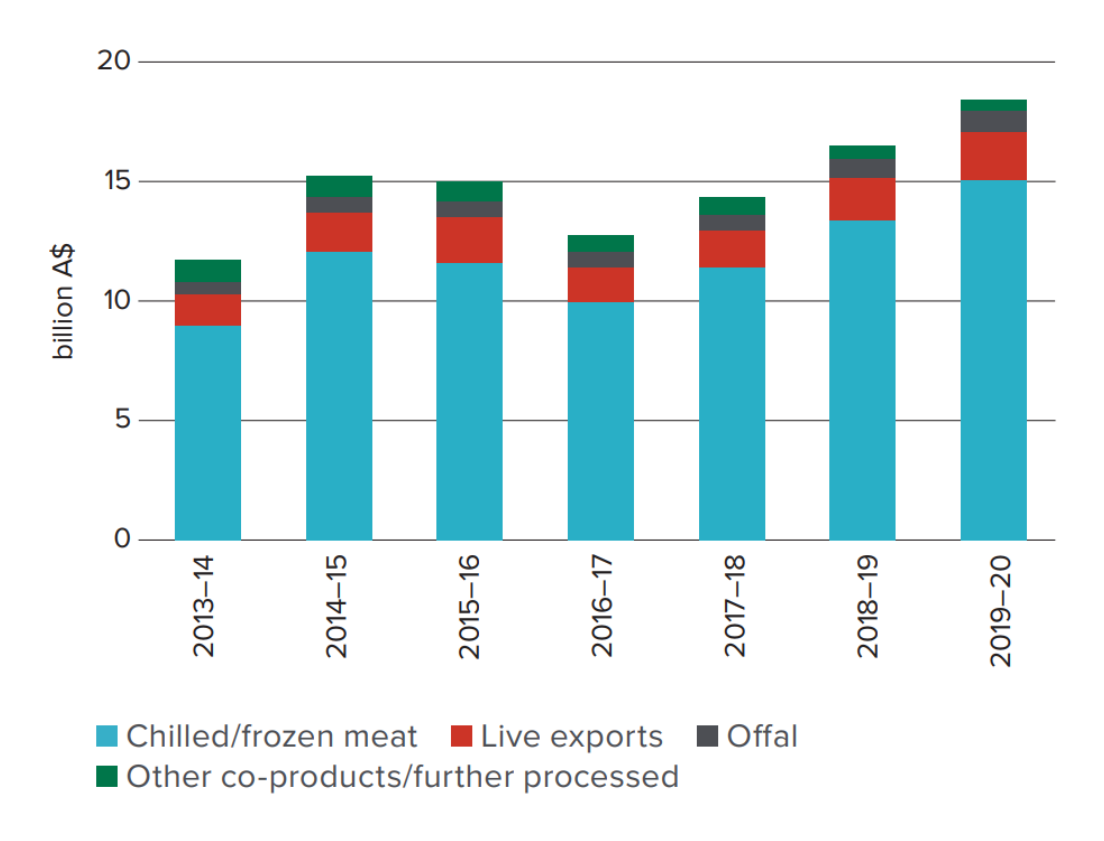


Figure 1-4: The significance of the export value of the processing sub-sector within the red meat industry. Source – (Ernest & Young, 2021)

When comparing the value add of processing of beef exported (including processing costs), in contrast to the exporting of livestock calculated as a value per equivalent weight (\$/kg), the processing of beef offers an additional \$4.31/kg gross beef product value-add. This highlights the value of the red meat processing industry for Australia's economy as opposed to live exporting of cattle.

#### 1.1.1 The Challenges of Australia's Red Meat Industry

The red meat industry faces a number of operational challenges and risks surrounding the access to, and retention of, skilled labour. According to a study conducted by the Australian Meat Industry Council (AMIC), there are currently 10,000 job vacancies in the red meat processing industry (Carter, 2022), with many processing plants unable to operate at full capacity due to national labour shortages for the red meat processing industry.

According to Carter (2022) there are several significant factors that limit the talent pool of the red meat processing industry, including:

- the negative perception of the red meat processing industry particularly prominent in younger generations,
- the lack of education and educational pathways to develop an understanding of, and skills within, the red meat processing industry, and
- the strenuous physicality of many roles in the processing plant that do not lend themselves to a female or younger demographic as well as the location of the majority of abattoirs, the significant majority of which are based in regional or remote communities.

In addition to the difficulty of attracting skilled labour, the red meat processing industry also struggles to retain the skilled labour force. According to a study conducted by The Response Group, on average the annual turnover rate of the labour force of the Australian red meat processing industry was 62% (Carter, 2022) with the highest staff turnover in the most skilled jobs in the processing plant (78% in the slaughter room; 56% in the boning/slicing room). A significant factor contributing to this turnover rate is the high rate of incidents and severity of injuries sustained by the labour force. This is predominantly injuries such as: sprains/strains, lacerations, injuries from working at heights, burns and injuries associated with animal handling, due to the repetitive, strenuous physical demands. Another significant factor that affects workforce retention is that a significant percentage of the workforce consists of migrants who are employed through Government supported migration initiatives. These programs are typically 24 months in duration, and the immigrant workforce typically use these initiatives as a shortterm opportunity to earn money to then return to their families in their native countries (Carter, 2022). The cultural diversity of the labour force

can also create language barriers that contribute to difficulties in training, and training costs.

The Australian Meat Processor Corporation (AMPC), a rural research and development corporation for the red meat processing industry of Australia, has identified the costs associated with labour as one of their most pressing issues. Past AMPC Chairman, Peter Noble, stated that the Australian red meat industry is struggling to retain its export market due to "Australia's red meat processing costs (being) the highest in the world" (Australian Meat Processor Corporation, 2016). This is illustrated in Table 1-1 which shows that the United States of America, Brazil and Argentina face only 66%, 57% and 75% respectively of the processing costs (per kilogram) to operate compared to Australia's red meat processing industry. Of all cost categories, labour-related costs most significantly contribute to Australia's cost to operate being substantially higher than competitors. Australia's labour-related costs are 63%, 178% and 138% higher than the United States of America, Brazil and Argentina respectively (see Table 1-1). This highlights the need to consider solutions that may reduce the significance of labour-related costs in the red meat processing sector.

The report by S.G. Heilbron Economic & Policy Consulting (2018) concludes that for Australia to remain sustainable "the industry will be required to identify ways in which it can reduce costs or improve productivity and product quality", which aligns to the core priorities reflected in the Meat Industry Strategic Plan (MISP) of 2020 developed by the Red Meat Advisory Council (RMAC). There is a strong focus in both the strategic plans of RMAC and AMPC outlining the commitment to improving access to labour, increasing productivity, and reducing processing costs (Red Meat Advisory Council, 2020; Australian Meat Processor Corporation, 2020).

Table 1-1: Typical operating costs of global beef processor competitors. Source – (Australian Meat Processor Corporation, 2017)

	Australia		United States		Bra	azil	Argentina		
Cost category	Cost per head (AU\$)	As % of total costs (excl. livestock purchases)							
Labour-related costs	\$210.54	58.4%	\$129.46	44.6%	\$75.63	43.9%	\$88.31	42.9%	
Utilities-related costs	\$21.62	6.0%	\$12.26	4.2%	\$19.93	11.6%	\$13.05	6.3%	
Certification- related costs	\$7.29	2.0%	\$1.49ª	0.5%	\$0.52	0.3%	\$2.28	1.1%	
Total (excl. livestock costs)	\$360.62	100.0%	\$290.15	100.0%	\$172.29	100.0%	\$205.96	100.0%	
Cost per kg HSCW	\$1.22		\$0.80		\$0.70		\$0.92		

The challenges of labour availability and the high cost to operate, predominantly due to labour-related expenses, highlight the significant need for Australia's red meat processing industry to be further automated.

# 1.1.2 Limitations of Conventional Technology in Red Meat Processing

Automation offers significant benefits, yet the processing industry remains relatively untouched compared to other large production sectors. When compared to highly automated industries like car manufacturing, it becomes evident that implementing conventional robotic technologies within red meat processing factories presents additional challenges (see Figure 1-5).



Figure 1-5: A juxtaposition of manufacturing: automotive (left) VS red meat processing (right).

Source – (Al-Naif Group, 2013; Farmers Weekly, 2018)

Some of the additional challenges with operating robotics in a red meat processor include:

- Variance in workpiece dimensions: The natural products
  have differences in shape, position, and many other qualities.
  The variability in the input product means that assumptions that
  are typically made to simplify the process cannot be reasonably
  made.
- Complex components: Biological products cannot be reasonably quantified by simple approximations due to the complex relationships between intra-product structures (e.g., bone, muscle, fat) that are inherent in such workpieces as red meat. This is contrary to conventional manufacturing production lines whereby parts are generally made from quite easily describable structures or assemblies.
- Non-homogeneity: By design, the components handled by robotic systems in typical production lines are consistently homogeneous to tight tolerances to optimise the automatability of the production line. With many uncontrollable inputs that have contributed to this product (e.g., chemical composition of the food, the variability between species, gender and age and

geographical origin of the animal) determining a consistent behaviour or developing an accurate relationship to describe for a control algorithm is difficult.

- Flexible: As opposed to car manufacture, the rigidity of the environment and stiffness of the product is assumed to ensure that positional coordinates remain relevant even at the point of contact by the system's actuators. Red meat is a flexible product and thus, even for the particular characteristic of this product, the assumptions underpinning the entire control mechanisms of the robot are void. Without real-time sensory perception and continuous real-time modification of control strategy automation will unlikely be successful.
- Hard-to-fixate: Red meat products are difficult to fix due to the size variabilities, non-uniformity of structure, slipperiness, and non-destructive handling requirements. Additionally, even in cases where effective fixation is possible, many complications exist such as considerations relating to contamination due to wear, down-time for servicing and maintenance and cleanability of fixtures.
- Challenging Operating Environment: For red meat processing all hardware is required to be made from only particular materials with high manufacture ratings (IP67) such that the system is required to be dustproof, waterproof and food-grade compatible with the versatility to work at high precision and accuracy, in low temperature environments and be easy to clean.

Due to these limitations, the majority of operations that have been automated for this industry are those that are repetitive, require heavy handling or require very minimal dexterity or skilled butchery such as packaging and storing, carcass splitting equipment and visual inspection. The current capability of robotic butchery is restricted to low-value operations where the sensitivities of the red meat product's mechanical properties may be rendered insignificant through 'brute force' and the positioning of a cutting tool in reference to easily definable visual markers. The primary factor preventing robotic systems from being implemented to undertake the more complex operations in red meat processing applications is the lack of sensing capability. This capability typically requires the means to measure or estimate the subsurface features of red meat products for which high value products are cut with respect to. Without these sensing capabilities, robotics will remain unable to emulate the skilled butchery of human operators with the capability of cutting with reference to the flexible, biological interfaces within the meat products. The lack of literature for these types of advancements in the domain of red meat processing highlights the need for further work in this area (Abolhassani, Patel & Moallem, 2007; Kettenbach et al., 2006). Hence, the research conducted in this thesis will focus upon addressing this gap in literature by exploring, and developing, a system capable for sensing subsurface interfaces for automating applications within the red meat processing industry.

#### 1.1.3 Automation Focus: Uniform Fat Trimming of Beef Striploin

A single processing task of a meat product was chosen to define the scope of this research to provide a focused investigation into the development of a sensing system capable of achieving automated, skilled butchery. The processing task chosen was the uniform fat trimming of a beef product known as the boneless striploin. The selection of this particular processing task and red meat product was based upon the significant contribution that automating this task would have on the red

meat processing industry. Beef processing accounts for 74.5% of the total processed red meat in Australia and provides 69.3% of the total export value (see Table 1-2). Additionally, the significant variability between carcasses (due to carcass size, feed types, genetic breed, etc.) was considered advantageous as it enabled the developed system to be most impactful if successful.

Table 1-2: Comparison of species in the Australian Red Meat Industry calculated by statistics available online. Source – (Meat & Livestock Australia, 2018a; Meat & Livestock Australia, 2018b; Meat & Livestock Australia, 2018c; Meat & Livestock Australia, 2018d)

Comparison: Red Meat Processing Species (Statistics from 2018)							
Categoy	Beef & Veal	Lamb	Mutton	Goat			
Stock	26.2 million head (2% of world supply)	23.1 million head (7% of world supply)	49 million head	N/A			
Processed (head)	7.2 million head	22.4 million hea	22.4 million head				
Processed (cwt)	2.24 million tonnes	531,793 tonnes	203,724 tonnes	31,414 thousand tonnes			
Exported	71%	61%	96%	91%			
Export Value	\$7.45 billion	\$3.04 billion		\$260 million			
Ave Value (\$/kg)	595 c/kg	629 c/kg	446 c/kg	585 c/kg			

Within beef processing there are several products that could be examined from the carcass (see Figure 1-6). Through an evaluation of primal (a large 'primary' meat product removed from a carcase) weights in bovine carcases on average, and the wholesale value of these primals, the striploin was found to be the most valuable primal (13.3% of the total carcass value) for a standard MSA-graded (Meat Standards Australia) beef carcass (see Table 1-3).

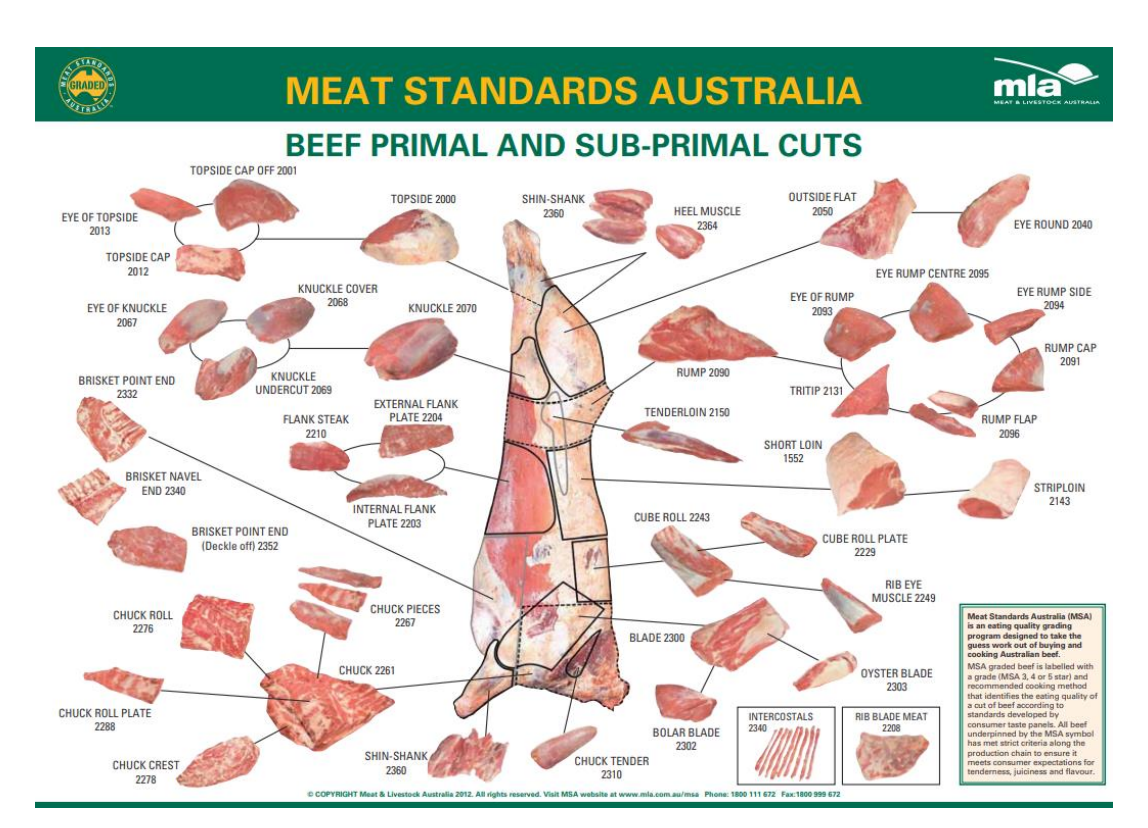


Figure 1-6: Beef carcass breakdown of primal and sub-primal MSA cuts. Source – (Meat & Livestock, 2018e)

Table 1-3: Evaluation of entire beef carcase for to identify value significance by primal using statistics available online. Source – (Meat & Livestock, 2018a; Meat & Livestock 2018b; Meat & Livestock 2018c; Meat & Livestock 2018d)

Beef Primal and Sub-Primal Comparison								
	Cut Name MSA Name		Carcass Proportion (%)	Weight (kg)	Wholesale MSA Price (\$/kg)		lue per rcass (\$)	Value per Carcass (%)
Hindquarter	Topside		6.2%	16.1 kg	\$ 7.05	\$	113.51	8.2%
	Thick Flank	Knuckle	3.7%	9.6 kg	\$ 7.11	\$	68.26	4.9%
	Outside	Silverside	5.7%			\$	104.34	7.5%
	D-Rump	Rump	3.8%	9.9 kg	\$ 9.05	\$	89.60	6.5%
	Tenderloin	Butt fillet	1.6%	4.2 kg	\$ 25.81	\$	108.40	7.8%
	Striploin	Sirloin	4.4%	11.4 kg	\$ 16.09	\$	183.43	13.3%
Forequarter	Navel End Brisket	t	3.3%	8.6 kg	\$ 5.55	\$	47.73	3.5%
	Point End Brisket		3.8%			\$	54.95	4.0%
	Cube Roll	Cube Roll	1.7%	4.4 kg	\$ 24.02	\$	105.69	7.6%
	Blade	Blade	5.5%	14.3 kg	\$ 6.00	\$	85.80	6.2%
	Chuck Roll		4.5%	11.7 kg	\$ 5.81	\$	67.98	4.9%
	Chuck Tender	Stir Fry	0.9%	2.3 kg	\$ 5.81	\$	13.36	1.0%
	Shin Shank	Diced	4.6%	12.0 kg	\$ 5.55	\$	66.60	4.8%
	Thin Skirt		0.2%	0.5 kg	\$ 5.55	\$	2.78	0.2%
	Flank Steak		0.4%	1.0 kg	\$ 5.55	\$	5.55	0.4%
	Trimmings		18.4%	47.8 kg	\$ 5.55	\$	265.29	19.2%
Components	Meat Yield		68.7%	178.6 kg	\$ 5.32	\$	950.15	-
	Fat		12.0%	31.2 kg	\$ 0.30	\$	9.36	-
	Bone		19.3%	50.2 kg	\$ 0.05	\$	2.51	-
Total	HSCW Equivalent		100.0%	260.0 kg	\$ 3.70	\$	962.00	-

The processing of the beef striploin is primarily the trimming of excess subcutaneous fat to ensure a uniform layer of fat at a depth determined by market specifications remains on the primal. An investigation conducted by Khodabandehloo for AMPC estimated a cost in yield losses of \$263k per year for a typical work shift for each processor for a 1 mm over-trim from the target product specification (Khodabandehloo, 2018). An industry survey conducted by Palmer for MLA identified that processors consider the capability of trimming subcutaneous fat to specification the most beneficial development for processing (Palmer, 2015).

This is supported by general managers of processors that process over 70% of Australian red meat have reported significant losses in the processing of beef striploin including Kilcoy Global Foods (KGF), JBS Foods (JBS) and Teys Australia (J McCormack 2018, pers. comm., 21 October). Shane Clancy, General Manager of KGF, reported that the operation of beef striploin fat trimming amounts to a loss of \$20/head (a loss of 4.1% to 4.5% yield) simply due to the inability of skilled labour to consistently trim to the market specification of the customer. Clancy estimates that, with a throughput of 4,000 head per week, this amounts to \$80k/week (over \$40m per year) and have employed various techniques such as selling half-striploins which have been unsuccessful (S Clancy 2019, pers. comm., 12 May). This was emphasised at the International Food and Automation Networking Conference (IFAN) in 2018 by Tom Maguire, General Manager of Teys Australia (Maguire, 2018). Maguire reported:

"anyone who can come up with a solution for striploin fat trimming will dominate the industry"

Much of the common tasks of red meat processing consists of cutting with respect to subsurface, biological interfaces to ensure that these products can be supplied to the consumer with a high degree of consistency, and thus, be highly valued with respect to the price that can be charged - particularly for the application of trimming excess subcutaneous fat from primals. Thus, by investigating the task of trimming subcutaneous fat the findings and conclusions of this thesis can be highly relevant for the industry in general.

#### 1.2 Research Objectives

This dissertation is an investigation conducted towards developing the capability of robotics to address the limitations preventing the automation of the red meat processing industry. This investigation aims to focus on the application of uniform fat trimming of beef striploin, and more generally, the capability of a system to ascertain, within an acceptable tolerance, the position of the fat-lean interface within the primal. The most significant and foremost limitation for this task involves acquiring the necessary information to inform the cut path of a tool for trimming subcutaneous fat in accordance with industry specifications. The numerous complexities associated with the task make this a novel undertaking worthy of study.

The following objectives have been defined for the study:

**Objective 1:** To identify the most feasible sensing technologies for the application of automated uniform fat trimming of beef striploin through conducting a literature review.

**Objective 2:** To define the key parameters that inform the system capabilities for the task of uniform fat trimming of beef striploin through analysing fat characteristics and industry standards.

**Objective 3:** To establish a framework for evaluating sensor performance that outlines the process of ranking sensors against metrics important for the automation of beef striploin fat trimming.

**Objective 4:** To develop, implement and evaluate novel ultrasound sensing systems capable of integration into an automated system to measure fat depth across an untrimmed beef.

**Objective 5:** To conclude upon evaluations of sensing systems and provide recommendations to inform the development of practical sensing systems for integration into an automated system capable of uniform fat trimming of beef striploin.

#### 1.3 Thesis Outline

This thesis is ordered as follows:

**Chapter 2** presents the current progress towards automation of uniform fat trimming before summarising the various sensing technologies that may be employed to measure the subcutaneous fat thickness on a beef striploin primal. This desktop literature review applies criteria, developed in consideration with the task-specific requirements of beef striploin fat trimming, to identify the most promising methods to be further investigated through this research.

**Chapter 3** is a collection of smaller experiments that provide the context of the product and process to inform the methodological approach of the thesis. These experiments present findings pertaining to the variability of the striploin product presented for trimming, an approximation of the processing time for striploin trimming and an evaluation of fat thickness across the striploin. Through these analyses this chapter provides rationale that informs the development of a

performance evaluation framework and the sensing systems developed for analysis within this thesis.

**Chapter 4** presents the evaluation of CT technology for the application of measuring the fat depth of a beef striploin primal. This chapter disseminates the results of the 'gold standard' sensing technology to benchmark performance and develop a framework to evaluate the performance of the candidate technologies for industry use in automation of the trimming task.

**Chapter 5** contains the evaluation of the first candidate sensing technology — B-Mode ultrasound technology. This chapter provides the rationale employed to determine the feasibility of the selected B-Mode ultrasound sensor before outlining the process of developing this sensor into a system for measuring subcutaneous fat depth on a beef striploin primal. The results obtained were evaluated by applying the sensor evaluation framework to conclude on this system's capability to be employed for the sensing of an automated beef striploin fat trimming system.

**Chapter 6** contains the evaluation of the second candidate sensing technology — A-Mode ultrasound technology. This chapter provides the rationale employed to determine the feasibility of the selected B-Mode ultrasound sensor before outlining the process of developing this sensor into a system for measuring subcutaneous fat depth on a beef striploin primal. The results obtained were evaluated by applying the sensor evaluation framework to conclude on this system's capability to be employed for the sensing of an automated beef striploin fat trimming system.

Chapter 7 concludes upon the processes and methodologies employed to develop, evaluate and implement a system to measure or estimate the fat depth of a beef striploin primal. The results of each system are compared and recommendations upon the most promising technology and technique for implementation upon automated beef striploin fat trimming is provided. A reflection is provided upon further sensing work and integration insights, both particular to beef striploin fat trimming and alternative tasks in the red meat processing industry.

# **CHAPTER 2: LITERATURE REVIEW**

This chapter defines the beef striploin product and the processing task of uniform fat trimming, present the current progress towards automation of uniform fat trimming of beef striploin and summarise the various sensing technologies and techniques that may be employed to measure, or ascertain, the fat thickness on a beef striploin primal. This desktop literature review applies criteria, developed in consideration with the task-specific requirements of beef striploin fat trimming, to identify technologies that are most promising to be further investigated through this research (Research Objective 1). Through this process this literature review aims to recommend the technology most suitable for consideration in the context of an automated trimming system.

#### 2.1 Defining Uniform Fat Trimming of Beef Striploin

The trimming of subcutaneous fat from the striploin primal is a process that requires skill and judgement. This is a complex process due to the need to leave a uniform thickness of subcutaneous fat on the striploin primal which requires trimming in reference to the fat-lean tissue interface of the product. Currently, this remains to be a labour-intensive process which, due to the inability of the slicer (the person 'slicing'/'finishing' the large meat components into meat products) to see this interface prior to making an incision, creates large yield losses.

The following subsection presents key information regarding the primal (beef striploin), current process (uniform fat trimming) and product (fat specifications) for the application considered in this research.

## 2.1.1 Beef Striploin Primal

According to Aus-Meat standards (AUS-MEAT Limited, 2005): "Striploin is prepared from a Hindquarter by a cut at the lumbosacral junction to the ventral portion of the Flank.

The Flank is removed at a specified distance from the eye muscle (M. longissimus dorsi) at both cranial and caudal ends."

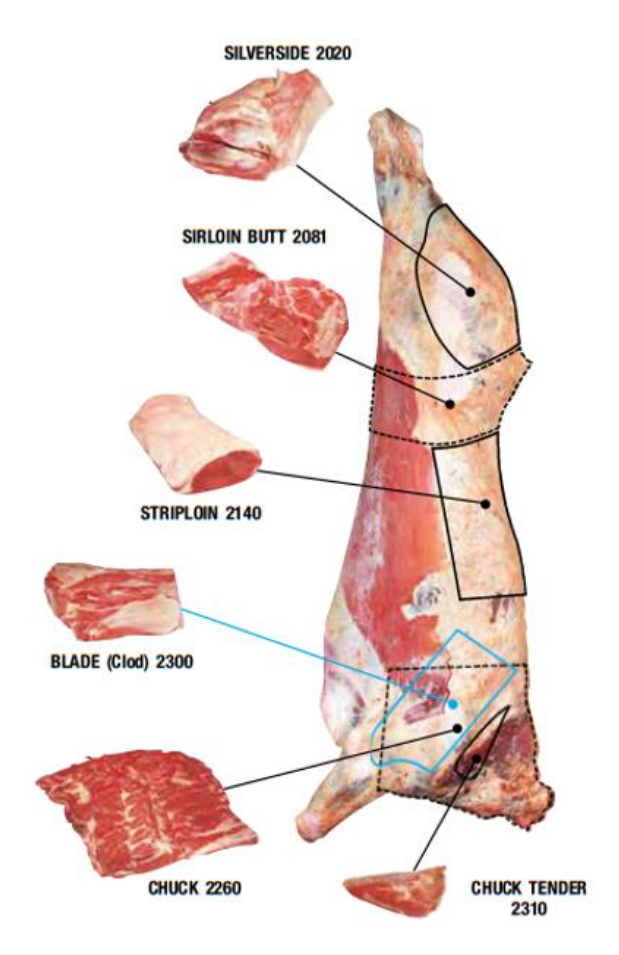


Figure 2-1: Anatomical location of a typical striploin primal on a bovine carcase. Source – (AUS-MEAT Limited, 2005)

The location of the striploin primal is presented anatomically in Figure 2-1. The striploin primal is considered particularly high value of all within the bovine carcass due to the tenderness and flavour of the M. Longissimus dorsi muscle (commonly referred to as the 'eye' muscle) that it is comprised of. A few anatomical variations are sold within the hindquarter to include the striploin primal within a product such as shortening (e.g., short loin) or lengthening (e.g., Rump and Loin, pistola

hindquarter) products (see Figure 2-2), or creating boneless or bone-in (0, 1, 2 or 3 rib) products (Figure 2-3).

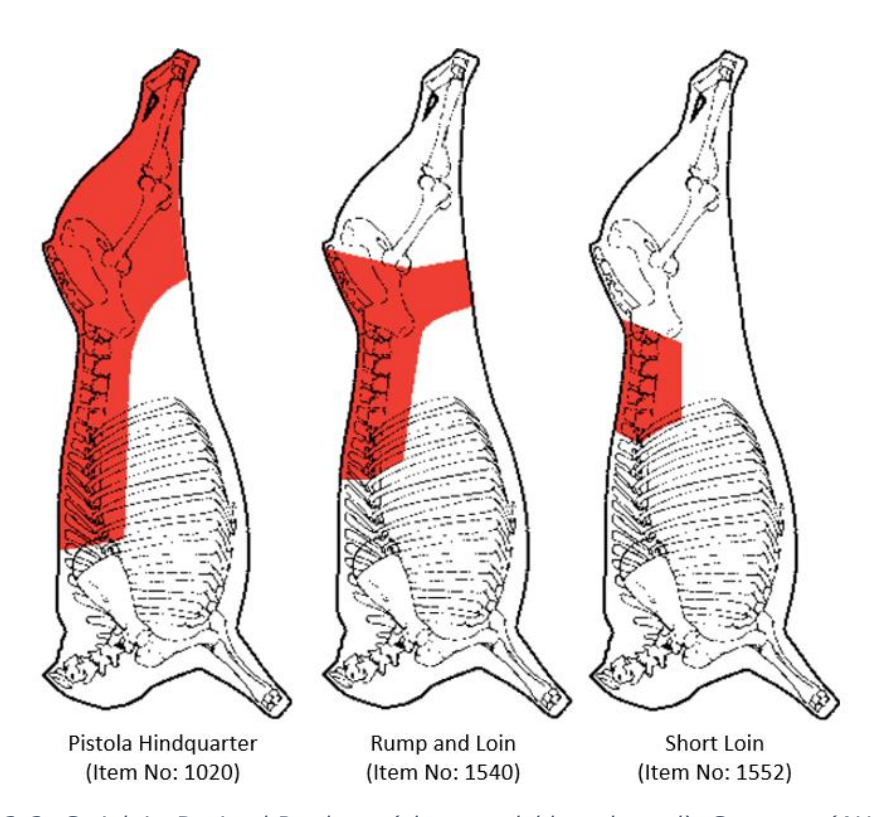


Figure 2-2: Striploin-Derived Products (shortened / lengthened). Source – (AUS-MEAT Limited, 2005)

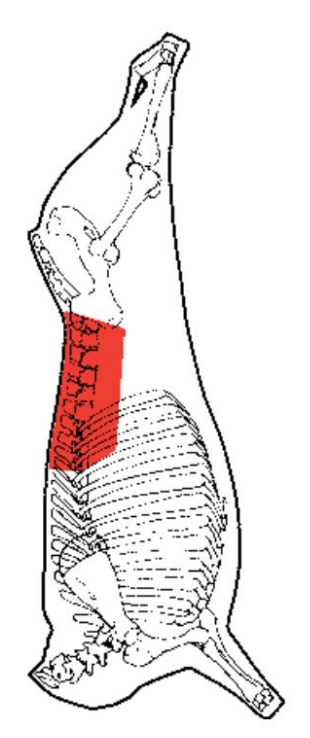


Figure 2-3: Striploin products: Boneless (0 rib) / Bone-In (1-3 rib). Source – (AUS-MEAT Limited, 2005)

Though this research could be applied to all striploin products, and perhaps many other beef and lamb products that require similar subcutaneous fat specifications, the focus of this research is the boneless (0-rib) striploin defined by Aus-Meat's unique time number: 2141 (AUS-MEAT Limited, 2005). Typically, processors sell this boneless primal as a vacuum-packed product to wholesalers or restaurants to then be portioned into high value steaks and roasts of varying thicknesses to sell to consumers (see Figure 2-4).

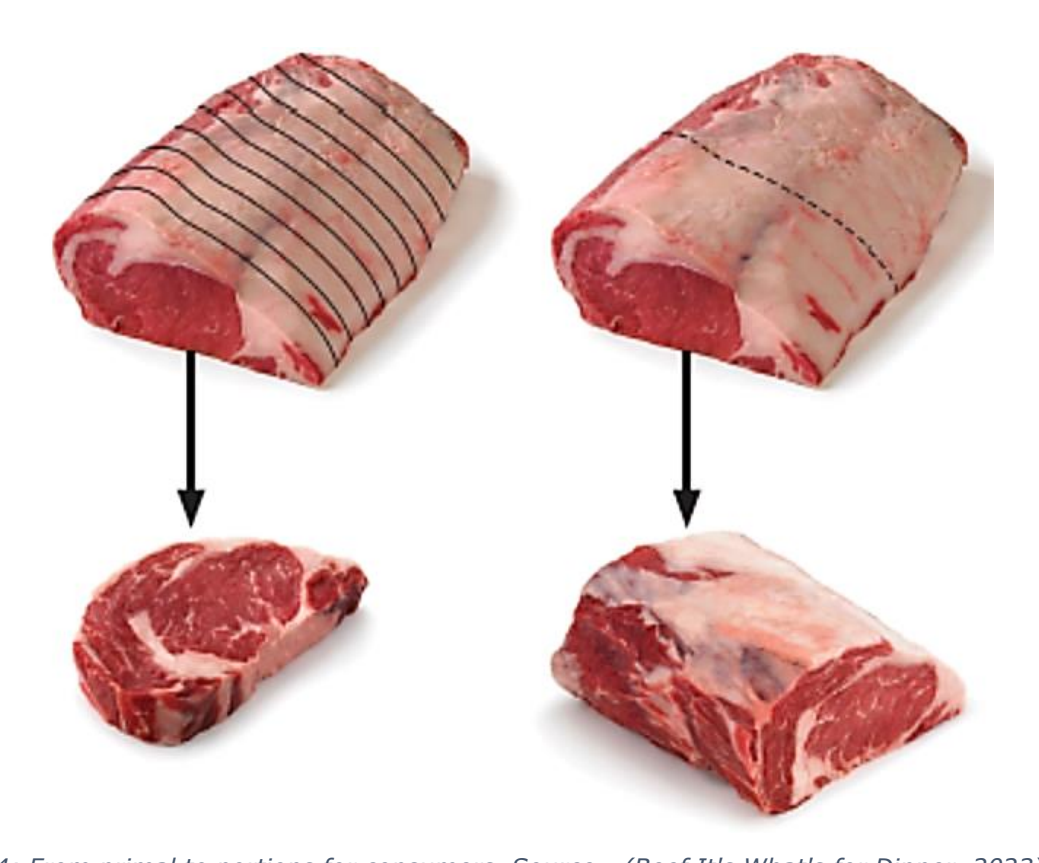


Figure 2-4: From primal to portions for consumers. Source - (Beef It's What's for Dinner, 2023)

Figure 2-5 illustrates the anatomical terminology and planes that may be used to precisely reference biological features of the bovine carcase and striploin primal. Throughout the thesis the use of this anatomical nomenclature is used to reference features within the striploin primal consistently.

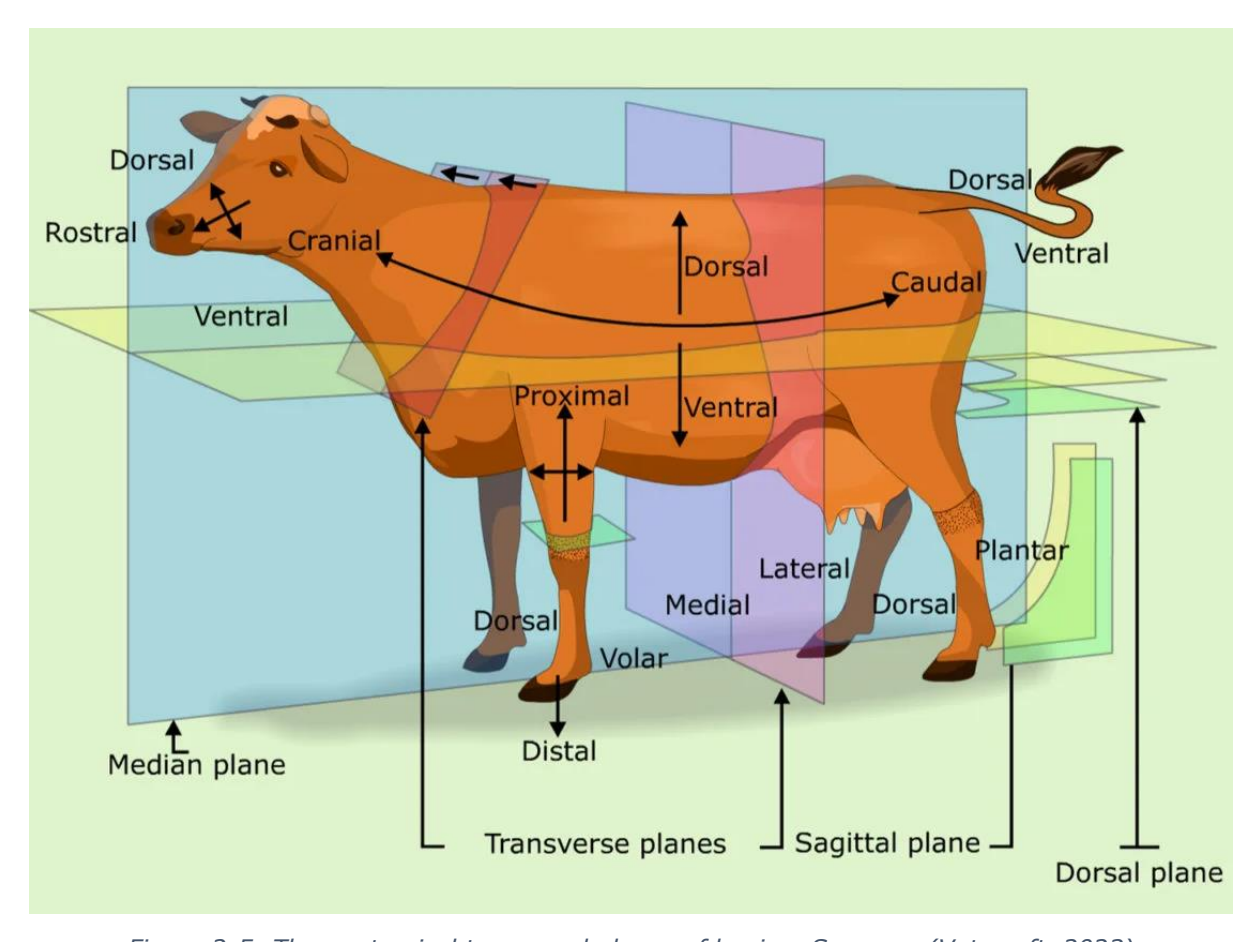


Figure 2-5: The anatomical terms and planes of bovine. Source – (Vetscraft, 2023)

A bovine carcase is sawn down the centre of the spine through the median plane of the carcase. This is commonly referred to 'carcase splitting' and is a process that creates a 'left' and 'right' carcase body, which in turn, creates two anatomically mirrored striploin orientations: left-hand side (referred to as 'LHS' striploin) and right-hand side (referred to as a 'RHS' striploin). A transverse (cross-sectional) view of a bovine carcase is presented in Figure 2-6 to illustrate how mirrored striploins (LHS and RHS) are created after carcase splitting.

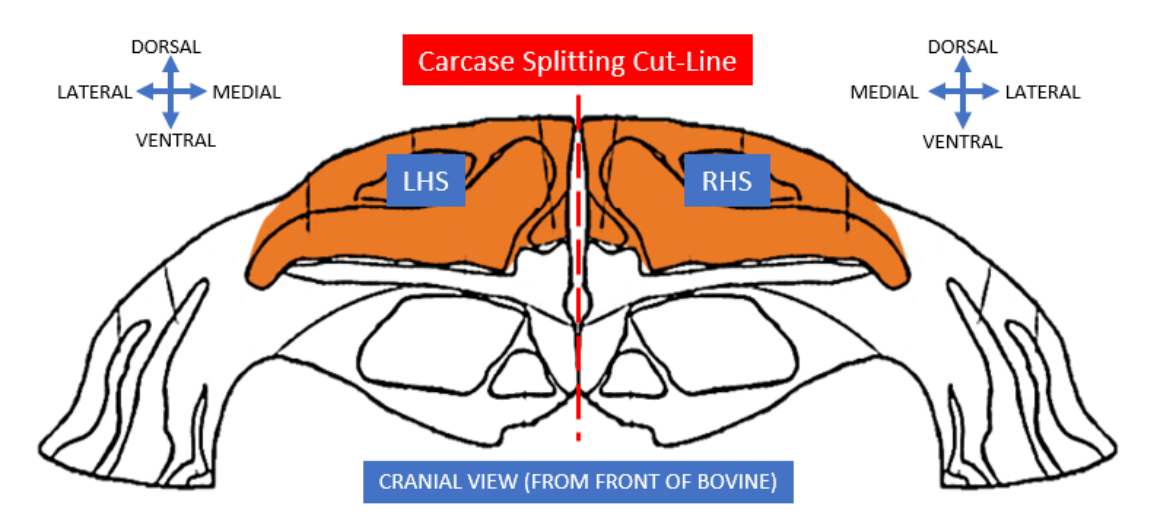


Figure 2-6: An illustration of how LHS and RHS striploins are created from bovine carcase. Source – (Government of Canada, 2023)

The anatomical planes and axes, as well as the colloquial terminologies used by slicers to refer to external features of, and internal tissues within, the striploin will be used within this research. This terminology is shown respectively in Figure 2-7 and Figure 2-8.

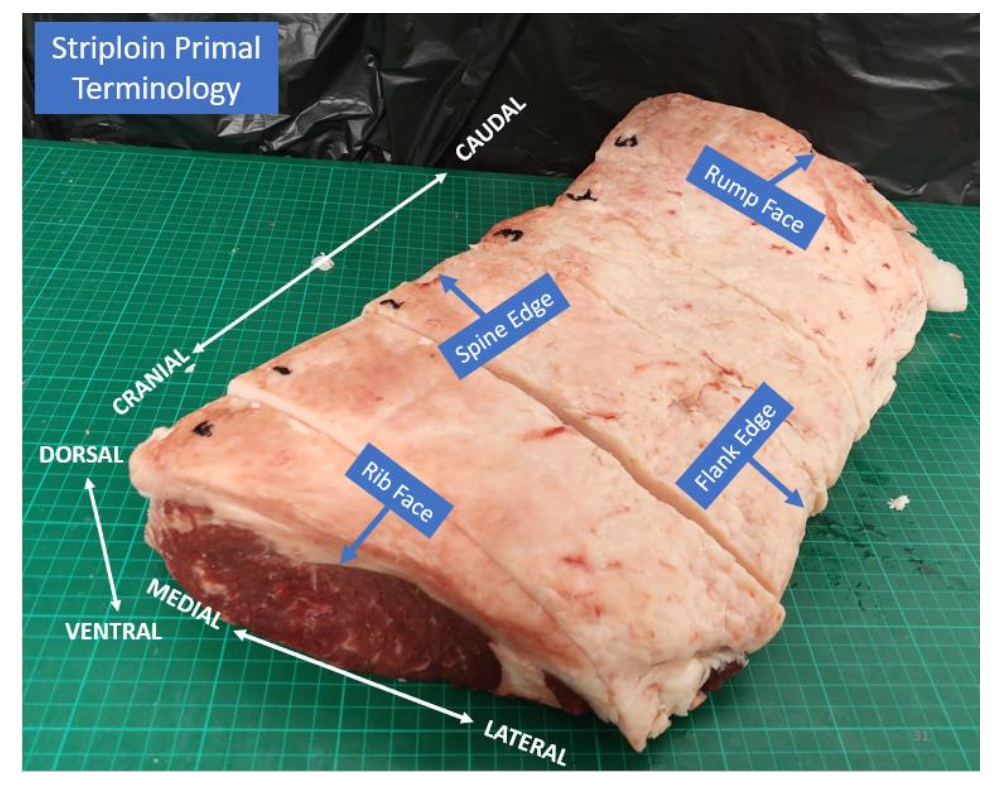


Figure 2-7: The anatomical (white) & slicer nomenclature (blue) used refer to features of the beef striploin primal illustrated for a RHS striploin.

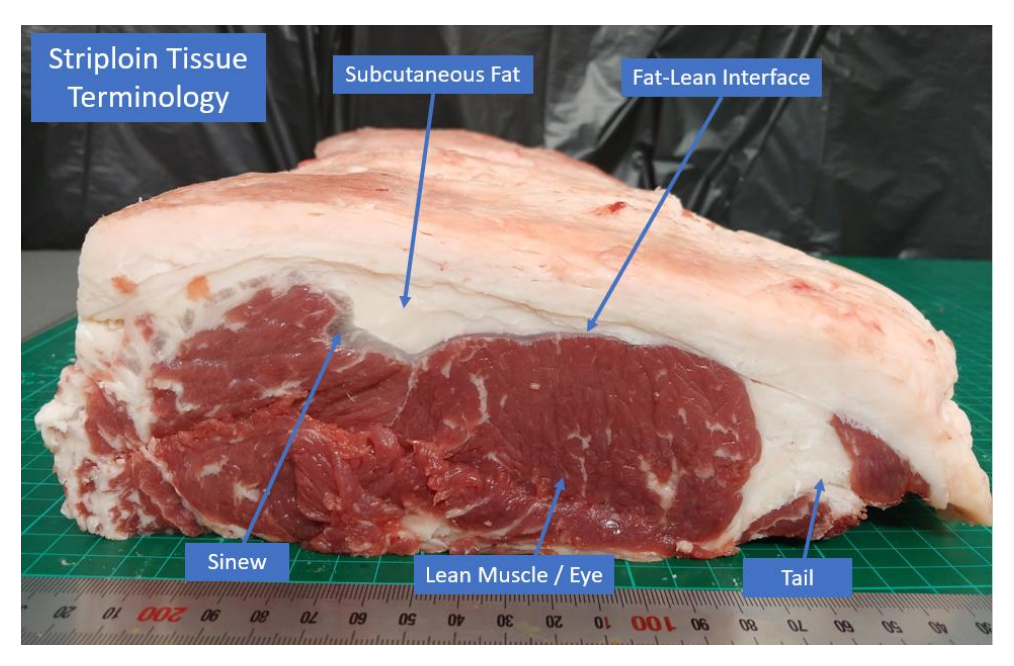


Figure 2-8: The slicer nomenclature (blue) used refer to features of the beef striploin primal illustrated for a RHS striploin.

## 2.1.2 Uniform Fat Trimming Process

Currently the fat trimming process is performed manually by slicers who use boning knives or various electric or pneumatic powered tools with reciprocating blades or shaving mechanisms (see Figure 2-9). The domestic and international markets that Australian processors sell boneless striploin have differing fat depth requirements typically ranging between 0 mm (denuded) and 25 mm (United Nations Economic Commission for Europe, 2007). The typical range of fat thickness requirements is shown in Table 2-1. The collaborating processor's most common fat specification was 12 mm, and hence this is the specification considered within this research.



Figure 2-9: Manual fat trimming methods for beef striploin. Source – (Khodabandehloo, 2018)

Table 2-1: Fat thickness specifications of beef striploin. Source – (United Nations Economic Commission for Europe, 2007)

Fat thickness code	Category
(Data field 10)	
0	Not specified
1	Peeled, denuded, surface membrane removed
2	Peeled, denuded
3	Practically free (75% lean/seam surface removed)
4	3 mm maximum fat thickness or as specified
5	6 mm maximum fat thickness or as specified
6	13 mm maximum fat thickness or as specified
7	25 mm maximum fat thickness or as specified
8	Chemical lean specified
9	Other

The complexity of trimming accurately to achieve a consistent (uniform) fat depth across the striploin is largely due to the large variations in subcutaneous fat thickness across the striploin. Due to the lack of perception that slicers have during trimming there is a high probability that the striploin products produced through manual trimming methods are not trimmed precisely to the fat specification. An ideal trimming to a 12 mm fat thickness specification is visualised on a cross-section of a boneless striploin in Figure 2-10. An under-trimming of the

striploin (fat depth larger than the product specification) could result in a 'fat claim' whereby processors are financially penalised by customers. Alternatively, an over-trimming of the striploin (fat depth smaller than the product specification) reduces the saleable weight of the product whereby the yield of these products for processors is reduced. Though there is yet to be a conclusive analysis of the degree of imprecision and inaccuracy that occurs during manual fat trimming, or the cost associated with this, a 1 mm over-trimming error is estimated to cost processors up to \$263,000 per typical work shift in direct yield losses (Khodabandehloo, 2018).

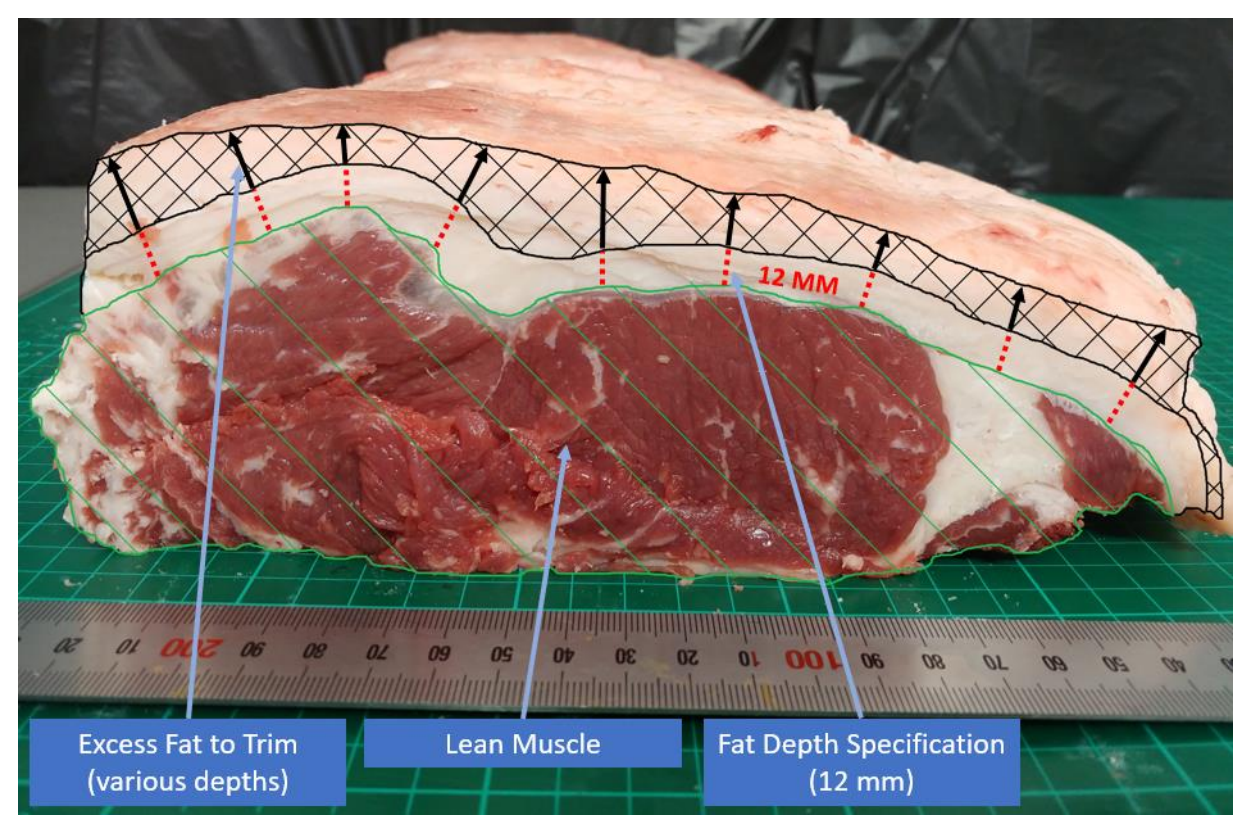


Figure 2-10: An ideal trimming of a striploin for a 12 mm fat depth specification.

### 2.1.3 Product Fat Specifications

The product of focus for developing an automated system for trimming is defined by the Aus-Meat code 2141 (0 rib / boneless beef striploin). In addition to the Aus-Meat specifications, the product is also required to adhere to international standards as defined by the United

Nations Economic Commission for Europe (UNECE Standard, 2016) which defines that:

"The purchaser can specify the maximum fat thickness of carcases, sides and cuts."

UNECE (2016) further defines the requirements of fat trimming with the following statements:

- a) Sufficient care to maintain cut integrity and identity and avoid scores in the lean [muscle].
- b) All cross-sectional surfaces [of a product] shall form approximate right angles with the skin surface [of the carcase].
- c) Trimming of external fat shall be accomplished by smooth removal along the contour of underlying muscle surfaces.
- d) Bevelled fat edges alone do not substitute for complete trimming of external surfaces when required.
- e) Fat thickness requirements may apply to surface fat (subcutaneous and / or exterior fat in relation to the item), and seam (intermuscular) fat as specified by the purchaser.

UNECE (2016) provide further definitions of two methods that may be used to describe fat trim limitations:

- Maximum fat thickness at any one point: Evaluated by visually determining the area of a cut which has the greatest fat depth and measuring the thickness of the fat at that point.
- Average (mean) fat thickness: Evaluated by visually
  determining and taking multiple measurements of the fat depth
  of areas where surface fat is evident only. Average fat depth is
  determined by computing the mean depth in those areas.

For each of these methods, the measurements of fat thickness

"... are made on the edges of cuts by probing or scoring the overlying surface fat in a manner that reveals the actual thickness and accounts for any natural depression or seam which could affect the measurement."

These natural depressions capable of causing measurement discrepancies are intra-muscular and inter-muscular subcutaneous fat deposits defined by UNECE (2016) as:

- **Bridging:** When a natural depression occurs in a muscle, only the fat above the portion of the depression, which is more than 19 mm in width is considered [in fat depth measurements]
- Planing: When a seam of fat occurs between adjacent muscles, only the fat above the level of the involved muscles is measured [in fat depth measurements]

Instances of bridging and planning are illustrated in Figure 2-11. Illustrations to exemplify the cross-sections of a "perfectly" trimmed striploin primal according to these fat specifications are exemplified in Figure 2-12.

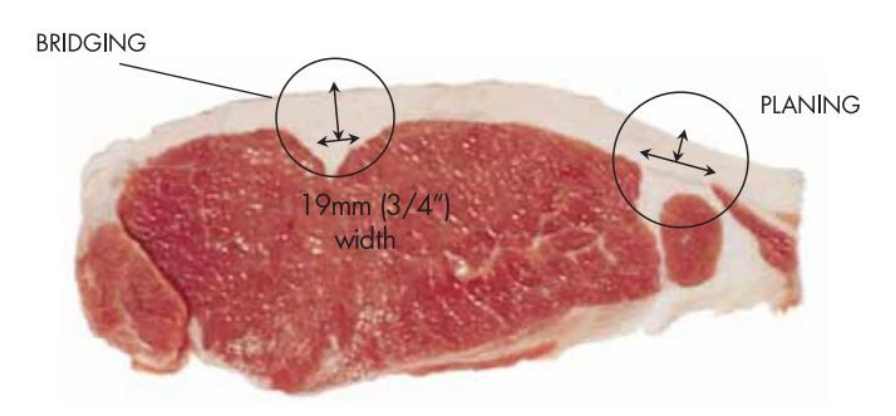


Figure 2-11: Defining the measurement of fat thickness for cases of intra-muscular ('bridging') and inter-muscular ('planing') fat deposits. Source – (UNECE, 2016)



Figure 2-12: Cross-sectional examples of the "perfect" trimming of beef striploin according to a 12 mm fat thickness specification.

## 2.2 Progress Towards Automated Beef Striploin Fat Trimming

The following progress has been made towards informing the automation of uniform fat trimming of beef striploin.

## 2.2.1 Registered Patents

There are several patents that have been submitted in anticipation of creating an autonomous system with the capability of uniform fat trimming, yet all of these have since expired or have not been developed.

A patent submitted by Leblanc (1990) expired in 2010 described a system capable of trimming the subcutaneous fat of pork loin. This patent illustrates a highly mechanised system which utilises many gear, pulley, belt and chain arrangements to achieve trimming. The system includes an endless chain system to provide compression and tension to fix the striploin against the conveyor whilst an arcuated blade is used to trim back fat and a 20-teeth chain is used to smooth the remaining trim. The mechanism of this design allows the articulated blade to replicate the curvature of the loin's subcutaneous fat surface (see Figure 2-13).

This mechanised system may provide a means of trimming uniform fat layers from the striploin, yet without a means of sensing the fat depth along the loin, there is not capability of trimming to leave uniform fat on the striploin. For use on a striploin sensing is required and therefore this patent doesn't provide a valid solution for leaving the product with uniform fat for this trimming application. This suggests that these mechanisms would likely be unsuccessful for beef striploin fat trimming applications.

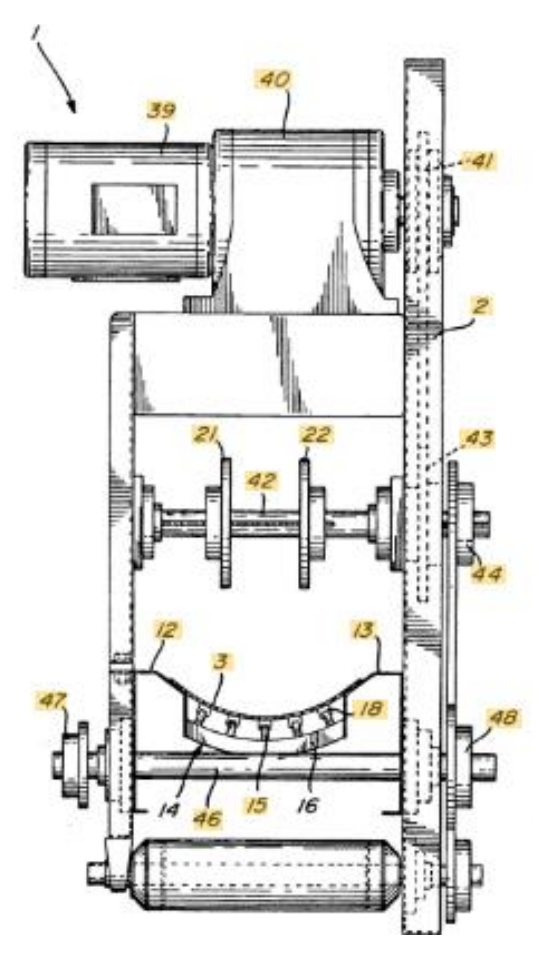


Figure 2-13: A registered patent for a mechanised system of trimming pork fat uniformly. Source – (Leblanc, 1990)

A patent submitted by Matthews et. al (1976) expired in 2005 described a process of simulating a natural fat-lean meat product using forming techniques to replicate the presentation of a genuine trimmed striploin. This process outlines the co-extrusion of meat and a fat-simulated, emulsified mixture (fabricated from lean meat, fat, salt, skin and other extenders) into fitted non-toxic plastic sleeves to simulate the shape of natural meat products with fat cover. To assist to bond the emulsified fat mixture with the lean meat an adhesive emulsion (meat, water, polyphosphate and salt) may be added (see Figure 2-14).

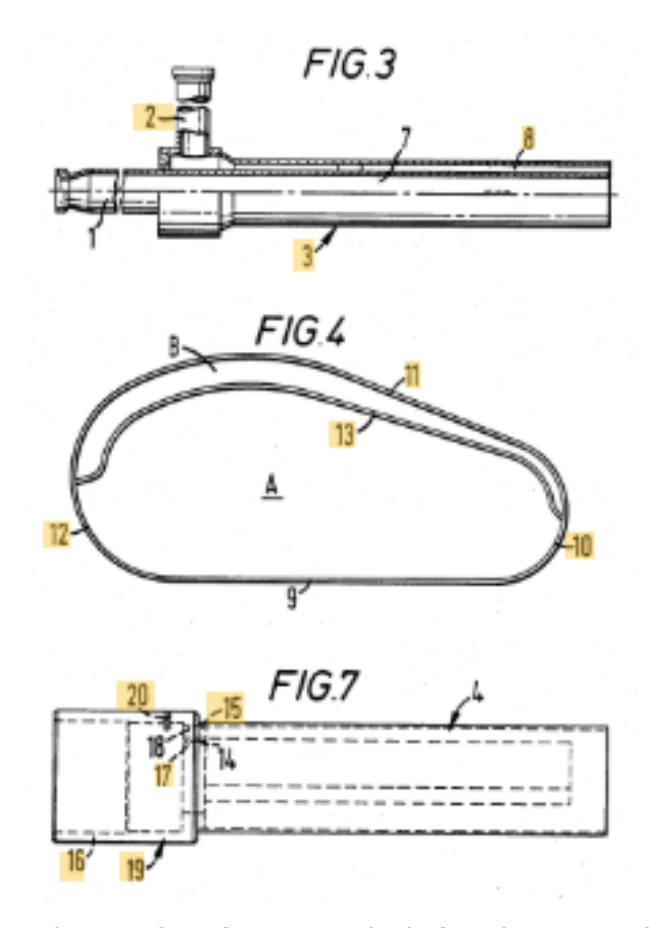


Figure 2-14: A registered patent for a forming method of producing a uniform fat thickness on a meat product. Source – (Mathews et al, 1976)

Whilst the system presented may be suitable for high-end 'designer' steaks that are perfectly formed, the forming process would not be scalable for the large volumes of meat that is processed. This process would also introduce larger processing costs due to the need to denude (remove) subcutaneous fat from the striploin and then reform this fat on the primal.

A patent submitted by Long & Thiede (1994) illustrates a mechanism that uses an inclined conveyor to force the subcutaneous fat of a striploin against a rotating trimming blade. This patent outlines that the amount of material trimmed from the meat product will be dependent on the number of rotations allowed for the contact between the trimming blade and striploin product determined by setting the rotational and

translational speed of the trimming blade and conveyor moving the striploin respectively (see Figure 2-15).

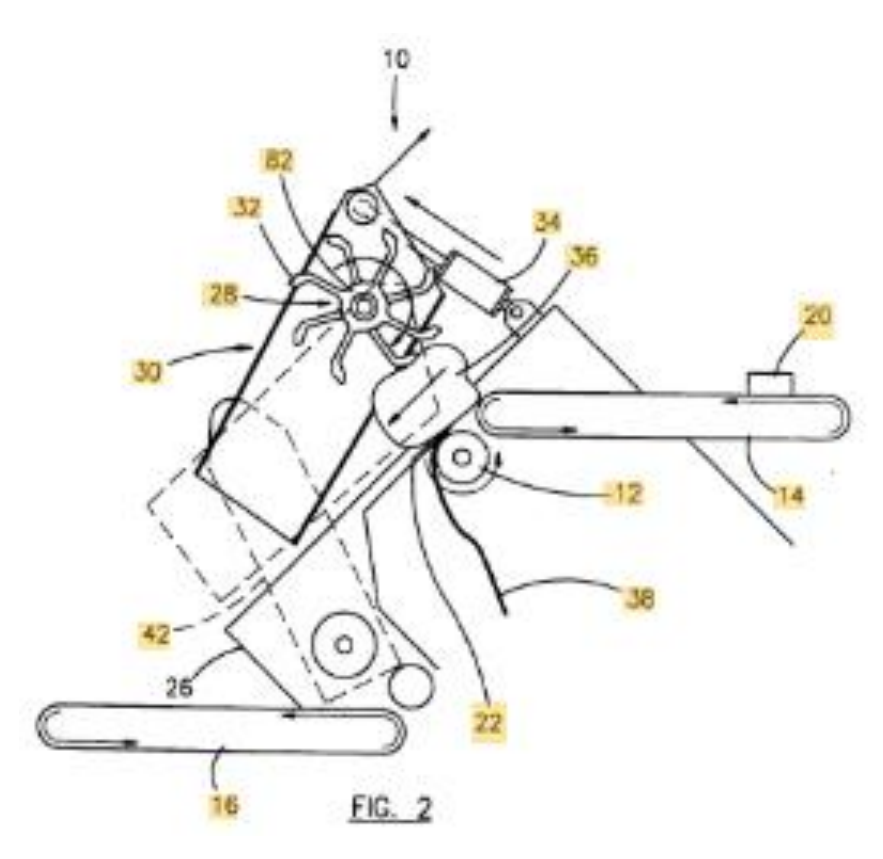


Figure 2-15: A registered patent for a mechanised system of trimming fat uniformly. Source – (Long & Thiede, 2014)

Similar to the patent registered by Leblanc (1990), there currently exists no method for quantifying fat depth at various points along the striploin. Consequently, the ability to maintain a consistent fat layer on the striploin product is limited. While it is asserted that this approach is applicable to various meat products such as beef, pork, poultry, and fish, there is an absence of empirical data or presented research substantiating this assertion. The rigidity of beef fat raises uncertainties regarding the feasibility of fat trimming as outlined by this system.

In summary, there are no feasible patents that have been found to present a uniform fat trimming solution for beef striploin in the surveyed literature.

## 2.2.2 Commercial Systems

The four largest international robotics companies servicing Australia's red meat processing industry are: Frontmatec (Denmark), Marel (Iceland), Scott Automation & Robotics (New Zealand) and Mayekawa (Japan). Many operations that have been automated by these companies for the meat processing industry are tasks that are repetitive, require heavy handling or require very minimal dexterity or skilled butchery such as: packaging and storing, carcass splitting equipment and visual inspection. Presented below are the commercial solutions most relevant to the application of beef striploin fat trimming characterised by the capability to measure to, and position a cutting tool in respect to, a subsurface biological interface.

**Frontmatec:** Frontmatec, a Danish food automation company, has developed a number of fat trimming systems to the commercial market such as: the automatic loin trimmer (model ALTL-1100) and the 3D loin trimmer (model ALTD-450).

Model ALTL-1100 is a commercial system developed for the automated trimming of subcutaneous fat of pork products (see Figure 2-16). This system features a pressure wheel and plastic guides to both mould the primal into a pre-defined shape and feed it through a static blade to uniformly remove excess subcutaneous fat (see Figure 2-17).

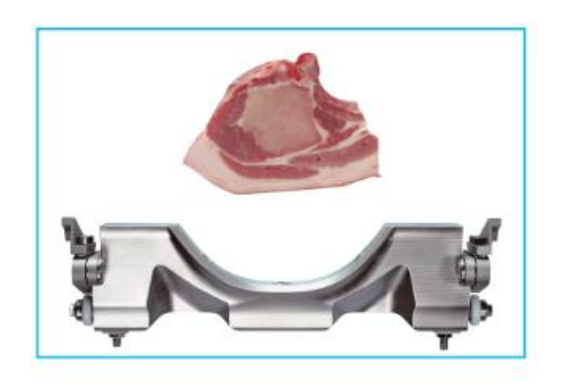


Figure 2-16: Frontmatec's automatic loin trimmer system. Source – (Frontmatic, 2020a)



Figure 2-17: The mechanism of feeding and moulding the pork loin through a cutting blade of Frontmatec's automatic loin trimmer. Source – (Frontmatic, 2020a)

There are three pressure wheel designs that assist to mould the different pork products, boneless/bone-in loin and back, as they are fed through the cutting knife. Two blade configurations for pork loin or back that have been designed to approximate the contour of the fat-lean interface of the moulded product (see Figure 2-18). During installation the machine is fitted with one of these blades depending upon the product to be trimmed.





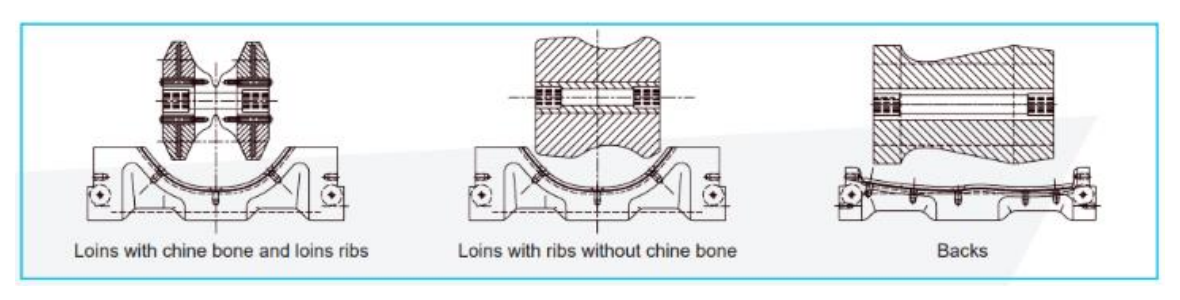


Figure 2-18: The numerous pressure wheel and blade contours for trimming pork loin (bone-in and boneless) and back of Frontmatec's automatic loin trimmer. Source – (Frontmatic, 2020a)

An optical probe is inserted into the product from the surface of the fat into the lean muscle to ascertain a fat thickness measurement at a single location of the product (Frontmatec, 2020a). This measurement is used to adjust the gap between the knife and the infeed conveyor to provide a depth of cut specific to the product (see Figure 2-19) which enables the subcutaneous fat to be removed from the pork primal (see result in Figure 2-20).

As with many other designs, this mechanism is restricted to trimming uniform subcutaneous fat with reference to the surface of the product rather than the fat-lean tissue interface required of market specifications. The sensing technique of acquiring a single measurement to approximate the fat depth across the entire pork primal indicates that this system cannot account for fat variability along the length of the primal. The mechanism of feeding the primal through a fixed contour blade indicates that the system cannot account for the fat variability across the width of the primal.



Figure 2-19: The optical probe (spike at centre of image) for acquiring fat depth of the pork primal for adjusting the trimming depth of Frontmatec's automatic loin trimmer. Source – (Frontmatic, 2020a)



Figure 2-20: The finished output of pork loin through Frontmatec's automatic loin trimmer. Source – (Frontmatic, 2020a)

The 3D loin trimmer was developed by another Denmark automation company called Attec which was acquired by Frontmatec in July of 2016. In comparison to Frontmatec's automatic loin trimmer, this commercial system has the capability to adjust trimming depth lengthwise

and widthwise across boneless pork loin and back primals (see Figure 2-21).



Figure 2-21: Frontmatec's 3D loin trimmer system. Source – (Frontmatic, 2020b)

The 3D loin trimmer employs a similar handling technique as the automatic loin trimmer where a deliberately shaped pressure wheel moulds the primals into a specific shape while also feeding against a static blade arrangement. The 3D loin trimmer has an arrangement of eight 'planer' blades that are positioned in a similar contour to the previous single contoured blade, and each of these individual blades that can be positioned to change the trimming depth along the width of the primal (see Figure 2-22).

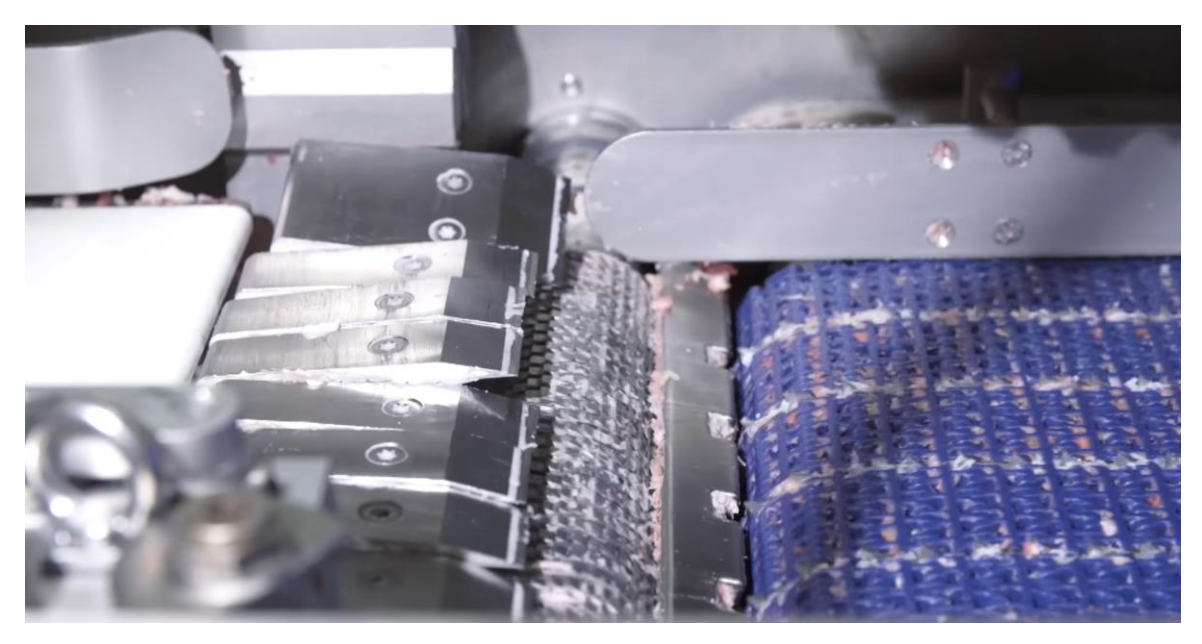


Figure 2-22: The 'planer' blade arrangement used to vary the trimming depth of Frontmatec's 3D loin trimmer. Source – (Attec Denmark A/S, 2014)

The blades are controlled through a servo-driven mechanism that resembles a camshaft; small rotations of a shaft below will push on the blades through a connecting rod. Through this mechanism, the gap between each blade and the conveyor (which the primal is being forced onto through the pressure wheel) can be controlled with precision (see Figure 2-23 & Figure 2-24).

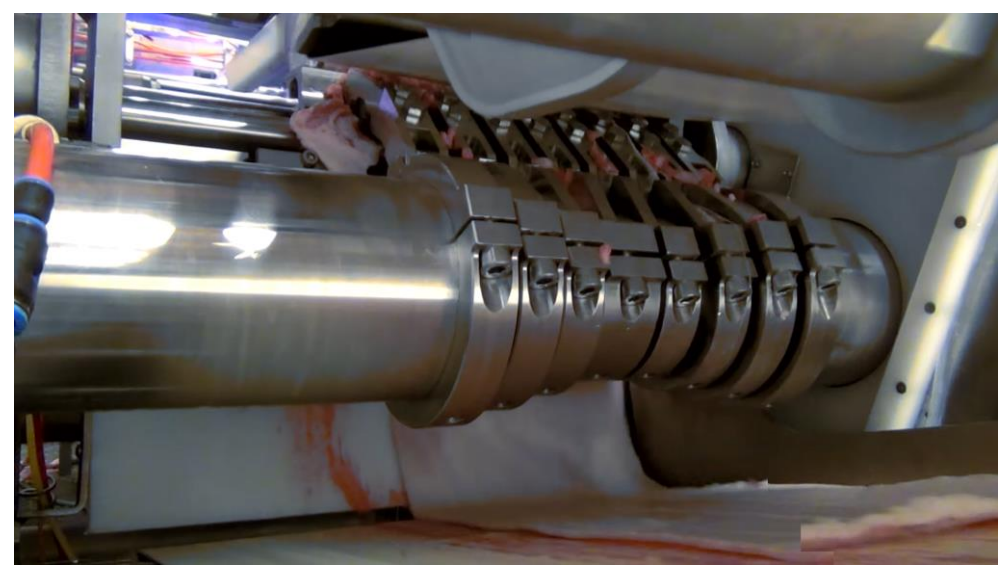


Figure 2-23: Back View: The mechanism for positioning each blade in the trimming arrangement used to vary the trimming depth of Frontmatec's 3D loin trimmer. Source – (Attec Denmark A/S, 2014)

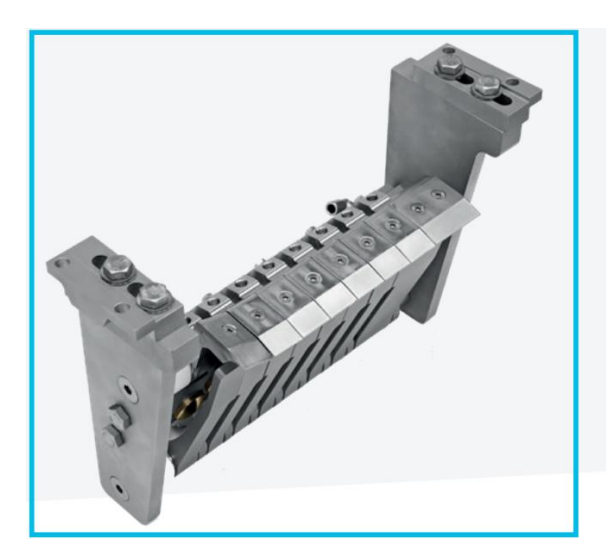




Figure 2-24: Isometric View: The mechanism for positioning each blade in the trimming arrangement used to vary the trimming depth of Frontmatec's 3D loin trimmer. Source – (Frontmatic, 2020b)

According to Frontmatec (2020b), the ALTD-450 model acquires the fat depth data across the primal using an array of ultrasound sensors and a camera-based vision system at the system's inlet (see Figure 2-25). For pork back primals 15 individual measurements are taken to ascertain the fat depth at particular locations of the primal (see Figure 2-26).

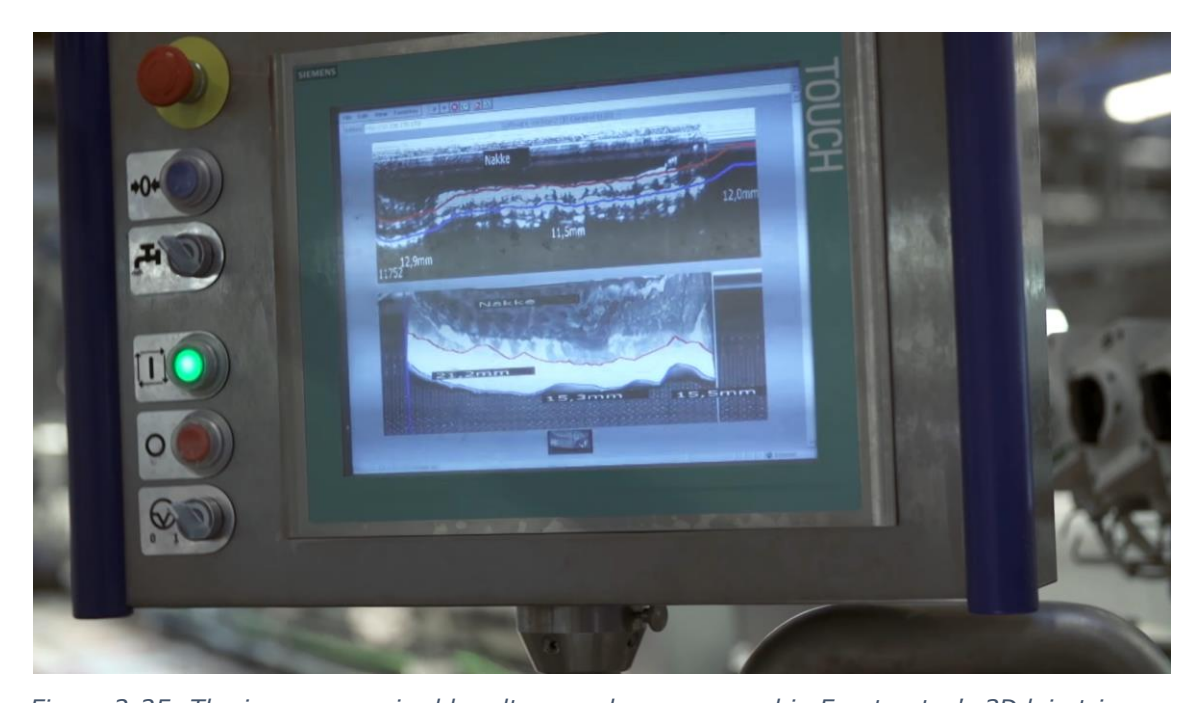


Figure 2-25: The images acquired by ultrasound sensors used in Frontmatec's 3D loin trimmer system. Source – (Attec Denmark A/S, 2014)

# Metrics for testing measurements of 3D trimmed backs

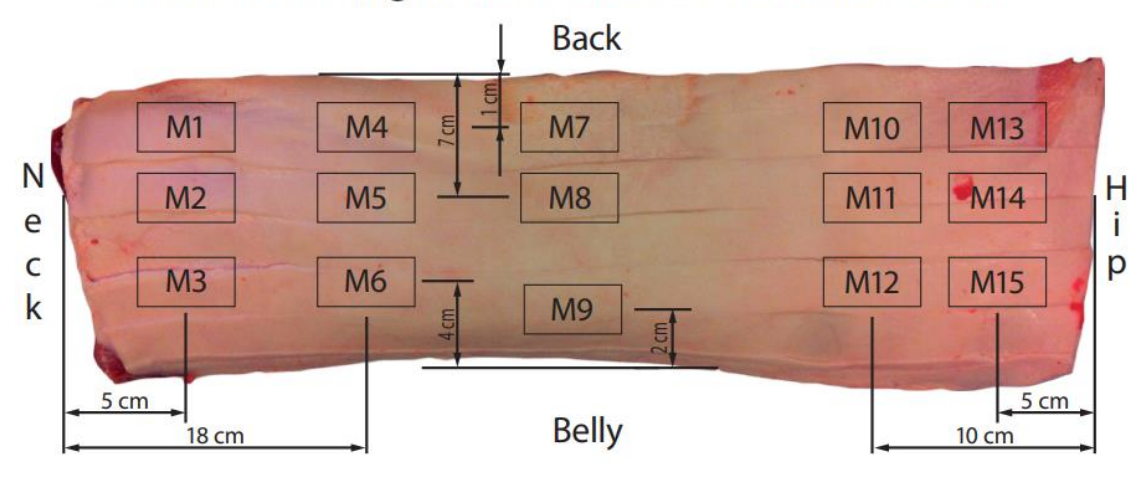


Figure 2-26: The location of ultrasound measurements for estimating the fat depth across pork back of Frontmatec's 3D loin trimmer system. Source – (Frontmatic, 2020b)

A study by Khodabandehloo (2018) conducted using this system illustrated that a plastic guide is used to compress the primal for the ultrasound probes to contact, and measure tissue depth from, the surface of the lean muscle. The interruption of a laser sensor to gauge the leading edge of the primal and the known, constant feed-rate of the conveyor enabled the positioning of the ultrasound probe at the measurement sites within the pork primal (see Figure 2-27). Through combining sensing information and registering the data acquired from the camera-based and ultrasound sensing systems a 3D model is created for each primal (see Figure 2-28).

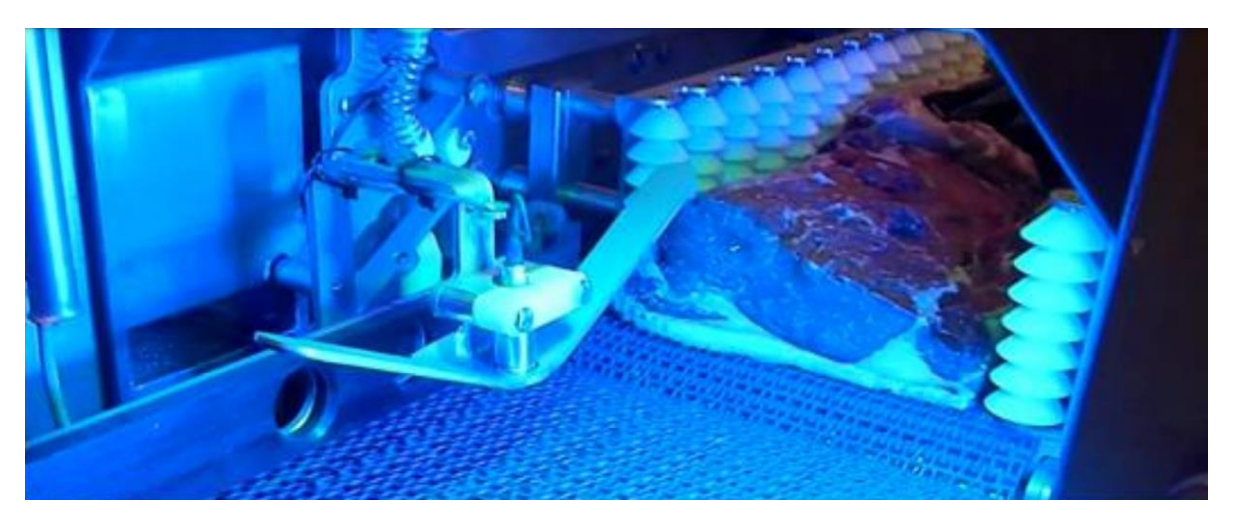


Figure 2-27: The mechanism of locating the ultrasound probe (centre of image) at measurement sites within the pork back of Frontmatec's 3D loin trimmer system. Source – (Khodabandehloo, 2018)

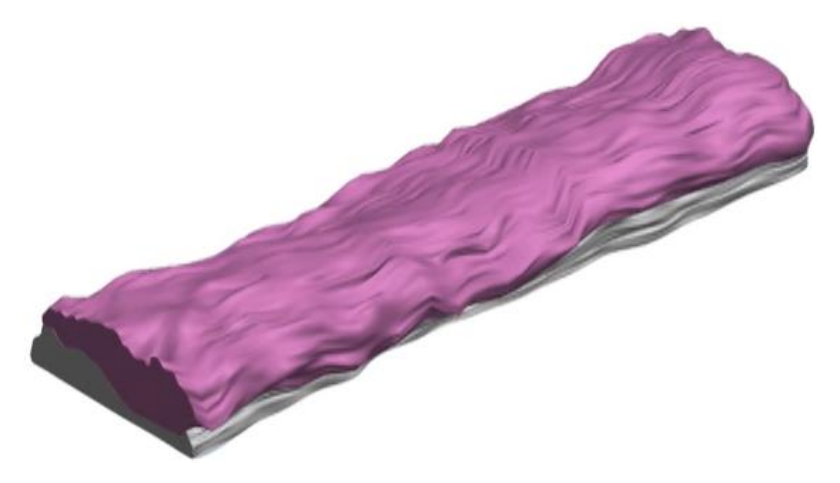


Figure 2-28: The 3D model generated by combining the ultrasound and imaging information acquired by Frontmatec's 3D loin trimmer system. Source – (Attec Denmark A/S, 2014)

The camera and ultrasound measurements acquired across the pork primal are used to position the trimming blades as the primal is indexed though to leave a uniform fat depth across the pork primal (see Figure 2-29). It is likely that by utilising the pressure wheel applying force onto the primal it has been assumed that the fat surface is uniformly positioned against the conveyor belt. This provides a constraint to the fat surface of the volumetric model of the primal to be defined if the conveyor belt is kept tight. In order for the camera system to identify the fat and lean tissues on the exposed cross-section of the model, at least one of the cameras must be positioned to acquire an image of this cross-section (blue lighting is used to assist the visual thresholding to

differentiate between fat and lean muscle). It is likely that this image is used to define the initial position of the blades before beginning the trimming of the primal.



Figure 2-29: The resulting uniform fat trim of pork primals using the Frontmatec's 3D loin trimmer system. Source – (Attec Denmark A/S, 2014; Frontmatic, 2020b)

Whilst this commercial system is seen to deliver the capability of leaving a uniform fat trim on the loin product, the specific development is limited to pork processing applications. A feasibility study conducted by Khodabandehloo (2018) to assess the feasibility of the application of this solution to trim beef striploin deemed Frontmatec's 3D loin trimmer to be incompatible for such applications due to the higher degree of trimming controllability. The product characteristics of typical beef striploin are out of scope of the limits of Frontmatec's 3D loin trimmer as summarised in Table 2-2 (Khodabandehloo, 2018; Frontmatec, 2016).

Table 2-2: Limitations of a Frontmatec 3D Loin Trimmer for Beef Striploin Applications. Source – Khodabandehloo, 2018; Frontmatec, 2020b)

	3D Loin Trimmer (System Limits)	Beef Striploin (Product Characteristics)
Maximum Width	< 225 mm	< 245 mm
Minimum Fat Depth	> 8 mm	> 2 mm
Maximum Fat Depth	< 40 mm	< 75 mm

**Marel:** Marel have commercialised the following automated solutions in similar applications as Frontmatec: the Loin Trimmer (model 6000DHT), AutoTrimmer (model AT21–620) used for pork butts and the Auto Shoe Adjust Skinner (model SK 15 – 350).

Marel's 6000DHT Loin Trimmer (see Figure 2-30) utilises an infeed conveyor to a heavy-duty shoe and tooth roll at a pre-set height in order to trim a uniform layer of fat and skin from bone-in pork loins (Marel, 2020a). A promotional video of the product indicates that a pre-set height of the shoe, and hence trim depth, is selected manually (Marel, 2018). A conveyor is used to apply downward force on the lean meat face of the primal as shown (see Figure 2-31). The manufacturer claims that the system can trim beef striploin to leave uniform fat cover, however this is not shown publicly and without sensing capabilities would not be able to trim to the correct depth.



Figure 2-30: Marel's 6000DHT Loin Trimmer system. Source – (Marel, 2020a)

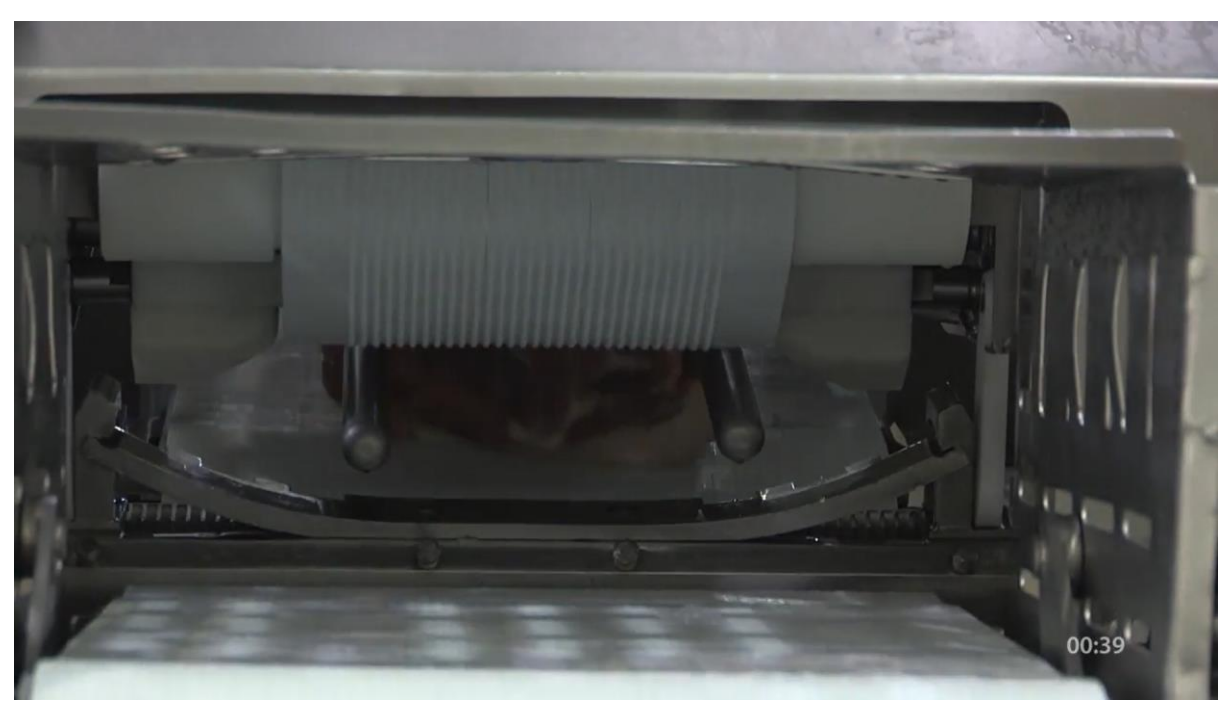


Figure 2-31: Marel's 6000DHT Loin Trimmer forces the pork primal through a shoe that trims to a manually selected depth with a particular profile. Source – (Marel, 2018)

The Townsend AT 21-620 AutoTrimmer is the successor to the 6000DHT Loin Trimmer which utilises a single measurement from an optical probe to adjust the height of the trimming shoe (see Figure 2-32). This enables an automated adjustment of the trim thickness through the vertical positioning of the shoe. Similar to the 6000DHT Loin Trimmer, this system uses a plastic guide to force the primal onto the surface of the conveyer to ensure the blade of the shoe cuts at a depth above the conveyor (see Figure 2-33). This product is very similar to the Auto Shoe Adjust Skinner, which features the ability to select vertical shoe positions to select up to 4 pre-programmed trim depths (Marel, 2020c).



Figure 2-32: The optical probe (centre of image) used within Marel's AutoTrimmer system. Source – (Marel, 2020b)

Due to the use of a shoe profile cutting blade the shape of the trim of this design is restricted to the blade profile. Additionally, whilst the optical probe may approximate the fat depth of the product, this single measurement allows only an estimate of the fat depth along the entire product. Hence, whilst these products may trim fat, without additional sensing capabilities and adjustment the cutting profile this system would

not be able to leave uniform fat cover behind. As with Frontmatec, there is no published evidence to support the claim that beef products may be similarly trimmed using these automated pork trimming solutions.

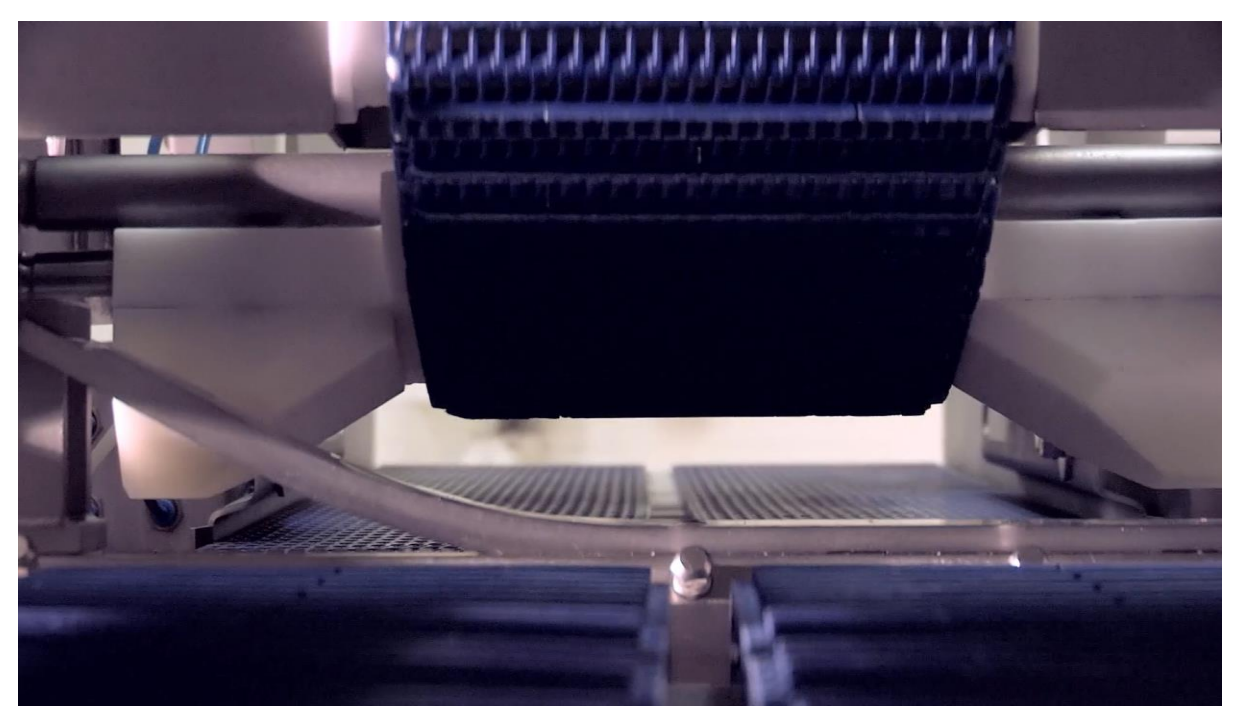


Figure 2-33: A View of Marel's AutoTrimmer System along the conveyor belt. Source – (Marel, 2020b)

Whilst Frontmatec and Marel have several, both Scott Automation and Robotics and Mayekawa have no commercial automated systems for uniform fat trimming applications. Frontmatec provides the only solution (3D loin trimmer) that has the capability required to meet market specifications of trimming to a uniform fat cover on the product. This has been proven for pork loin trimming but within a feasibility study this system has been deemed inappropriate for beef striploin applications due to the vastly incomparable fat characteristics of beef to pork (Khodabandehloo, 2018). This review concludes that an automated system developed with the capability of uniform fat trimming of beef striploin is yet to be developed.

## 2.2.3 Summary of Automation Progress

Within literature it has been identified that there remains to be a system capable of automating the trimming of subcutaneous fat for beef striploin primals. Whilst there are many aspects still requiring work to develop a system technically capable of automated trimmings (e.g., methods of handling and fixation, designing trimming tools, etc.), there remains to be a significant gap in knowledge of developing a practical sensing system using existing technologies for this application. The sensing technologies utilised in the reviewed systems primarily focused upon ultrasound and optical sensing technologies. All these systems were developed for the application trimming subcutaneous fat from pork. This highlights the significant gap in literature focused on automated fat trimming applications for beef processing. The remainder of this literature review considers all sensing technologies that may offer the capability to measure fat thickness and is practical for beef striploin fat trimming applications.

# 2.3 Desktop Evaluation of Sensing Technologies

This literature review subsection evaluates potential technologies that may be used for developing a sensing system capable for measuring the fat depth of a beef striploin primal. For a technology to be appropriate for this application there are a few core requirements that need to be met:

**Sensing Capability:** As defined by product specifications the fat specification is measured as the fat remaining on the striploin measured from the subcutaneous fat surface to the fat-lean interface. Therefore, sensor must have the capability to measure, or ascertain, the subcutaneous fat thickness with respect to the fat-lean interface.

**Accurate & Precise:** The cost to a meat processor for poor accuracy is high – estimated by a feasibility report by AMPC (2018) as

over \$1 million per year for a 1 mm over-trim on striploin product. This means that a target accuracy and precision of a few millimetres would be ideal and lower accuracies would weigh heavily in the sensor selection process.

**Deep Penetration Range:** For this sensor to be effective it must be capable of penetrating and providing measurements to tissues in a range of approximately 2 mm – 75 mm (Khodabandehloo, 2018).

In addition to meeting core requirements an appropriate sensing technology must be practical for integration for processors. The following functionality will be considered in reviewing feasible sensing technologies to account for the nature of the striploin product, processing procedures, operating environment, and market specification for the product.

**Non-Destructive:** It should be noted that whilst devices typically used for grading, such as the Hennessy Grading Probe and the SFK Fat-O-Meater, may cause carcass damage during use, this is an industry required necessity restricted to specific measurement sites of the carcass (Kempster, Chadwick & Jones, 1985). In the specific evaluation of sensors for striploin fat trimming it remains ideal to avoid significant damage to the product due to the potential risk of devaluing the striploin primal.

**Robust in Harsh Environments:** The developed system and its sensing components must be designed to withstand the harsh environment of the processing facility. Therefore, the following must be considered mandatory for practical application:

- cleanable (IP67-rated sealed from water and dust)
- durable to operate at low temperatures (3–7 degrees Celsius)
- robust to breakdown

**High Throughput:** According to an AMPC (2018) report the fat trimming process needs to be delivered at line speed, which in the abattoir surveyed (Dinmore - JBS) is 240 striploins per hour, or 4 striploins per minute. Whilst in this evaluation it would be inappropriate to stringently apply such a criterion this does set a measure to gauge technology feasibility. It may also be possible to increase the throughput of these technologies by employing multiple sensors or automated systems in parallel.

**Small Footprint:** One of the most significant constraints of implementing automated solutions for industry use is the footprint required of the system. This is particularly important for this application as slicer stations are typically quite small and confined to fit around a central conveyor for which striploins are retrieved from. The ideal footprint for a solution is comparable to a human operator station (e.g., approximately a 2 m x 2 m area).

**Cost Effective:** As reported by industry R&D Program Manager at AMPC, the general rule considered for the red meat processing industry is that a system should have a payback period of approximately 1.5 – 2 years (S Shaw 2021, personal communication, May 9, 2021).

From literature survey there many techniques of measuring the fat deposits of pork products that have been developed, validated, and compared (Hambrock 2005; Zhou, Peng & Liu 2014). The sensing technologies and methods presented in this section are particular to the application of beef striploin fat trimming and therefore specific to measuring the subcutaneous fat of the striploin for the potential integration into an automated trimming system.

## 2.3.1 X-Ray

CT (Computed-Tomography) is a medical imaging technique that uses X-rays and computer algorithms to create detailed images of the tissues within body or, in this case, primal. The process involves multiple steps, including data acquisition, image reconstruction, and image post-processing. During the data acquisition step, a motorised table or conveyor is used to position the cross-section of the tissue location to be scanned within the aperture of the CT machine (see Figure 2-34). The CT scanner emits a series of narrow X-ray beams that rotate around the patient, each producing a set of 2D X-ray images. The X-ray images are captured by detectors on the opposite side of the patient and are converted into digital signals (see Figure 2-35).



Figure 2-34: A typical Computed-Tomography system. Source – (Radiology Key, 2021)

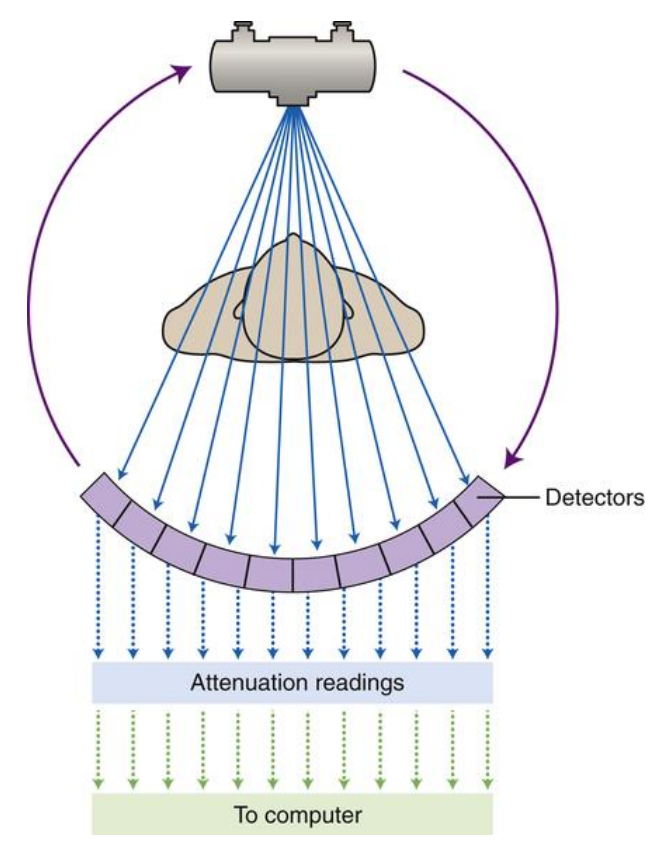


Figure 2-35: The imaging mechanism of Computed-Tomography. Source – (Radiology Key, 2021)

The attenuation of X-rays as they pass through different materials is a fundamental principle that underlies CT imaging. The X-rays used in CT imaging have a high energy level, and when they pass through the body, they interact with the atoms and molecules of the tissues they encounter. The amount of attenuation that occurs depends on the material properties of the tissue, including its density, atomic number, and thickness. Materials with higher density, such as bone, attenuate more X-rays than materials with lower density, such as muscle or fat. This is because the high-density materials have more atoms per unit volume, which increases the probability that the X-rays will interact with the material and be absorbed or scattered. The attenuation of X-rays leads to the creation of bright and dark pixels in the CT image. Regions of the body that attenuate more X-rays appear brighter, while regions that attenuate fewer X-rays appear darker. For example, bone appears bright

in CT images because it attenuates a lot of X-rays, while air appears dark because it attenuates very few X-rays.

The use of X-ray to acquire images that enable the discrimination and measurement of tissues has been researched in the context of red meat processing since 1998 (Meat & Livestock Australia, 2011). X-ray imaging is a process whereby a beam of electromagnetic radiation is transmitted through an object which, depending on X-ray absorption properties (primarily thickness and density) of the tissue, will result in varying amounts of X-ray being measured by a detector positioned on the opposing side of the object (see Figure 2-36). This creates a 2D image with pixels with varying values of brightness used to visualise the areas of high absorption (high value / bright pixels) and low absorption (low value / dark pixels).

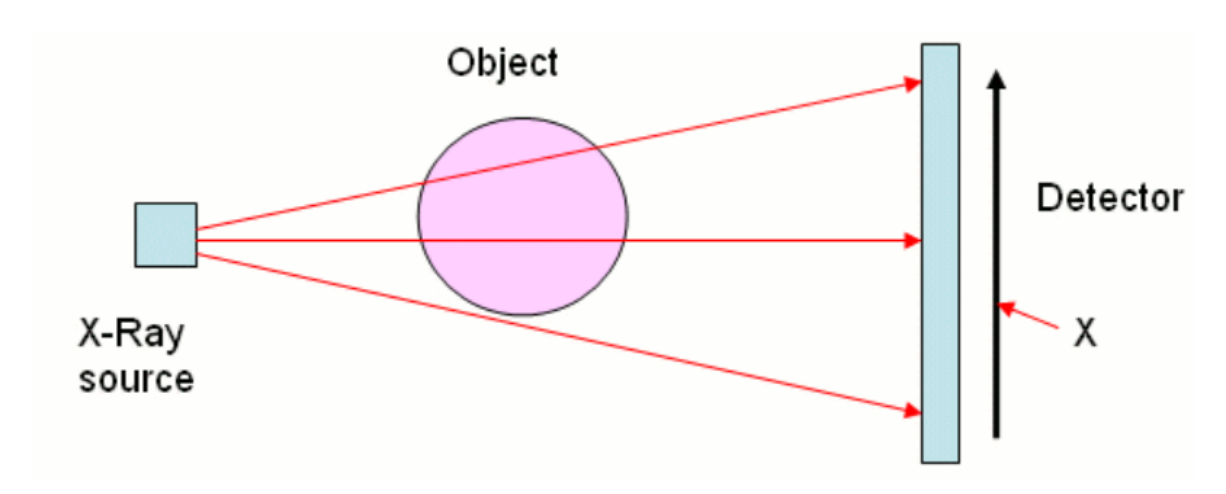


Figure 2-36: Illustration of how the x-ray technology can detect sub-surface tissues based on their x-ray absorption properties. Source – (Plus Maths, 2021)

Computed-Tomography (CT) images are by combining multiple X-ray images acquired at multiple orientations. This enables a 3D image can be created which typically provides greater detail and information than standard X-Ray imaging.

Numerous trials have been funded, and conducted, by MLA and AMPC to explore the commercial viability of using X-ray technologies and techniques for the red meat processing industry (Cook & Anderson, 2017; Meat & Livestock Australia, 2014; McPhee M. 2014a; McPhee M. 2014b, Brumby, Shirazi, & Starling, 2016; Cook, Shirazi & Gardner, 2016; Morton, 2020; Four Dimensional Digital Imaging Inc, 2021; Calnan et al., 2021; Mata et al., 2021). These trails including the following methods.

- 2D imaging using single image capture:
  - SEXA (Single Energy X-ray Absorption),
  - DEXA (Dual-Energy X-ray Absorption),
  - MEXA (Multiple Energy X-ray Absorption),
- 3D imaging using multi-image capture in conjunction with tomosynthesis to interpolate in 3D:
  - Multibeam X-ray which is a method of using a cone beam or multiple pairs of emitters and receivers.
- 3D imaging using multi-image capture in conjunction with constructing images taken over 360 degree captures:
  - CT (Computed-Tomography) both medical grade and non-medical grade CT.

In summary, it is seen that X-ray technologies have been demonstrated successful for OCM and eating quality measurements such as intra-muscular fat (IMF) in the significant majority of trials. Various X-ray technologies with the capability of generating 3D images have been trialled for fat depth measurement applications. Only medical-grade CT technology was shown to be capable of measuring subcutaneous fat depth, and is considered the 'gold standard' of tissue measurements for red meat processing which is what other methods are compared to (Cook & Anderson, 2017). However, the power requirements of medical-grade CT system cannot provide operate at line speed or operate continuously without causing damage. According to Cook & Anderson (2017):

"The scan range of the system, in both distance and time, is restricted by heat dissipation of the X-ray tube. Thus, a trade-off must be made between duration of scan and energy levels (equating to image quality), a balance which is bounded by the machine firmware and software to prevent damage to the system."

CT imaging machines that have been custom-designed for lowpower, high-throughput without the clarity of medical CT would be a more feasible X-ray technology for this application. The only two manufacturers of this technology are RapiScan Systems, who manufacture airport CT imaging machines, and the Danish Meat Research Institute (DMRI), who support the pork processing industry in Europe, both of which are conducting trials to demonstrate their systems' capability for Australia's red meat processing industry with a focus on beef. Testing of the RapiScan RTT110 CT system (RTT referring to Real-Time Tomography) have concluded that this system is not suitable for red meat applications due to the lack of resolution (Calnan et al., 2021). In this analysis, the imaging resolution (illustrated by pixel count) of RapiScan's RTT110 can be seen to be a magnitude of 10 less than medical CT imaging (see Figure 2-37). RapiScan is currently conducting further work to improve the image construction filter to enable the image clarity required for red meat processing applications (Morton, 2020).

In addition to resolution issues trials highlighted cost of the RTT110 RapiScan system as an adoption constraint of processors. A feasibility study conducted by McPhee in 2014 by estimated that the cost to processors to adopt CT technology would be \$3.63m over a 15-year period (McPhee, 2014b). In addition to the prohibitive cost, the legislative requirements of lead shielding for CT installations, the lack of space and the impracticality of altering the infrastructure of processing plants makes this CT technology more difficult to justify (Australian Radiation Protection and Nuclear Safety Agency, 2008).

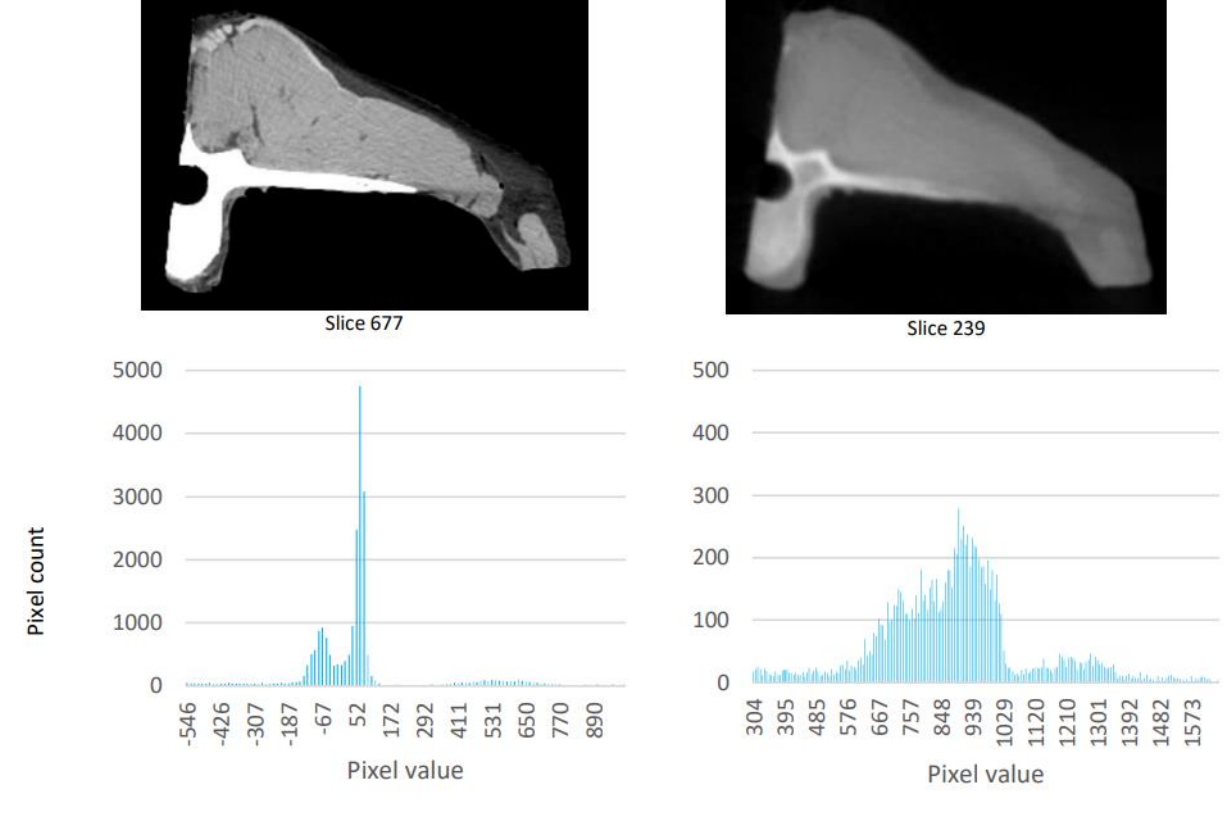


Figure 2-37: A comparison between medical-grade CT and the RapiScan RTT110 System. Source – (Calnan et al., 2021)

In summary, at the time of publishing there was no feasible X-ray imaging system commercially demonstrated for the red meat processing industry.

### 2.3.2 Ultrasound

Ultrasound is a rapid, non-invasive sensing technique that utilises high frequency soundwaves (generally 20 kHz to 15 MHz) to locate various objects or layers of various densities within a medium. This technology utilises the principle of acoustic propagation through media where the boundary of differing tissue types (signified by density) will reflect soundwaves due to an introduction of impedance (Brøndum, 1998; Pathak, Singh & Sanjay 2011). An ultrasonic probe will transmit sound at a particular frequency and detect the receival of this reflected soundwave through a piezoelectric transducer. This is diagrammed illustrated in Figure 2-38.

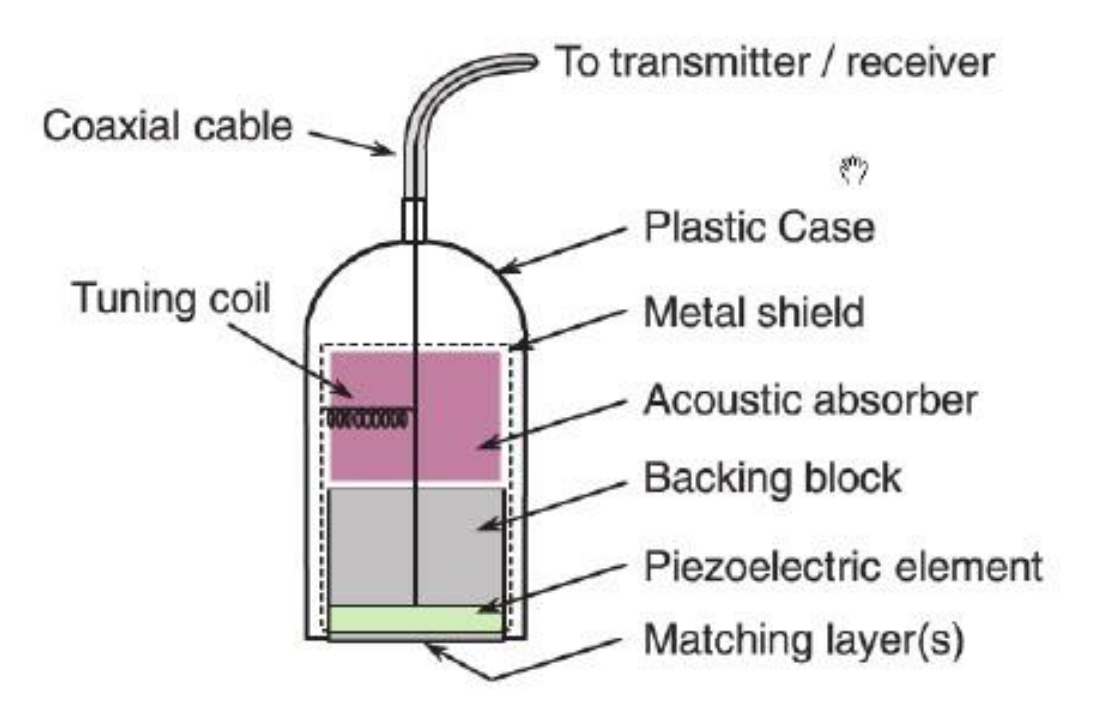


Figure 2-38: The internal structure of a piezoelectric ultrasound transducer. Source – (Medical Radiation Resources, 2012)

The two parameters measured by the transducer are the amplitude of echo and time taken to receive the echo (referred to as time-of-flight or TOF). The amplitude of soundwave reflection is proportional to the electrical signal generated by the transducer when switched to 'receiving' mode (Pathak, Singh & Sanjay, 2011). The measurements of these two parameters provide a means of characterising the tissue and the tissue position within the medium soundwaves are transmitted through. Using the measured TOF parameter and considering the velocity of the soundwave propagating through the medium (dependent upon the specific acoustic property of the material), a distance measurement of the tissue from the transducer can be ascertained. This is illustrated with a diagram shown in Figure 2-39 and can be estimated formulaically using the expression presented in Equation 2.1.

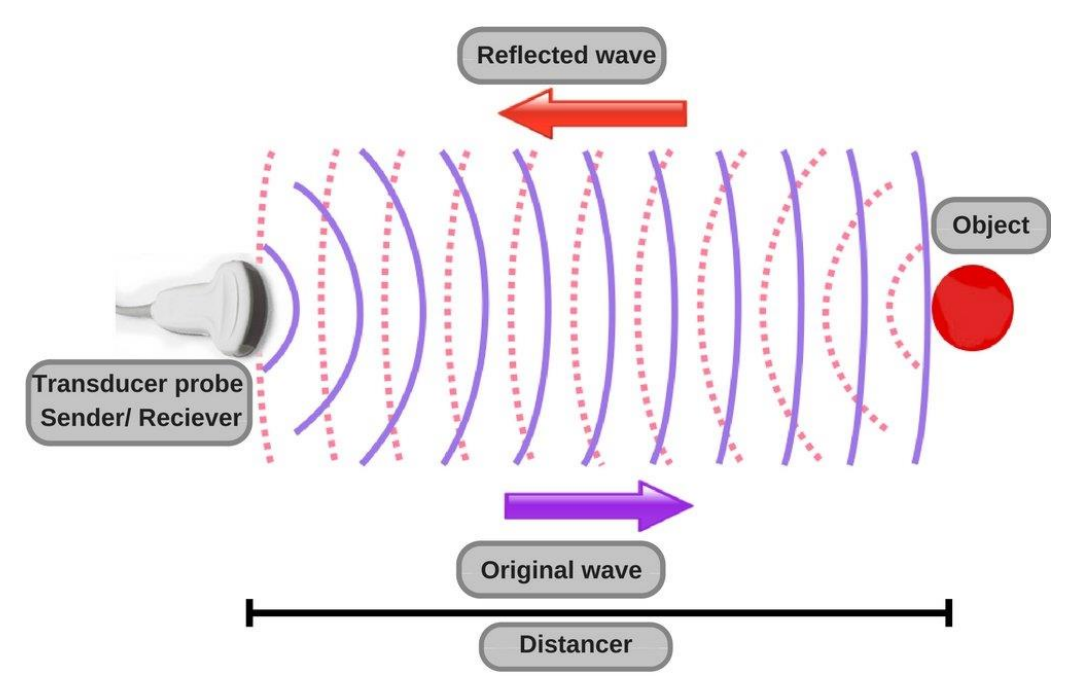


Figure 2-39: An illustration of how the TOF of reflected waves can be used to calculate distance of an object. Source – (Science ABC, 2022)

Equation 2.1: Calculation of tissue depth using ultrasound TOF principles

Tissue Distance,  $d_t = v_S * \frac{t_R}{2}$ ,

### where:

 $v_S$  = the speed of sound propagation through fat tissue wave through subcutaneous fat is generally considered to be 1,450 m/s (Johnson & Wales University, 2019)

 $t_R$  = the time taken for the soundwave to reflect and be read by the ultrasonic transducer

The operational state of ultrasound for meat is typically A-Mode or B-Mode (Schulze, Curic & d'Hoedt, 2002). A-Mode, referred to as amplitude modulation, plots the amplitude as a vertical spike (strong echo), signifying a detected tissue interface, of the received soundwave (y axis) with the depth ascertained by this soundwave (x axis). A-Mode

ultrasound technology employs only a single transducer, allowing examination of echoes along a one-dimensional axis. Tissue interfaces, characterised by large amplitude signals generated by soundwave reflections, are plotted against depth (calculated using TOF). This produces a graph of spikes with height indicating echo strength and tissue acoustic properties (Pathak, Singh & Sanjay, 2011). The means of acquiring a depth measurement of a tissue interface from transducer signals are illustrated in Figure 2-40. The amplitude captured by the transducer can be used to differentiate tissues of differing densities by considering acoustic properties and principles of soundwave propagation through mediums. The amplitude measured by the transducer depends upon various factors (University of Washington, 2017) including:

- The proportion of the soundwave that is absorbed, refracted, and reflected at the tissue interface.
- The degree of attenuation of the soundwave travelling through the medium (typically referred to as an attenuation coefficient)

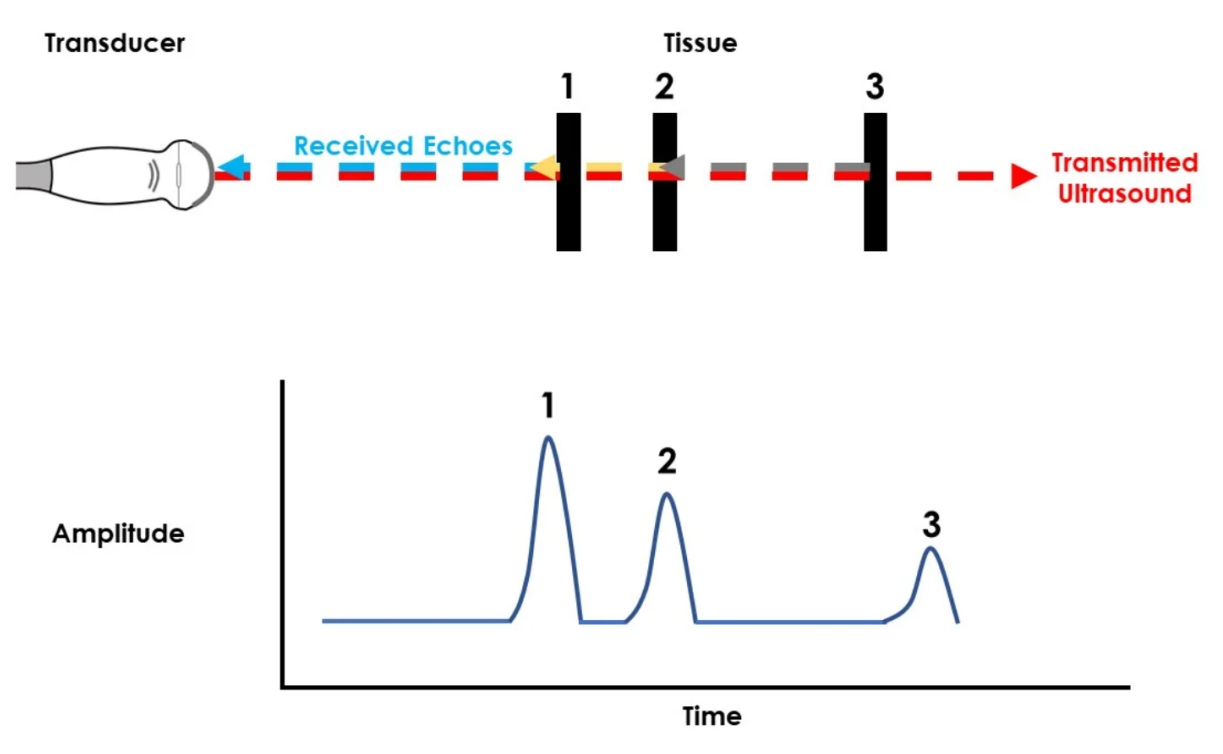


Figure 2-40: Illustration of A-Mode ultrasound technology to take depth measurements. Source – (IMV imaging, 2023)

A-Mode provides a simple means of interrogating data to acquired fat depth measurements. Instead of analysing a 3-dimensional dataset of an image (X - pixel position, Y - pixel position, greyscale value using machine vision algorithms to differentiate and locate tissues, simple thresholds (e.g. noise filtering, signal amplification, time-gain compensation) can be applied to a 1-dimensional dataset (Pathak, Singh & Sanjay, 2011; Wagner et al., 2019). The data acquired using A-Mode is relatively straightforward to understand and interpret, making it an excellent tool for quick, qualitative assessments of tissue depth and boundary identification. A-Mode ultrasound is simpler to analyse and more cost-effective than B-Mode ultrasound with the trade-off of less information per reading. The contrast of how A-Mode and B-Mode systems present these echo signals are shown in Figure 2-41.

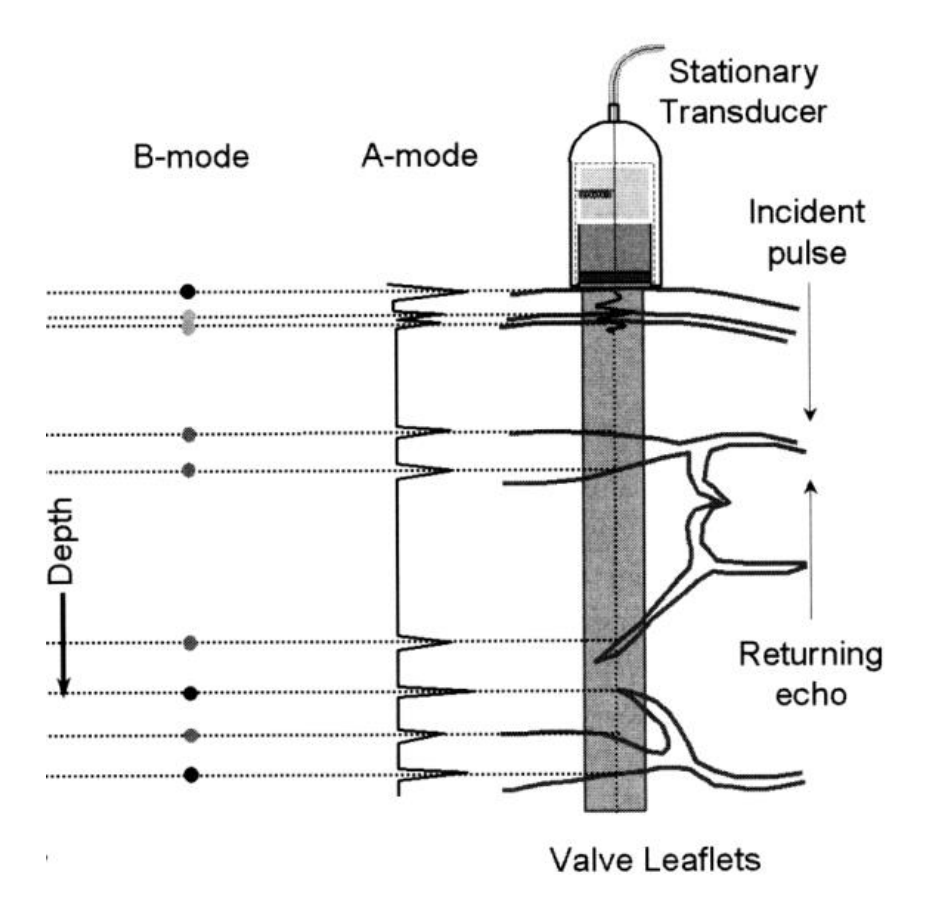


Figure 2-41: A comparison of ultrasound (Mode A vs Mode B) in displaying depth and amplitude of tissue reflections. Source – (University of Washington, 2017)

Whilst A-Mode (amplitude modulation) ultrasound indicates a depth measurement with an amplitude 'spike' in 1-dimension, B-Mode (brightness modulation) ultrasound integrates multiple A-mode signals to create a 2-dimensional, greyscale image (see Figure 2-42). In this way, B-Mode ultrasound greyscale images consists of pixels, where the brightness of each pixel is determined by the amplitude of the echoes at that pixel location. This location is determined by the time-of-flight of the reflected soundwave along the axis of the ultrasound transducer. These echoes are reproduced as varying shades of grey in the resulting ultrasound image, with B-mode using 64 shades of grey. This grey scale allows for visualization of differences in acoustic properties of the tissue, making B-mode ultrasound useful for providing the sensitivity to identify and distinguish between different types of tissues and structures within the medium, such as differentiating between fat and muscle layers

(Pathak, Singh & Sanjay, 2011). The use of B-Mode ultrasound to differentiate between lean muscle and fat tissue is illustrated by the varying brightness of pixels in Figure 2-43.

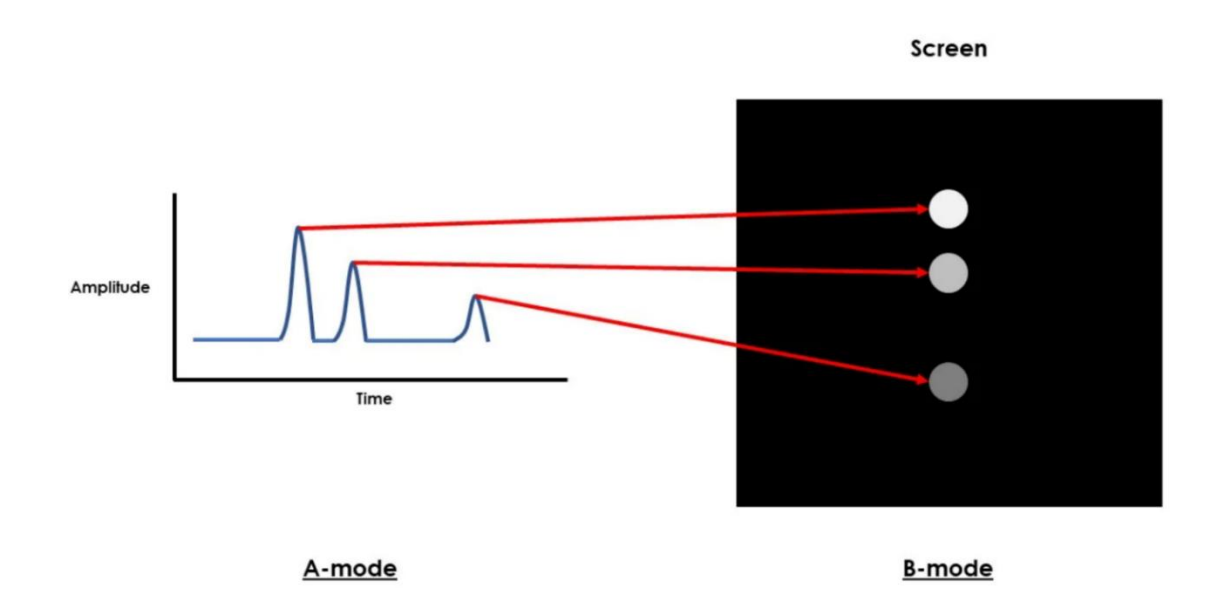


Figure 2-42: Illustrative comparison between A-Mode and B-Mode of how information is displayed. Source – (IMV Imaging, 2023)

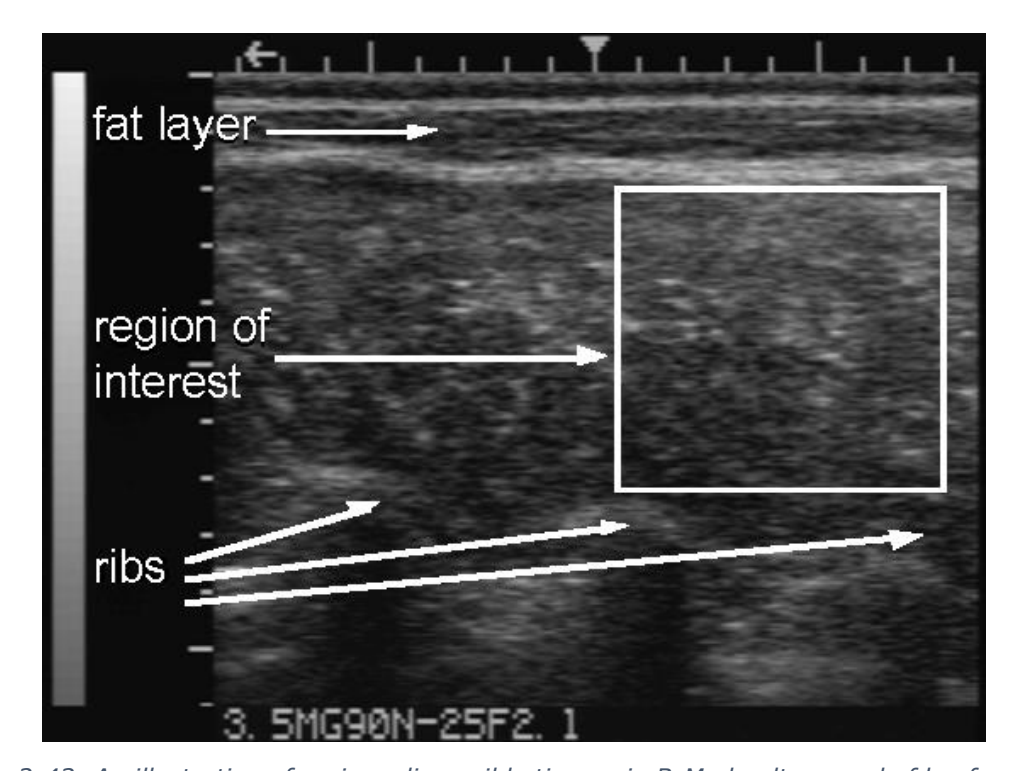


Figure 2-43: An illustration of various discernible tissues in B-Mode ultrasound of beef carcases. Source – (Leaflet, 1997)

There are numerous configurations of transducer arrays that B-Mode ultrasounds can consist of. The particular configuration type determines the representation of the data as an image and typically the shape of the probe. By sequencing the triggering of each transducer separately (referred to as beam sweep), and knowing the orientation of each transducer's measurement axis, an image can be created from the array of ultrasound readings (see Figure 2-44).

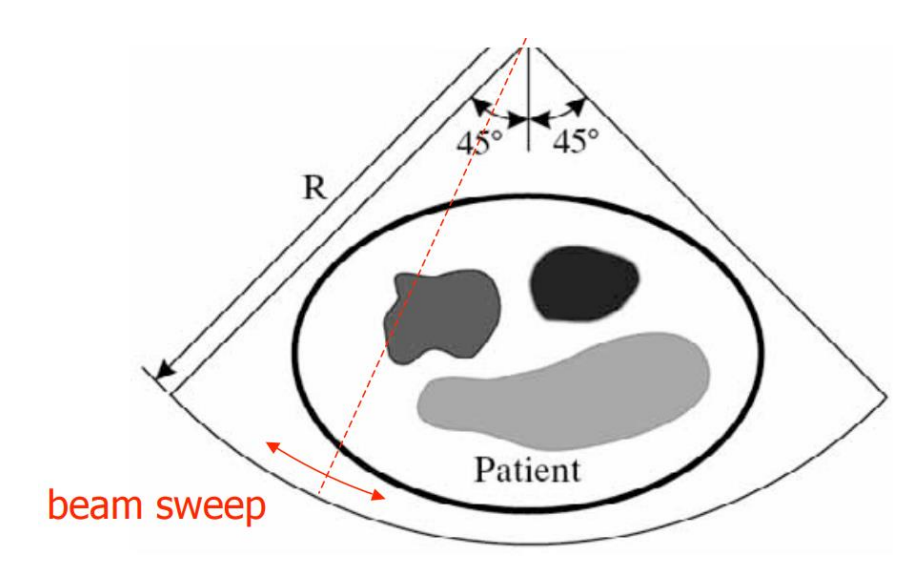


Figure 2-44: A convex array of ultrasonic transducers used in sequence to construct a B-Mode image. Source – (university of Washington, 2017)

There are a number of hardware and software configurations which create varying performance characteristics of ultrasound devices. A hardware configuration typically describes the arrangement of piezoelectric crystal arrangement within, and footprint of, the probe head of the ultrasound. The selection of a probe head is an important factor to consider as for the ultrasound to be emitted into a medium consistent contact between the probe and the surface must be made to eradicate any air gaps impeding the propagation of soundwaves. A few common configurations include linear, convex and phased array; these produce differing displays and have different advantages (see Figure 2-45 & Figure 2-46):

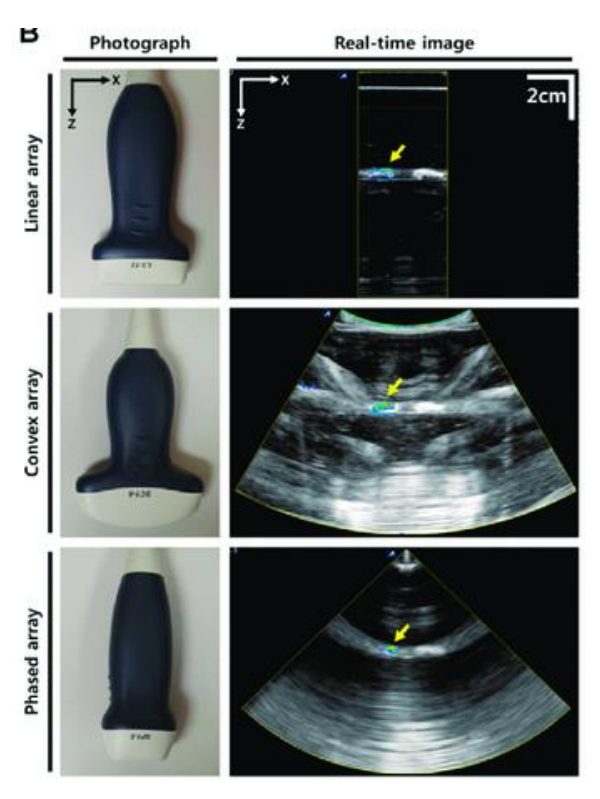


Figure 2-45: Linear vs Convex vs Phased Array ultrasound array configurations. Source – (Wen et al., 2022)

**Linear:** In a linear configuration, the transducer elements are arranged linearly in a straight line. This configuration is commonly used for imaging superficial structures, such as blood vessels, tendons, and musculoskeletal tissues. It provides high-resolution images with a narrow field of view.

**Convex:** In a convex configuration, the transducer elements are arranged in a curved or convex shape. This configuration is suitable for imaging deeper structures, such as abdominal organs and foetal imaging. The convex shape allows for a wider field of view, facilitating imaging of larger areas.

**Phased-Array:** Phased array ultrasound systems use a matrix of transducer elements that can be electronically controlled to steer and focus the ultrasound beam. This allows for real-time imaging in multiple

directions without physically moving the transducer. Phased array systems offer adjustable beam steering, variable focus, and sector scanning capabilities. They are particularly useful in applications where dynamic imaging, precise targeting, and real-time visualization are required, such as cardiac imaging and interventional procedures.

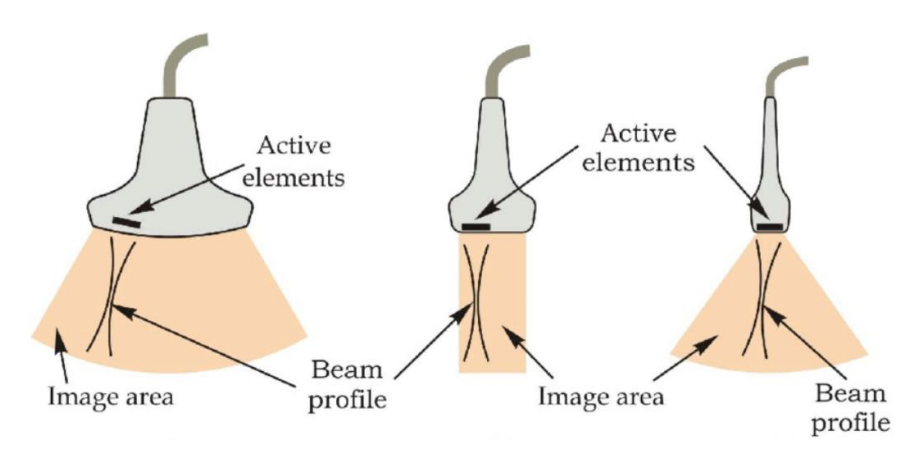


Figure 2-46: Convex (left) vs Linear (middle) vs Phased Array (right) B-Mode ultrasound transducer configuration profiles. Source – (Khaled, 2023)

For ultrasound wave propagation there is a beam profile that describes the volume of measurement in the axis of measurement for each transducer in the array. This beam profile narrows to a focal length, dependent upon the transducer frequency and aperture of the transducer array, before diverging into an unfocused wave (Ng & Swanevelder, 2011). At the penetration depth of the focal length the highest concentration, and therefore resolution, of the ultrasound is emitted. The focal length of transducers can be visualised using visualisation software (Garcia, 2023). The beam concentration of an ultrasonic transducer is visualised in Figure 2-47.

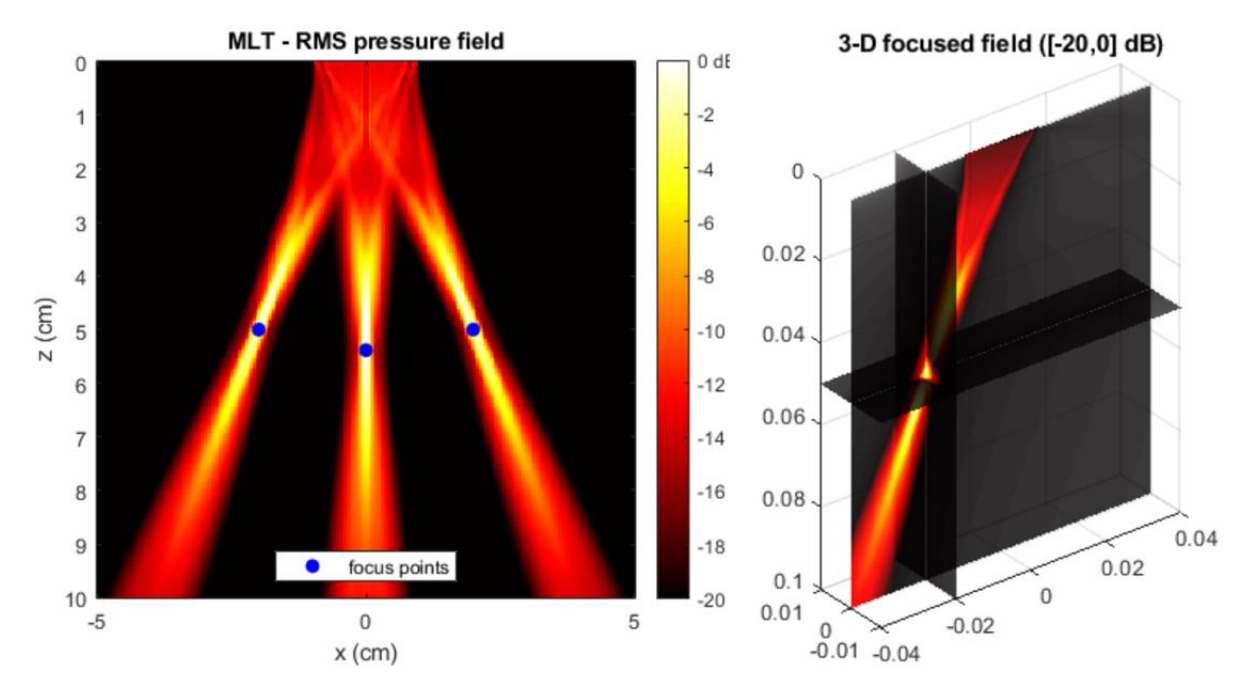


Figure 2-47: Visualisation of focal lengths of ultrasonic transducers. Source – (Garcia, 2023)

Many modern ultrasound devices have the capability to allow the user to adjust this focal length through transducer beam steering to provide a focus beam, employing concave or acoustic lenses or adjusting the soundwave frequency (e-Echocardiolography, 2023). Many modern devices also provide pre-set software modes for various permutations of settings for each of these parameters.

To ensure that the particular point of interest to be measured is referenceable in the B-Mode ultrasound image precise positioning of the probe head is required. Typically, this means alignment of the centre of the transducer array aperture in the X (azimuth) and Y (elevation) axes with the point of interest to ensure that this measurement is centred in the image frame. Acoustic frequencies have a trade-off between resolution and depth penetration due to energy absorption, and so frequency selection is highly dependent on the application (Houghton & Turlington, 1992). The soundwave frequency needs to be selected to ensure that the ultrasound penetration depth in the Z (axial direction) axis is sufficient to measure the point-of-interest (see Figure 2-48). The

selection of frequency is a trade-off between image resolution (higher frequency) and penetration depth (lower frequency). Balancing acoustic parameters to define the focal length at the depth of the tissue interface is ideal. A frequency of 2.5 MHz is typical for meat sensing applications which permits high resolution to a depth of approximately 75 mm (Brøndum, 1998).

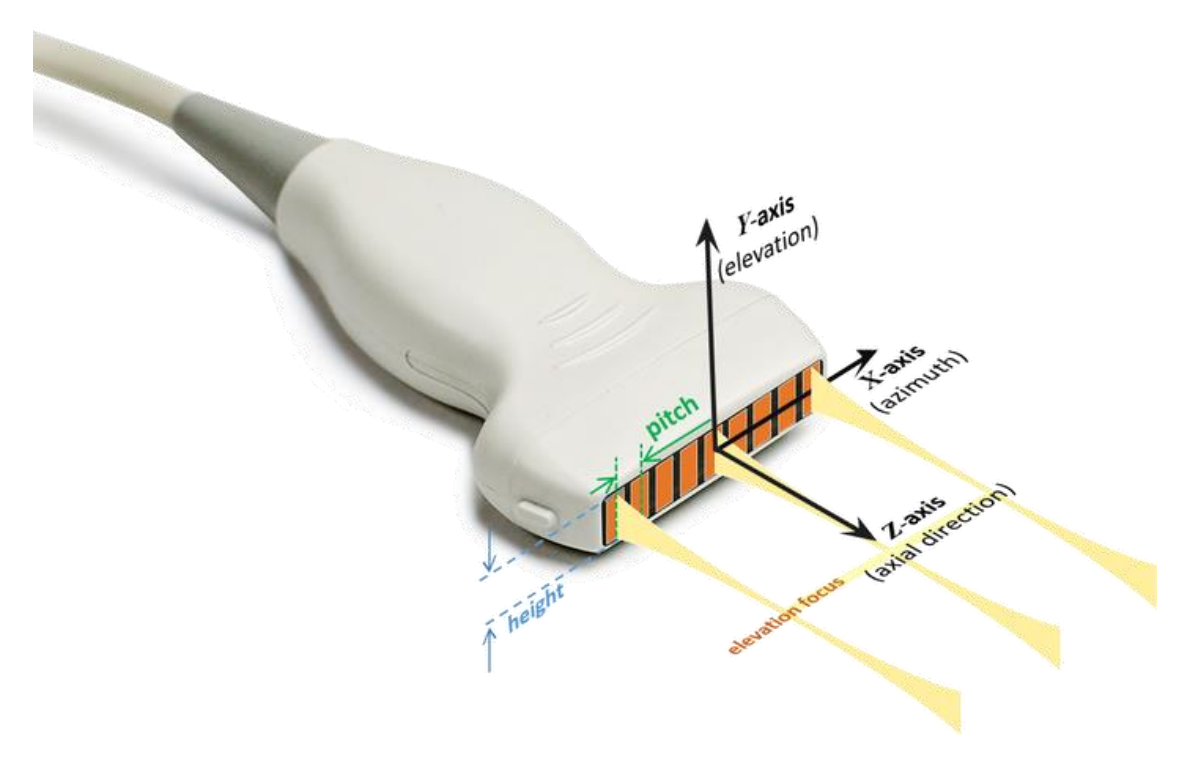


Figure 2-48: The reference coordinate frame of the ultrasound probe. Source – (Garcia, 2023)

In many live animal and meat product applications B-Mode ultrasound is applied to constantly update an image real time ultrasound (RTU), enabling this data may be presented as an imaging sensor (Silva & Cadavez, 2012). Whilst this technology is primarily used in the medical industry it is highly prominent in numerous carcass measurements such as fat depth, muscle depth and muscle area for beef grading and quality evaluation systems in food (Morlein et al., 2005; Busch, Dinkel & Minyard, 1969; Shepard et al., 1996; Bergen et al., 1997). There has been a long history of ultrasound technology being used in red meat processing applications for measuring backfat and loin eye fat in various species

including beef (Pathak, Singh & Sanjay 2011; McLaren, McKeith & Novakofski, 1989; Hedrick, 1983; Houghton & Turlington, 1992).

One of the world's most effective examples of ultrasonic-based grading systems is used in pork and called Autofom. This is a U-frame arrangement of 16 A-Mode ultrasonic probes which perform 200 scans along the back of a pork carcass at a line speed of 1,250 carcasses per hour (Brøndum et al., 1998)

Ultrasonic sensing has several distinct advantages in the application for beef striploin fat trimming:

- It is non-invasive, safe and hygienic sensing method
- Relatively low cost
- Well-developed, trusted technology
- It is easily implementable with completely within a real-time autonomous system

There are also additional sensing considerations when using ultrasound (Hazwan et al., 2013; Mueller 2018):

- It requires consistent contact to the measurement site with a lubricant/gel that can act as a medium for soundwaves to propagate through to measure fat and meat
- A skilled operator is required to ensure a consistent, reliable reading to be measured
- Measurements are affected by angle of probe, water content in the medium, temperature, non-homogeneity of medium
- The dehiding process can disturb tissue interfaces air pockets that prevent ultrasound measurements to be accurately collected (Khodabandehloo, 2018)

In many instances ultrasonic measurements are subsequently analysed though machine vision and machine learning applications (see

Figure 2-49) to create an observation that can be action by robotics. Many systems have been developed using machine learning algorithms (e.g. Support Vector Regression, Neural Networks) in combination of key features extracted from analysing frequencies (e.g. applying the Fourier Transform) obtained through ultrasound reflectance signals (Park et al., 1994; Halim et al., 2013; Simianer et al., 2013; Pathak, Singh & Sanjay, 2011). In the case of RTU applications machine vision algorithms have been applied to determine automated location and measurement of subcutaneous fat during post-mortem scanning (Pathak, Singh & Sanjay, 2011; Jung et al., 2015; Scholz, 2015).

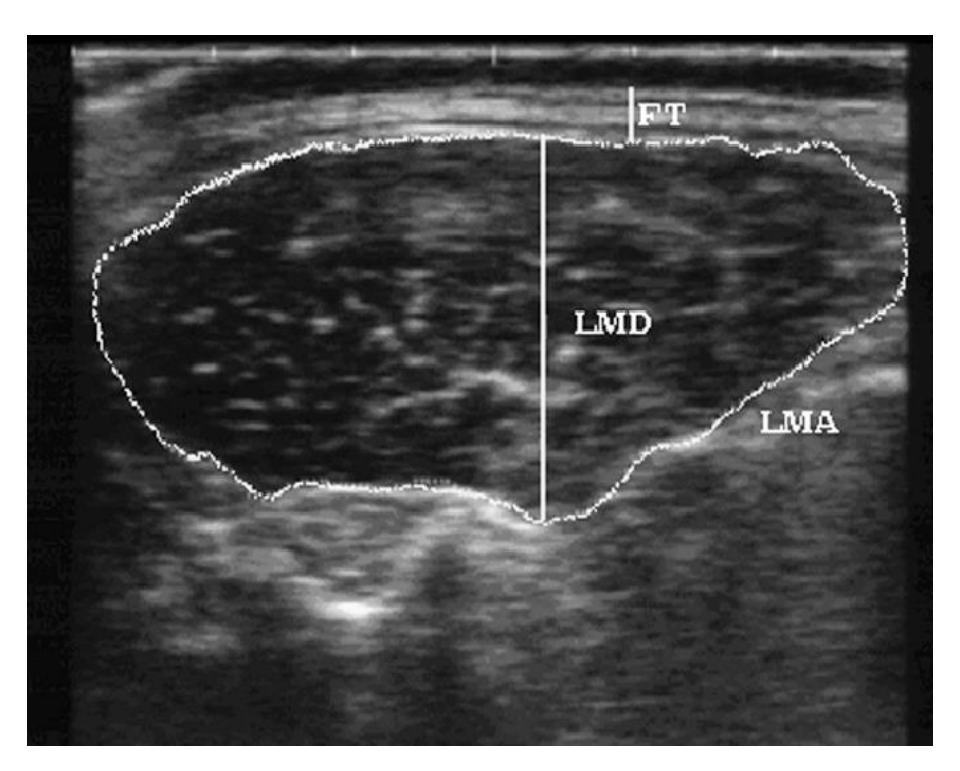


Figure 2-49: An example of a typical ultrasound image of the depth of muscle that imaging processing techniques could be used for automation. Source – (Sahin et al., 2008)

# 2.3.3 Vibrational Spectroscopy

Spectroscopy is a means of exciting vibrational states of a material to determine informational characteristics through the interpretation of its response to various frequencies of light (Whitman et al., 1996). Both Raman and Near Infra-Red (NIR) spectroscopy have been employed for the application of fat measurement (Prieto et al., 2017), and use different

methods of interrogating information due to the way in which light energy interacts with the material. The intensity of light that is absorbed within, transmitted through or scattered by (referred to as 'back scatter') a material can be measured to determine various material properties (Prieto et al., 2017; Jespersen & Munch, 2009). The backscatter profile, which represents the distribution of reflected light intensities across a spectrum of wavelengths, can be effectively utilized to infer various quality parameters. This profile provides insights into the size and intensity of the backscatter can be correlated with key quality attributes such as composition, the separability of fat, and the hardness of fat (Narsaiah & Jha (2012). The interrogation of light backscatter profiles allows vibrational spectroscopy to measure fat thickness with a great deal of success with many commercial products on the market for pork - the modified fat-o-meter (manufactured in Denmark), the Hennessy and Chong fat depth indicator (manufactured in New Zealand) and the Ulster probe (manufactured in Ireland) (Agri-Food and Biosciences Institute, 1982; Jones, Allen & Haworth, 1982, Brøndum et al., 1998).

One of the most successful NIR reflectance devices has been the Fat Quality Meter (FQM) developed by the Danish Meat Research Institute (DMRI). This device has been calibrated to employ the judgement of an expert classifier to classify samples based upon 8 NIR sensors reading numerous signals between 800–1800 nanometre wavelengths (Brøndum et al., 1998). Similar applications of statistical methods (e.g. multi-variate classifiers and parameter transformations) have been employed as machine learning in practice to describe the state or material through the classification of sensory signatures (Bacci, Porcinai & Radicati, 1997).

NIR Reflectance spectroscopy has a number of advantages such as:

- Relatively low cost
- Well-developed, trusted technology

- Various meat characteristics may be identified additionally to fat depth (e.g. meat colour)
- It may give real-time measurements
- Easy to use, robust

This technique has the following limitations:

- It requires extensive calibration to classify composition
- It is unable to measure in the presence of multiple fat and muscle layers due to the misalignment of the probe with the required anatomical position (Hambrock, 2020)
- Computational processing is required
- Insertion of optical diodes through meat to measure fat thickness do cause mild damage to product

The exact numerical measurements as a backscatter profile are not important, yet these can act as predictors/characteristic parameters that can be manipulated. Techniques such as Principal Component Analysis (PCA) can be used to extract relationships out between the readings and characteristic properties (e.g. skin, skin + fat, skin + muscle) with machine learning techniques (Roberts et al., 2017). Figure 2-50 illustrates the implementation of a machine learning technique (clustering) to determine the type of tissue from the spectroscopic signal acquired.

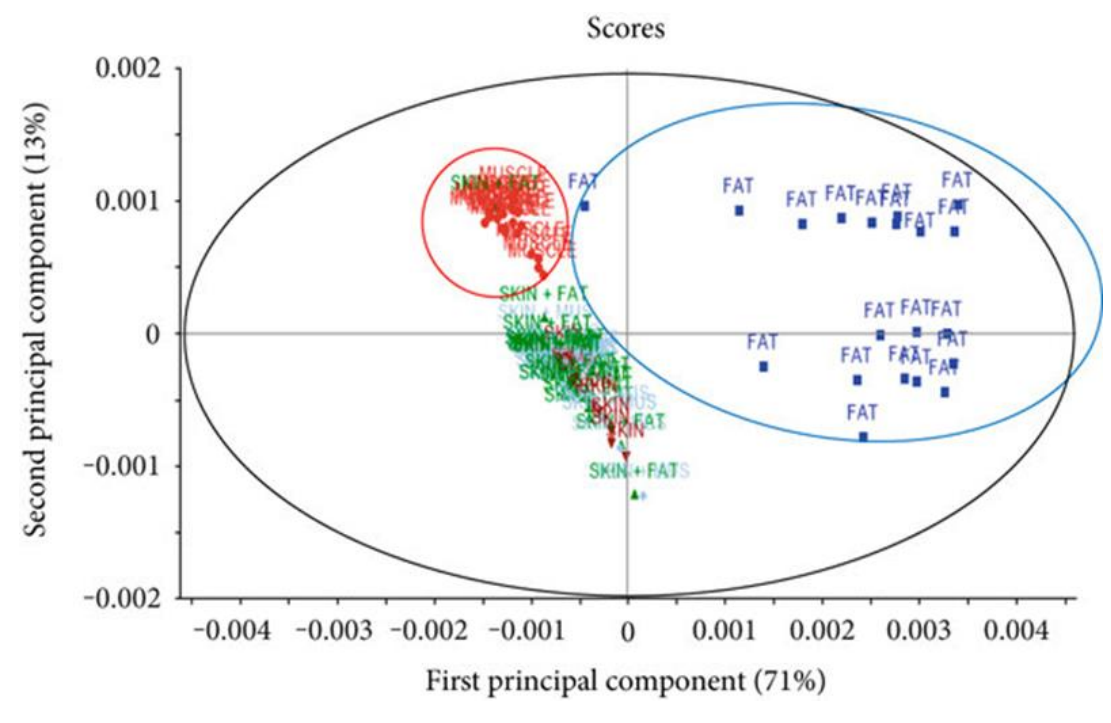


Figure 2-50: NIR Spectroscopy can provide signals that can be classified using Principal Component Analysis and clustering algorithms. Source – (Roberts et al., 2017)

## 2.3.4 Electrical Impedance

Through the technique of electrical stimulation both resistance and capacitance may be measured in a medium between an electrode and probe arrangement. Many manufacturers have developed these probes for fat measurements with positive results world-wide predominantly in pork (Brøndum et al., 1998). This technology is documented to have been first implemented in an Australian plant since 1971 to measure hot and cold carcass fat thickness with findings reporting up to  $\pm$  2 mm tolerance in 70% of cases (Meat and Livestock Australia, 2020). A typical example of this technology is the Meat-Fat-Automatic or KS-meter developed by SFK Ltd in Denmark (Stavrev, 1997). The Meat-Fat-Automatic is a handheld device that e handheld and drives an electrode on a probe tip through the fat until it penetrates the meat whereby this increase in the electrical conductivity of the medium is sensed by a change of current draw at a given voltage exceeding a predetermined, calibrated threshold.

Advantages of this technology include (Meat and Livestock Australia, 2020):

- Measurements could be obtained quickly and at a high frequency (up to every 5 seconds in operation)
- Has been previously trialled with success in industry applications.
- Relatively low cost

Limitations of the technology include (Meat and Livestock Australia, 2020):

- The maximum fat thickness of this technology is 28 mm
- False readings have been observed whereby electrical conductivity was tampered with due to fat smearing on the electrodes as well as high pH levels in the lean meat muscle
- Of the instrument's errors (16% of readings were out of +/-3 mm tolerance), it is presumed that 10% of these were from incorrect operating technique, with the remaining errors being due to unusual physical factors of the meat product such as low conductivity in the lean, and inclusions of lean / conducting fluid in the fat layers.
- Probe insertion deformation, varying with the degree of chill of the carcass (yet this has been accounted for to some degree using a simple linear equation)
- Relative position of the electrode to the probe tip
- Number of electrodes
- Disposition of the electrodes along the stem of the probe
- Probe traverse speed
- Is an invasive sensing technique

The measures this sensor provides (resistance or capacitance) are not informative on their own, but through association to the reference voltage these devices are able to inform fat depth between the inserted electrodes (Meat and Livestock Australia, 2020). The use of multiple

frequencies can enable these devices to more precisely discriminate between lean muscle and fat to improve fat depth measurement accuracy (see Figure 2-51).

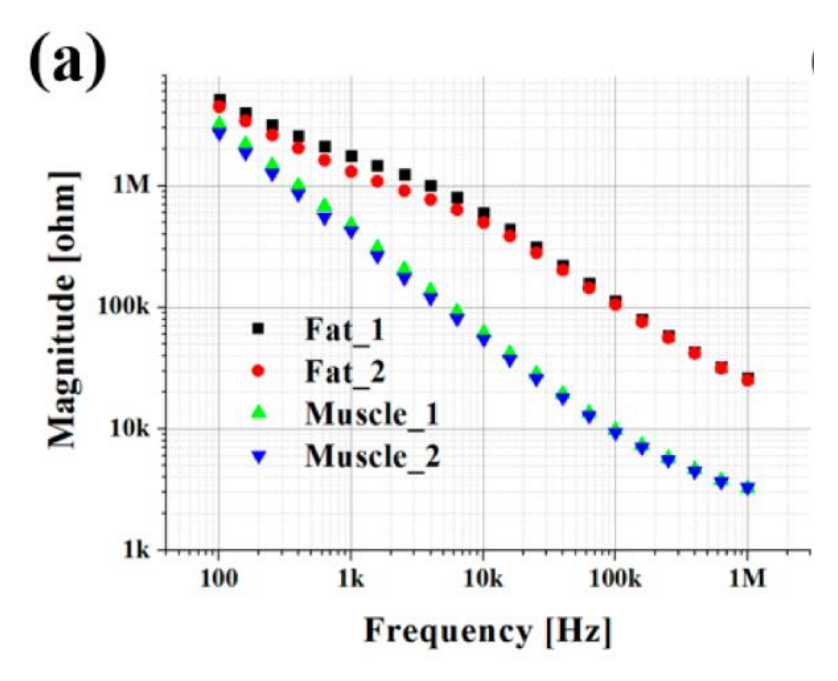


Figure 2-51: A typical measurement of electrical impedance measured for fat depth. Source – (Kim et al., 2016)

## 2.3.5 Tactile

Tactile sensing is the provision of perception acquired through sensing the contact of a tool and its operating medium through kinaesthetic (force) and cutaneous (tactile) feedback (Okamura, 2009). In such cases the goal of this technology is to "detect local mechanical properties of tissue such as compliance, viscosity, and surface texture – all indications of the health of the tissue – or to obtain information that be used directly for feedback to a human operator, such as pressure distribution or deformation over a contact area" (Eltaib & Hewit, 2003).

In practice, there is a substantial amount of information that can be used to perceive complex movements of natural tissues as opposed to other sensing techniques (den Boer et al., 2014; Guo et. al. 2018). Several applications of tactile sensing technologies have been developed

for surgical applications such as robot-assisted minimally invasive surgery (RMIS) where fine tool adjustments need to be made with accuracy and precision within a flexible workpiece.

The importance of a sense of "feel" to enable this skilled surgical capability of manipulating tools in reference to biological tissue has been recognised by both surgeons and robotic engineers and supporting research (Xin, Zelek & Carnahan, 2014; Ortmaier et al., 2007). Numerous examples of haptic technology improving RIMS outcomes including increasing accuracy of surgical skill in both surgeons and non-surgeons, reducing unintentional tissue damage and injuries during dissection and suture tasks (Wagner & Howe, 2007; Talasaz, Trejos & Patel, 2012; Ortmaier et al., 2007). The notable success of the employment of haptic perception in surgical robotics was first exemplified through the development of a hand-held drill for cochleostomy surgical procedures (Brett et. al. 2014).

Only until recently the implementation of force-sensing, particularly over vision, has considered as an ideal mechanism for red meat processing applications. Literature shows a prevalence of utilising e force-control in automating complex red meat processing applications (i.e. beef forequarter deboning) over the past 30 years (Purnell, Maddock & Khodabandehloo 1990; Australian Meat Processor Corporation, 2020b). A report recently conducted for AMPC (Australian Meat Processor Corporation, 2018a; Australian Meat Processor Corporation, 2018b; Australian Meat Processor Corporation, 2019) explicitly support this by highlighting the lack of research yet current demand for integrating real-time, tactile sensing for cut path determination within red meat processing applications.

Force sensor feedback from the cutting tool as it progresses through the meat will give different readings depending on whether it is cutting through muscle, fat or even bone. This varying feedback could potentially be used to generate tool paths for the robot in real time. As opposed to pre-determining the path using external or penetrating sensors such as vision or ultrasound. Further research needs to be undertaken to determine if force sensor feedback-based path generation is feasible and what meat processor tasks it could be applied to.

Tactile sensing has several distinct advantages in the application for beef striploin fat trimming (Tiwana, Redmond & Lovell, 2012):

- It can be non-invasive, safe and hygienic sensing method.
- Low cost
- Potential to gather extremely informative data about tool-workpiece interaction.
- Great sensing repeatability, range, and sensitivity
- It is implementable within a real-time autonomous system.
- Can be designed with simplicity.

There are also several limitations to tactile sensing methods:

- Requires cleaning and hygienic design consideration.
- A skilled operator or controlled interaction is required to ensure a consistent, reliable reading to be measured.
- Measurements are affected by meat characteristics such as muscle grain direction, water content, temperature, nonhomogeneity of medium.

Full tactile perception more than just basic transduction of tactile data — it also requires the computational processing of data to guide control. However, real-time computational processing of tactile data can be difficult, and so other less complex mathematical approaches have been investigated (Du et. al., 2018). An example of this control is the cochleostomy drill which informed control by discriminating pertinent conditions of a cutting process in tissue mediums from which automated

control strategy can be implemented. Du et. al. (2018) was able to discriminate the character of drilling non-uniform, flexible media within microns of accuracy by interpreting relationships between transient force and torque responses (see Figure 2-52).

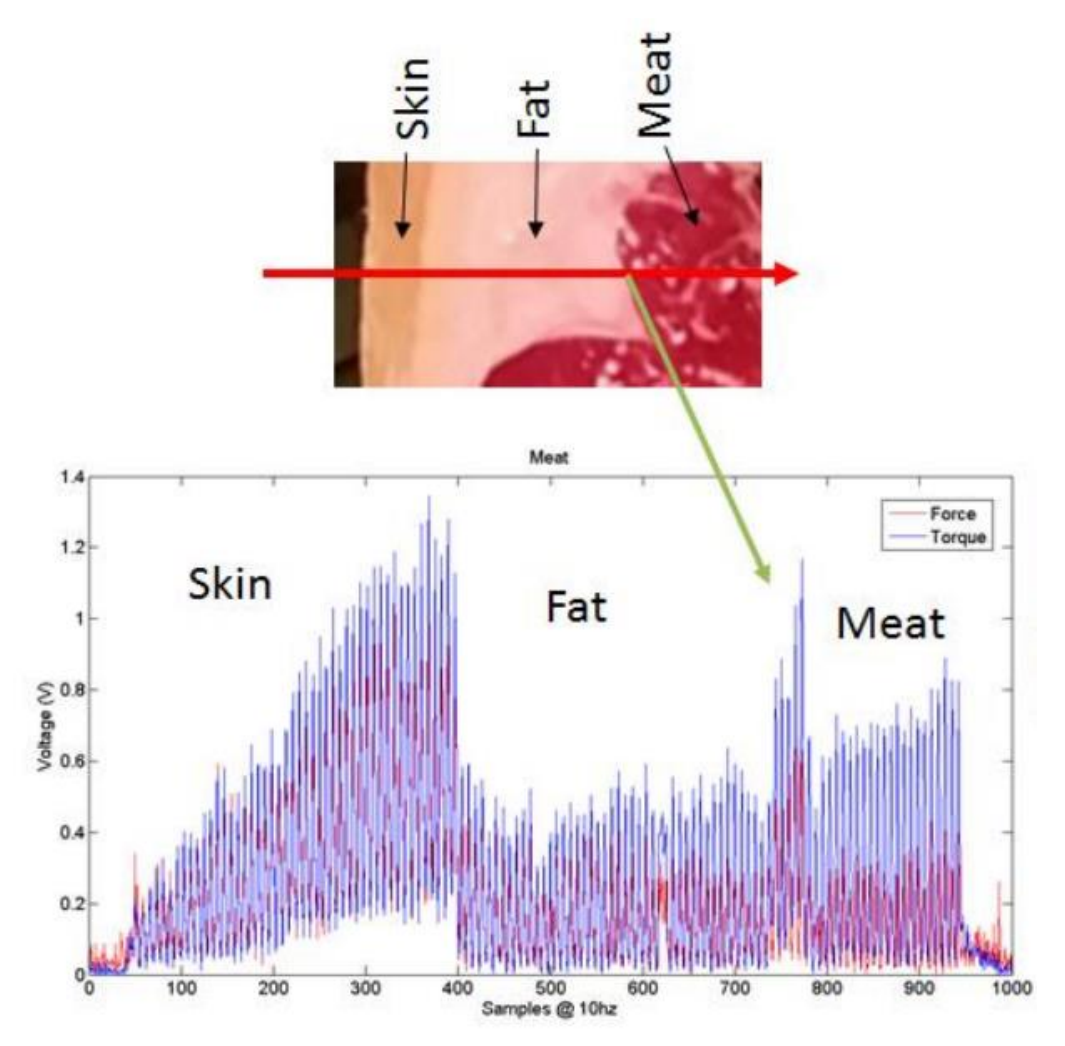


Figure 2-52: Discrimination of beef striploin tissues using force and torque transients. Source – (Khodabandehloo, 2018)

The state of the system (i.e. cutting skin, fat or lean meat) is determined by analysing transient responses of parameters such as torque and force. This approach is similarly applied in other medical applications as a means of determining state from physically based models based upon reactive force measurements to inform the tool positioning for percutaneous operations (Rosen et al., 2006; van den Gobbelsteen, 2012; Petra et al., 2006). With a traditional, non-temporal

force-torque sensing method gravitational, Coriolis and inertial forces can bias the force response characteristics of the tool-workpiece interaction (Fumagalli et al., 2010). Brett's (2014) method of classifying signatures of known descriptors of the task (i.e. force and torque with respect to displacement or time) enables measurements inflicted by these factors to be irrelevant as well as simplifying the computation of the state of the task (see Figure 2-53).

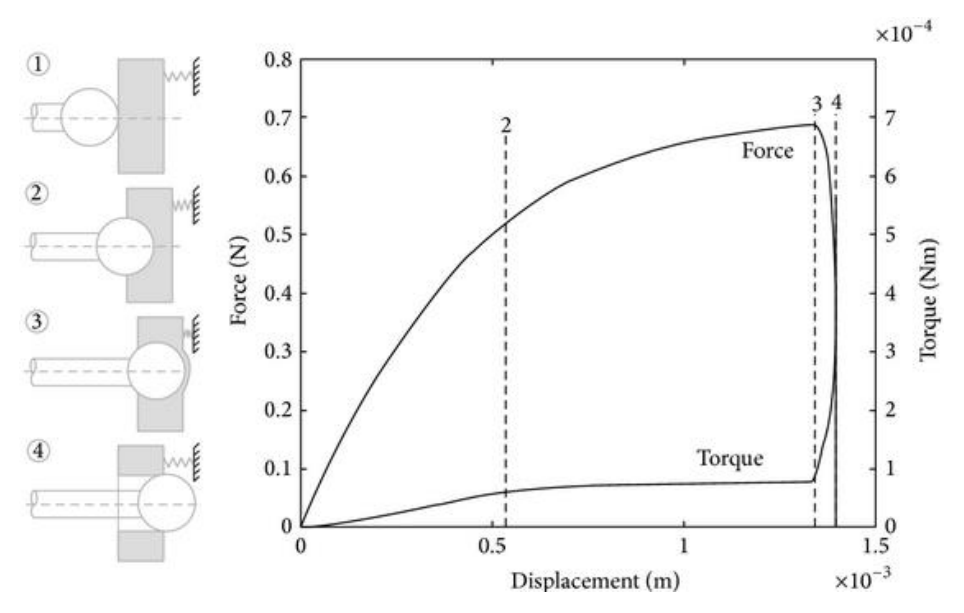


Figure 2-53: Using transient tactile measurements (force and torque) for discrimination of tissues

Source – (Brett et al., 2014)

## 2.3.6 Discussion

The following list of criteria was formed from the core and functional requirements to assess each of the four sensing technologies against each other:

- a) Non-Destructive
- b) Robust for Environment
- c) High Throughput
- d) High Accuracy & Precision
- e) Small footprint
- f) Cost Effective
- g) Large Penetration Range

For each of the criteria, each technology will be rated as:

- D: Desirable (worth 2 points)
- F: Feasible (worth 1 point)
- I: Infeasible (worth 0 points)

**Ultrasound:** Ultrasound is a non-destructive, contact or contactless device that has been employed in the applications of pork processing, thus confirming its robustness for the operating environments of processing facilities. Frontmatec's 3D loin trimmer exemplifies that this technology facilitates the capacity of sensing up to 750 products per hour which is more than adequate for beef striploin trimming applications. The high accuracy of ultrasonic measurements in meat applications is evident in a number of studies summarised in literature (Halim et al., 2013). The ultrasonic probes generally are very compact (e.g. 20 mm diameter x 15 mm long) and are sold by a large number of retailers for less than \$60,000 making this technology affordable for system implementation. Selecting an ultrasonic technology according to its rated frequency will determine penetration depth, compromising resolution, yet can measure the maximum striploin fat of 75 mm. With the ability to utilise both Amode and B-mode, in real-time, this sensor offers much versatility and capability to create an informative sensing technique for this application (University of Gelph, 2020).

**Vibrational Spectroscopy:** This technology has been employed successfully (e.g., Fat-o-Meater) to measure pork fat, hence whilst showing evidence of a robust system integration, it does show the invasive, mildly destructive nature required of this sensing technique. Due to its mechanical nature requiring insertion, measurement, retraction and cleaning for each measurement cycle its throughput was determined as feasible. According to the University of Gelph (2020), this technology has an accuracy of 0.5 mm over 180 mm measurements and is packaged as a

hand-held device, hence performing well in categories d), e) and g). Due to its simple, mechanical nature the cost-effectiveness of this technology is extremely high yet, without taking a significant number of readings (and causing damage to the product) this technology is limited as a real-time, informative sensor even through applying machine learning algorithms to differentiate fat and meat readings.

**Electrical Impedance:** Whilst electrical impedance technologies are invasive, they have been developed and trialled in processing plants with a degree of success. Due to this sensors accuracy being determined by insertion accuracy, meat pH levels and the potential of fat smearing on the device, all of which are likely issues within a production environment, this technology was rated infeasible for commercial robustness. Studies have found that the throughput attainable for this technology is more than adequate for the line speed of striploin processing (Meat and Livestock Australia Limited, 2020). Due to its mechanical nature requiring insertion, measurement, retraction and cleaning for each measurement cycle its throughput was determined as feasible. This handheld technology was deemed a desirable footprint yet the accuracy of  $\pm$  3 mm as evaluated in (Meat and Livestock Australia Limited, 2020) was deemed infeasible due to the extremely high yield loss value expected with this magnitude of error. Due to the similarity of electrical impedance and vibrational spectroscopy technologies for this application, electrical impedance performed similarly in the categories of cost-effectiveness (f), real-time (h) and informative sensing capabilities (i). Due to the limitation of sensing up to 28 mm of fat thickness at a time this sensing technologies was rated as 'infeasible' for its penetration range (g).

**Tactile:** Although tactile sensing does require the contact and an applied force to the product, there is no requirement to puncture, disfigure or damage the striploin. Hence, this technology is deemed to be desirable in category (a). Force modules require deflection to measure

tactile features and are generally packaged in small, sealed components meaning that robustness of system integration is desirable. Many studies, particular to the medical field, have exemplified the development of realtime, informative sensing techniques for accuracy of less than 1 mm is possible (Rosen et al., 2006; van den Gobbelsteen, 2012; Petra et al., 2006). This as such deems tactile sensing a highly desirable technology for considerations d), h) and i). The cocleoscopy drill developed by Brett et. al. (2018) illustrated that such technology could be packaged in the form of an extremely inexpensive (less than \$2,000), handheld device (deeming e) and f) as desirable). With the validation of this technology's ability to sense the thickness of fat (Khodabandehloo, 2018) the only questionable consideration, whilst expected to be similar to spectroscopy and impedance probes, is that of its capability to match the throughput required for striploin trimming.

**Summary:** The desktop feasibility evaluation of the sensing technologies considered for fat trimming is summarised in Table 2-3. From the review of sensing technologies that have potential to be or have been employed within red meat processing for fat measurement applications it is evident that there is no single optimal technique. Two tied for the highest score and are recommended to be developed further: ultrasound and tactile sensing technologies.

Table 2-3: Comparison of sensing technologies to determine most feasible for further development.

Criteria	Ultrasound	Spectroscopy	Impedance	Tactile
Non-Destructive	D	F	F	D
Robust	D	D	I	D
High Throughput	D	F	F	F
Accurate & Precise	D	D	I	D
Small Footprint	D	D	D	D
Cost-Effective	F	D	D	D
Deep Penetration	D	I	I	D
TOTAL SCORE	<u>13</u>	<u>10</u>	<u>4</u>	<u>13</u>

Note: 'I' is infeasible, 'F' is feasible, and 'D' is desirable (for each category)

**Ultrasound:** With the prior success of implementing ultrasonics within Frontmatec's 3D Loin Trimmer, ultrasonic sensing should be further explored for beef fat applications. Whilst this system is not able to be applied directly for beef fat developments based upon similar sensing techniques is highly recommended. Yet much development is needed to ensure ultrasound technology is practically developed within a system capable of measuring fat thickness across beef striploin primals. This desktop review has highlighted the following challenges for development of an ultrasonic sensing system as:

- ensuring adequate contact with the ultrasound probe and the primal
- ascertaining which type of ultrasound is most appropriate

- Developing a means of using measurements to create a cut path for an automated system

Tactile: Tactile sensing also scored strongly against the criteria and has been successfully deployed in similar fields i.e. the surgical field with some initial exploration in the red meat industry (Brett et al., 2018). The potential to extract real-time tactile information as shown in the medical field may revolutionalise the means of perceiving and anticipating the cutting tool position with reference to the fat-lean interface. Yet much development is needed to develop the capability of ascertaining a means of discriminating the cutting of lean meat and fat tissue for a practical tool that can be used on an automated system.

Of the two sensing technologies ultrasound was selected for development within this research due to this technology being most proven in the applications of fat depth measurement and commercial pork trimming systems. The prior work identified in literature also supported the readiness for ultrasound to be implemented within a fat depth sensing system moreso than tactile sensing technologies.

#### 2.4 Conclusion

The literature review conducted fulfilled the goal to *recommend the technology most suitable for consideration in the context of an automated trimming system*. A survey of patents and commercial systems found that no automated fat trimming system exists for beef striploin. In surveying technologies, based upon the considerations deemed important and nonnegotiable to the holistic characteristics of an automated fat trimming system, ultrasound was identified to be most promising.

It is evident that there are several unknowns surrounding the requirements and benchmarks of the process of uniform fat trimming of

beef striploin. In the survey of patents and commercial systems there was very little representation in beef processing within automated fat trimming systems. These systems were not designed to be cross-compatible with beef either suggesting that the characteristics of the fat trimming process between pork and beef are significantly different. Many of these systems either estimated fat depth (did not acquire measures) or estimated the entire subcutaneous fat profile with few measurements. This suggests that it is likely that the characteristics between beef and pork processing are significantly different, and that an analysis of the striploin variability and subcutaneous fat profile and the trimming process of fat trimming should be undertaken.

The learnings from the literature review inform the development of a methodology for sensor evaluation. The learnings also inform the study of other variables within a processing plant that may impact system design and sensor selection, which is further evaluated in the next chapter (Chapter 3) before defining a benchmark performance using CT imaging in Chapter 4.

# CHAPTER 3: SENSING SYSTEM DEFINITION FOR BEEF STRIPLOIN FAT TRIMMING

This chapter presents preliminary experimentations that provide an in-depth analysis of the striploin primal variability, the processing requirements for uniform fat trimming for the specific collaborating processor and the product specifications of trimmed beef striploin. These investigations inform the automation constraints and sensing considerations of a system that can meet the performance requirements (Research Objective 2). The preliminary experiments presented in this chapter provide specifics to the functional requirements of the sensor evaluation framework developed in Chapter 4, and again for the development of ultrasound systems in Chapter 5 and Chapter 6.

### 3.1 Introduction

This section presents a review of the striploin product and the processor-specific processes important for consideration to develop the experimental aims and processes required to inform the methodology of this thesis.

## 3.1.1 Preliminary Work

Prior to the beginning of this thesis there was a striploin fat trimming feasibility study conducted (Khodabandehloo, 2018). The focus of this study was to identify the range and variability of striploin primals and therefore the measurements presented were based upon the smallest and largest striploin that could be collected during the survey period at an undisclosed processing plant. The findings pertaining to variability of the striploin primal relevant to this thesis are summarised in Table 3-1. The dimensions referenced in this table were measured as illustrated in Figure 3-1.

Table 3-1: Variability of physical characteristics of untrimmed beef striploin primal.

Quantity		Smallest	Largest	Range
Dimension:	Length (mm)	470 mm	605 mm	135 mm
Dimension:	Width (mm)	200 mm	245 mm	45 mm
Dimension:	Height (mm)	90 mm	125 mm	35 mm
Weight:	Primal (kg)	15 kg (nominal)		
Fat Thickness:	Depth (mm)	2 mm	75 mm	73 mm
Fat Thickness:	Gradient (degrees)	60 (across length of striploin)		
		66 (across width of striploin)		

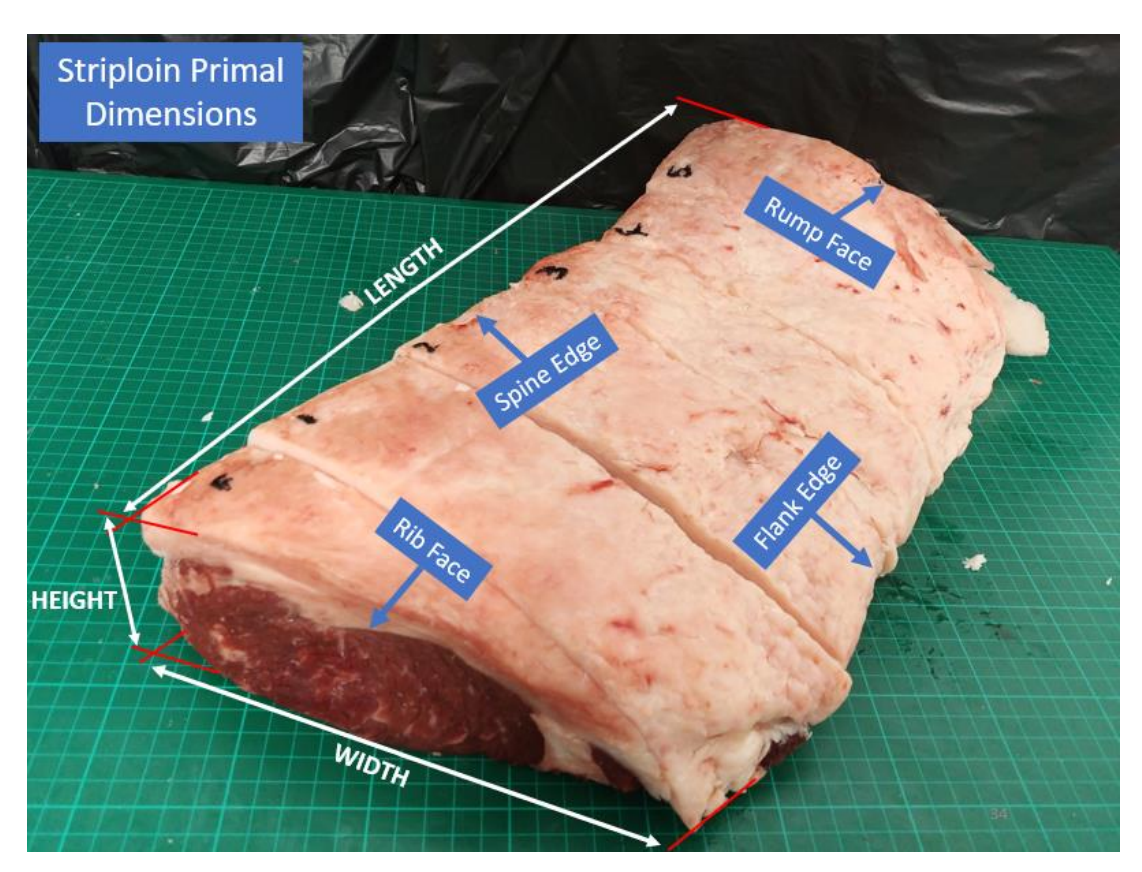


Figure 3-1: The definition of measurements (length, width and height) of a beef striploin primal.

This study highlighted the possible presence of delamination of fat layers in the subcutaneous fat of striploins surveyed as well as the potential for fat cover damage to be introduced by the 'hide puller' mechanism used in processing process prior to striploin fat trimming (Khodabandehloo, 2018). The 'hide puller' mechanism employed in beef processing that, in some cases, causes damage to the fat cover of the

striploin. Typically hides are 'pulled' from carcases in processing plants to 'dress' the carcase for further processing. Based on these observations the author suggested that the sensing be conducted on the medial surface (lean meat surface) of the striploin to avoid complications of 'no contact' instances inhibiting ultrasound sensing performance.

Khodabandehloo's (2018) investigation provides valuable insights for considerations in developing a feasible automated striploin fat trimming system. The biggest limitation of the statistics presented within this study was the very limited sample dataset (2 striploins) that were acquired from the line of a different processor. The collaborating processor for this thesis runs a 100 to 120-day grain-fed feeding programme that produces uniquely consistent (dimensions and fat profiles) striploin products. Due to such a small sample size and concerns for representativeness, it was determined that an independent study using striploins supplied by the collaborating processor was required for defining the sensing capabilities for this application.

# 3.1.2 Processor-Specific Context

Though there are some operations that are performed by all beef processors in Australia there are many variations of tasks that occur throughout the processing workflow (Cross, 2011a; Cross 2011b; Cross 2011c). These processor-specific operations will determine how the boneless striploin product is presented to the slicer, or automated system, for fat trimming. These processor-specific operations for the collaborating processor are presented, in order of occurrence, in the following subsection.

## **De-hiding Carcase:**

As mentioned by Khodabandehloo (2018) one such processing method that may cause damage to the fat cover on beef striploin primals is the 'hide puller'. Typically hides are 'pulled' from carcases in abattoirs

to 'dress' the carcase for further processing. The predominant types of hide pullers are upward (see Figure 3-2) and downward (see Figure 3-3). Australian processors typically employ the downward hide pulling mechanism due to the reduced likelihood of faecal contamination introduced during this process (Thompson, 2009). Though, the drawback of this method is the possibility of causing fat tears from the loin and hindquarter regions of the carcase which create inconsistent intra-striploin fat profiles. Though the collaborating processor confirmed the use of downward hide pulling the significance of the phenomena of 'fat tears' will be investigated in this chapter (C Anderson 2019, pers. comm., 13 November).



Figure 3-2: The mechanism of upward 'hide pulling' to dress the carcase. Source – (Thompson, 2009)



Figure 3-3: The mechanism of downward 'hide pulling' to dress the carcase typically used by Australian processors. Source – (Thompson, 2009)

# **Process of Boning Striploin:**

The boning processes employed will determine the physical dimensions of the striploin. The following processes are employed by the collaborating processor:

1) Carcass Splitting: The process after de-hiding whereby the carcase is split in half by sawing through the spine (mid-sagittal plane) to create two beef sides (see Figure 3-4).



Figure 3-4: Bovine carcase splitting using a saw to create beef sides. Source – (Savell, 2015)

This operation separates the carcase into 2 sides ('left' and 'right') and thus 2 separate striploin primals that are anatomically mirrored at the spine in the transverse plane. During carcase splitting the saw cuts the spine in the direction of most caudal (Rump face) to cranial (Rib face) end and defines the most medial edge (referred to as the spine edge) of each striploin primal.

**2) Chilling Beef Sides:** The process whereby the beef side is rapidly cooled in a chiller to prolong meat shelf life by preventing microbial growth occurring (see Figure 3-5).



Figure 3-5: Beef sides being cooled in a processor's chiller prior to grading. Source – (Betancourt, 2019)

This operation rapidly cools the beef side which causes the contraction of muscles to the degree that the carcase frame permits (which resists these contraction forces) during the time in the chiller (Husband, 1993). Though there is no literature defining the degree of this phenomena, and how the cutting of the carcase for grading may exacerbate this, the contraction of muscles is likely the cause a curvature of varying significance of the spine edge of each striploin primal.

**3) Carcase Grading & Quartering:** Typically, whilst the beef side is in the chiller it is cut between the 12th and 13th thoracic rib to expose the eye muscle for grading and mark the position to use to quarter the beef side (see Figure 3-6).



Figure 3-6: Beef sides cut between the  $12^{th}$  and  $13^{th}$  rib for grading whilst in the chiller. Source – (Konopacki, 2006)

This operation is a straight cut parallel to rib bones and separates the beef side into 2 quarters ('hindquarter' and 'forequarter'). This cut defines the anatomical cut plane of the "rib" face of each striploin. This cut line is parallel between the 12<sup>th</sup> and 13<sup>th</sup> rib, cut from the medial (spine) to the lateral (flank) direction. The skeletal structure of the bovine carcase provides a guide for the boner's knife, and upon cutting past the

end of the rib, the boner cuts out of the carcase "straight" by eye. This provides explanation of the 2 different angled cuts that typically create the rib face of the striploin, which at their intersection identifies the end of the 12<sup>th</sup> rib bone when the boning knife changes orientation (see Figure 3-7). This also provides an explanation as to the varying degrees of chamfers (the cut line defining the rib face from the end of the 12<sup>th</sup> rib to the flank end) that have been observed in striploins.

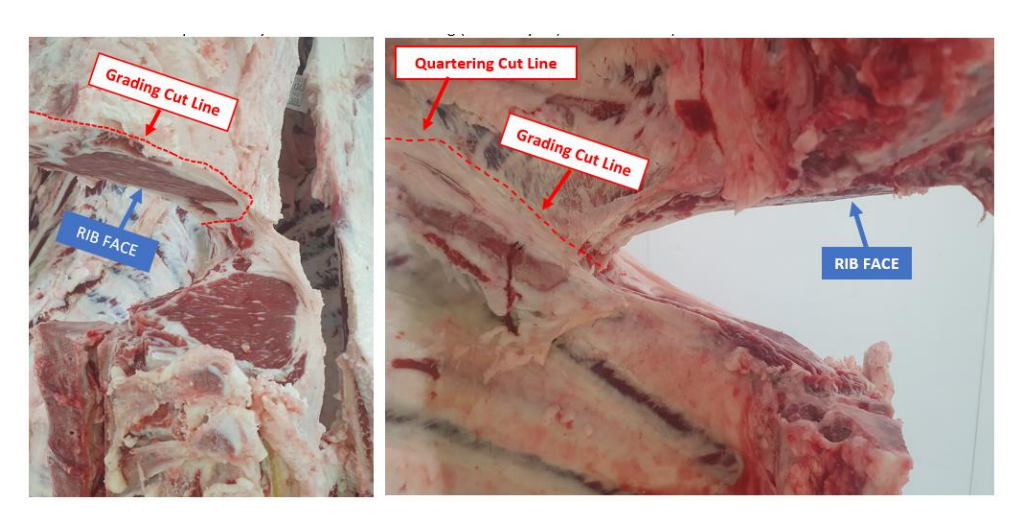


Figure 3-7: Two distinct cut lines used to define rib face of striploin at the collaborating processor's facility. Original image source – (McDonald-Keating, 2021)

**4) Hindquarter Boning – Flank Removal:** The hindquarter is cut along a seam of fat to remove the flank from the hindquarter (see Figure 3-8).

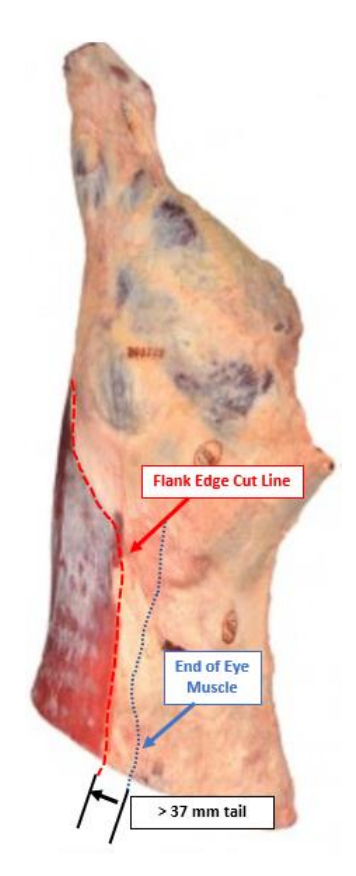


Figure 3-8: Removal of the flank from the hindquarter by cutting along fat seam. Original image source – (John the Butcher, 2018)

This operation is a straight cut along a fat seam to remove the flank from the striploin leaving at least 37 mm of fat after the eye muscle in the most ventral direction (commonly referred to as "tail"). This cut defines the anatomical cut plane of the "flank" edge of each striploin and is typically quite consistently cut perpendicular to the "spine" edge (see Figure 3-9).

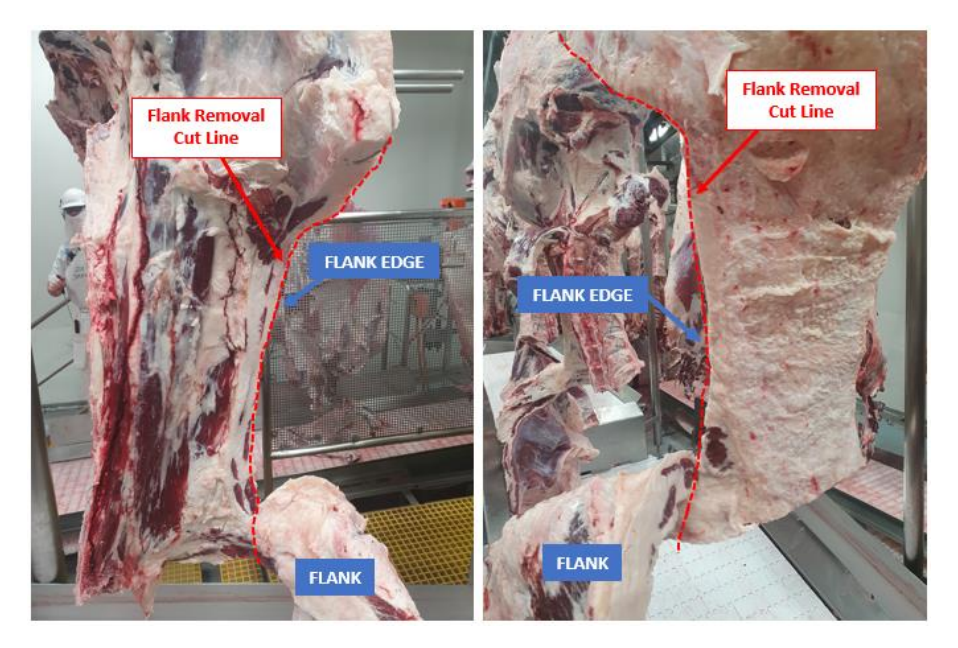


Figure 3-9: The cut line that removes the flank from the hindquarter to define the flank edge of the striploin at the collaborating processor's facility. Original image source – (McDonald-Keating, 2021)

**5) Hindquarter Boning – Striploin Removal:** The hindquarter is cut straight between the lumbar junction and 1st sacral vertebrae to remove the striploin from the hindquarter (see Figure 3-10).



Figure 3-10: Removal of the striploin from the hindquarter by cutting straight from between the lumbar junction and  $1^{st}$  sacral vertebrae. Original image source – (John the Butcher, 2018)

This operation is a straight cut straight between the lumbar junction and 1st sacral vertebrae to remove the striploin from the hindquarter. This cut defines the anatomical cut plane of the Rump face of each striploin (see Figure 3-11).

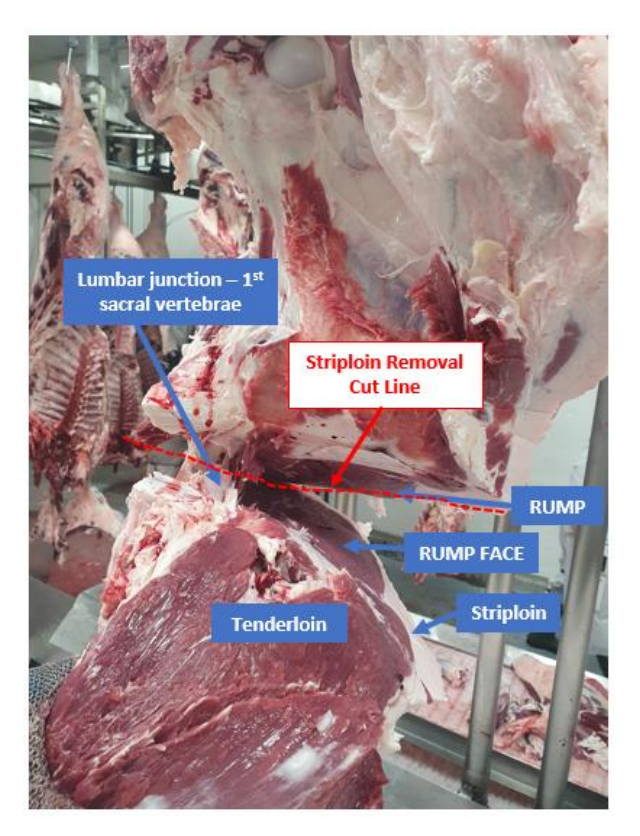


Figure 3-11: The cut line that removes the striploin (and tenderloin) from the hindquarter to define the rump face of the striploin at the collaborating processor's facility. Original image source – (McDonald-Keating, 2021)

**6) Striploin Boning – Chine Sawing:** After removing the tenderloin a bandsaw is used to cut the 13<sup>th</sup> rib extending from the striploin and then to cut the chine bone along the length of the striploin to separate this with the feature bones into easy-to-remove flat and button bones (see Figure 3-12).

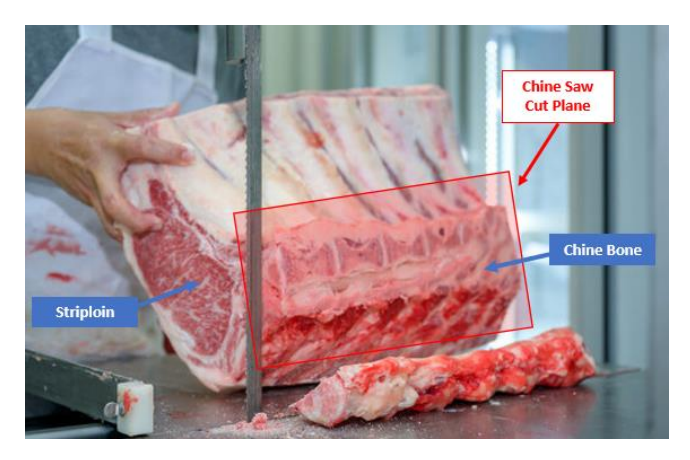


Figure 3-12: Chine sawing to disconnect the chine and feather bones for easier removal of smaller bones. Original image source – (Adobe, 2021)

Through this process of chine sawing bones are released so that a table boner can remove bones (the 13<sup>th</sup> rib, the remainder of the chine bone along the chine edge, and several button bones and flat bones) with as little yield loss as possible.

**7) Striploin Boning – Table Boning:** The striploin is then boned on the table to remove the rest of the bones underneath the striploin (see Figure 3-13).

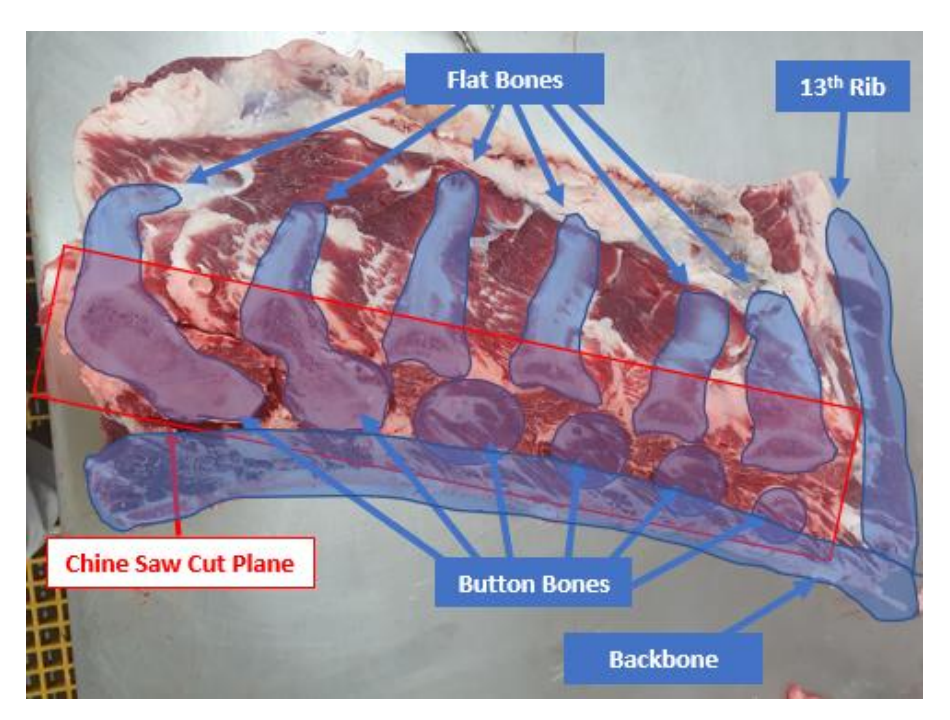


Figure 3-13: An illustration of the bones that are under the striploin after chine sawing. Original image source – (McDonald-Keating, 2021)

A brief study was conducted to investigate the cavities that are created on the medial surface (lean meat surface) upon table boning the striploin, and what the approximate positions and extent of these cavities were (see Appendix A.1: Cavities Created by Table Boning). A summary of this analysis revealed that post-chine sawing the striploin had 7 sets of button and flat bones in addition to those along the spine (see Figure 3-14). When removed the button and flat bones left cavities in the lean meat surface of the striploin 10 - 20 mm deep spaced on average 55 mm from each other.

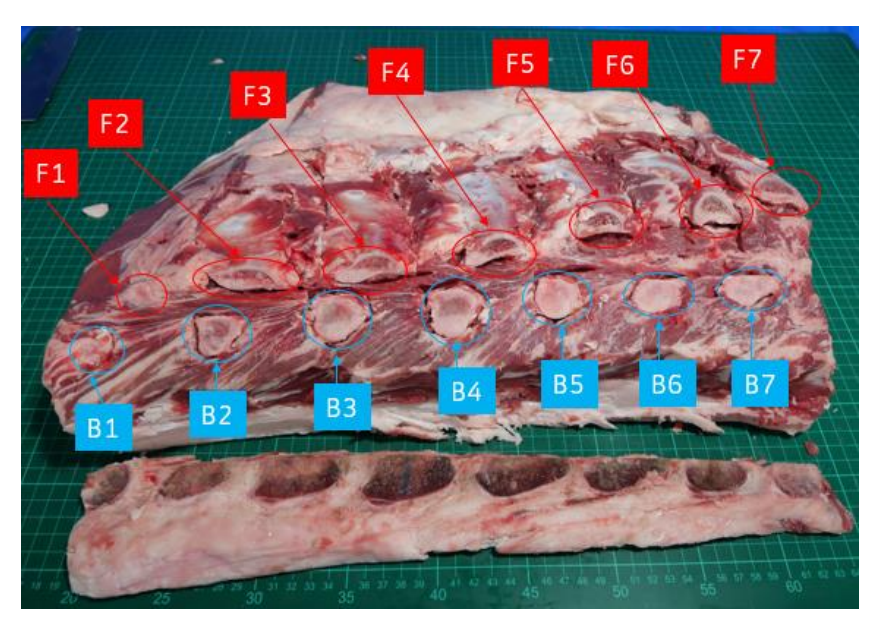


Figure 3-14: An analysis of flat bones (F1, F2, ...) and button bones (B1, B2, ...) removed from the medial surface (lean) of the striploin prior to fat trimming.

# **Fat Specifications and Trimming:**

There are many fat thickness specifications used by processors to produce striploin products depending upon the market the product is sold to. The fat thickness specification chosen for this thesis was selected as 12 mm as this was the most common customer requirement of the collaborating processor (C Anderson 2019, pers. comm., 13 November).

The processor provides products to customers according to the 'maximum fat thickness at any point' method with the exception of 'bridging' and 'planing' scenarios (C Anderson 2019, pers. comm., 13 November). In the case whereby a customer identifies a beef striploin with a fat thickness of more than the maximum 12 mm fat thickness a 'fat claim' against the processor may be actioned. In such a scenario, the processor is required to refund the cost of the entire striploin product to the customer (C Anderson 2019, pers. comm., 13 November). In order to reduce the number of fat claims that are lodged for reimbursement the processor instructs slicers to purposeful over-trim striploin products (C Anderson 2019, pers. comm., 13 November). The yield losses incurred from over-trimming this product is estimated to be significantly greater, though less visible, than fat claims. Until there is a mechanism of measuring the fat depth within a striploin there will not be the precision required to trim accurately to the desired fat thickness specification.

The task definition of the 'fat trimming' and the time taken to by slicers to complete are processor-specific constraints that are important to consider in the development of an automated fat trimming system. These processes will be documented for the collaborating processor and further analysed to provide these insights for system development in subsequent chapters.

## **Summary of Processor-Specific Considerations**

The key product specifications that inform the development and evaluation of the sensing system for automated trimming are summarised in Table 3-2. These processor-specific factors contribute to defining the scope of an automated system capable of fat trimming for this application in this processing facility.

Table 3-2: Key product constraints to consider for the development of an automated system capable of trimming to specifications.

Product Specification	Sensing System Considerations
Fat Specification:	A maximum fat specification of 12 mm will be
Commonly 12 mm	considered as per the typical customer
	requirements of the processor. Practically,
	this would be a perpendicular measurement
	from the fat-lean interface as opposed to
	vertically (as this would yield a measurement
	of the maximum fat depth)
Trimming Standards:	In addition to decreasing yield over-trimming
Avoid scores in the lean	fat may also significantly devalue the product
	if lean muscle is scored during trimming.
Trimming Standards:	A sensing mechanism/configuration needs to
Smooth trimming along the	be considered to acquire enough fat depth
contour of underlying	measurements to generate a contour
muscles	representative of underlying tissues
	throughout the striploin primal.
Measurement Method:	An under-trimming-related failure is clearly
Maximum fat thickness at	defined as fat thickness over the maximum
any point measured at the	specified at any point. Though, it should be
edges of cuts	highlighted that the nature of retailers
	portioning striploin means that only a limited
	number of edges (e.g., cross-sections / faces
	of steaks) will be seen. In addition to this,
	these cross-sections are likely only measured
	(and fat claimed) if large deviations from the
	fat specification are observed. This suggests
	that an 'unspoken' error tolerance exists in
	the practical application of specifications.
Measurement Method:	This introduces the need for some degree of
Fat depth accounts for	path planning using fat depth measurements
'bridging' and 'planing'	to optimise automated trimming for yield.

Cost of Failure:	Further investigation is required to quantify
Fat Claims vs Loss of Yield	the cost of both failures (over-trimming and
	under-trimming) to determine what failure
	should be prioritised and to what degree. This
	will inform the performance evaluation.

### 3.1.3 Chapter Aims

More processor-specific information is required to better define the considerations and capability scope for a suitable automated fat trimming system. The analyses to presented in this subsection address these knowledge gaps.

## **Investigation 1: Product Variability & Processing Constraints**

There has been very little work conducted to quantifying the variabilities of the striploins presented for fat trimming, and the prior processes that create such variabilities. These variabilities are important to consider for developing an automated solution to ensure that the automated system is capable of servicing the range of striploins, or to define the scope for which the system can cater for. This has a significant impact on the following aspects of the automated fat trimming system:

- The surface area of the striploin will determine the sensing area (and number of nodes) to be considered.
- The sensing area will contribute towards defining the number of nodes, and the spacing within the nodes which will create a trade-off between the sensing time required (in total and per node) and the representativeness of sensor data to the striploin.
- The temperature of striploin primals will determine ultrasound settings which are typically considered for calibration.
- The significance, and likelihood, of product surface deformations (e.g. fat cover damage, fat delamination, etc.)

present in the fat and lean surfaces of striploins will determine the sensing orientation that would be best for ultrasound sensing.

A survey of the physical attributes (dimensions, weight, temperature, surface deformations and fat cover damage) of untrimmed striploins will be conducted at the processor's facility to better define the input variability of the system with respect to the overall dimensions and general characteristics of untrimmed striploins, and the processing methods that contribute to this.

### **Investigation 2: Time Motion Study of Uniform Fat Trimming**

There is yet to be data collected defining the processing speed that is currently being adhered to within the fat trimming operation of beef striploin at the collaborating processor's facility. This line speed is a constraint that needs to be considered in the development of a feasible automated system capable of striploin fat trimming in this processing plant. This has a significant impact on the following aspects of the automated fat trimming system:

- The total time permitted for the entire system's cycle time which assists to define the time (in total and per node) for sensing. This also then provides insight towards the trade-off between: the number of sensing nodes in the node mesh, the cycle time of the sensing process, and the response time of the sensor per measurement.

Therefore, a time-motion study was conducted on slicers performing fat trimming at the processor's facility to better define the response time of a sensor and the sensing cycle time of a system feasible for fat trimming system at this line speed.

### **Investigation 3: Subcutaneous Fat Characteristics**

Whilst Chapter 2 identified ultrasound to be the most promising technology for the application of measuring fat thickness on a beef striploin further investigation is required to determine the characteristics of which an appropriate ultrasound device can be selected using. This has a significant impact on the following aspects of the automated fat trimming system:

- The range of fat thickness measurements that can be expected at the sensing nodes of striploins from the processor's processing line. This will assist to define the minimum and maximum penetration depth of an appropriate ultrasound device.
- The maximum gradient between fat thickness measurements that can be expected at the sensing nodes of striploins from the processor's processing line. This will assist to define the cut path considerations for a robotic automated solution.
- An evaluation of the fat distribution and the variability of fat distributed inter-striploin and intra-striploin will provide insight towards optimising the trade-off between measurement representativeness and sensing cycle time through the number of sensing nodes in the node mesh.

An in-depth analysis of the subcutaneous fat profile of untrimmed striploins at the processor's facility will be conducted to better define the context that the sensing system will be applied within.

## 3.2 Product Variability & Processing Constraints

This experiment quantified the product variability and the processing processes and constraints important for the collaborating processor.

### 3.2.1 Experimental Set-Up

The processing steps that occur before the striploin primal is presented to the slicer impacts the size and dimensions of the primal. The processing steps presented are specific to defining the presentation of a beef striploin primal for fat trimming at the collaborating processor's facility (P McDonald-Keating 2021, pers. comm., 20 July). An example of the overall shape and dimensions of a typical striploin at the collaborating processor's processing line is illustrated in Figure 3-15.

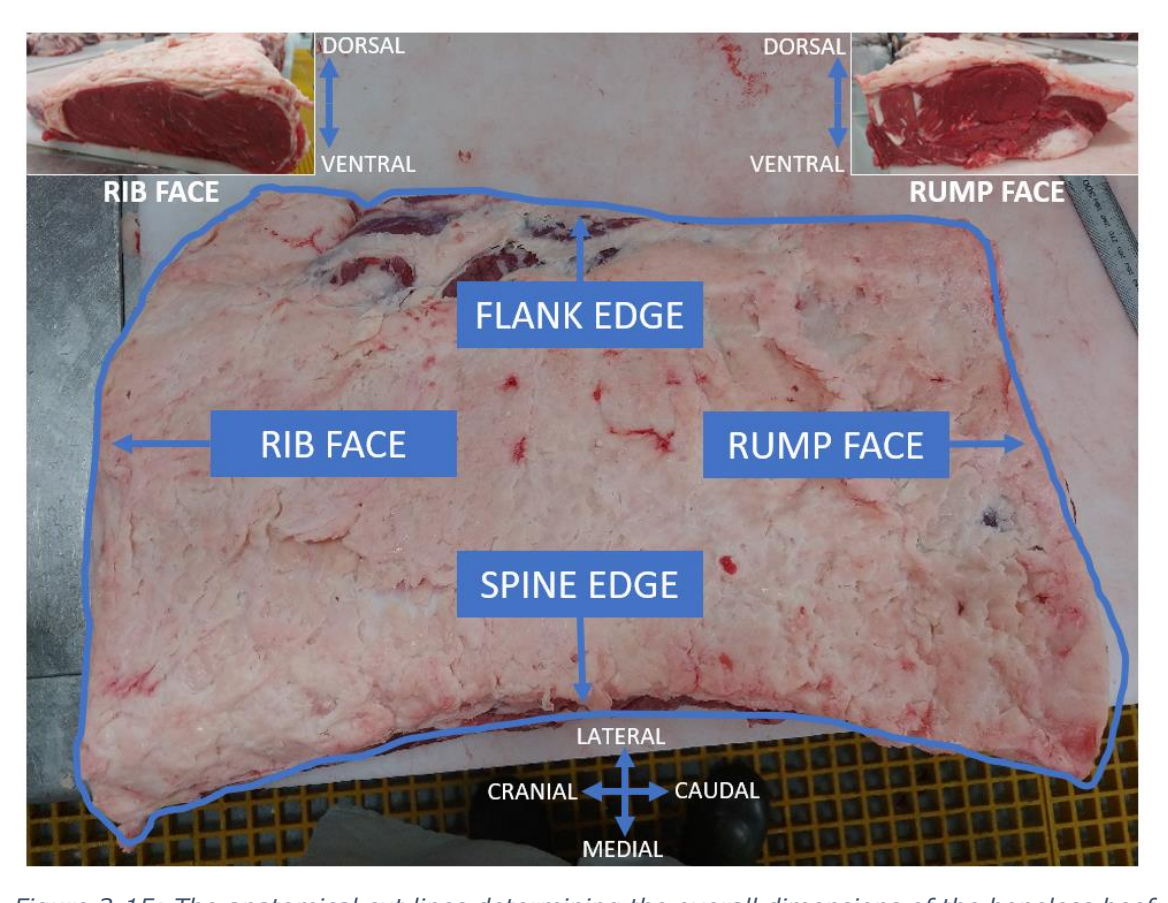


Figure 3-15: The anatomical cut lines determining the overall dimensions of the boneless beef striploin primal presented for fat trimming at collaborating processor's facility illustrated on a LHS striploin.

A survey was conducted to ascertain the typical dimensional variations of 100-day grain-fed beef striploin primals at the collaborating processor's site on the late morning shift (11:30 AM – 1:00 PM) on the 28th of April 2021. For this survey, twenty untrimmed beef striploin primals were acquired during a typical run at the processor's facility.

Detailed information defining the characteristics of the striploins used in this survey is outlined in Appendix A.2: Dataset for Product Variability of Untrimmed Striploins.

The length, width, and height of the primals were measured using a stainless-steel ruler, the weight was measured using digital scales in the processor's facility, and the average temperature of the primal was measured using an infrared digital thermometer. A qualitative description of the fat cover over each striploin was reported, and each face of each striploin was photographed (see Figure 3-16).



Figure 3-16: The set-up for the survey of the physical characteristics of untrimmed striploin primals.

### 3.2.2 Experimental Analysis

The dimension and weight measurements of the twenty untrimmed striploins surveyed were averaged (mean) with the calculation of 2 standard deviations to define the variance of these characteristics to a 95% confidence interval. This gave clarity in defining the percentage and variance of products that are not in scope for an automated system.

According to MLA (2022), considerable fat cover damage is defined as areas of more than  $10 \text{cm} \times 10 \text{cm}$  that were void of fat. For the purposes of fat trimming, these affected areas were only considered

significant whereby this area was in a position that it may inhibit the capability to acquire a fat thickness measurement (e.g. the fat cover damage was on a location that was at least 20 mm from an edge). As such, these instances were counted from observations of the fat cover on each striploin. Statistically, the expected probability was calculated to estimate the likelihood of fat tear-related damage being presented on striploins based on this sample dataset.

### 3.2.3 Results

The twenty (20) striploins surveyed were measured in length (spine edge), width (rump face cross-section), height (maximum at rump face) and weight (overall primal) and results were tabulated (see Table 3-3) with the five number summary plus the confidence interval bounds (± 2SD) presented in Table 3-4. This analysis quantified the typical striploin (within a 95% confidence interval) presented for fat trimming being 388 – 456 mm in length, 221 – 309 mm in width and 72 – 103 mm in height.

Table 3-3: Measurements of the 'typical' untrimmed striploins acquired from the collaborating processor's conveyor.

Measurement of Untrimmed Striploin Primals								
Date & Time Measured	Striploin #	Feed Regime	L/R	Lspine (mm)	W <sub>RUMP</sub> (mm)	Нмах (mm)	Weight (kg)	
28/04/2021 11:39	1	100-120 day grainfed	R	430	270	101	8.66	
28/04/2021 11:43	2	100-120 day grainfed	R	451	309	81	9.31	
28/04/2021 11:47	3	100-120 day grainfed	R	446	292	77	9.12	
28/04/2021 11:50	4	100-120 day grainfed	R	412	261	105	8.17	
28/04/2021 11:53	5	100-120 day grainfed	R	448	288	83	9.27	
28/04/2021 11:56	6	100-120 day grainfed	R	393	229	74	6.78	
28/04/2021 11:59	7	100-120 day grainfed	R	401	246	82	6.99	
28/04/2021 12:02	8	100-120 day grainfed	R	405	254	90	7.22	
28/04/2021 12:05	9	100-120 day grainfed	R	422	261	88	8.65	
28/04/2021 12:05	10	100-120 day grainfed	R	414	257	83	8.51	
28/04/2021 12:08	11	100-120 day grainfed	R	412	249	84	8.4	
28/04/2021 12:10	12	100-120 day grainfed	R	423	265	87	8.36	
28/04/2021 12:13	13	100-120 day grainfed	R	433	273	96	8.71	
28/04/2021 12:17	14	100-120 day grainfed	R	405	231	98	7.08	
28/04/2021 12:19	15	100-120 day grainfed	R	412	252	92	8.57	
28/04/2021 12:23	16	100-120 day grainfed	R	431	271	87	8.75	
28/04/2021 12:26	17	100-120 day grainfed	R	397	234	86	6.87	
28/04/2021 12:30	18	100-120 day grainfed	R	427	267	86	8.61	
28/04/2021 12:35	19	100-120 day grainfed	R	434	279	84	9.04	
28/04/2021 12:38	20	100-120 day grainfed	R	445	306	82	9.01	

Table 3-4: Statistical summary of untrimmed striploin dimensions.

Statistical Summary								
LSPINE WRUMP HMAX Weight								
Statistic	(mm)	(mm)	(mm)	(kg)				
Min	393	229	74	6.78				
Median	423	263	86	8.59				
Average	422	265	87	8.30				
Max	451	309	105	9.31				
SD	17	22	8	0.81				
Lower Bound (2SD)	388	221	72	6.67				
Upper Bound (2SD)	456	309	103	9.93				

Observations were also made regarding the shape of the twenty striploins. It was seen that the most perpendicular face to the spine edge of the striploin was the caudal/cranial edge with the cranial/rib edge being curved at the ventral/flank edge. This finding supports using the caudal/cranial edge and spine edge to reference the origin of the node mesh of the sensing system proposed in the third experiment of this chapter (Section 3.4). In addition to this, the temperature was made with a digital infrared thermometer which revealed the average surface temperature of the subcutaneous fat being 8.1 degrees Celsius. This temperature was considered in the experimentation procedure outlined in Chapter 5 and 6.

Observations regarding the significance of fat cover damage were made from the twenty striploins within this dataset (see photographs taken of fat cover for each striploin in Appendix A.2: Dataset for Product Variability of Untrimmed Striploins). Two instances of significant fat cover damage were identified for the location of measurement for the prescribed node mesh. Using this sample size (twenty) the expected probability was calculated to be 10% for instances of fat tears affecting measurements for a fat trimming system. Furthermore, there was a pattern observed that fat tear damage typically occurred on the ventral

edge at approximately 100–200 mm from the caudal (rump) face as shown (see Figure 3-17).

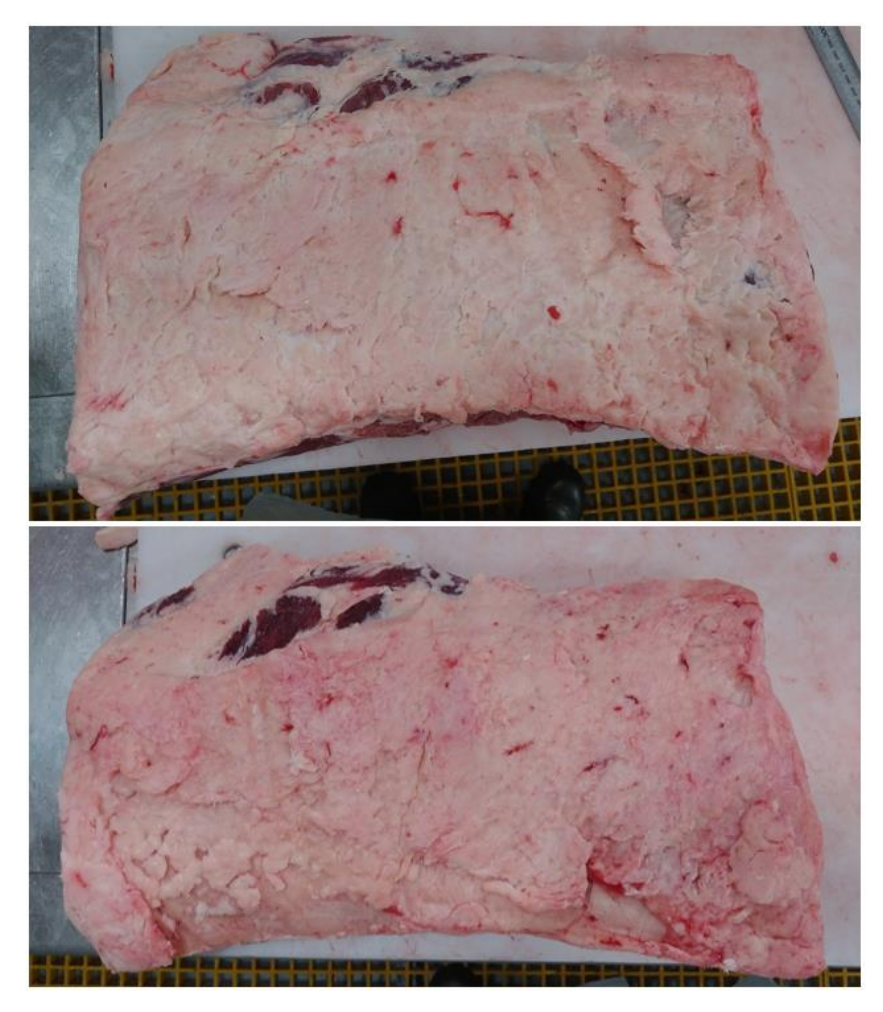


Figure 3-17: Illustration of fat tear damage found on two of the twenty surveyed striploins.

#### 3.2.4 Discussion

The variability of the striploin primal presented to the slicer is a significant factor that influences the effectiveness of developing an automated fat trimming system. This variability has been characterized by differences in length, width, height, weight, and the condition of the fat cover.

The striploin primal's length, width, height, and weight show a significant difference to the striploin characteristics presented in

Khodabandehloo's (2018) preliminary study. The contrasting striploin characteristics supports the significance of bovine breeds, feeding regimes and processing methods that translate to significant differences within striploin dimensions, and inter-striploin variability within a typical processing run (see Table 3-5). The significant differences between preliminary work and the experimental survey presented within the results section of this subsection confirm the decision to conduct the survey using the particular striploins of the collaborating processor.

Table 3-5: Comparison of typical striploin dimensions with preliminary work.

Quantity	Study	Smallest	Largest	Range
Length	Khodabandehloo	470 mm	605 mm	135 mm
	Border	393 mm	451 mm	58 mm
Width	Khodabandehloo	200 mm	245 mm	45 mm
	Border	229 mm	309 mm	80 mm
Height	Khodabandehloo Border		125 mm	35 mm
			105 mm	31 mm
Primal Weight	Khodabandehloo	15 kg (nominal)		
	Border	8.30 kg (mean)		

This highlights the need for automation to be designed to accommodate for such a large deviation of striploin primals or that of the chosen processor. As shown in Table 3-5, the width and weight of the striploin primal exhibit the most variability, as indicated by the standard deviation values. Considering all striploins surveyed were from the same 'processing run' (a term used to describe the carcases were from the same lot and roughly the same breeds and quality). For the trial conducted at the site of the collaborating process this was reported to be a processing run of mixed breed MSA 0-3 quality, and so there is little case for variability being assigned to breed or genetic deviations.

The variability in striploin boning, particularly in the precision of cuts, is noteworthy. Edges cut based on visual estimation (lateral/flank edge) exhibit more variability compared to those made along anatomical landmarks such as tissues and bones (medial/spine edge, caudal/rump face, cranial/rib face). This supports the argument that the variability of the width is due to human error due to approximation of cutting lines. In combination with the curvature of the cranial/rib face observed on the striploins surveyed, the decision to position of the origin location in reference to the medial / spine edge and the caudal / rump face has been supported. This enables a more consistent approach of acquiring measurements that can be registered between different striploins and striploin types (LHS / RHS). This method also provides a means of measuring a uniform mesh spacing without the complication of a node mesh significantly skewed to the orientation of the striploin.

The condition of the fat cover also shows variability, with instances of fat cover damage observed in only a small number of striploins. This damage typically occurs on the ventral edge at approximately 100-200 mm from the caudal (rump) face (see Figure 3-17). The expected probability for instances of fat tears affecting measurements for a fat trimming system was calculated to be 10%. Whilst this observation was used in Khodabandehloo's (2018) preliminary study to recommend applying ultrasound sensing, the insignificance of this phenomena recontextualises the recommendation for this study. In the worst case, the general location of this fat cover damage may contribute towards recommending an altering of the node mesh to node place measurement nodes on this region or else omit this node from the mesh. In addition, and the lack of observations of fat delamination being unobservable in the striploins surveyed did not make a definitive case to conclude that sensing from the subcutaneous fat surface would yield ineffective results. Through studying the process of boning the striploin it was identified that the cavities created by table boning of the flat and button bones from the

striploin could impose issues when measuring from the lean surface with an ultrasound device. As such, the recommendation made in this study was not deemed completely valid and further preliminary testing will be conducted for the sensing orientation of systems presented in Chapter 5 and 6.

The average temperature of the striploin at the fat trimming operator table was 8.2 degrees Celsius. This temperature will be considered in the parameter settings of the ultrasound device to properly tune this correctly (see Chapter 5 and 6).

### 3.3 Time Motion Study of Uniform Fat Trimming

This section presents a time motion study that was conducted to define the processing speed benchmark for uniform fat trimming.

### 3.3.1 Experimental Set-Up

For the time-motion analysis of uniform fat trimming, slicers were observed on a typical run at the processor's facility on 6 June, 2021. Through these observations, and the timing of slicers' actions, the particular actions required to perform the task of uniform fat trimming, and the average processing time for the task, was defined (see Figure 3-18).



Figure 3-18: A slicer performing uniform fat trimming of beef striploin at the collaborating processor's facility.

# 3.3.2 Experimental Analysis

The process of uniform fat trimming was documented as a series of sequential tasks performed by slicers during fat trimming. Several personnel (slicers, trainers and the leadership team) were consulted to confirm the tasks that consist of fat trimming as well as photographs were taken during observations. There were tasks conducted by slicers on the lean muscle surface that were considered supplementary to fat trimming and hence omitted from the time-motion study analysis conducted. These 'lean surface' type tasks are described in Table 3-6. De-identified results were tabulated over four slicers trimming 25 striploins to ascertain the time taken for this operation. Mean processing time, and the 95% confidence interval / within 2 standard deviations (SD).

#### 3.3.3 Results

The results of the time-motion analysis identified the following subtasks performed by slicers to 'finish' the striploin (see Table 3-6).

Table 3-6: Motion analysis of fat trimming beef striploin

Motion Analysis of Finishing Beef Striploin						
Туре	Sub-Task					
	Inspecting and removing any stray bones / bone chips.					
Lean Surface	Squaring off the underside to reduce the divets made by removing the button and flat bones.					
	Removing a large portion of the tail by cutting at a 45 degree angle from the medial to the lateral surface, cutting along the length. Then cutting this portion to remove small amount of lean meat from the fat.					
	Cutting along the spine to square up this edge.					
	Square up the rib and rump faces with a perpendicular cut.					
Fat Surface	Trim fat using long knife strokes lengthwise. The tail gets trimmed significantly. The technique of each slicer differed as to where they cut in general.					

The time taken to trim both the lean and fat surface separately was recorded for four unidentified slicers over 25 observations. The raw data of this time motion study has been included in an appendix (see Appendix A.3: Time-Motion Analysis of Striploin Fat Trimming). A summary of the timings of each slicer for only the fat trimming component of these observations is tabulated in Table 3-7 and presented as a box-and-whisker plot to evaluate the spread of these individual measurements in Figure 3-19. The timing of the fat trimming tasks identified an average processing time of 27 seconds, with a 95% confidence interval for a processing time range of 12–42 seconds. During this survey it was observed that there were four slicers allocated for the fat trimming of beef striploin each positioned in a 1m x 1.5m workspace. This observation provides the space constraints of a feasible footprint for an automated system to adhere to.

Table 3-7: Summary of time recordings from fat trimming observations (n = 25)

Time Summary of Fat Trimming								
Statistic	Slicer A	Slicer B	Slicer C	Slicer D	Overall			
Min	22.0	16.0	21.0	13.0	13.0			
Median	30.5	26.0	33.5	21.0	29.0			
Average	30.0	25.5	31.7	22.6	27.2			
Max	36.0	32.0	42.0	38.0	42.0			
Standard Deviation	4.1	5.7	7.5	7.7	7.4			
Lower Bound (2SD)	21.8	14.1	16.7	7.2	12.4			
Upper Bound (2SD)	38.2	36.9	46.6	37.9	42.1			

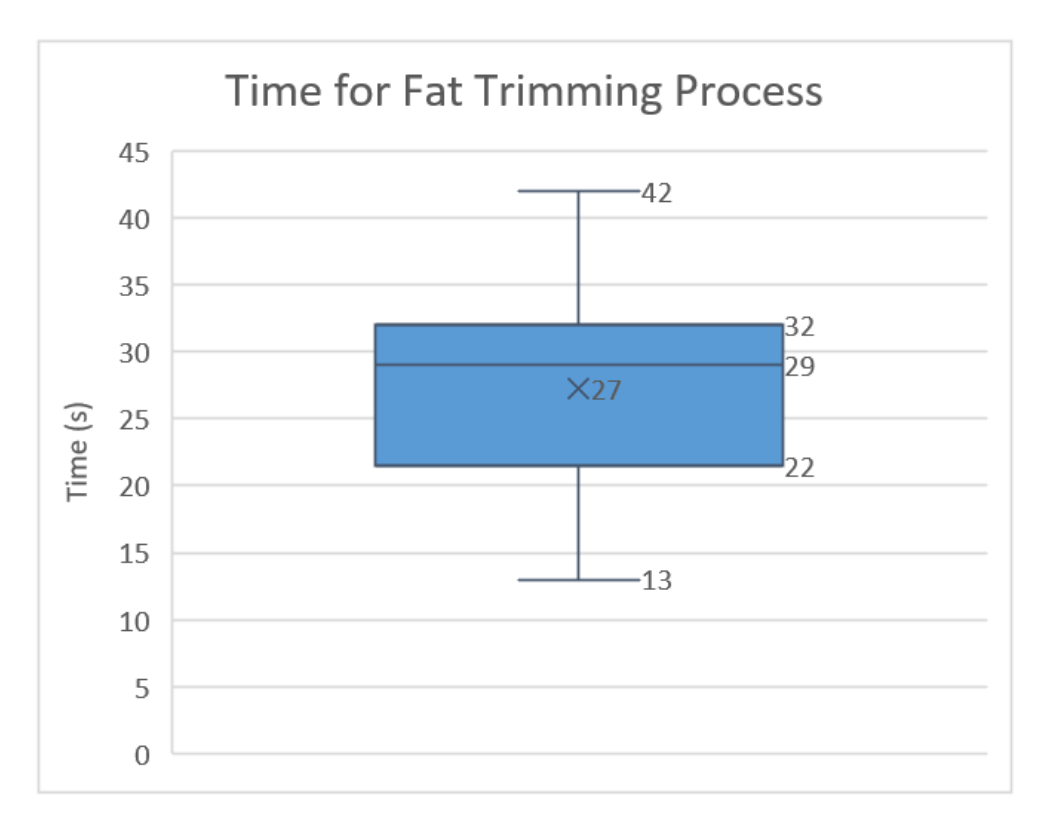


Figure 3-19: The fat trimming times from trimming observations (n = 25) presented in a box-and-whisker plot.

### 3.3.4 Discussion

The time-motion analysis identified an average processing time of 27 seconds for the fat trimming element of the slicers' trimming tasks, with a 95% confidence interval for a processing time range of 12 – 42 seconds. Quantifying this processing timing provides a benchmark for the

response time that a feasible sensing technology must be capable of. This response time will be considered in the preliminary investigations of Mode-A and Mode-B ultrasound systems developed in Chapter 5 and 6.

The footprint of a workstation was measured to be 1.5m x 1m could be considered equivalent for a robot station, and perhaps initially this system could be installed in series with slicers who can continue to deal with peak loads by storing striploins could operate to similarly deal with peak loads. With four stations for fat trimming the number of units that may be installed could be reasonably presumed to be two (leaving two stations for manual trimming until breakdown frequency is evaluated). This provides an approximate limit for the number of units that could be installed for such a processing line, which further constrains the maximum cycle time of both units to achieve the line speed.

#### 3.4 Subcutaneous Fat Characteristics

This section evaluates the subcutaneous fat distribution characteristics of a typical striploin to inform the requirements for a suitable sensing system for this application.

### 3.4.1 Experimental Set-Up

For this analysis, four striploins were selected from the processing line of the processor as samples to conduct the analyses presented in this investigation. The striploins acquired for this experiment had characteristics that aligned to those identified as a 'typical' striploin in the previous experiment in Section 3.2. The striploins were labelled with a number and orientation (Striploin 1R, 2R, 3L, 4L) where 'L' and 'R' denoted a LHS and RHS striploin respectively. The dimensions and weights of the striploins used in this experiment are shown in Table 3-8.

Table 3-8: A summary of the striploin dataset characteristics (dimensions & weight).

Striploin Dataset Characteristics							
Date & Time Measured	Striploin #	Feed Regime	L/R	L <sub>SPINE</sub> (mm)	Wrump (mm)	H <sub>MAX</sub> (mm)	Weight (kg)
08/12/2021 11:20:00	1	100-120 day grainfed	R	428	282	89	8.846
08/12/2021 22:05:00	2	100-120 day grainfed	R	435	305	92	6.582
09/12/2021 13:05:00	3	100-120 day grainfed	L	410	235	88	6.581
27/11/2021 00:45:00 4 100-120 day grainfed L 445 235 76 6.679							
Averages & Totals				430	264	86	7.17

To draw more insight into the fat characteristics, a node location convention was created to ensure that inter-striploin measurements could compared and intra-striploin patterns could be recognised. Since the spine and rump edges were most consistently cut square between striploins (identified in Section 3.2), the origin of the sensing mesh was measured in reference from the Caudal (Rump) face and Medial (Spine) edge. A permanent marker was used to mark the location of the origin of a sensing node mesh on the plastic wrapping of each striploin on the face of the subcutaneous fat. With the origin defined, a template created from clear plastic 10 mm x 10 mm grid was used to both align to the rump face and mark the measurement nodes array on each striploin (see Figure 3-20). The final origin locations of each striploin are defined in Table 3-9.



Figure 3-20: A clear, plastic grid was aligned with the origin and used to mark up the 25 mm X 50 mm spacings to create the node mesh on each striploin.

The variability of striploin dimensions in the dataset meant that the origin placement varied slightly with placement being as to ensure as many nodes as possible in the mesh would be marked on the surface of the striploin. By defining the origin similarly and aligning the node mesh perpendicular to the Caudal face, which was generally cut perpendicular to the spine edge, this enabled the spatial relationship of fat depth to be evaluated across the entire striploin dataset despite variance in dimension (length and width) and orientation (LHS/RHS).

Table 3-9: A summary of the measurement node mesh for the striploin dataset.

Measurement Nodes of Striploin Dataset								
Striploin #	Striploin # L / R Faces (X) Markings (Y) Nodes Origin, X (mm) Origin, Y (mm)							
1	R	8	9	72	30	45		
2	R	9	9	81	42	45		
3	L	8	7	56	45	85		
7	┙	8	8	64	35	35		
Averages	& Totals	38	52.5					

The chosen spacing of measurement nodes was predetermined to align with industry work being conducted simultaneously. The spacing used for this node mesh was 50 mm in the X direction (across the length / medial-ventral anatomical plane of the striploin) and 25 mm in the Y direction (across the width / caudal-cranial anatomical plane of the striploin). This created a node array of measurements that could be spatially registered for evaluation between other striploins regardless of dimensions and type (both LHS and RHS). In addition to numbering each node (i,j) based upon its x and y coordinate the terminology of "point" (y) and "face" (x) was used (see Figure 3-21).

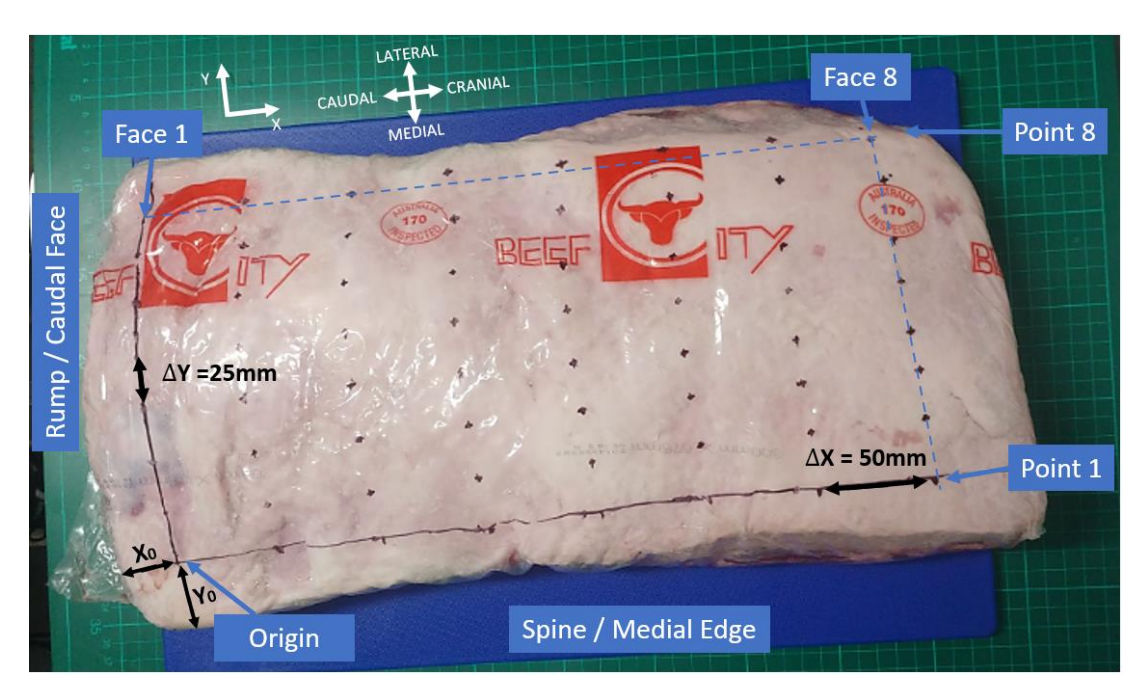


Figure 3-21: The location of the measurement nodes marked for each striploin illustrated on a RHS striploin.

The plastic wrapping of the striploin was pierced using a stainless-steel skewer and marked with black, food-grade gel on the surface of the fat to ensure these measurement points remained at the same location (see Figure 3-22). A sharp boning knife was used to make a cross-sectional cut along the transverse plane of the striploin to expose the measurement nodes on each face (see Figure 3-23).

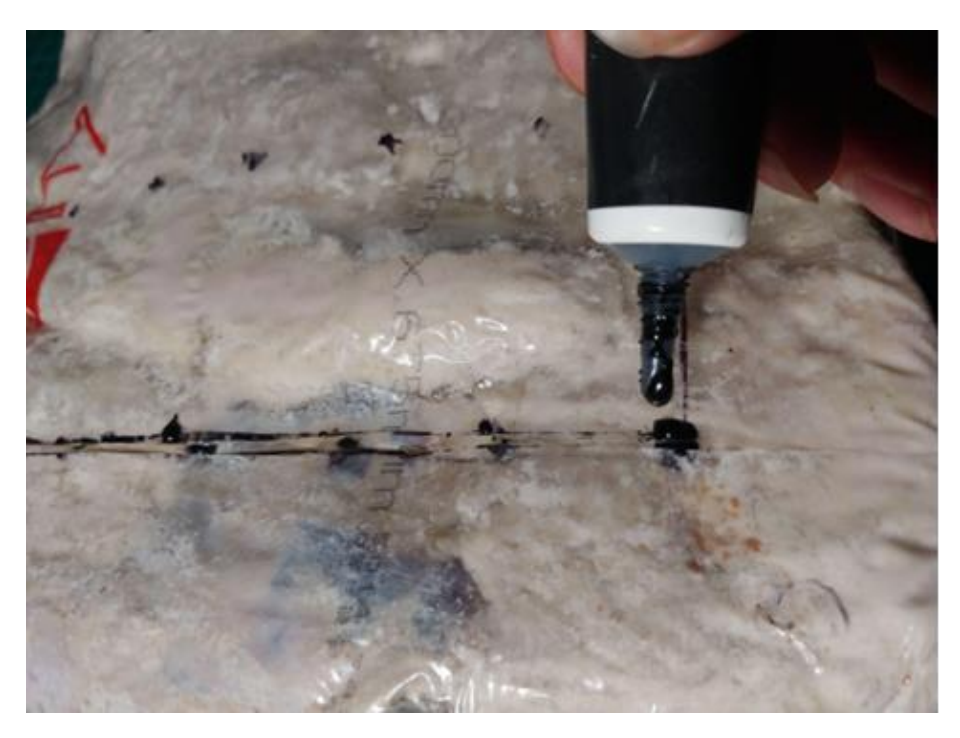


Figure 3-22: Marking the location of the measurement nodes on the striploin fat surface using food-grade gel.



Figure 3-23: Plastic wrapping was cut to create the cross-section face to measure fat thickness at each of the nodes.

The fat depth at each node was measured at each face using a stainless-steel ruler (see Figure 3-24). The fat depth measurements for all nodes were recorded and tabulated on Excel. Comments were also recorded for the instances of discrepancies and interesting phenomena

with regards to the interfaces seen within the cross-section of the striploin. The depth of fat is determined to be the distance from the fat surface to the fat-lean or fat-sinew interface measured perpendicular to the fat surface. The measurement axis of the ruler taken for a cross-section / face is shown in Figure 3-25.



Figure 3-24: Manual measurements of fat depth at each node were taken using a stainless-steel ruler aligned perpendicular to the fat surface at each face.

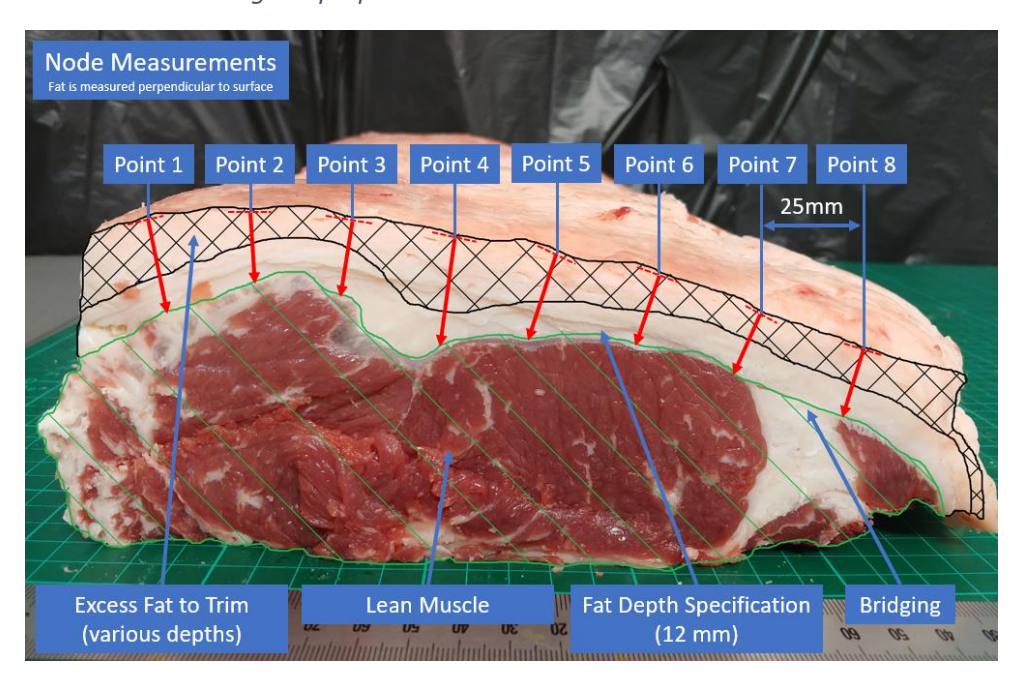


Figure 3-25: The fat depth measurements (red arrow) at each node was measured perpendicular from the fat surface to the fat-lean or fat-sinew interface at a 25 mm pitch (for cross-sections at 50 mm thick) illustrated on a RHS striploin.

One limitation of the measurement process is that there will always be a discrepancy between fat depth measurements taken prior to, and after, trimming. This is due to the product specifications measuring maximum fat depth radial from the fat-lean interface of the striploin, though without the capability of offsetting the trim tool perpendicular to the fat-lean surface there will be a misalignment of the pre-trim and post-trim measurement planes. This is illustrated below for a method of measuring fat depth perpendicular from the fat surface (see Figure 3-26).

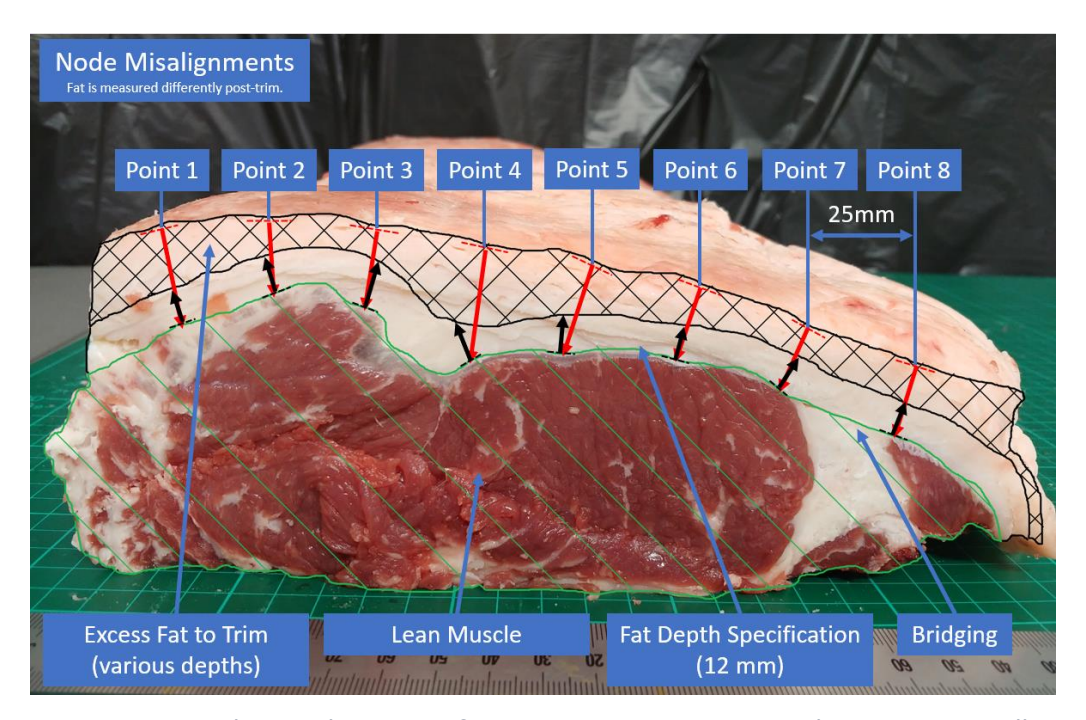


Figure 3-26: The misalignment of measurement axes prior and post trimming illustrated on a RHS striploin is deemed insignificant in this analysis.

The magnitude of measurement misalignment error  $(\theta_e)$  between the fat thickness measurements, pre-trimming  $(FT_{Pre})$  and post-trimming  $(FT_{Post})$ , is dependent upon the difference in angle between the fat surface and fat-lean interface at each considered node and the desired fat trim specification  $(FT_{Post})$ . This unavoidable error is visually illustrated in Figure 3-27.

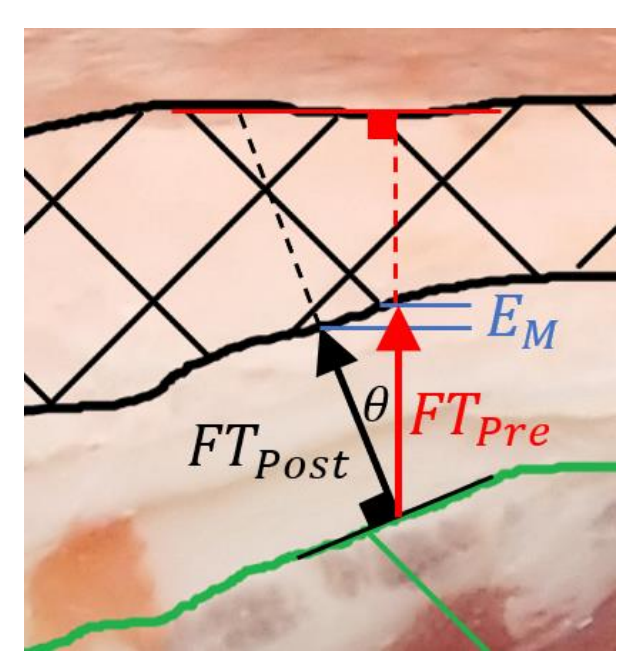


Figure 3-27: An illustration of the insignificant error between pre-trim (measured by a sensor) and post-trim (measured by quality assurance) that occurs due to misalignment of measurement axes.

This error is expressed formulaically in Equation 3.1.

Equation 3.1: Unavoidable misalignment error between sensor and post-trim fat depth Misalignment Measurement Error,  $E_M = FT_{Pre} - FT_{Post}\cos(\theta)$ ,

where:

 $FT_{Pre}$  = target fat thickness pre-trim  $FT_{Post}$  = final fat thickness post-trim  $\theta$  = the angle difference between  $FT_{Pre}$  and  $FT_{Post}$  measurement axes (perpendicular to the fat surface)

It should be noted that the 'bridging' definition used to accept or reject fat trim (see Section 2.1.3) substantially reduces the likelihood of a significant angular error due to omitting steep, intramuscular fat seams being considered the point of measurement against fat specifications. As such, an angular difference between the fat surface and fat-lean interface may be considered to be within the magnitude of  $\pm 30$  degrees ( $30^{\circ} < \theta <$ 

30°). Using the formula above (see Equation 3.1), an approximation of this misalignment error for a 12 mm fat specification is calculated below.

$$E_M = 12 - 12\cos(\mp 30^\circ)$$
  
 $E_M = 12 - 10.39$   
 $E_M = 1.61 \, mm$ 

An error of 1.61 mm has been considered negligible compared to several more substantial errors that are present within such validation processes (e.g., human measurement, sensor measurements, deformation during trimming, etc.). As such, whilst it is important to acknowledge this error it is considered insignificant to the work conducted further in this research.

## 3.4.2 Experimental Analysis

A statistical analysis of the manually measured fat depth dataset  $(f_M)$  of the untrimmed beef striploin was conducted to provide information important to define the operational context (e.g., required sensing depth, node spacing, etc.) to aid the development of a suitable sensing system and sensor performance matrix.

Literature suggests investigation of the dataset distribution of this fat depth dataset ( $f_M$ ) using the Kolmogorov-Smirnov Test (K-S Test) to determine the most appropriate statistical measures to be identified (Jakob, 2021; Specht, 2020; Lall, 2015). In applying the K-S Test it was identified that this dataset was not dissimilar enough to a normally distributed dataset of the same characteristics to reject the null hypothesis of being normally distributed. The conclusion that this dataset is normally distributed is further supported by the kurtosis and skewness statistics shown in the results of this section. Therefore, mean-derived statistical measures (mean, standard deviation and confidence interval) were used for this analysis.

For this application it is critical to identify the range of fat depth to ensure that this can be considered in the selection of a sensor. This is calculated using the unfiltered dataset due to the insignificant skew introduced by outliers in this dataset (see Equation 3.2).

Equation 3.2: Range of Fat Depth

Range of Fat Depth,  $R(f_M) = Max(f_M) - Min(f_M)$ ,

where:

 $f_M$  = the total dataset of fat depth measurements acquired using a ruler (manual measurements)

The addition of a spatial analysis of the fat depth distribution across the untrimmed striploin dataset will enable location-specific insights to be identified. This will inform conclusions that optimise the sensing mesh and cut path generation of an automated system. As such, the following node location and the coordinate system will be employed to enable a spatial description of each node as a unit volume (see Figure 3-28 & Figure 3-29).

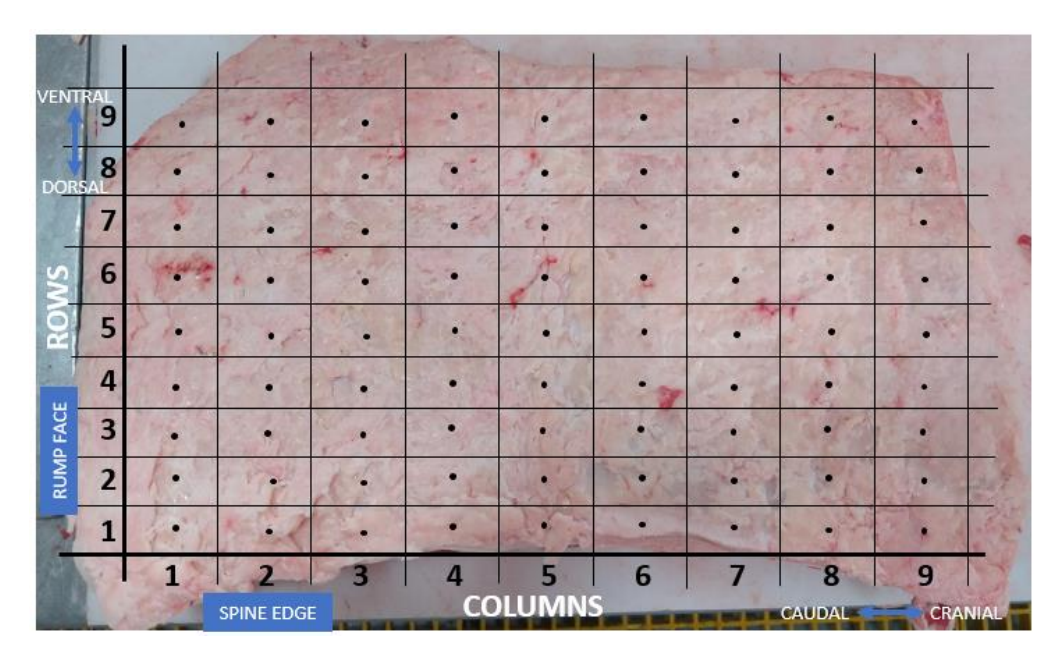


Figure 3-28: Unit volume for each measurement node illustrated on a RHS Striploin. Note: 1R had 8 x 9 & 2R had 9 x 9 node mesh (faces/columns X points/rows).

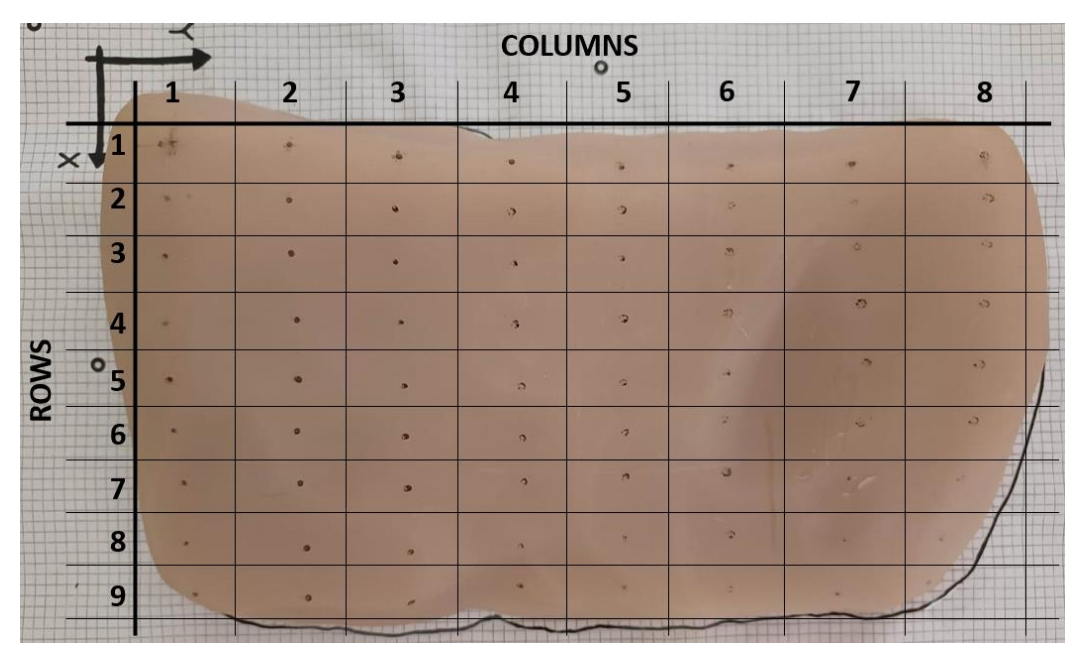


Figure 3-29: Unit volume for each measurement node illustrated on a LHS Striploin. Note: 3L had 8 x 7 & 4L had 8 x 8 node mesh (faces/columns X points/rows).

The striploin fat depth measurements for each node would be averaged across each type, RHS (1R & 2R), LHS (3L & 4L) and in entirety (1R, 2R, 3L, 4L), according to each node position (i, j). In the case whereby there are no measurement acquired from a striploin at a particular node (due to differing node meshes) the node was not

considered in the calculation of average fat depth. This will be calculated as shown in Equation 3.3.

Equation 3.3: Calculations for average fat depth at each node (LHS, RHS & Combined)

Average fat depth at each node (RHS Striploin Dataset),

$$\overline{F_{RHS_{i,j}}} = \sum_{i=1}^{m} \sum_{j=1}^{n} \frac{F_{1R_{i,j}} + F_{2R_{i,j}}}{n_{i,j}},$$

Average fat depth at each node (LHS Striploin Dataset),

$$\overline{F_{LHS_{l,j}}} = \sum_{i=1}^{m} \sum_{j=1}^{n} \frac{F_{3L_{i,j}} + F_{4L_{i,j}}}{n_{i,j}},$$

Average fat depth at each node (Combined Striploin Dataset),

$$\overline{F_{C_{i,j}}} = \sum_{i=1}^{m} \sum_{j=1}^{n} \frac{F_{1R_{i,j}} + F_{2R_{i,j}} + F_{3L_{i,j}} + F_{4L_{i,j}}}{n_{i,j}},$$

where:

 $F_{1R_{i,j}}, F_{2R_{i,j}}, F_{3L_{i,j}}, F_{4L_{i,j}}$  = the manual fat depth measurement matrices for each striploin (1R, 2R, 3L, 4L) with dimensions (n,m)

 $n_{i,j}$  = the number of measurements acquired for the striploin node (i,j) for each dataset (LHS, RHS, combined)

Visualisations were developed to graphically evaluate the spatial relationship of fat depth across the striploin dataset fat depth measurements. The number of nodes were equal to or less than the fat specification (12 mm), as well as the respective distribution of fat throughout the striploin considering measures of mean-derived distribution measures. This will inform automation optimisation through defining the location of nodes that are most likely to not require sensing, or trimming, and the capability of estimating fat depth based upon spatial location of the node within the primal.

Evaluating the gradient of the change in fat depth across the striploin will provide insight into the mechanism of sensing and trimming for a production system. This would include considerations such as: the number, and location of, nodes (optimised for less nodes that are more descriptive to the fat profile) and the most appropriate trimming orientation (the gradient of fat depth introduces complexity within actuation and fixation). The nodes within the combined average fat depth matrix ( $\overline{F_{C_{i,j}}}$ ) that is less than the fat specification (12 mm) will be overridden as 12 mm to then calculate the gradient of the trimming blade for automated trimming of this dataset (as there is no need to trim values of fat depth less than the fat specification of 12 mm). This will be denoted by a trimming cut path dataset,  $T_{C_{i,j}}$ , which was calculated by applying the filter as denoted in Equation 3.4.

Equation 3.4: Filtering of combined average fat depth dataset  $(\overline{F_{C_{i,j}}})$  for nodes with <12 mm fat thickness to create the trimming cut path dataset  $(T_{C_{i,j}})$ .

$$\left[\overline{F_{C_{l,j}}} > 12\right] = \begin{cases} 1 & T_{C_{l,j}} = \overline{F_{C_{l,j}}} \\ 0 & T_{C_{l,j}} = 12 \end{cases}$$

The forward gradient of fat thickness with respect to both width and length travelling out from the sensing mesh origin can be calculated using Equation 3.5.

Equation 3.5: Forward Gradient of the trimming cut path dataset  $(T_{C_{i,j}})$ .

Gradient of Average Trim Cut Path Dataset, 
$$\nabla T_C = \frac{\partial T_C}{\partial x} \hat{\imath} + \frac{\partial T_C}{\partial y} \hat{\jmath},$$

where:

 $T_C$  = the trimming cut path position represented as a matrix of coordinates

The gradient was calculated between nodes in x and y directions independently for comparison, where 'x' is considered to be along the length of the striploin and 'y' is considered to be along the width (trimming from medial to lateral nodes). The forward gradient along the striploin length and width is illustrated in red and blue respectively in Figure 3-30.

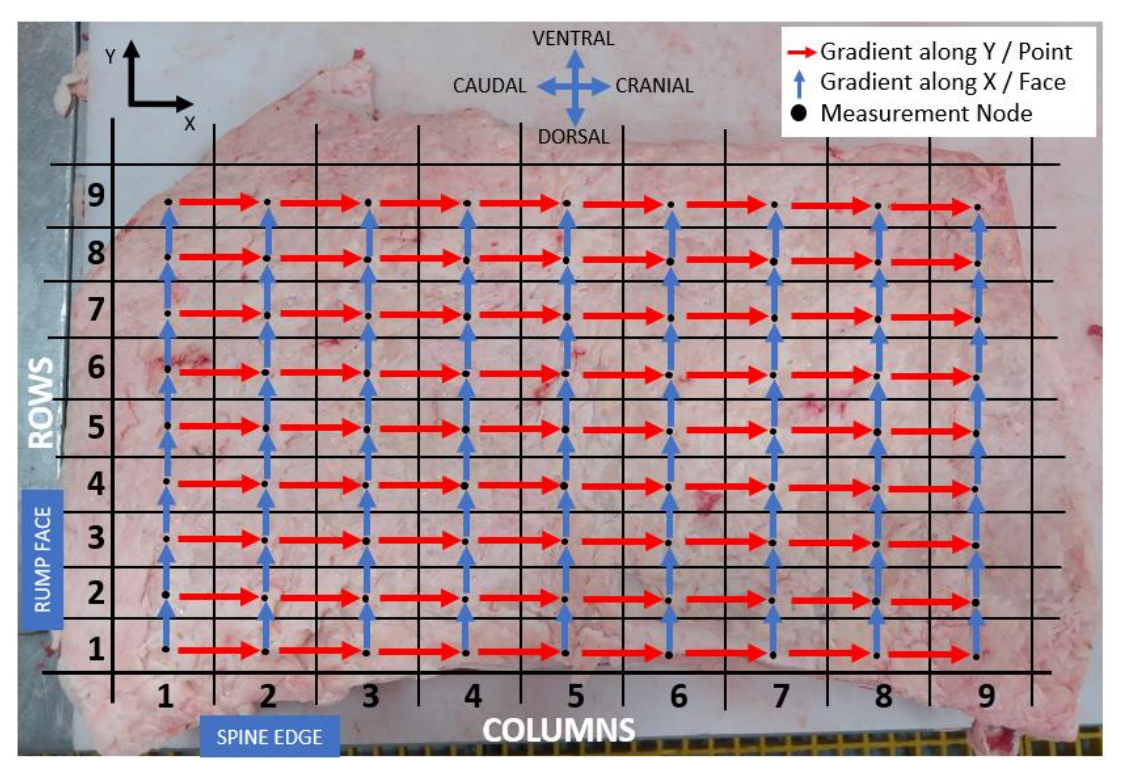


Figure 3-30: An illustration of gradient vectors calculated from average fat depth at each node of striploin datasets developed using a RHS striploin image.

The scalar gradients of the trim cut path for each direction, individually, can be expressed formulaically (see Equation 3.6).

Equation 3.6: Scalar Forward Gradient of the trimming cut path dataset  $(T_{Cij})$ .

Gradient of Trim Cut Path Dataset in X direction,  $T_{C_x}' = \frac{\partial T_C}{\partial x} = \sum_{i=1}^{n-1} \frac{T_{C_{i+1}} - T_{C_i}}{\Delta x},$ Gradient of Trim Cut Path Dataset in Y direction,  $T_{C_y}' = \frac{\partial T_C}{\partial y} = \sum_{j=1}^{m-1} \frac{T_{C_{j+1}} - T_{C_j}}{\Delta y},$ 

where:

 $T_{C_{i,j}}$  = the trimming cut path position at the particular node (i,j)

 $\Delta x$  = the average node spacings in the x direction (50 mm)

 $\Delta y$  = the average node spacings in the y direction (25 mm)

To practically consider the effect of fat thickness gradient in each direction  $(T_{C_x}, T_{C_y})$ , the gradient matrices were evaluated for maximum absolute gradient, maximum positive gradient and average absolute gradient. This is calculated, for both 'x' and 'y' components of  $T_c$ , to compare, and provide insight towards, the trimming orientation of beef striploin. In practicality, difficulties arise in particular trimming scenarios as identified in previous trials delivered upon with industry (Khodabandehloo, 2019), such as:

- A) a large change in blade/trimming tool position (gradient): due to the potential of 'scalloping' and disfiguring the presentation of the striploin surface,
- B) a large, upward of position (positive gradient): due to the potential of the blade lifting the striploin upon rapidly changing orientation within the fat,
- C) the average change in position of the trimming tool: due to the additional programming complexities and the movement time of the robot.

## 3.4.3 Results

The analysis of the fat depth measurements using reference measurements was conducted for all measured nodes (n=272) with additional tables and figures included in Appendix B: Dataset for Manual Fat Depth Measurements. The results of the K-S test for normality are presented in Table 3-10. These results indicate that there is a non-

significant difference between this unfiltered dataset and the equivalent normal distribution dataset (D(272) = 0.062, p = 0.243), and so the dataset was determined to be normally distributed.

Table 3-10: K-S Test results for manual fat depth measurements generated using an online K-S Test statistics tool (Statistics Kingdom, 2022)

Parameter	Value
P-value	0.2429
D	0.06161
Sample size (n)	272
Average (x̄)	16.0018
Median	15.5
Sample Standard Deviation (S)	7.8747
Sum of Squares	16804.7491
K	1.0161
Skewness	0.4865
Skewness Shape	Asymmetrical, right/positive (pval=0.001)
Excess kurtosis	0.4278
Kurtosis Shape	Potentially <b>Mesokurtic</b> , normal like tails (pval=0.146)

Unfiltered and outlier-filtered (+- 3SD from the mean) datasets were statistically evaluated to evaluate the effect of these outliers to the manual measurement dataset. These datasets are seen to be similar as shown in Table 3-11.

Table 3-11: Statistical summary of manual fat depth measurements (n = 272)

Fat Depth of Striploins (n = 272) for Manual Dataset								
Statistical Measures	Unfiltered Dataset	Filtered Dataset (3SD)						
Minimum Fat Depth (Q <sub>0</sub> )	0 mm	0 mm						
25th percentile of Fat Depth (Q1)	11.0 mm	11.0 mm						
Median of Fat Depth (Q2)	15.5 mm	15.0 mm						
Mean of Fat Depth	16.0 mm	15.7 mm						
75th percentile of Fat Depth (Q <sub>3</sub> )	21.0 mm	21.0 mm						
Maximum Fat Depth (Q4)	44.0 mm	38.5 mm						
Interquartile Range (IQR)	10.0 mm	10.0 mm						
Standard Deviation (SD)	7.9 mm	6.8 mm						
Range (Max - Min)	44.0 mm	38.5 mm						
Lower Outlier Boundary (3SD)	-7.6 mm	-4.8 mm						
Upper Outlier Boundary (3SD)	39.5 mm	36.1 mm						

Three outliers (3SD) were identified within the unfiltered dataset (40 mm, 40.5 mm and 44 mm); though the slightly positive skewed distribution (right tailed) was not particularly created from these outliers. Instead, the skewness of this dataset was primarily due to the significant number of measurements below the dataset mean. The unfiltered dataset was concluded to be representative of the fat depth measurements and therefore used for further analysis. The distribution of this dataset is illustrated in Figure 3-31 & Figure 3-32.

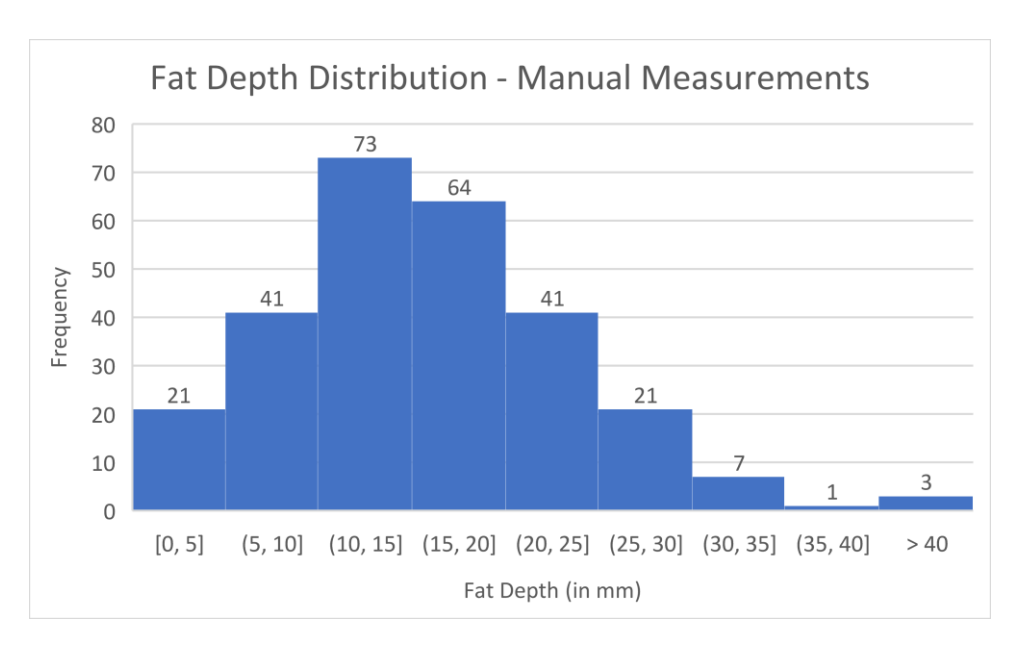


Figure 3-31: Histogram plot for the fat depth across measurement nodes.

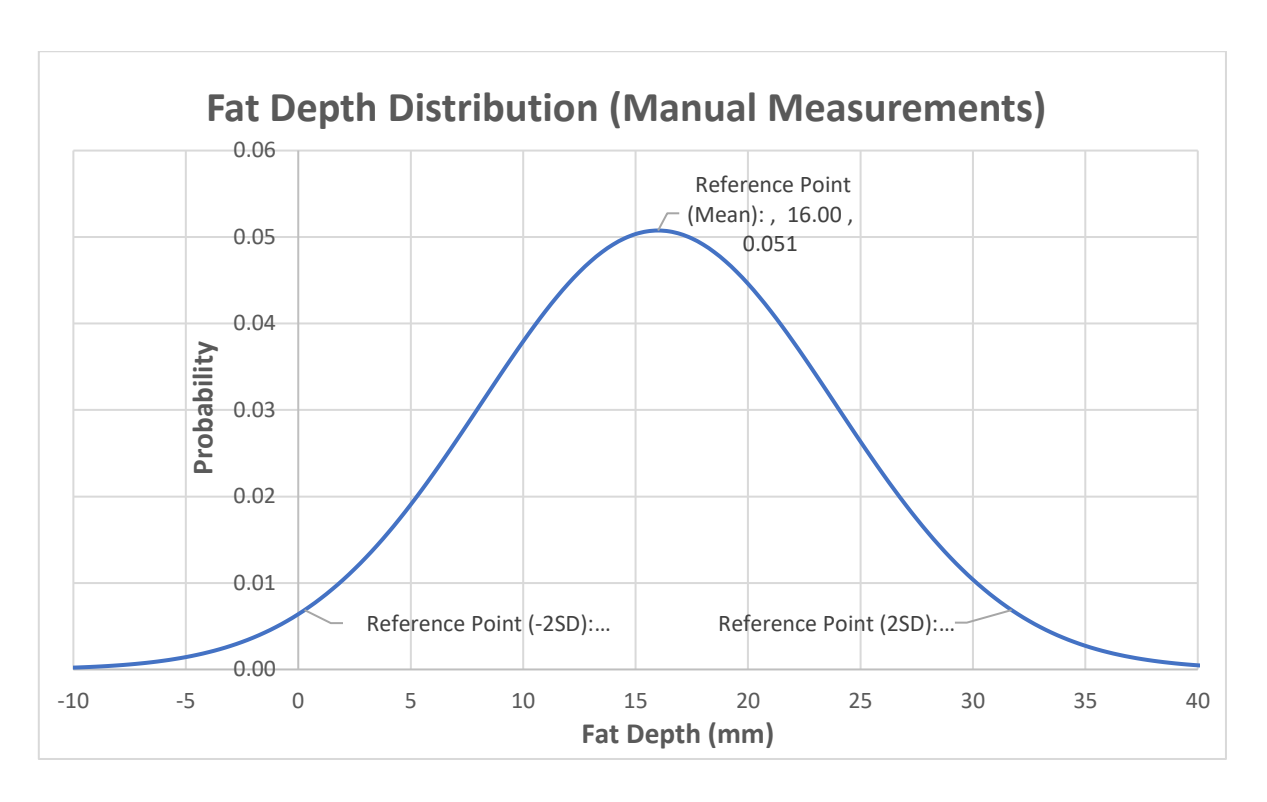


Figure 3-32: Distribution plot for the fat depth across measurement nodes.

The histogram and distribution of the fat depth measurements (manual measurement) reflects a normally distributed dataset and highlights the significant distribution of measurements being centrally distributed at the mean (16 mm). This analysis quantifies the characteristic fat depth of the striploins that are to be presented for fat

trimming. For a 95% confidence interval, the subcutaneous fat depth of 0 – 32 mm can be expected for an untrimmed striploin with the maximum depth being 44 mm. This is an important consideration for defining the range of a suitable sensor to measure fat depth of untrimmed striploin primals.

The cumulative histogram illustrated in Figure 3-33 highlights that approximately 45% of all nodes measured for this analysis have less than 12 mm of subcutaneous fat depth. If the trimming threshold was increased to 17 mm (since trimming at a depth of only 5 mm could be difficult for a slicer or robot) then the number of nodes required to be trimmed would be further reduced to 28% of those surveyed.

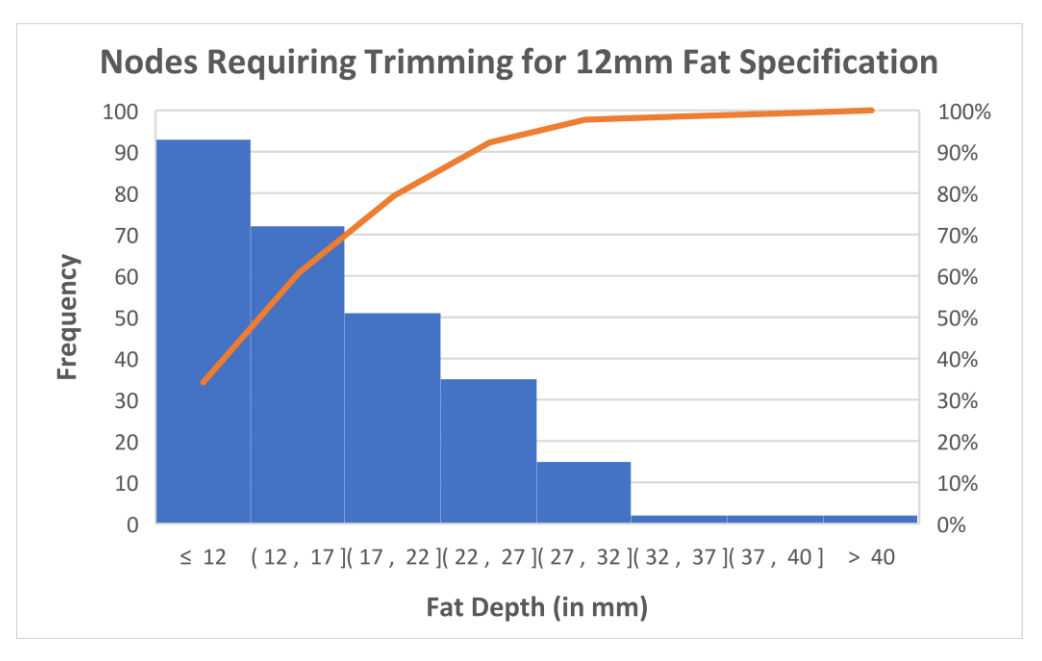


Figure 3-33: Nodes requiring trimming for the fat trim specification of 12 mm.

The spatial analysis the average fat depth for untrimmed striploin types, LHS & RHS, is illustrated separately (see Figure 3-34). These figures illustrate the locations of nodes that have 12 mm of less fat depth (coloured red) and hence do not require trimming or sensing. Note: The LHS striploin is vertically flipped to align to anatomical planes (caudal-cranial, lateral-medial) of the RHS to visualise spatial patterns more easily

		1	3					-	RH	S
VENTRAL 9	16	18	18	18	35	33	21	20	26	
DORSAL T	12	21	15	16	21	30	19	20	20	
7	22	22	20	15	12	13	15	17	19	
§ 6	15	26	24	19	16	12	10	11	13	
2 5	10	21	24	17	14	14	8	8	11	
4	8	11	23	16	18	15	10	12	12	The second
A CE	8	13	15	11	12	5	7	11	28	
RUMP FACE	5	11	7	4	6	8	9	18	5	
<sup>2</sup> 1	11	6	9	6	9	11	15	20	9	
	1 SPINE ED	2	3	4	l 5 DLUMN	6	7	8	9	
		JUE			4-4-4111	THE RESERVE AND PERSONS NAMED IN		CAUDAL	- C 192	WIAL
		NGE	-					CAUDAL	To State of	S
, a		, de	NO		OR RO		INT 9	CAUDAL	LH	
VENTRAL 8	20	18	NO 20			W / PO	INT 9	21	To State of	
VENTRAL					OR ROV	W / PO			H	
VENTRAL 8 DORSAL 6	20	18	20	DATA F	OR ROV	W / PO 1 2 8 2	22	21	27	
VENTRAL 8 DORSAL 6	20 23	18 20	20 24	DATA F - 28	OR ROV 3 3 2:	W / PO 1 2 8 2 1 1	22	21 30	27 23	
VENTRAL 8	20 23 18	18 20 26	20 24 23	DATA F - 28	OR ROV 3. 3. 2. 2. 2. 1.	W / PO 1 2 8 2 1 1 8 1	22	21 30 16	27 23 17	
DORSAL P	20 23 18 20	18 20 26 22	20 24 23 25	DATA F	OR ROV 3.3.3.2.2.2.2.2.1.3.0.2.2.2.2.1.3.0.2.2.2.2.2.2.2.2.2.2.2.2.2.2.2.2.2.2	W / PO 1 2 8 2 1 1 8 1	22 2	21 30 16 13	27 23 17 14	
DORSAL P	20 23 18 20 15	18 20 26 22 24	20 24 23 25 23	DATA F	OR ROV  3 3 2 2 1 2 1 2 2 1 2 2	W / PO 1 2 8 2 1 1 8 1 1 1	22 22 .6 .3	21 30 16 13	27 23 17 14 16	
DORSAL P	20 23 18 20 15	18 20 26 22 24 23	20 24 23 25 23 17	DATA F  28  22  22  20  21	OR ROV 3. 3. 2. 2. 1. 2. 2. 2. 3. 4. 2. 4. 5. 6. 6. 7. 8. 8. 8. 8. 9. 9. 9. 9. 9. 9. 9. 9. 9. 9	W / PO  1 2  8 2  1 1  8 1  1 1	22 22 .6 .3 .6	21 30 16 13 13	27 23 17 14 16 19	
DORSAL P	20 23 18 20 15 9	18 20 26 22 24 23 20	20 24 23 25 23 17 14	DATA F  28 22 22 20 21 12	OR ROV  3. 3. 2. 2. 2. 1. 2. 4. 2. 8. 9.	W / PO  1	22 22 .6 .3 .6 .5	21 30 16 13 13 16 15	27 23 17 14 16 19 22	

Figure 3-34: RHS & LHS striploin datasets highlighting unit volumes with 12 mm or less fat depth (highlighted red)..

By combining all corresponding nodes of the total striploin dataset and mapping averaging fat thicknesses (e.g. average fat thickness for node i,j for all LHS and RHS striploins) this spatial fat distribution pattern is further emphasised (see Figure 3-35). The pattern illustrates that measurement nodes within 50-75 mm of the striploin spine edge (both LHS and RHS) will typically not require trimming or sensing. This pattern illustrates the exception of a fat deposit approximately found 50 mm from the cranial face of the striploin.

			1			TO THE				COMBI	NED
VENT	9	16	18	18	18	35	33	21	20	26	
DORS	8	16	19	17	16	26	26	20	23	20	
	7	23	21	22	21	20	18	23	20	19	
NS	6	16	26	23	20	18	14	13	14	13	
ROWS	5	15	21	24	19	16	14	11	11	11	
	4	11	18	23	18	19	15	12	14	12	THE STREET
RUMP FACE	3	9	18	16	16	16	10	12	15	28	
RUM	2	/7	15	10	8	7	8	12	20	5	
N	1	11	7 <	8	7	9	12	16	18	9	
		1	2 SPINE EDGI	3	4 CC	5 LUMN	6	7	8 CAUDAL	9 CRAI	NIAL

Figure 3-35: Combined striploin dataset highlighting unit volumes with 12 mm or less fat depth (highlighted red) illustrated on a RHS striploin primal.

For each of these datasets (LHS, RHS and combined) the fat depth distribution dataset (normally distributed) can be spatially observed considering their respective mean and standard deviation (see Table 3-12).

Table 3-12: Statistical summary of fat depth measurements for LHS, RHS and Combined Striploin Datasets

Statistical Summary of Striploin Dataset Fat Depth							
RHS LHS Overal							
Minimum	-	-	-				
Q1 (25%)	9	13.25	11				
Median	13.5	18	15.5				
Mean	14.6	17.8	16.0				
Q3 (75%)	18	22.5	21				
Maximum	44	40.5	44				
Standard Deviation	7.6	7.9	7.9				

These datasets are illustrated with the average fat depth highlighted red for unit volumes with less than or equal to their average and the atypically large average fat depths more than 1 standard deviation above the mean (the largest 32%) being highlighted green (see Figure 3-36 & Figure 3-37). These figures illustrate the large deviations of fat depth across the striploin. The LHS striploin in Figure 3-36 is vertically flipped to align to anatomical planes (caudal-cranial, lateral-medial) of the RHS to visualise spatial patterns more easily.

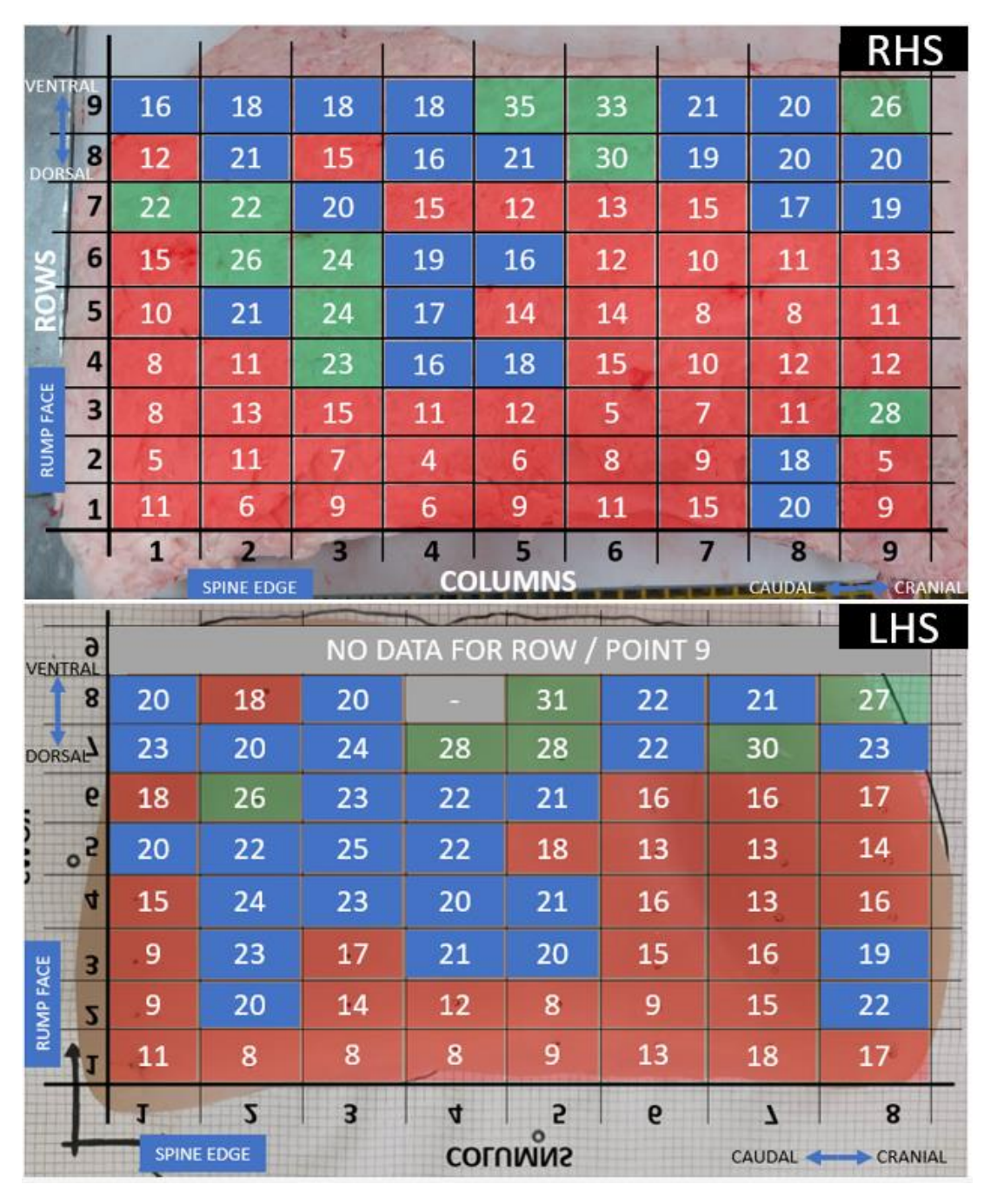


Figure 3-36: RHS (top) & LHS (bottom) striploin datasets highlighting large deviations of fat depth across the striploin.

		1			Same o		1	1	COMBI	NED
VENTRAL 9	16	18	18	18	35	33	21	20	26	
DORSAL DORSAL	16	19	17	16	26	26	20	23	20	
7	23	21	22	21	20	18	23	20	19	
SN 6	16	26	23	20	18	14	13	14	13	
ROWS 2	15	21	24	19	16	14	11	11	11	
4	11	18	23	18	19	15	12	14	12	
3 A Z	9	18	16	16	16	10	12	15	28	
RUM 2	7	15	10	8	7	8	12	20	5	
1	11	7 <	8	7	9	12	16	18	9	2
	1	SPINE EDG	3	4 CO	5 LUMN	6	7	8 CAUDAL	9 CRA	NIAL -

Figure 3-37: Combined (RHS & LHS) striploin datasets highlighting large deviations of fat depth across the striploin.

The forward gradient across the typical striploin using the cut path for the average fat depth of the combined striploin dataset is shown in Figure 3-38 and Figure 3-39. A summary of the gradient measures of each direction of cutting is shown in Table 3-13 which identifies significant gradient statistics for trimming along the striploin length (X) and width (Y). These gradient measures differ significantly for trimming cut paths along the length and width of the striploin. For trimming across the length (X direction) of the striploin it would be approximately half of the gradient, both on average and as a maximum, in comparison to trimming across the cross-section of the striploin.

VENTRAL 9	3	0	0	19	-2	-14	1	6	1
DORSAL T	4	-2	-2	12	0	-7	4	-4	
7	-2	1	-1	-1	-3	6	-3	-1	
S 6	11	-3	-4	-2	-5	-2	2	-2	
2 5	7	3	-6	-3	-3	-2	0	0	
4	7	6	-5	1	-4	-4	2	-2	
3 — Sump FACE	7	-2	0	0	-5	0	3	15	
2	3	-3	0	0	0	0	9	-9	
1	0	0	0	0	0	5	2	-7	
1	2 SPINE EDGI	3	4 CO	5 LUMN	6	7	8 CAUDAL	9 CRA	NIAL

Figure 3-38: Forward gradient of the tool cut path moving along the length of the striploin calculated with combined average fat thickness dataset.

	11			2 30		2000		-			
VENT	9	1	-3	2	5	20	17	2	-8	13	
DOR	8	-16	-3	-10	-12	13	19	-7	8	2	
	7	14	-12	-3	3	4	7	23	14	15	
NS	6	3	10	-3	2	5	1	1	4	1	
ROWS	5	7	8	3	2	-7	-4	0	-4	0	
	4	0	0	17	5	7	8	0	-2	-36	
RUMP FACE	3	0	7	9	9	9	0	0	-11	36	
RUM	2	0	7	0	0	0	0	-10	3	0	4
31	1	4:1	1		1		1	1	1	1	1000
		1	2 SPINE EDGE	3	4 CO	5 LUMNS	6	7	8 CAUDAL	9 CRA	NIAL

Figure 3-39: Forward gradient of the tool cut path moving along the width of the striploin calculated with combined average fat thickness dataset.

Table 3-13: Summary of Gradient Measures for Striploin Dataset

Summa	Summary of Gradient Measures for Trim Cut Path (Tc)								
Direction	Absolute Average (degrees)	Absolute Maximum (degrees)	Positive Maximum (degrees)						
X	3.5	18.9	18.9						
Υ	6.9	35.5	35.5						
Relative Difference	51%	53%	53%						

## 3.4.4 Discussion

The findings within the analyses presented on the subcutaneous fat distribution of beef striploins highlight several insights for informing the automation of fat trimming beef striploin.

The striploin primal's length, width, height, and weight show considerable variability, with the width and weight exhibiting the most variability. This variability is largely due to human error in the approximation of cutting lines and the curvature of the cranial/rib face. This finding supports referencing the node mesh from the spine edge and the caudal cross-section to define the sensing mesh for the remainder of the research and is recommended in future work. This will provide a more accurate reference between the sensing nodes with respect to locations on the striploin and therefore enable node-by-node spatial relationships to be comparable in future work.

The fat depth measurements, conducted for all measured nodes (n = 272), were identified to be normally distributed (at a 95% confidence level) without major outliers skewing the characteristics of the dataset. evaluated for normality using the K-S test at a 95% confidence level. This suggests that statistical analyses that derive from the mean may be adequate for characterising the fat distribution of a striploin by meanderived statistics for comparative evaluations. This is useful for the

application of developing fat depth models based upon typical fat depth characteristics. For example, perhaps interpolation by the mean may be used for developing an automated system for use in a different processing plant if the means can be compared. Additionally, this analysis has highlighted the typical range of fat depths that a sensing system will need to measure to. The mean fat depth was found to be 16 mm, with a 95% confidence interval indicating that the majority of measurements will be at fat depths between 0 – 32 mm. The deepest measured fat depth in this dataset (n = 272) was identified to be 44 mm. In contrast, literature suggests that the fat depth of an untrimmed beef striploin is 2 mm - 75 mm though this investigation was conducted at a single processing plant which differs from the processing plant consulted for this thesis (Khodabandehloo, 2018). To ensure that the maximum range is designed for, the fat depth range for untrimmed beef striploin will be considered 0 - 75 mm. This range is an important consideration in Chapter 5 and 6 for defining the depth penetration capabilities of a suitable ultrasound sensor to measure fat depth of untrimmed striploin primals.

The analysis of fat depth characteristics revealed insights useful for the development of an automated fat trimming system. Overall, it was found that 45% of nodes are typically less than 12 mm in fat thickness with an average fat depth of 16 mm (72% of nodes). Such findings provide insight into the possibility of determining erroneous values that can occur through sensor malfunctions and therefore prevent instability in the control system in generating cut paths.

The spatial patterns presented with reference to the anatomical location on the striploin provide insights towards the optimisation of the sensing and trimming node mesh and the cycle time of an automated system. The key anatomical patterns identified for striploin fat thickness datasets (shown in Figures 3-38 & 39) that inform practical optimisation strategies are provided below:

- Typically, nodes that were within 50 mm from the spine edge of the striploin exhibited a fat thickness of less than 12 mm.
- As such, 22.2% of the node mesh may be omitted from the sensor node mesh. With generalised presumption that 4 mm error is unnoticeable the nodes within 75 mm from the spine edge can be omitted (33.3% of nodes).
- A region of significant fat depth significantly higher than the mean of the distribution located at 50 200 mm from the caudal face and from past 75 mm from the spine edge to the flank edge. This area of interest travels from the flank edge into the striploin along a 45-degree cross-section between the caudal face and flank edge. An optimisation strategy would be to reduce the node spacing within this region (more nodes per area) and increase the spacing in other areas of the striploin that has a more uniform fat thickness distribution. This would enable the sensor node measure to better fit the striploin fat profile without increasing the number of nodes and extending the cycle time of the sensing routine.
- The striploin tail has a significantly higher distribution of fat thickness that typically extends 50 mm from the flank edge. This fat thickness is consistent across the entire length except for the centre and the cranial face which spikes with large fat deposits. An optimisation strategy would be to reduce the node spacing in the centre to capture the fat profile in more resolution at the deep fat deposit and perhaps use a camera to measure fat thickness on the cranial face of the striploin. This would enable the sensor node measure to better fit the striploin fat profile at the area of large fat deposits without increasing the number of nodes and extending the cycle time of the sensing routine.

An even more substantial optimisation could be achieved if the fat thickness at the anatomical location of these nodes could be estimated without as many or any sensing nodes at all based on a heuristic model or estimate. The normally distributed fat depth dataset suggests that simple mean-derived heuristics may be employed to estimate fat depth but further work with a significantly large dataset is required to conclude on this hypothesis.

The gradient measures, which differ significantly for trimming cut paths along the length and width of the striploin, clearly indicate that the least complex orientation of trimming is along the X axis (lengthwise). The average gradient changes mean that a more complex cut path is required in the widthwise direction. The maximum gradient, which is twice as complex when travelling across the faces, poses challenges in robotics due to the potential of lifting of the primal (prone to occurring with steep positive gradients) or the inability to manipulate the tool within the meat without deviating from the generated cut path through deforming the striploin. As such, with the findings presented (see Table 3-13), it was recommended that trimming lengthwise be advantageous for considerations of the tool cut path gradient. This would further ensure that the automated trimming system is capable to perform without the limitation of the cutting tool being dextrous enough to cut into sudden, deep pockets of subcutaneous fat.

#### 3.5 Conclusion

The research conducted in this chapter has provided significant insights into the key parameters and characteristics that need to be considered for developing an automated fat trimming system for beef striploins:

 The physical characteristics (dimensions, weight, shape, fat cover), and variability of these dimensions, for a typical striploin presented to Slicers through the processes implemented by the collaborating processor.

- The processing constraints (time, space) to be considered for the process of fat trimming beef striploin.
- The range and spatial distribution of subcutaneous fat tissues across beef striploins to be considered for defining the sensing node mesh and trimming cut path of an automated system.

The striploin's dimensions and weight ranges and variability inform the definition of the work volume and payload requirements of an automated system. This processing cut path variability that occurs largely due to human error in the boning process causing curvature of the cranial/rib face and variation of the flank edge identifies the caudal/rump face and the spine edge being most consistently cut. This finding supports referencing the node mesh from the spine edge and the caudal cross-section to define the sensing mesh for the remainder of the research and is recommended in future work. This will provide a more accurate reference between the sensing nodes with respect to locations on the striploin and therefore enable spatial relationships to be implemented to optimise the sensing node mesh and robotic cut path development.

The condition of the fat cover also shows variability, with instances of fat cover damage observed in some striploins. However, the expected probability for instances of fat tears affecting measurements for a fat trimming system was calculated to be only 10%, which was considered insignificant to the sensing node mesh. As a result, for this study the subcutaneous fat surface will still be considered for ultrasound sensing in contrast to the recommendation from Khodabandehloo (2018).

The time-motion analysis identified an average processing time of 27 seconds for the fat trimming element of the Slicers' trimming tasks, with a 95% confidence interval for a processing time range of 12 – 42 seconds. Further, only 2 units could be reasonably installed for fat trimming due to the limited number of fat trimming stations available, all

with the approximate footprint of 1x1.5m. These constraints further inform that the total cycle time (sensing and trimming) of a feasible automated system will need to be between one to half of the processing line speed. This timing provides a guideline for the response time that an automated system should aim for when completing automated fat trimming operation. With the presumption of operating at the same speed as a human operator, this constraint defines the cycle time to approximately 27 – 54 seconds per striploin. This provides an estimate for which to aim towards for both sensing and trimming to be completed within and gives an appropriate benchmark for determining response time of a suitable sensor (see Chapter 4) and an appropriate number of nodes in the sensing mesh of a feasible automated system.

Due to the requirement to apply 'bridging' and 'planing' techniques to suitably trim striploin to specification a path-planning sensing approach is required. This highlights the importance of using a sensing node mesh to define a cut path as opposed to simply generating a cut depth at each node independently. This highlights the importance of optimising the sensor node mesh to balance the need of completing the sensing cycle as soon as possible (dependent upon the sensor response time and the number of nodes in the mesh) whilst representing the fat profile as precisely as possible to provide the best capability to trim to a maximum fat specification of 12 mm on a continuous path.

The analysis of the subcutaneous fat depth of beef striploin has revealed several key characteristics that have significant implications for the development of a suitable sensing system and an automated system for uniform fat trimming. The fat depth measurements were identified to be normally distributed, with a mean fat depth of 16 mm and a 95% confidence interval indicating that the majority of measurements will be at fat depths between 0 - 32 mm. The deepest measured fat depth was

identified to be 44 mm – hence this will be considered for the penetration depth range of a suitable ultrasound sensor.

With further insights from applying sensing to acquire fat depth measurements, and further analysis of fat distribution, an optimisation of node locations are likely to contribute towards automation optimisation. A probabilistic approach, based upon spatial relationships of fat depth distribution across the striploin would enable many nodes to be omitted from the sensing and trimming processes of the automated system. The normality of fat distribution, and the spatial patterns observed suggest that through further analysis spatial modelling may assist or enhance fat depth estimations alongside, or in replacement, of sensing techniques as well as the capability to apply generalised cut path and fat depth learnings between processors through a comparison of mean fat depth of 'typical' striploins.

The gradient measures indicate that the least complex orientation of trimming is along the X axis (lengthwise). As such it is suggested that the trimming orientation, and therefore if sensing is to occur just in front of the trimming, the sensing process should also be measured lengthwise.

In conclusion, the findings of this chapter provide a comprehensive understanding of the key parameters and characteristics that need to be considered for developing an automated fat trimming system. The insights gained from this study contribute towards the broader objective of developing an automated system capable of trimming excess fat on beef striploins, informed by a thorough analysis of fat characteristics and industry standards. This chapter contributes towards the following chapter to describe the parameters to be considered within a sensor performance metric to define feasibly ultrasonic sensors for development within sensing systems presented in Chapter 5 and 6.

# CHAPTER 4: SENSOR PERFORMANCE METRICS USING CT BENCHMARKING

This chapter outlines the development undertaken to enable computed-tomography technology to be used for the application of measuring the fat depth of a beef striploin primal. The output of the CT analysis is the estimation of the 'gold standard' for which more practical sensors may be evaluated against. In addition to providing benchmarking, CT imaging measurements were utilised to evaluate the fat depth of beef striploin primals prior to trimming to inform the operating range required of a sensor for this application.

The output of this chapter is a weighted performance evaluation matrix to define the minimum feasible requirements and best possible performance for a sensing system capable for integration within an automated beef striploin fat trimming system. This performance evaluation matrix identifies the key performance metrics deemed most appropriate to the application of beef striploin fat trimming is presented as well as their significance to evaluating an appropriate sensing system (denoted by a metric weighting).

## 4.1 Introduction

To benchmark these performance metrics a sensing system was developed using CT imaging that was capable of acquiring the measurements that could inform automated trimming. Aligned to literature, this investigation enables the approximation of what is possible using the 'gold standard' of medical-grade sensing and, in conjunction with considering the context of this application, provides insight into how a suitable sensing system may perform with respect to these metrics (Merriam, 2005; Cook, Shirazi & Gardner, 2016; Cook & Anderson, 2017, Morton, 2020; Four Dimensional Digital Imaging Inc, 2021). This

evaluation will also define the significance of each of these metrics to inform a suitable sensing system will be investigated.

## 4.1.1 Performance Metrics

Within literature it is common for a sensor evaluation framework to be applied in order to evaluate the performance of a sensor for a particular application (Coravos et al., 2020; Kuorilehto, Hännikäinen & Hämäläinen, 2008). To design such a framework, the key metrics that are of high importance for the particular application, and context the sensor is used, needs to be identified (Border, 2016). Once these performance metrics are defined weightings can be associated with these to ensure that each metric is considered proportional to their importance (Zhao, Song & Xin, 2011; Rieger & Majchrzak, 2016).

The selection and prioritisation of performance metrics for sensor evaluation are highly application-specific. To effectively assess sensor performance in the context of automated beef striploin fat trimming, it is crucial to consider the unique requirements of this application (Niesten et al., 2019; Brooke, 2016). The relevant performance metrics will be identified, substantiated by literature, and then used to establish a tailored evaluation framework for this specific application (Drury et al., 2022; Song et al., 2022).

The tolerances and numerical targets of the metrics for an evaluation framework must be defined within the context of the specific application. The flexible and non-homogenous nature of meat products means that 'true' reference measurements are difficult to define. As such, to better define these performance metrics a 'gold standard' sensing system is appropriate to provide a measurement of the best available performance per consensus as a reference (Versi, 1992; Goldsack, 2020). This approach is typically used within literature to define the performance metrics, and thus the performance of sensors, in comparison to the

sensor that has consensus to provide the best performance (Godfrey et al., 2015; Müller et al., 2017). For the application of sensing tissue interfaces within red meat processing the 'gold standard' sensing technology is considered to be medical grade CT imaging (Meat & Livestock Australia, 2022).

## 4.1.2 Chapter Aims

The aim of this chapter was investigated through the two research questions posed to focus this chapter to address the various considerations within the objective.

- **1)** What is the 'gold standard' performance for sensing fat depth using CT imaging according to the performance metrics considered important for developing a fat trimming automated system?
- **2)** Considering performance metrics, context-derived weightings, and 'gold standard' benchmarks, how can a sensor performance evaluation matrix be created for the context of automated fat trimming?

## 4.2 Experimental Setup

This section provides the data collection and data analysis methods implemented to benchmark a medical-grade CT imaging system. This sub-section includes the methods for CT imaging of striploins, the registration of nodes between CT and manual measurements, and the calculation of error between the CT and manual measurements.

**Experiment Samples:** The same samples (Striploin 1R, 2R, 3L & 4L) were used as those selected for the analyses presented within Chapter 3. These 4 striploins deemed to be 'typical' as their dimensions and characteristics were within 2SD of the survey conducted in Chapter 3 (see Table 4-1).

Table 4-1: Comparison of striploin dataset with 'typical' striploin characteristics.

Dataset vs Typical Striploins										
Carin lain #	1.75	LSPINE	WRUMP	Нмах	Weight					
Striploin #	L/R	(mm)	(mm)	(mm)	(kg)					
1	R	428	282	89	8.85					
2	R	435	305	92	6.58					
3	L	410	235	88	6.58					
7	L	445	235	76	6.68					
Average	Average 430 264 86 7.17									
Lower Bou	Lower Bound (-2SD) 387 220 72 6.63									
Upper Bou	nd (+2SD)	457	310	103	9.98					

**Node Marking:** The nodes were marked on the plastic of the striploin fat surface as shown in Chapter 3 before CT imaging (see Figure 3-21).

Fat Depth Measurements using CT Imaging: A Siemens Somato GoUp CT machine was used to acquire the reference measurements for this experiment. Striploins were stored in a refrigerated trailer before and after CT scanning and were not unwrapped or cooled during the scanning process which took approximately 10 minutes including preparation. A simple rig was used to allow the striploins to lay flat on a board to prevent the deformation of this fat profile during scanning. The striploins were aligned using the laser sight of the CT to ensure that the cross-sectional images of the CT were close-to perpendicular (see Figure 4-1). This plane alignment simplified the visualisation of the fat profile throughout the striploin and assist in providing a means of calibrating images.



Figure 4-1: The laser lines of the CT imaging system were used to align to the front edge of the striploin (rump / cranial face) to align nodes to appear on similar cross-sectional images.

In preliminary CT imaging trials it was found that this alignment method was not accurate enough to use to determine the position of nodes within CT images without additional aids. Medical-grade CT markers which consisted of 2.1 mm ball bearings embedded within adhesive tags were attached to the nodes of the striploin prior to scanning (see Figure 4-2). In doing so, the position of these nodes was able to be visualised in 3D space within CT images (see Figure 4-3).



Figure 4-2: The adhesive CT markers were attached on the plastic at the locations of the prescribed measurement nodes.

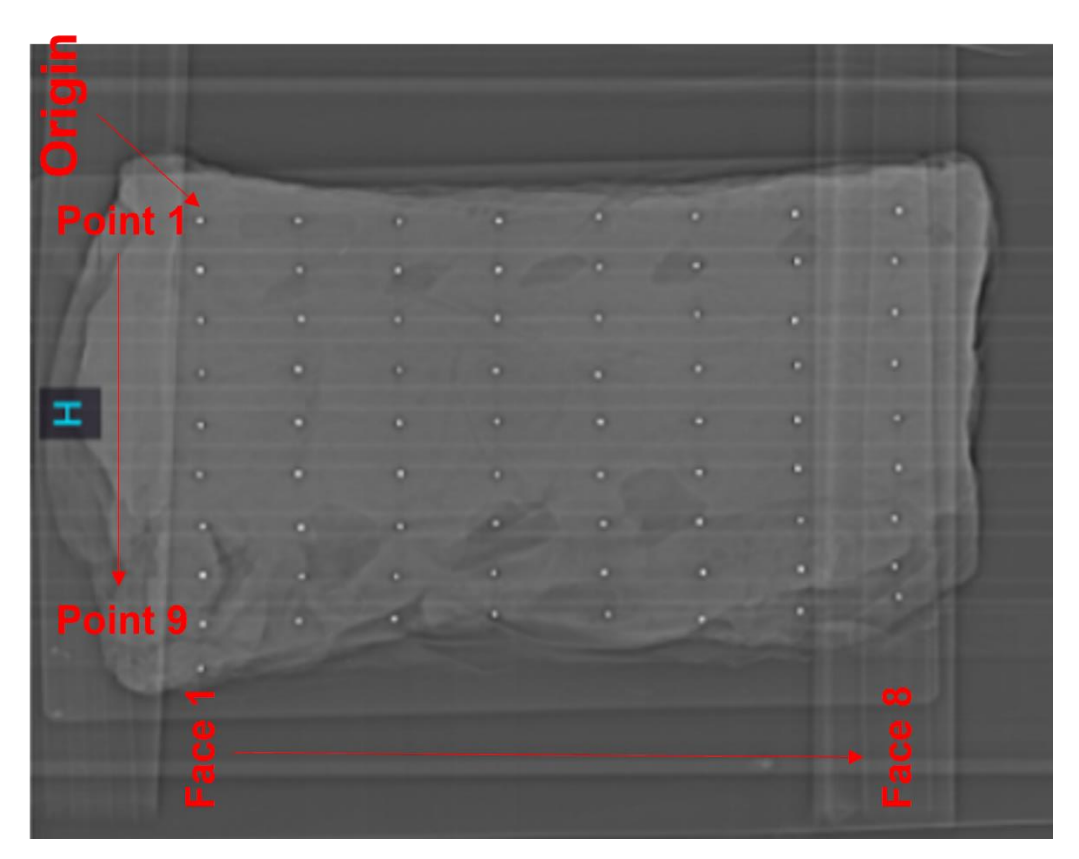


Figure 4-3: Screenshot of CT images illustrating CT markers highlighting measurement node locations shown on Striploin 1.

Although the CT markers provided referencing positions (nodes) to be identified these caused image distortion commonly referred to as artifacting. Thes CT markers affected image clarity and the ability to clearly identify the fat surface to measure from (see Figure 4-4). To avoid artifacting issues a nearby image was chosen to measure from. As each image is a 0.6 mm slice it was deemed that offsetting a few images would be an acceptable compromise. In this analysis the maximum number of images offset to avoid artifacting was 4, and hence a maximum offset of 2.4 mm from each measurement node (see Figure 4-5).

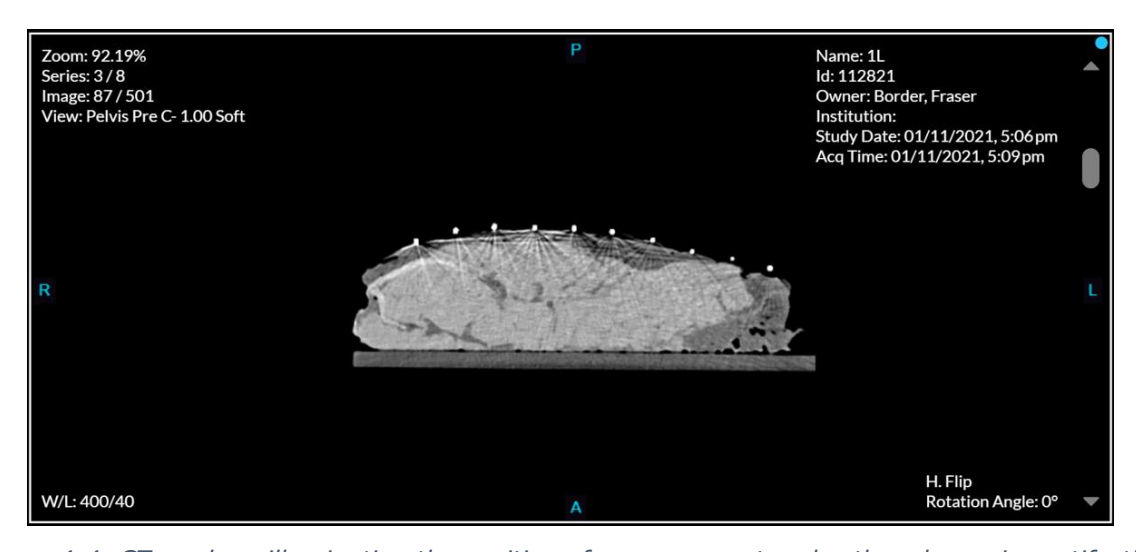


Figure 4-4: CT markers illuminating the position of measurement nodes though causing artifacting within CT images.

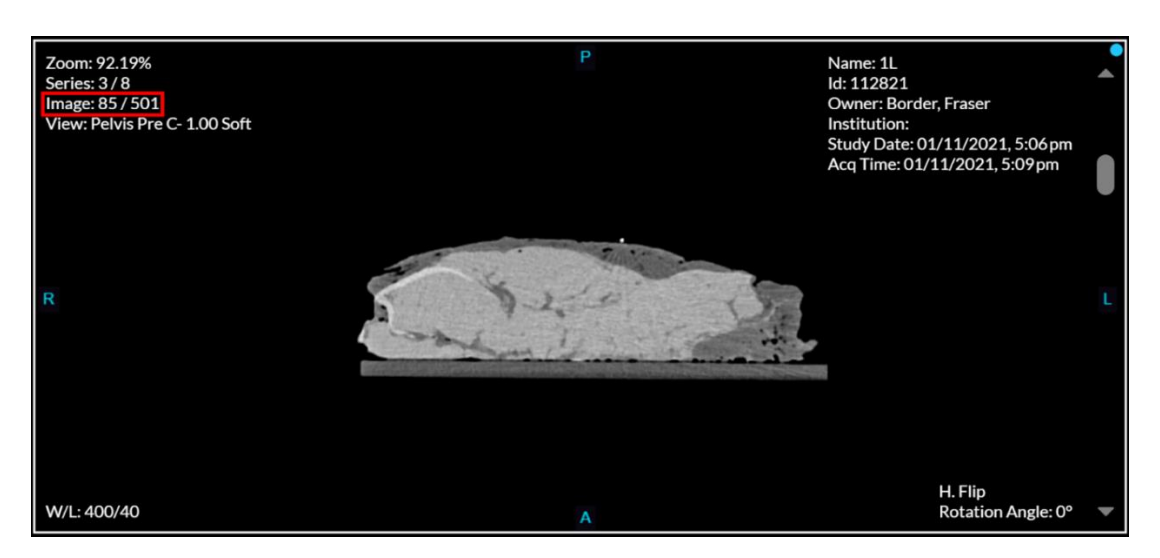


Figure 4-5: An example of offsetting by 2 images (e.g., from Image #87 to #85) to remove artifacting in an image for Striploin 1.

The collection of images within the CT scan of each striploin were uploaded to the Siemens cloud repository (called Asteris Omni). The pixel per mm calibration of these images was conducted by correlating an image and physical measurement. The known width of the plastic board the striploin was scanned on was used. Measurements were made using the 'ruler' software tool at the locations of the visualised measurement nodes and tabulated in Microsoft Excel (see Figure 4-6).

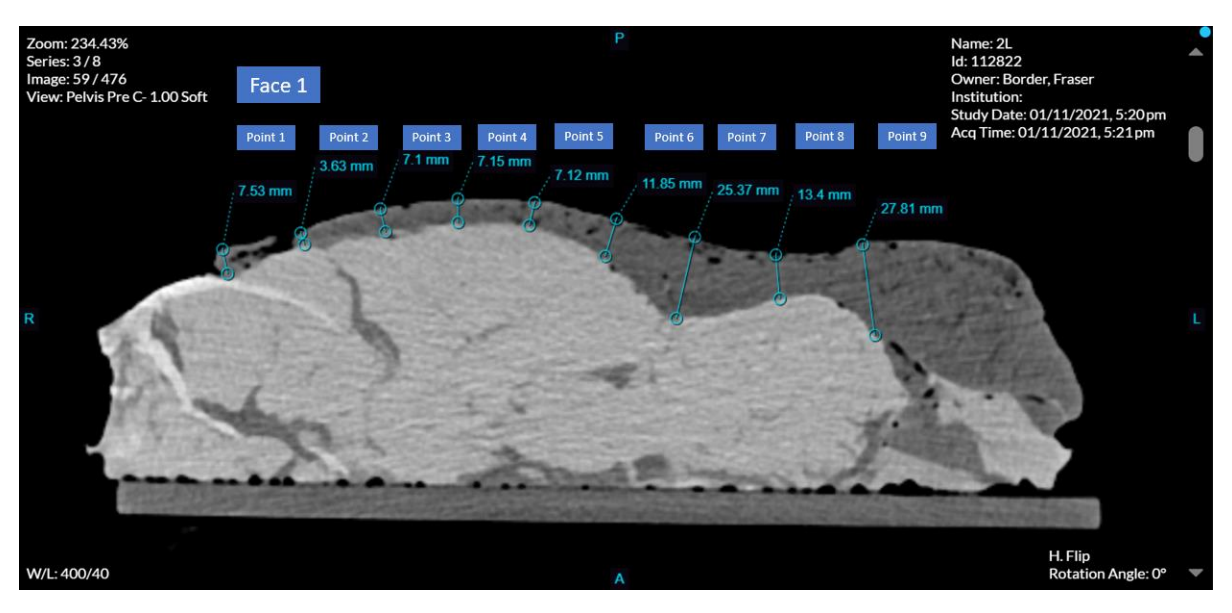


Figure 4-6: An illustration of the fat thickness measurements acquired from CT images acquired for rows (1 - 9) on face 1 of striploin 2R.

Fat Depth Measurements using a Ruler: The process of acquiring fat thickness measurements through a manual process using a stainless-steel ruler is outlined in Chapter 3. CT imaging was conducted prior to manual measurements whereby the striploin was sealed in plastic wrapping. After CT imaging each striploin was carefully unwrapped to ensure the accurate preservation of the node locations. When the CT markers were removed, at the same location (marked by the permanent marker on the plastic), a stainless-steel skewer was used to pierce the plastic slightly to mark the striploin surface (see Figure 4-7). This enabled the registration of points between the manual measurements and the

location of the CT markers in CT images by then using black, food-grade dye ink to mark these nodes for manual measurement.

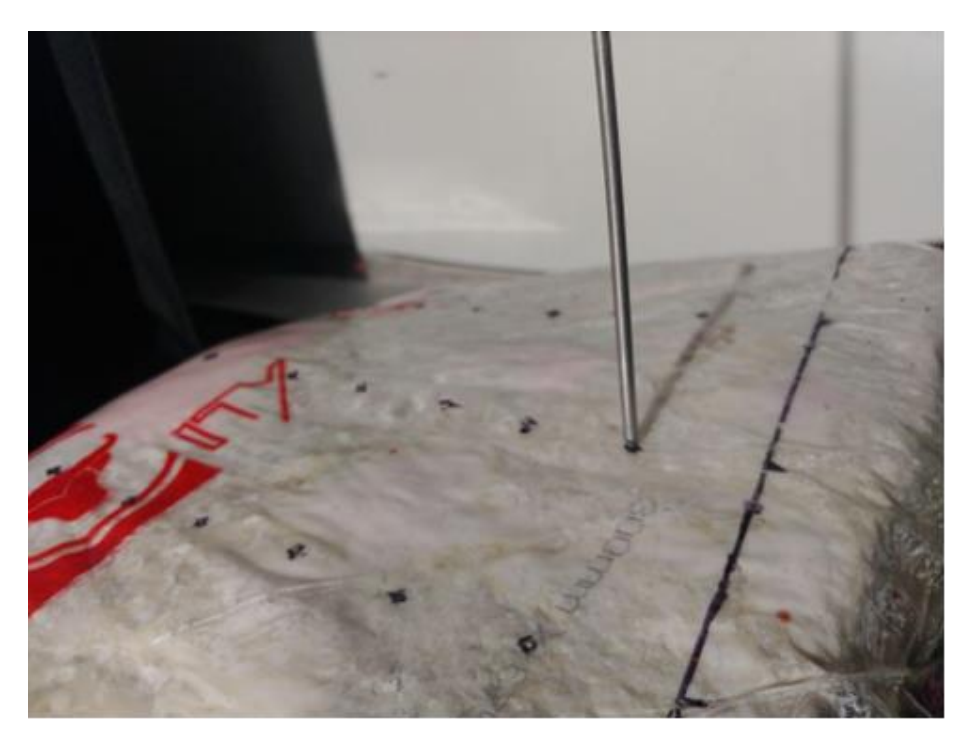


Figure 4-7: Method for registering nodes between CT imaging (using CT markers) and manual measurements.

## 4.3 Experimental Analysis

The assessment of CT imaging for beef striploin fat trimming focuses on identified performance metrics (accuracy, precision, reliability), excluding those metrics observable only upon implementation (operating range and response time). This benchmarking approach facilitates a standardised evaluation of CT imaging as a sensor, compared to manual measurements, and serves as a model for evaluating other sensing technologies.

The following performance metrics for this application are proposed and defined from drawing on the literature (Lewis & Groth, 2022).

Accuracy & Precision: Accuracy is a performance metric that refers to how closely the sensor's measurements correspond to the true value of the quantity being measured, whilst precision refers to the consistency of the sensor's measurements over time. These performance metrics are typically considered most important for sensor evaluations across literature (De Ponte Müller, 2017). The system's capability to trim and to leave a uniform fat thickness as outlined in the fat specification is dependent upon acquiring accurate measurements of fat depth along the striploin. The outcome of trimming to leave a uniform fat thickness of 12 mm is required by industry, yet there is no acceptable error tolerance that has been identified within literature or standard industry practice (AUS-MEAT Limited, 2005).

Two methods of analysing the difference between reference and sensor datasets are commonly cited within literature (Tomazevic, Likar & Pernus 2004; Shcherbina et al., 2016). This may be through a statistical comparison between means of the 2 datasets (reference and sensor measurements), or else through the analysis of error (determining the corresponding error between values within these datasets). The latter analysis method best aligns with the aims of this thesis as it enables a more in-depth analysis of evaluating sensor biases and systematic differences as opposed to an evaluation predominantly focused upon dataset correlations and describes the sensing system output in a form more important for the overall system functionality (measurement error). Literature evaluating sensor performance with similar research aims to this investigation reflect the choice of this analysis method (Tomazevic, Likar & Pernus 2004; Shcherbina et al., 2016; Kollman et al., 2005; Fischer et al., 2021). This is further reflected in literature through research that highlights the pitfalls of evaluating correlations of datasets as an alternative to applying descriptive statistics on the differences between sensor and reference measurements (Kollman et al., 2005; Rodbard, 2014). This also ensures that the distinction is made that

despite CT imaging being the "gold standard" in fat depth measurement, it is not used to provide the reference measurements of which the final system is judged. In actuality, the reference values, and how specification is confirmed by the Quality Assurance (QA) process and the customer, is the manual method (using a stainless-steel ruler). As such, the better method for comparing all sensors for this application is through defining the error between the reference value (ruler) and the sensor (in this case, CT imaging). Therefore, this analysis will rely upon calculating the measurement error ( $E_{M-S}$ ) between ruler (manual measurement) and CT fat depth measurements. This is expressed formulaically in a generalised notation to be used with all evaluated sensing technologies of CT (Chapter 4), B-Mode ultrasound (Chapter 5) and A-Mode ultrasound (Chapter 6) and shown in Equation 4.1.

Equation 4.1: Error between CT and manual fat depth measurements (CT – manual)

Error,  $E_{M-S} = f_M - f_S$ 

where:

 $f_M$  = the fat thickness measurement acquired manually using a ruler (considered the reference measurement).

 $f_S$  = the fat depth measurement acquired using the sensor to be evaluated (considered the estimated measurement)

The inclusion of dataset outliers, and their significance to the distribution of the dataset, was considered and informed whether they should be filtered. If these were deemed to be considerably influencing the dataset, they were removed using the 1.5IQR filtering method, also known as Tukey's Method (Hoaglin, Iglewicz & Tukey, 1986). In literature this statistical method is seen to be used as a means of outlier identification for non-gaussian data (normally distributed data) similar to the dataset presented in this chapter and those preceding (Durai & Shamili, 2022; Dash et al., 2023; Carling, 2000). The method for

identifying outliers between reference and observed measurement errors is used by Carling (2000). The following set of equations were used to identify and remove outliers from the error dataset across all statistical evaluations in this research (see Equation 4.2).

Equation 4.2: Identifying outliers within the error dataset (E).

Lower Bound Outliers  $\leq Q_1(E) - 1.5 * IQR(E)$ 

*Upper Bound Outliers*  $\geq Q_3(E) + 1.5 * IQR(E)$ 

#### where:

 $Q_1(E)$  = the first quartile (25th percentile) value of the error measurement dataset  $(E_i)$  and considered the lower bound / minimum value of this trimmed dataset  $Q_3(E)$  = the third quartile (75th percentile) value of the error measurement dataset  $(E_i)$  and considered the upper bound / maximum value of this trimmed dataset IQR(E) = the difference between the first (25th percentile)

Whilst a number of statistical analyses were considered in order to gain an understanding of the error between CT and ruler measurements, only a few metrics were used to evaluate sensor performance in terms of accuracy and precision. As suggested in the literature, measurement error datasets typically do not follow a parametric or normal distribution and display the characteristic of homoscedasticity and hence this assumption is usually violated within statistical analysis methods (Kollman, 2005; Rodbard, 2014; Álvarez et al., 2019; Falbriard et al., 2018; Anderson, Moore & Cohn, 2000). As such, non-parametric statistical methods that account for non-normality, skewed distributions and heteroscedasticity (variance of residuals in a regression model isn't constant across all values of the independent variable) should typically be considered when expressing statistical measures of accuracy and precision. The literature

and the third quartile (75th percentile) values

suggests the most representative, and easy-to-compare, statistical descriptors are median or median-derived (median difference, median absolute difference, average median error, etc.) as this is applicable for both unskewed and skewed datasets (Kollman, 2005; Nam, 2016; ). For this application, the polarity of error is a critical component of the analysis due to the significantly different consequences of error in the positive from the negative direction. This is similar to research conducted by Klonoff (2004), which supports describing positive and negative errors separately whereby there are differing consequences of an erroneous measurement based upon an underestimate or overestimate. Therefore, aligned with literature (Shcherbina et al., 2016; Falbriard et al., 2018) the evaluation of CT imaging, and all other sensor evaluation analyses, will provide median error as a measure of accuracy and interquartile range as a measure of precision. Therefore, the following statistical measures were used to describe sensors' performance for accuracy and precision. For the evaluations conducted to benchmark the performance of CT, the error dataset relates to the difference between manual and CT measurements  $(E_{M-CT})$ , though the equations presented below are generalised for the evaluation framework that will be applied to other sensors. As such these equations will be denoted as the error dataset (E).

## **Accuracy Metric Calculation:**

- Median Error ( $E_{Med}$ ): is a measure of central tendency that describes the median of the difference between the reference measurement (ruler) and the sensor measurement. It is a useful measure of the performance of a prediction model when dealing with datasets that are skewed data or include outliers (see Equation 4.3).

Equation 4.3: Statistical descriptor of the accuracy performance metric (median error).  $Accuracy\ Performance\ Metric\ \equiv\ Median(E)$ 

#### **Precision Metric Calculation:**

Interquartile Range (IQR(E)): is a measure of spread or dispersion of a set of data and calculated as the difference between the upper quartile, Q3 (75th percentile) and the lower quartile, Q1 (25th percentile) of the dataset. It is a useful measure of the performance of a prediction model when dealing with datasets that are skewed data or include outliers (see Equation 4.4).

Equation 4.4: Statistical descriptor of the precision performance metric (IQR of error). Precision Performance Metric  $\equiv IQR(E)$ 

**Reliability:** Reliability refers to the ability of the sensor to produce valid measurements consistently over an extended period of time or operating conditions. In many cases, this becomes more important in spatial applications whereby missing data points introduce complexities for spatial modelling or measurement critical applications (De Ponte Müller, 2017). Reliability differs from metrics that describe error, such as precision and accuracy, and instead describes the likelihood of the sensor acquiring a complete set of measurements. According to Cai et al. (2018), this is commonly referred to in literature as data completeness (expressed as a "miss rate" probability). The chosen application of beef striploin fat trimming requires a spatial map to be generated for a cut path to be planned to use. The likelihood of acquiring a complete set of measurements is an important consideration for automating striploin fat trimming due to the necessity to trim with minimal time. The reliability of a sensor, overall or at particular locations, could inform an overall evaluation of a sensor and the location, or number of, sensing nodes and therefore is an important factor of consideration.

With respect to reliability, data completeness is expressed as a miss rate probability for the sensor's capability to acquire measurements for

the total nodes surveyed. The Miss Rate (PM) will provide a measure of reliability in terms of how likely it is that a node will not be measured by the sensor. This will provide a means of quantifying sensor-related failures whereby no measurement is acquired. Typically, this is defined as a value between 0 and 1 and can be expressed as an expected probability or percentage likelihood (Cai et al., 2018; Hodan et al., 2018; Zhang et al., 2021). This is expressed as a percentage in Equation 4.5).

Equation 4.5: Statistical descriptor of the reliability performance metric (Miss Rate).

Reliability Performance Metric  $\equiv$  Miss Rate,  $P_{M}$ 

Miss Rate, 
$$P_M = \frac{N_M}{N_T} * 100\%$$
, where  $0\% < P_M < 100\%$ 

where:

 $N_M$  = the number of measurements "missed" measurements  $N_T$  = the total number of measurement nodes investigated

Operating Range & Linearity: The operating range refers to the minimum and maximum values that the sensor can acquire measurements for. Literature typically suggests that the operating range, and the accuracy across the operating range, are key considerations in evaluating the performance of the sensor (De Ponte Müller, 2017; Lui et al., 2019; Islam & Mukhopadhyay, 2019). These considerations must be made in the context of the application for which the sensor will be applied within, beef striploin fat trimming. The system's capability to provide comprehensive fat depth information is dependent upon the operating range, and the accuracy across the operating range, of the sensor. As identified in Chapter 3, the maximum range of fat depth expected to measure will be considered to be the largest of the two. As such, the operating range of fat depth measurements is considered 75 mm.

Literature suggests that when evaluating the operating range of the sensor, the detecting range and the accuracy across the detecting range should be considered (De Ponte Müller, 2017). As such datasheets should be first consulted to ensure that the technical specifications of the sensor can detect for the range required by the application. For CT imaging there is significant research indicating that the depth of measurement is typically feasible for a human body (Lain, 2017; Fong, 2022). Though this is significantly larger than the fat thickness of beef striploin, this will be cross-examined within the statistical analysis presented within the results section. This will be by considering the following constraint to conclude on the feasibility of the sensor's operating range for this application. Therefore, the sensor is deemed feasible if the technical datasheet indicates that its minimum and maximum measurement (operating range) surpasses that expected of the reference fat depth dataset. Through the evaluation presented in Chapter 3 the minimum and maximum fat depth expected for this application is 0 mm and 75 mm respectively. As such, the following equation shows the minimum requirements for any sensor to be deemed feasible for this application (see Equation 4.6).

Equation 4.6: The operating range constraints of a feasible sensor.

Minimum Sensor Measurement Depth,  $D_{Min} \leq 0 \text{ mm}$ Maximum Sensor Measurement Depth,  $D_{Max} \geq 75 \text{ mm}$ 

Upon concluding upon a sensor's capability to acquire measurements the linearity of these measurements can be evaluated. To evaluate the sensor linearity across the operating range a statistical, linear regression analysis of the fat depth measurement error was undertaken as per numerous literature papers (Liu et al., 2020; Liu et al., 2019). This was calculated as the determination of coefficient value,  $R^2$ , which is seen to be a statistical measure of linearity. As such, literature suggests evaluating the residual plot's correlation to visualise homoscedasticity as well as statistically describe this with a linear

regression line ( $R^2$ ). According to Lui (2019), this is calculated as shown in Equation 4.7.

As a benchmark of linearity, CT imaging is concluded upon with the following measures:

Equation 4.7: Statistical descriptor of the linearity performance metric  $(R^2)$ 

Variance over Operating Range 
$$\equiv R^2 = 1 - \sum_{i=1}^n \frac{\left(f_{R_i} - f_{S_i}\right)^2}{\left(f_{S_i} - \overline{f_S}\right)^2}$$
,  $0 \le R^2 \le 1$ 

where:

 $f_{R_i}$  = all values (i) of the fat thickness dataset acquired using a ruler

 $f_{S_i}$  = all values (i) of the fat thickness dataset acquired using the applied sensor

 $\overline{f}_S$  = the mean of the values (i) of the fat thickness dataset acquired using the applied sensor

Response Time: The response time performance metric refers to the time it takes for the sensor to acquire a measurement. Literature for systems required to respond or actuate quickly typically consider response time an important factor that determines sensor performance (De Ponte Müller, 2017). The line speed of the processing plant determines the time constraints of the fat trimming processing task, and hence the sensors and sensing strategies that are viable to be implemented at these speeds. This constraint defines the suitability of a sensor, and sensing strategy, and informs considerations such as:

- Real-time vs non-real-time
- direct (e.g., numerical values) vs indirect sensing (e.g., images to later ascertain measurements through further processing)
- a small vs large number of nodes in the sensing mesh

As highlighted in previous analyses the typical time taken by personnel trimming fat from striploins is approximately 27 seconds on average (see Section 3.3). There are several integration contingencies that may be employed to adhere to this line speed (such as multiple parallel or in-series systems) depending on the magnitude of the response time. As such the response time will be considered an important performance metric in order to evaluate the suitability of a sensor and sensing strategy for this application.

There are a number of processes that need to be considered in the estimation of the time required to acquire a fat depth measurement for a final system. As such an approximate estimate will be provided from the observations and conclusions made from the development of this system as an opinion of feasibility for the application of beef striploin fat trimming. Through the evaluation presented in Chapter 3 the average response time of the system was identified at an approximate average of 27 seconds. As previously stated, a feasible time may be up to a number of magnitudes larger than this depending upon the yield improvement of the automated system. With the presumption that the trimming tool will trim slightly behind the sensor, and hence not add significant time to the cycle time of the system. It may be concluded that for a proposed 90 second trimming cycle time (a multiple of '3' longer than manual processing), the time allocated for sensing (considering some time for fixation/location of the striploin and trimming), the sensing portion of the automation may be 60 seconds. The following equation shows the minimum requirements for any sensor to be deemed feasible for this application (see Equation 4.8).

Equation 4.8: The response time constraint of a feasible sensor.

Response Time,  $T_R \leq 15$  seconds

### 4.4 Results

Through evaluating the CT and ruler measurements of four striploins (two each of LHS and RHS) a total data set of 272 nodes were considered in this investigation (see additional figures and tables in Appendix C: Computed-Tomography Error Dataset Measurements.

The error measurement dataset (E) was calculated to create a means of evaluating the distribution of error between the ruler ( $f_R$ ) and CT ( $f_{CT}$ ) fat thickness measurements. The comparison between the unfiltered and filtered error dataset is presented in Figure 4-8.

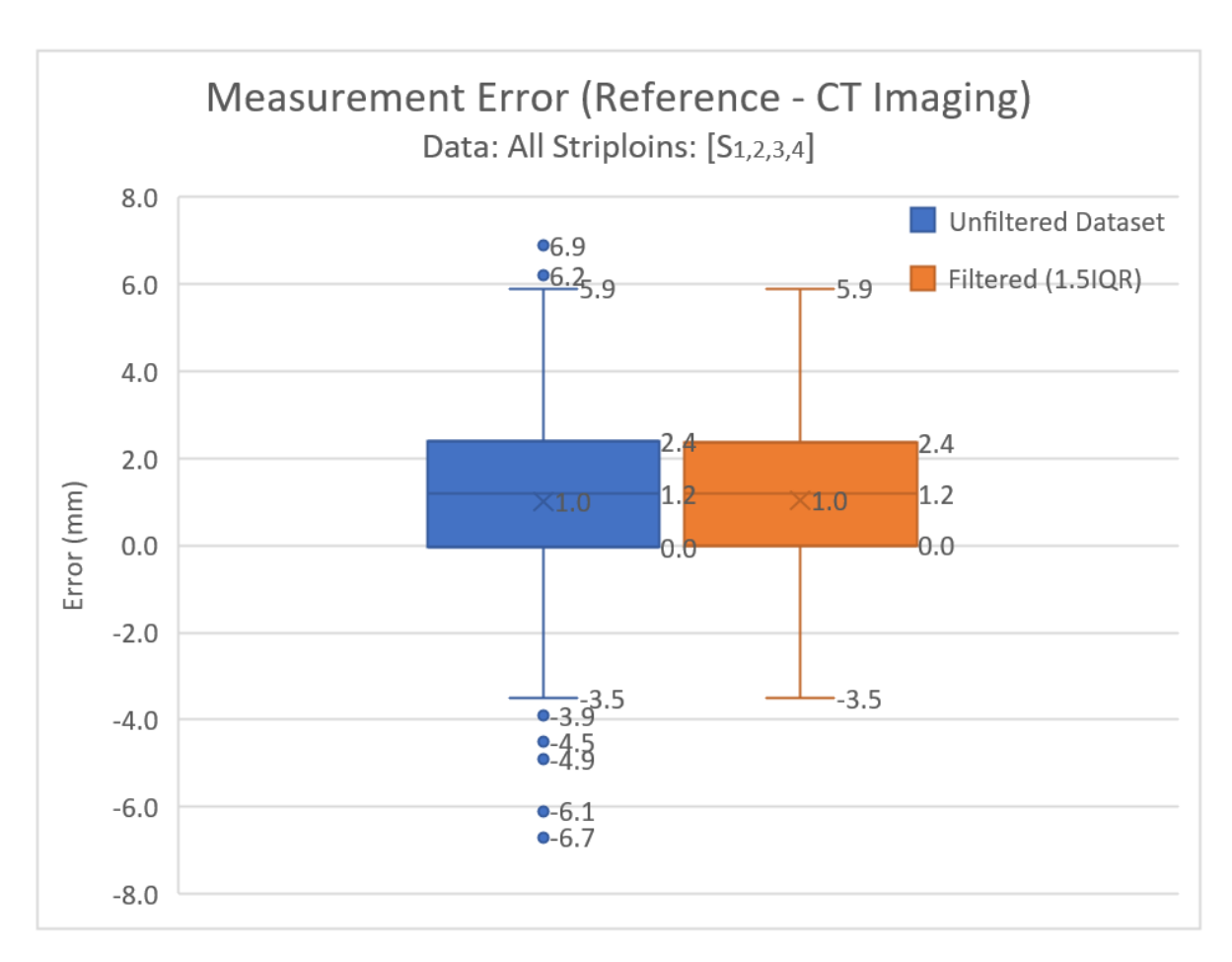


Figure 4-8: Statistical Summary of error measurement datasets (unfiltered vs filtered).

The key statistical measures are presented for the unfiltered dataset, and the filtered dataset (see Table 4-2). It should be noted that the filtered dataset was created from the unfiltered dataset by removing

all values identified as outliers using the 1.5IQR method presented in Equation 4.2.

Table 4-2: Statistical summary of error dataset (E) between ruler and CT measurements (n = 272)

Statistics	Unfiltered Dataset	Filtered Dataset
Minimum of Error Dataset, $Q_0(E)$	-6.7 mm	-3.5 mm
<sup>2</sup> 5th percentile of Error Dataset, $Q_1(E)$	-0.1 mm	0.0 mm
Median of Error Dataset, $Q_2(E)$	1.2 mm	1.2 mm
Mean of Error Dataset, $(\bar{E})$	1.0 mm	1.0 mm
<sup>7</sup> 5th percentile of Error Dataset, $Q_3(E)$	2.4 mm	2.4 mm
Maximum of Error Dataset, $Q_4(E)$	7.1 mm	5.9 mm
Interquartile Range of Error Dataset, <i>IQR(E)</i>	2.5 mm	2.4 mm
Standard Deviation of Error Dataset, SD(E)	2.1 mm	1.7 mm
Range of Error Dataset, $Range(E)$	13.8 mm	9.4 mm
Lower Outlier of Dataset, $Q_1(E) - 1.5IQR(E)$	-3.8 mm	-3.6 mm
Upper Outlier of Dataset, $Q_3(E) + 1.5IQR(E)$	6.1 mm	5.9 mm

Six lower and four upper bound outliers were identified in this dataset and removed for the creation of the filtered dataset:

Lower Outliers (
$$\leq -3.8 \, mm$$
): -6.7, -6.6, -6.1, -4.9, -4.5, -3.9 Upper Outliers ( $\geq +6.1 \, mm$ ): 7.1, 6.9, 6.4, 6.2,

With only a very slight reduction of IQR (precision) of 0.1 mm due to the impact of outliers causing the spread to be further towards negative errors (CT over-estimating fat measurements), the effect of outliers was deemed negligible and so the unfiltered dataset was concluded to be representative of the fat depth measurements and therefore used for further analysis.

The error dataset was plotted on a histogram using bin widths of 1 mm, with excess bins being used to group lower and upper bound outliers (see Figure 4-9). This error distribution is not normally distributed, and is negatively skewed, showing a bias for CT imaging to typically measure fat depth less than the ruler quite consistently. The largely distributed, central peak supports that there are no underlying subgroups trends.

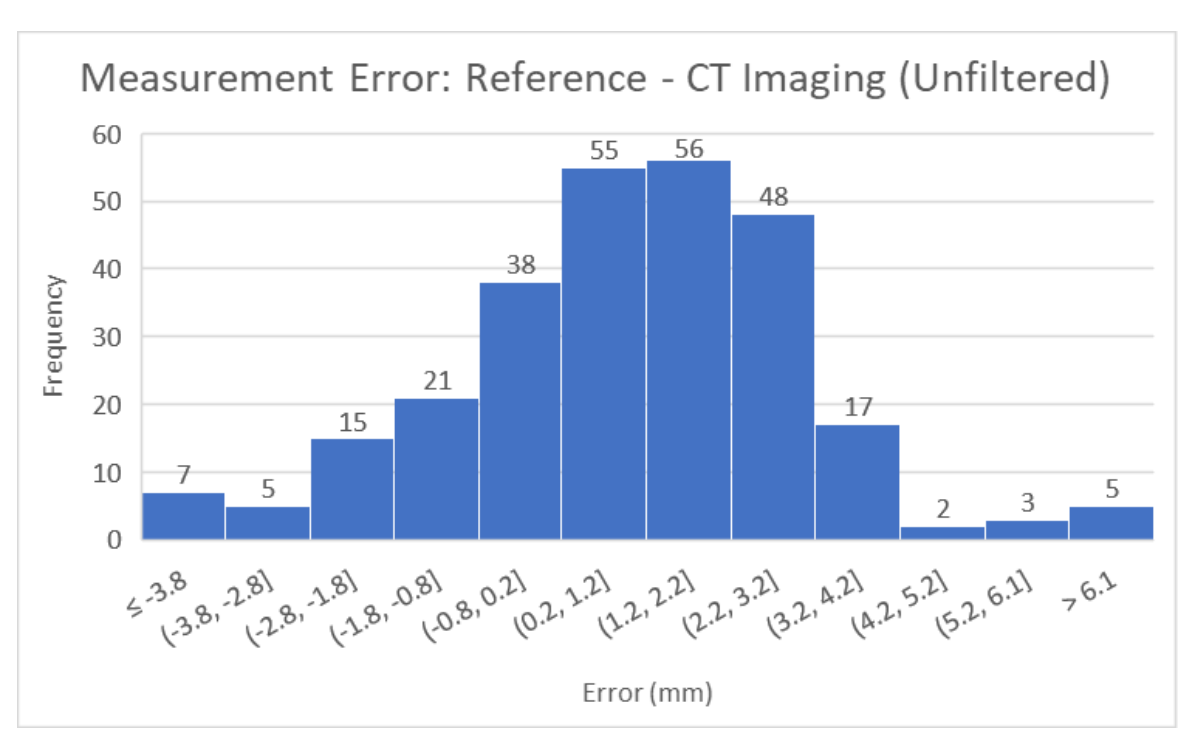


Figure 4-9: Error distribution of unfiltered data showing a non-normal distribution.

For this dataset the error of the CT imaging measurements compared to the manual measurements ( $\it{E}$ ) was calculated to be 1.0 mm and 1.2 mm for the average and median error respectively. This measurement error quantifies the combined discrepancies for the process of aligning nodes for CT and manual measurement comparisons. This statistic describes the imprecision of node alignment, the inaccuracies of human error including the precision tolerance of using a 0.5 mm resolution ruler, and the deformation of the striploin handling between CT imaging and manual measurements.

As a benchmark of accuracy and precision, CT imaging is concluded upon with the following measures:

Accuracy: Median of Error,  $E_{MDN}$  = +1.2 mm

Precision: Interquartile Range of Error, IQR(E) = 2.5 mm

Firstly, it should be noted that CT imaging was able to measure at any depth required within this analysis. For this subset of striploins, the minimum range and maximum ranges were found to be 0 mm and 44 mm respectively. The measurement error across the range of measurements acquired is described in Figure 4-10.

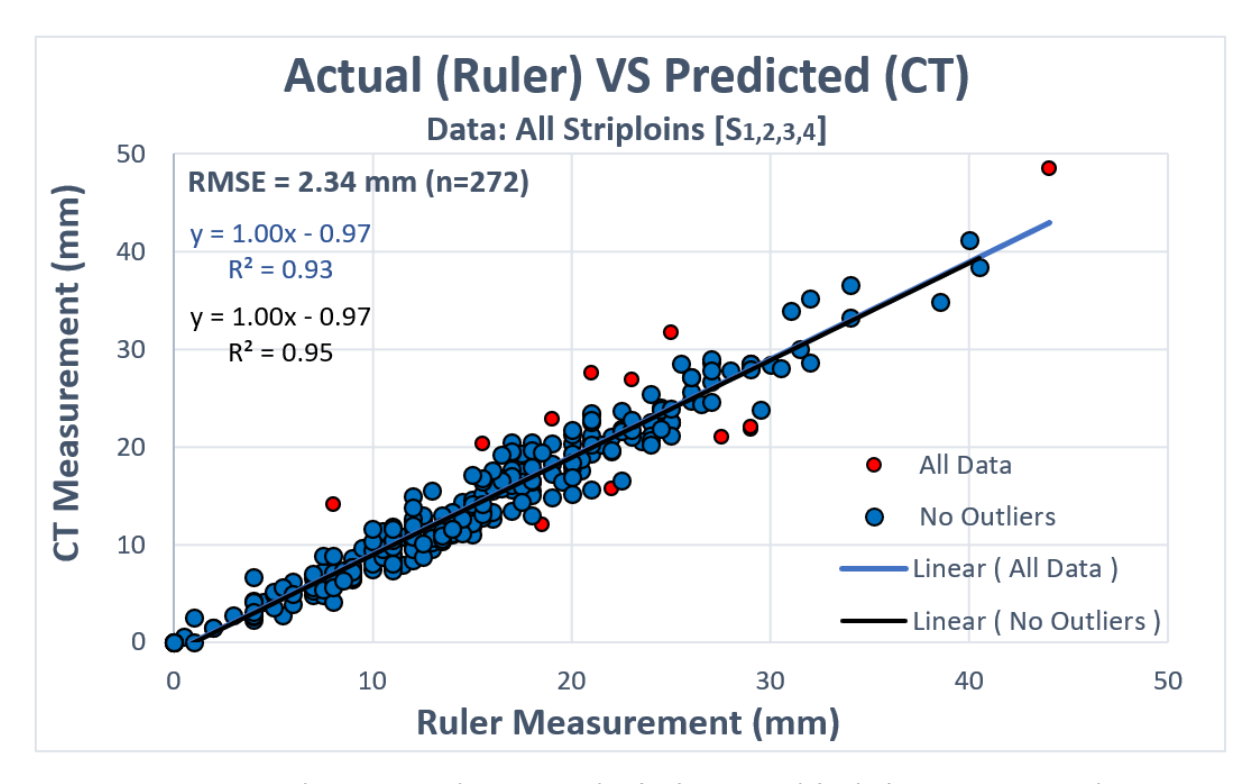


Figure 4-10: The Computed-Tomography (CT) vs actual (Ruler) measurement plot

The closeness of the correlation of determination ( $\mathbb{R}^2$ ) value of this linear regression to '1' indicates that spread of residual errors is narrow, and in general, the predicted and actual measurements are quite similar across the entire measurement error dataset. This is further reflected in the similarity of the outliers with other measurements within the dataset. A further analysis of heteroscedasticity is visualised in Figure 4-11 & Figure 4-12 which shows insignificant variation of error across the range of measurements (reference values). This analysis provides a conclusion upon the strong homoscedasticity error along the range of reference values of this dataset ( $\mathbb{E}$ ).

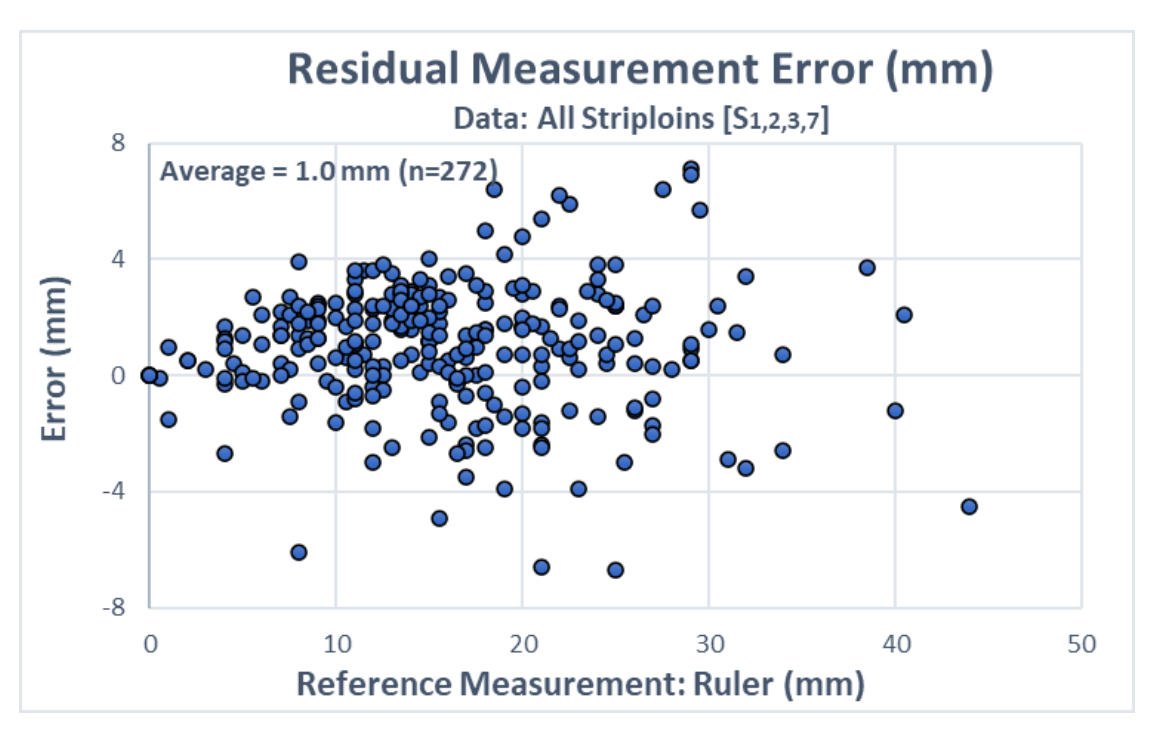


Figure 4-11: Residual error plot of CT-Ruler dataset (in mm)

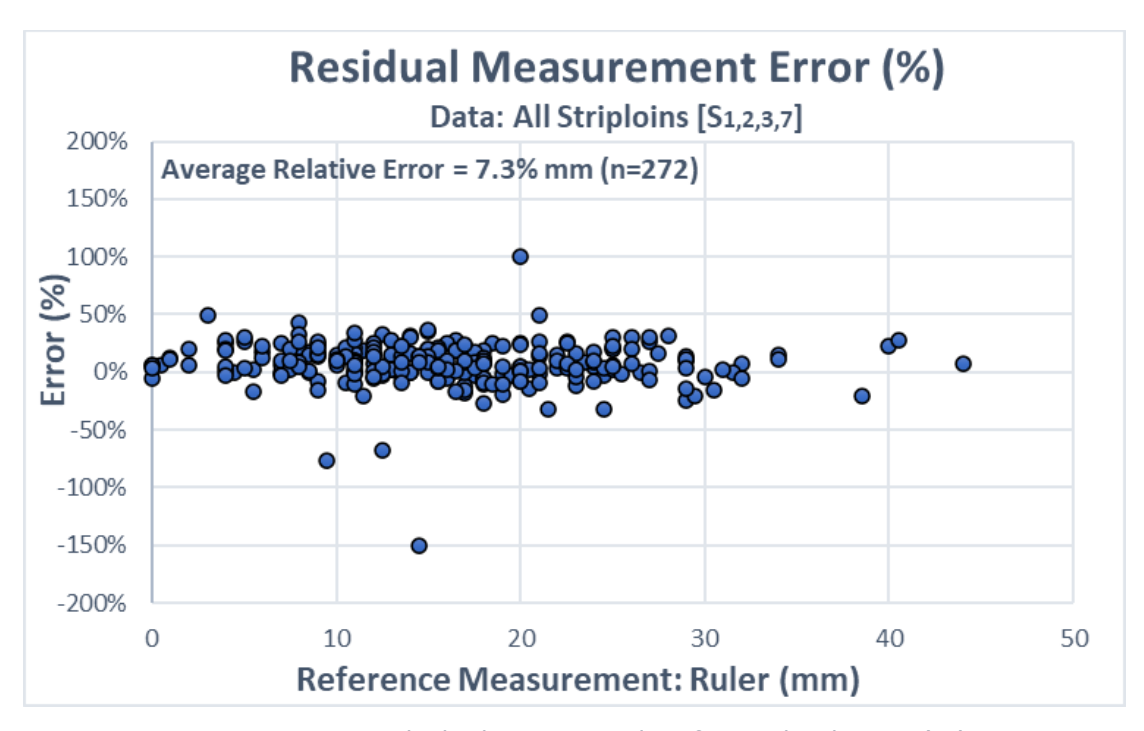


Figure 4-12: Residual relative error plot of CT-Ruler dataset (%)

As a benchmark of operating range, CT imaging is concluded upon with the following measures:

## **Range Requirements:**

Minimum Sensor Measurement Depth,  $D_{Min} \leq 0 \text{ mm}$ ,  $\therefore$  Feasible Maximum Sensor Measurement Depth,  $D_{Min} \leq 75 \text{ mm}$ ,  $\therefore$  Feasible

## **Linearity:**

*Variance over Operating Range*  $\equiv R^2 = 0.93$ 

There was only one instance whereby a manual fat depth measurement could not be taken after a CT image was taken. This was due to deformation of the meat between the sensor and physical measurements and not a limitation of CT imaging technology. As such, it was considered that no 'missed' measurements occurred and therefore the miss rate  $(P_M)$  for CT imaging was concluded to be 0%.

As a benchmark of reliability, CT imaging is concluded upon with the following measures:

### **Reliability:**

Miss Rate, 
$$P_{M} = \frac{0}{272} * 100\% = 0\%$$

The process of acquiring CT images of the striploins took approximately 10 minutes to perform though this included loading and precisely positioning the striploin in the CT (due to localisation requirements), running initialisation scans to identify the correct scanning parameters for the striploin (no pre-sets were made). The procedure was restricted to have all images uploaded to the cloud which took, on average, 5 - 7 days to complete and provide access to CT images.

### 4.5 Discussion

This section applies the results towards the specification of the weightings of, and the thresholds for ranking performance within, metrics to evaluate the performance of a sensor for the application of uniform fat trimming of beef striploin.

**Accuracy & Precision:** Acquiring accurate and precise fat depth measurements is crucial to enable the capability of the system to produce a trimmed striploin to fat specification. Though both performance metrics are important, there are several factors to be considered for deducing the weighting of these performance metrics.

A highly accurate but low precision sensor will provide a trimmed striploin that is close to 12 mm specification on average yet with low controllability. A highly precise yet low accuracy sensor will provide a trimmed striploin that is not close to 12 mm specification on average yet with high controllability. In a practical sense the processing plants, who would be the interested parties of such a system, have financial incentive to desire a controllable output moreso than an accurate output (within reason). The controllability of such a system enables the more precise tuning of how much error this system trims to.

For example, consider 2 systems with the following outputs:

- i) System A provides +2 mm of error (average) with a variance of error of  $\pm$  8 mm
- ii) System B provides +8 mm of error (average) with a variance of error of  $\pm$  2 mm

By creating offsets within the control algorithm of this system to be added to the measurements acquired of -2 mm and -8 mm to Systems A and B respectively we can reduce the average error to approximately 0 mm. Though, due to the variance of error, System A will vary between +

8 mm and - 8 mm (16 mm) and System B will vary between +2 mm and - 2 mm (4 mm). Thus, if we set the target of the control system to trim at 12 mm, the output of each system will vary for each system significantly:

- i) System A output will provide a trimmed fat depth of 4 mm to 20 mm
- ii) System B output will provide a trimmed fat depth of 10 mm to 14 mm

As such, due to the highly non-uniform trimming, there are instances in the trimmed striploin that largely vary from the fat specification. This large variation is significantly more easily detectable, due to being visibly apparent, as opposed to a striploin provided with a larger average error spread over the primal. In addition to this, the capability to control the average error precisely (e.g. less variance of error) enables the capability of a processor to fine tune the average error of the striploin. This is where this system can contribute significantly to the industry whereby a precise, yet inaccurate trimming performance, can lead to significant profit margins for this product.

For example, let's assume that an error of +8 mm (20 mm fat depth for a 12 mm specification) is deemed visibly erroneous to a customer and hence would create a scenario, or significantly increase the likelihood, of a fat claim being lodged. For System A, this would mean that this would just meet specification though sensing used to produce a striploin with an average error of 0 mm (hence a target fat depth at 12 mm). In comparison for System B, the average error could be increased to 6 mm (hence a target fat depth at 18 mm) and could similarly meet fat specifications as System A with significant additional economic benefit (see Table 4-3). At an average error of +6 mm over a typical striploin, for a throughput of 1,100 head per day over a 50-week operation, this controllable under-trimming could substantiate to a value-add of \$182.4 million per year to processors across Australia.

Table 4-3: Estimation of the value for a controllable error of +6 mm (under-trimming) for a typical beef striploin product.

Estimation of Yield Losses Reduction us	ing Visualis	ation
Statistical Measures	System A	System B
Overall Ave Error (mm) <sup>a</sup>	0	6
Average Surface Area per Striploin $(mm^2)^{\mathrm{b}}$	113,	495
Average Volume of Under-trim $(mm^3)^{\mathrm{c}}$	0	680,970
Average Volume of Under-trim $(cm^3)$	0	681
Density of Beef Fat $(g/cm^3)^d$	1.0	195
Mass of Under-trim $(g)$	0	694
Average Weight Gain due to Under-Trim $(kg)$	0	0.694
Value of Fat on Striploin ( $\$ / kg$ ) $^{\mathrm{e}}$	22	2.6
Value Fat as Tallow (\$ / kg) <sup>f</sup>	0.0	67
Net Value Difference (\$ / kg)	21.	.93
Net Value Add (\$ / striploin)	\$0.00	\$15.22
Relative Net Value Add to Striploin (%) <sup>9</sup>	0.00%	9.68%
Net Value Add Difference (\$ / striploin)		\$15.22
Annual Striploins at processor h	114,	400
Annual Value-Add to processor (million)	\$0	\$1.74
Value-Add for processor (million)		\$1.74
Annual striploins Australia (million) i	12.0	036
Annual Value-Add to Australia (million)	\$0.00	\$183.15

These calculations were made with the following assumptions:

- a) System A is considered the base case with 0 mm of average error (average) in comparison to System B with +6 mm (under-trimming) of average error
- b) The average surface area of striploins was calculated considering the average length and width of striploins used within this analysis (Length = 429.5 mm and Width = 264.5 mm)
- c) The average volume of fat was calculated considering by multiplying the average error with the average surface error of striploins

- d) The average density of fat was calculated between 1.006 1.033 g/cm3, and therefore "Density of Beef Fat (g / cm3)" is considered to be 1.0195 (Pan & Singh, 2001)
- e) According to meat wholesaler MOCO Food Services, Beef City Black boneless striploin sells for \$28.20/kg as of March 2023 (Moco Food Services, 2023). Hence, it is assumed that MOCO sells at a 20% mark-up, hence buys it from the processor for approximately \$22.60 / kg. This constant variable is used for the parameter referred to as "Value of Fat on Striploin (\$/kg)"
- f) According to MLA (2020c), tallow sold for \$963/tonne (\$0.963/kg) as of 2020. It is unknown if this price can be demanded by processors or wholesales; there is also likely a significant volumetric loss in the process of melting solid fat into tallow, and there are also additional processing and heating costs involved to do so. As such, a conservative estimate of 30% losses from this value can be considered, as such, 0.647. This constant variable is used for the parameter referred to as "Value of Fat as Tallow (\$/kg)"
- g) This was calculated by considering the net weight retained due to undertrimming divided by the average weight of striploins used within this analysis (Weight = 7.172 kg). This provided the parameter of "Net Value Add to Striploin (%)".
- h) Considering the throughput of a large processor to be 1,100 head per day (Goodwin, 2018). Hence, considering 2 striploins per head (2,200 striploins / day), operating for 5 weekdays (11,000 striploins / week), operating for 50 weeks per year (550,000 striploins / year)
- i) According to MLA (2022c), even at the lowest annual project in the past 36 years the projected slaughter for 2022 is 6.018 million head (12.036 million striploins)

The table above presents an approximation of the additional yield that is calculations, and assumptions, used to ascertain the additional yield for striploin fat trimming application for a system optimised for yield with a precision of  $\pm 2$  mm (System B) in comparison to a system with a precision of  $\pm 8$  mm (System A).

In conclusion, the performance metric of precision is most desirable in comparison to accuracy, yet both are important for evaluating a sensor

for this application. As such, the weighting of accuracy will be considered 3 / 5, whilst precision is determined to be 5 / 5.

To determine a weighting for the accuracy and precision performance metric the performance of medical-grade CT imaging should be considered the 'gold standard'. Therefore, a sensing system that exhibits a median error of 1.2 mm or less and an IQR of error of 2.5 mm or less will achieve a score of 5 for accuracy and precision respectively.

Whilst the specification exists as a maximum fat thickness definition, in practice, there is a tolerance of error that is commonly accepted by the customer, though this has not been agreed upon or defined. Without such data, it may be reasonable to assume that an error of 10 mm may be easily perceivable to customers, and hence, likely to be interrogated with a ruler to identify a product defect. Hence, equally spaced thresholds were created to develop a Likert scale to define the rating of a sensor for the metric of accuracy. This is shown in Table 4-4.

Metric	Weight			Perforn	nance Ran	k	
		0 Fail	1 Fair	2 Average	3 Good	4 Excellent	5 Exceptional
Accuracy $(E_{MDN})$	3	>10 mm	≤10 mm	≤ 7.8 mm	≤ 5.6 mm	≤ 3.4 mm	≤ 1.2 mm

Table 4-4: Thresholds for ranking sensor accuracy.

The IQR of the error dataset represents the middle 50% of errors values in the dataset. It was considered that intervals of the gold standard IQR (2.5 mm) was appropriate as it was decided that an IQR of a multiple of three of CT would be an appropriate / "average" performance of a sensor. As such, the following table was created to rate a sensor performance for precision (see Table 4-5).

Table 4-5: Thresholds for ranking sensor precision.

Metric	Weight			Perform	ance Ran	k	
		0 Fail	1 Fair	2 Average	3 Good	4 Excellent	5 Exceptional
Precision (IQR(E))	5	>12.5 mm	≤12.5 mm	≤ 10 mm	≤ 7.5 mm	≤ 5 mm	≤ 2.5 mm

It should be noted that the rating of "exceptional" is reserved for a sensor that performs equal or better than the gold standard of CT imaging. The '0' ranking is a failure and therefore any sensor that is determined within this ranking will cease to be considered a feasible option for this application due to its incapacity to acquire measurements with the accuracy and precision required for this application.

**Measurement Range:** It can be concluded from previous literature and analyses (presented in Chapter 3) that the measurement range of 0 mm to 75 mm is necessary, and hence will be considered as a prerequisite requirement prior to developing the sensing system with the chosen sensor. As such, the linearity of the sensor will be considered for evaluating the performance of the sensor. The linearity of the sensor, described as the coefficient of determination ( $R^2$ ) plotted for the sensor measurement and reference measurements plot, will be used to rank feasible performances (0 - 5). The R-Squared value of '1' suggests a perfectly linear correlation between sensor and actual measurements; the gold standard benchmark using CT imaging was calculated at 0.93 indicating a high linearity. In practice, the characteristic of linearity provides a measure of accuracy at a particular fat depth range which is a valuable metric for interpolating results and identifying inconsistencies with sensor interpretation. Though useful, this does not constitute failure

of a sensor independently as a performance metric. A 'good' coefficient of determination is subjective to many factors including sample size and biases, though it was determined that a value of '0.5' would be a 'fair' linear correlation between sensor and actual measurements. The thresholds for the linearity metric Likert scale were created between the 'fair' (0.5) and exceptional/gold standard (0.93) coefficient of determination values.

The performance metric of range was considered important enough to consider as this property enables the adjustment of error to be offset uniformly throughout the range of the sensor with a constant offset more accurately. From the analysis undertaken in Chapter 3 (mean = 16 mm, SD = 7.9 mm), 95% (2SD) of fat depth measurements were between approximately 0 - 30.6 mm although there was a maximum measurement of 44 mm. This narrow distribution exemplifies that for this application linearity is less important than that whereby fat depth measurements are more spread across the range, hence linearity evaluated across the range of fat depth measurements of the reference dataset has less of an informative description for sensor performance. Also, the smaller the measurement range, the less a sensor's description of linearity matters as this approaches a similar description of measurement accuracy. Thus, whilst considering the measurement range performance metric is important, this is accounted for in the feasibility evaluation of Measurement Range (ranking of '0'). For this application which has a high central distribution accuracy would take more of a weighting than linearity, as such measurement range was considered slightly less important and therefore weighted as a 2 / 5 (see Table 4-6).

Table 4-6: Thresholds for ranking sensor linearity.

Metric	Weight			Perform	ance Ran	k	
		0 Poor	1 Fair	2 Average	3 Good	4 Excellent	5 Exceptional
Linearity (R <sup>2</sup> )	2	< 0.5	≥ 0.5	≥ 0.6	≥ 0.7	≥ 0.8	≥ 0.93

Reliability: In respect to reliability, the performance of CT imaging was faultless, without a single missed measurement being observed over the 272 nodes measured. As such a rating, and allowing for a small amount of deviation, it was considered that  $P_M \leq 1 \%$  would be considered the gold standard (ranking of '5'). To identify the maximum value of  $P_M$  to be considered infeasible, the significance of a "missed" measurement must be considered within the context of this application. For every missed measurement there is a cost of time loss and substantial error that is introduced to the system due to the need to interpolate the missed measurement, or otherwise, a smaller number of measurement nodes that can provide an accurate estimation of the fat depth profile across the entire striploin. This creates a critical problem to consider due to the high cost to the system of such a missed measurement. Though, lots of measurements that are low quality (not accurate/precise) is less valuable than less measurements that are of high quality (accurate/precise). As such, it is reasonable to consider reliability to be weighted as less important than these metrics. As such, the weighting of reliability was considered to be 3 / 5.

Whilst CT imaging shows an incredible reliability (capturing every measurement at each node), it should be noted that literature shows successful trimming solutions that use as few as one fat depth measurement to trim subcutaneous fat in pork (see Chapter 2). In

conjunction with the narrow distribution of fat depth measurements presented in Chapter 3, the 'failure' threshold for reliability would primarily be centred around a percentage whereby there is a considerable likelihood that too much time would pass before getting one, or a few, measurements from the interrogated nodes. As such, it was defined that a system that 'missed' 75% of measurements of the nodes surveyed may the cut-off for an infeasible system as this would be a measurement of 4 points to get 1 valid reading. As such, this was used to establish the thresholds for the ratings for the reliability performance metric (see Table 4-7).

Performance Rank Metric Weight 0 3 5 1 Fail Fair Average Good Excellent Gold Standard Reliability 5 > 75% < 75% ≤ 50% ≤ 25% < 10% ≤ 1%  $(P_M)$ 

Table 4-7: Thresholds for ranking sensor reliability.

Response Time: It can be concluded from previous literature and analyses (presented in Chapter 3) that the response time of less than 15 seconds is necessary, and hence will be considered as a prerequisite requirement prior to developing the sensing system with the chosen sensor. As such, any response time faster than this can be used to evaluate the performance of the sensor. The determination of a feasible, and a fair to outstanding rank can only be based upon observations of the sensing system and foresight into how this system may be built in its final stages to enable it to perform according to time constraints. Whilst CT imaging has provided a benchmark for other performance metrics the benchmark for response time is dependent upon time constraints of the task of fat trimming. With the processing time of approximately 27

seconds per striploin, and with an average number of nodes being approximately 8 rows and 8 columns, a reasonable observation could be made that a robot could position sensors at all, or most nodes, take a measurement and then start slicing the striploin with multiple cutter assemblies to process this striploin in the cycle time required. Whilst the exact configuration of sensors, tools and robots are yet to be defined, it is possible to identify that for this to be plausible the sensing process at each node needs to take less time than 1 seconds for each node. As such, the infeasible ranking ('0') is considered for this sensing process taking longer than 15 seconds, which is scaled up to less than 1 second for an "exceptional" rating.

Similar to reliability, response time is a metric that measures the system's capability to measure more nodes for a given time. As such, this would be weighted less important than accuracy and precision for the similar reason that quality data at less nodes is more important than quantity of data over more nodes. Though, when compared to reliability, response time has less uncertainty than reliability, and therefore less important for a sensor to perform well in. In addition to this, it could be argued that a configuration with additional sensors would resolve the issue of increasing the number of measurements moreso, and more predictably, in a scenario of longer response time in comparison to less reliable sensors. As such, a sensor that performed comparatively better in reliability than response time would be more important, and therefore, the weighting of this performance metric is considered to be '2' (see Table 4-8). The thresholds of these performance ranks are chosen within multiples that enable a magnitude of sensing nodes to be measured within the absolute ideal (< 1 sec) and feasible (15 sec). For example, considering the maximum sensing time as 15 seconds, fail is no measurements (response time >15 second, fair would be 1 (response time <15 sec), average would be 2 (response time <7.5 sec), good would be 3 (response time <5 sec), excellent would be 6 (response time <2.5

sec), exceptional would be 15 (response time <1 sec). This approximation could be scaled to a magnitude depending upon the number of sensors used in the configuration.

Table 4-8: Thresholds for ranking sensor response time.

Metric	Weight			Perfo	rmance F	Rank	
		0 Fail	1 Fair	2 Average	3 Good	4 Excellent	5 Exceptional
Response Time $(T_R)$	2	> 15 sec	≤ 15 sec	≤ 7.5 sec	≤ 5 sec	≤ 2.5 sec	≤ 1 sec

Through the analyses presented in Chapter 3 and Chapter 4 the following sensor performance matrix was defined (see Table 4-9). This framework will be applied in the subsequent chapters by analysing the measurements acquired by sensors to identify their quantities for the selected performance metrics to then be evaluated considering the metric ranking and weighting to conclude on a sensor performance score.

Table 4-9: Performance evaluation framework for evaluating sensors for automated fat trimming of beef striploin.

Performance Metric	Quantity			Perform	ance Rank			Metric Weighting	Metric Score
		FAIL/POOR 0	FAIR 1	AVERAGE 2	GOOD 3	EXCELLENT 4	EXCEPTIONAL 5		
Accuracy $(E_{MDN})$		> 10 mm	≤ 10 mm	≤ 7.8 mm	≤ 5.6 mm	≤ 3.4 mm	≤ 1.2 mm	3	
Precision (IQR(E))		> 12.5 mm	≤ 12.5 mm	≤ 9.5 mm	≤ 6.5 mm	≤ 4.5 mm	≤ 2.5 mm	5	
Linearity (R²)		< 0.5	≥ 0.5	≥ 0.6	≥ 0.71	≥ 0.82	≥ 0.93	2	
Reliability $(P_M)$		> 75%	≤ 75%	≤ 50%	≤ 25%	≤ 10%	≤ 1%	3	
Response Time $(T_R)$		> 15 sec	≤ 15 sec	≤ 7.5sec	≤ 3 sec	≤ 2 sec	≤ 1 sec	2	
Sensor Perform	nance Scor	е					•		/ 75

### 4.6 Conclusion

The analyses presented within this chapter provide a means of defining the metrics, and their corresponding weightings, for integration into a framework to evaluate and compare sensors for the specific task of uniform fat trimming of beef striploin. These metrics are:

- Accuracy (Weighting: 3): statistically determined as the median of the error between the sensor and manual measurement dataset.
- Precision (Weighting: 3): statistically determined as the IQR of the error between the sensor and manual measurement dataset.
- Linearity (Weighting: 2): statistically determined as R-squared value of the regression line for the sensor (y) vs reference (x) measurement plot.
- Reliability (Weighting: 3): statistically determined as the percentage of "missed" measurements by the sensor.
- Response Time (Weighting: 2): estimated through observation of the developed sensing system for evaluation.

This framework, with thresholds determined in consideration to the gold standard of fat depth measurements (medical-CT imaging), will be applied to independently evaluate Mode B and Mode A ultrasonic sensors presented in Chapters 5 and 6 respectively. Through the uniform application of this evaluation framework a side-by-side comparison will be presented to recommend which sensor is most suitable for this application.

# CHAPTER 5: ANALYSIS OF B-MODE ULTRASOUND SENSING SYSTEM

This chapter focuses on the development and evaluation of B-Mode ultrasound technology for measuring the fat depth of a beef striploin primal. The objective is to assess the capability of Mode-B ultrasound to be employed in an automated system for uniform fat trimming of beef striploin through the application of the sensor evaluation framework developed in Chapter 4. The findings presented in this chapter contribute to the understanding of the potential of B-Mode ultrasound technologies and inform the design and optimization of future automated fat trimming systems.

### 5.1 Introduction

Through the literature review presented in Chapter 2 ultrasound was identified as the most promising, proven sensing technology for measuring fat thickness on a beef striploin. This chapter presents the development of a B-Mode ultrasound system in alignment with the key design considerations outlined in previous chapters. The performance of this system is evaluated using the sensor performance evaluation framework presented in Chapter 4.

In comparison to A-Mode, B-Mode ultrasound offers a more comprehensive view of internal tissues which can be beneficial in applications where a more detailed tissue structure is desired. In the context of measuring fat thickness and automatic fat trimming systems, B-Mode ultrasound can also provide a two-dimensional image of the area being evaluated, allowing for a better spatial understanding of the distribution of fat tissue. Additional to this, there is more certainty of acquiring a measurement to the correct interface due to the ability to locate this interface in a larger window that is easier to interpret visually.

This can be particularly useful in automated systems where precision and detailed information about tissue layout is required for optimal, more 'certain' measurements.

Commonly, ultrasound has been used for the measurement of subcutaneous fat depth over the rib, lumbar, and rump, and that of the longissimus muscle area (Houghton & Turlington, 1992; Pathak, Singh & Sanjay, 2011). Halim et al (2013) presents a comprehensive list of twenty-seven research papers that have explored the use of ultrasound as a fat measurement sensor between the period of 1990 and 2012. Within the review of literature conducted by Halim et al. (2013), research has predominantly favoured B-Mode ultrasound with ten of the eleven studies highlighted being using B-Mode (91%) compared to A-Mode (9%). Discussions regarding the context of using B-Mode ultrasound within an automated fat trimming are presented at the conclusion of this chapter.

## 5.1.1 Chapter Aims

The aims of this chapter were to develop and evaluate a B-Mode ultrasound system capable of measuring fat thickness and implemented within the context of an automated system.

Key design considerations that were highlighted in previous explorative work presented in Chapter 3 & 4 were implemented in the design of this system to provide insights towards how a B-Mode ultrasound sensing system may be developed. The performance of this system was evaluated through applying the sensor performance evaluation framework to conclude on its performance and compare with another sensing technology (A-Mode).

### **5.2 Experimental Setup**

This section presents the methods employed for the data collection of acquiring sensor and manual fat depth measurements as well as the data analysis method implemented to evaluate the performance of the sensor according to the sensor evaluation framework developed in Chapter 4.

## 5.2.1 Preliminary Investigation into Sensor Feasibility

According to analyses summarised in previous chapters (Chapter 3 & 4), it has been identified that the following parameters define a feasible sensor for measurement of fat depth for the context of automated beef striploin trimming. As such, preliminary analyses (see Methods section) were conducted to confirm the feasibility of the chosen sensor prior to the development of a fat depth measurement system. This includes evaluating:

- The sensor range / penetration depth of the ultrasound
- Sensor Response Time
- Fat Depth Measurements (in practice)

According to past work presented in Chapter 3, the sensing configuration chosen for this investigation was measuring from the surface of the subcutaneous fat to the fat-lean interface. Three B-Mode ultrasound systems were evaluated before selecting the final, most promising system. The two with the most promise after preliminary evaluations were conducted were: ReproScan Flexx and the Butterfly iQ+ (see Figure 5-1). These B-Mode ultrasound imaging systems provided a means of acquiring greyscale images for further analysis to determine fat depth at each node surveyed. The details for accessing product information and datasheets of these two systems are provided in Appendix D: B-Mode Ultrasound Device Datasheets.



Figure 5-1: B-Mode ultrasound systems evaluated in preliminary trials: ReproScan Flexx (top) and Butterfly iQ+ (bottom). Sources – (ReproScan, 2023; Butterfly, 2023a).

In comparison, both probes were developed for vastly different applications and therefore had distinct advantages. The ReproScan Flexx unit is an ultrasound device developed for on-the-go veterinary examinations of animals. One such advantage of the ReproScan Flexx unit was that through external hardware the image provided on the screen of the unit could be acquired into a laptop as a live webcam input. This enabled real-time machine vision to be applied to the acquired greyscale images using pixel value filters to identify interfaces and measure depth automatically (see Figure 5-2). Despite this, it struggled to consistently provide images that had clearly discernible tissue interface features in it (see Figure 5-3). It was ascertained that the 'grainy' image in addition to the image quality lost in the conversion from analogue to digital hardware affected the capability of providing clear images from this device.

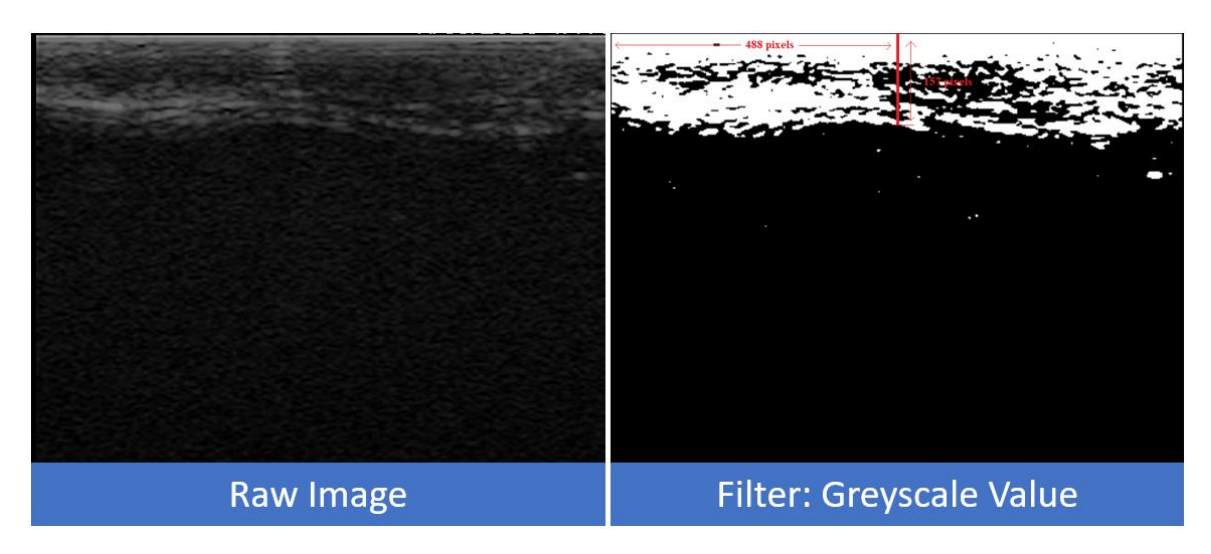


Figure 5-2: Machine vision algorithms applied to ReproScan Flexx system for automated fat depth measurement.

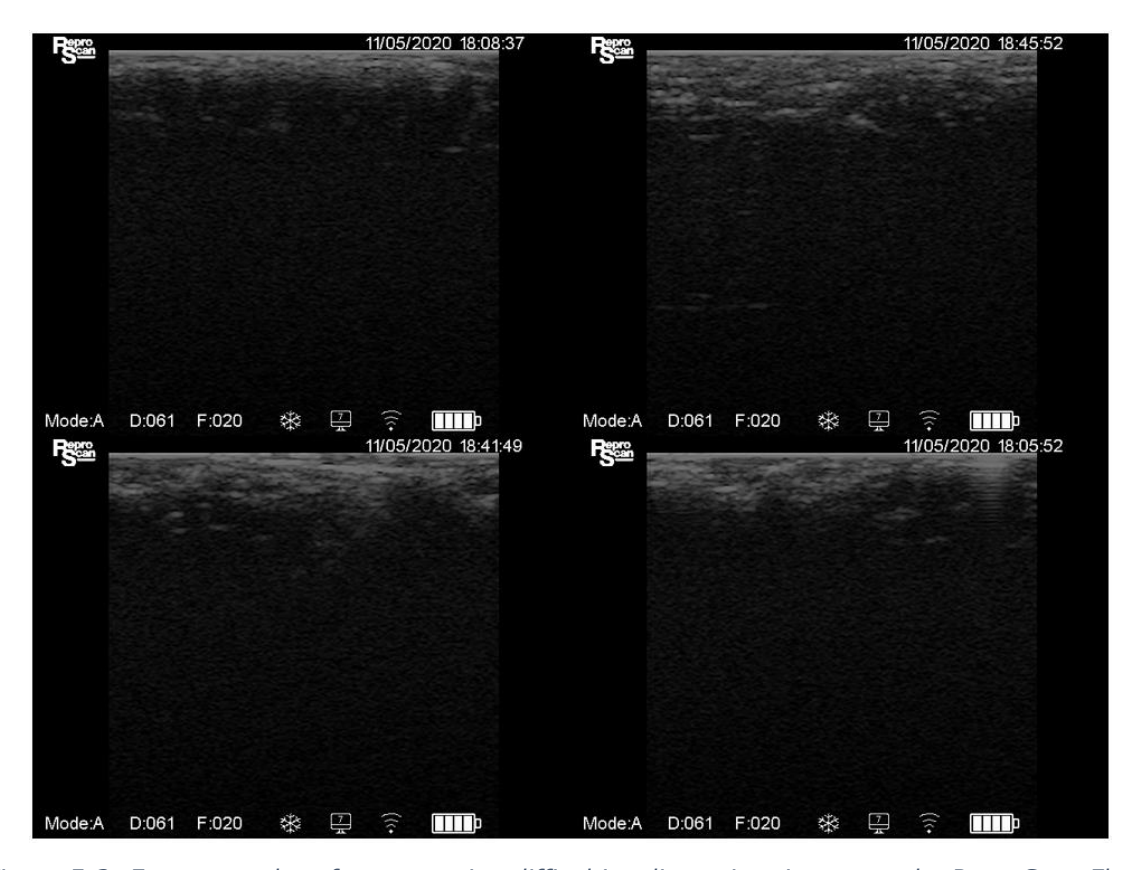
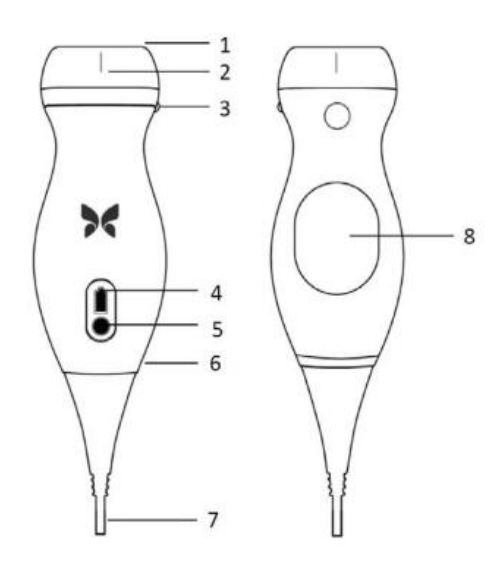


Figure 5-3: Four examples of encountering difficulties discerning tissues on the ReproScan Flexx.

As such, the Butterfly iQ+ device was trialled which provided images with more clarity and tissue discernability. This was the predominant basis for selecting the Butterfly iQ+ probe for this application.

The probe of the Butterfly iQ+ has 9000 capacitive micromachined ultrasonic transducers (CMUT) arranged in a 2D array with an adjustable frequency range of 1-10 MHz and penetration depth between 10-300 MHz mm (Butterfly, 2023a). The probe components are shown in Figure 5-4.



**Table 3-1 Probe Components** 

tem	Description	Item	Description
1	Lens	5	Battery Indicator Button
2	Midline Mark	6	Probe/Cable Boundary
3	Orientation Mark	7	Mobile Device Cable
4	Battery Indicator Lights	8	Charging Surface

Figure 5-4: Butterfly iQ+ probe components. Source – (Butterfly, 2023b)

A rubber standoff was purchased to ensure that contact on the non-planar surface of the striploin was achieved more consistently. In addition to better contact producing images that provided more discernible tissue interfaces, this standoff provided a 5 mm offset from the surface of the subcutaneous fat which provided a means of measuring nearer to the required minimum fat depth (see Figure 5-5 & Figure 5-6). In conjunction with this standoff, several food-safe lubricants were trialled for use before selecting extra virgin olive oil as the lubricant.



Figure 5-5: Photo of the Butterfly iQ+ with ultrasonic standoff attachment.

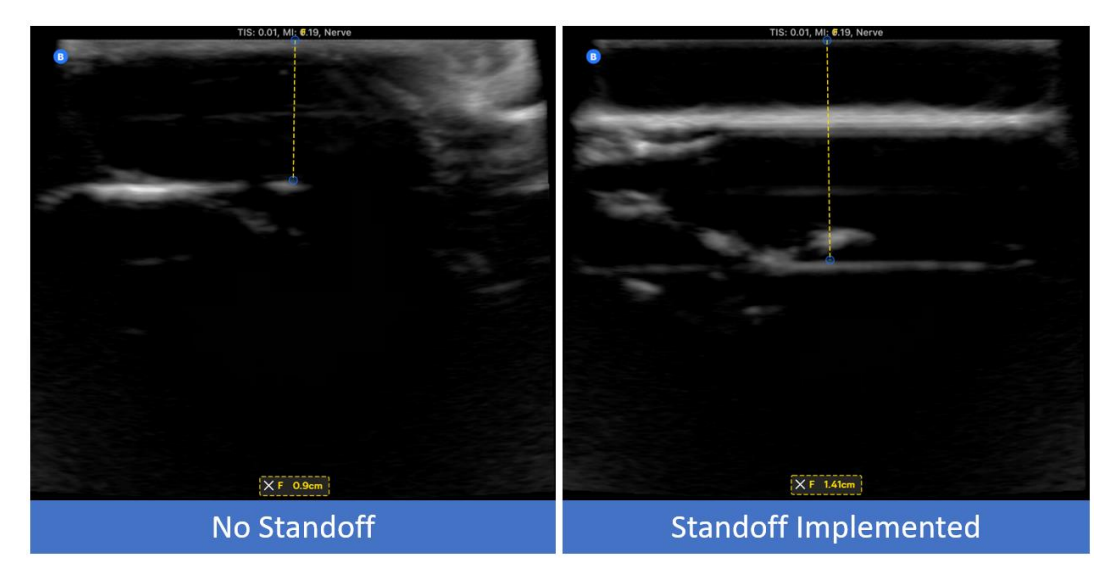


Figure 5-6: Improvement of tissue discernibility within an image taken at the same node on a striploin using ultrasonic standoff with Butterfly iQ+.

This probe and software package was used in-conjunction with an iPad mini (5<sup>th</sup> generation) to provide computational processing to the probe as well as save the images to the Butterfly network cloud where measurements could be taken (see Figure 5-7). For an automated system integration, a Wi-Fi communication from the iPad into a laptop could be created to enable the live feed to be used as a webcam for further machine vision processing.

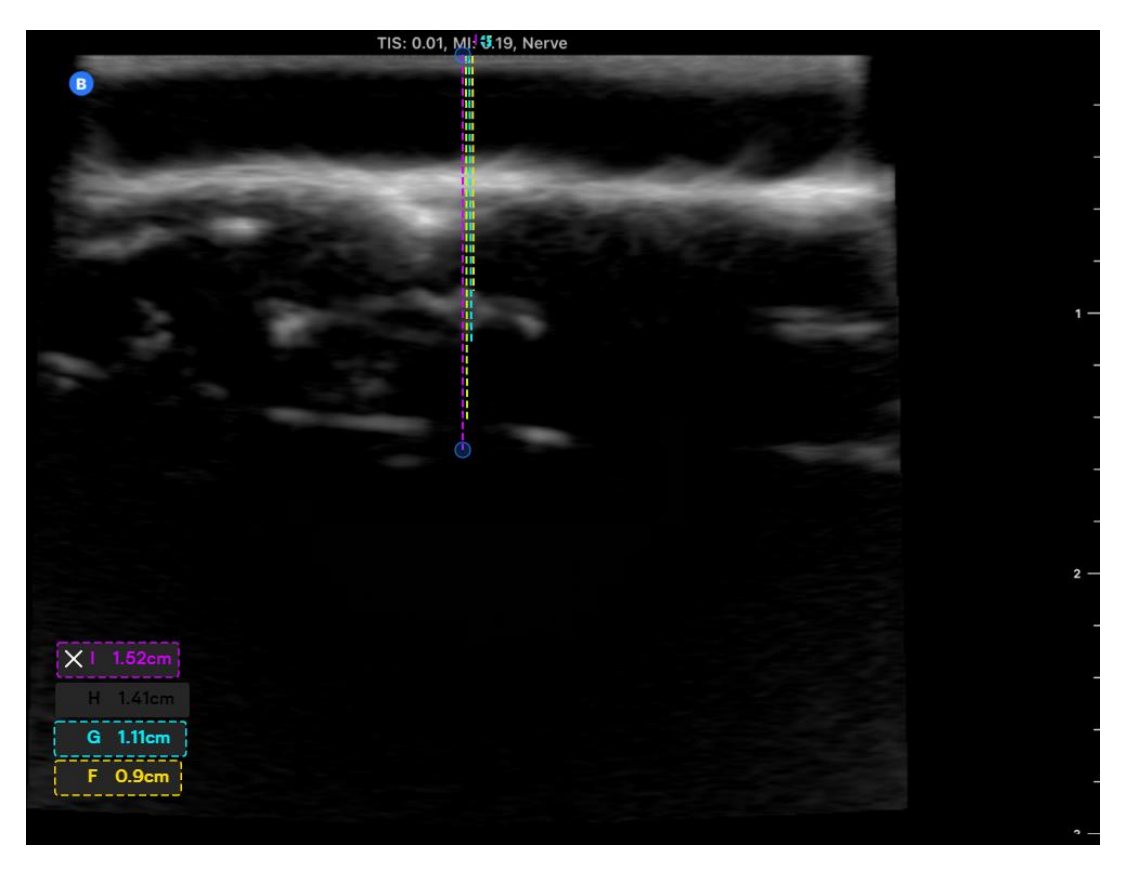


Figure 5-7: A screenshot of the user-interface for acquiring measurements from saved images stored on the Butterfly cloud.

The Butterfly iQ+ software system also enabled the tuning of parameters to ensure tissue echo, and its depth, could be measured. These parameters were set within preset configurations classified as medical practitioner applications (e.g. Abdomen, Cardiac, Soft Tissue, etc.). The presets defined the ultrasound frequency and penetration depth, focus/gain, transducer configuration and visualisation mode (Mode B was selected). Of all presets the most appropriate was "Nerve" which set a penetration focus of 30 mm depth. This aligned with the average fat depth of the striploin, which after the 5 mm thick standoff, provided the best focus for detecting superficial tissue interfaces near the surface of the striploin. The probe also calibrated itself based upon an on-board air temperature sensor that considered the temperature of the medium.

**Sensing Range:** The sensing orientation chosen for this experiment was from the fat surface. The delamination of fat layers that

were cited by previous research leading to measurements from the lean surface was not observed in surveys presented in Chapter 3 and hence, this was identified to be less prominent and risky than the interfaces seen in the lean muscle of striploins. The measurement depth would be significantly less through the fat as opposed to the lean meat of up to a penetration depth of 103 mm required (97.5% confidence interval) as opposed to a depth of an absolute maximum fat depth of 75 mm. The trade-off between penetration depth and image clarity was a more important consideration for B-Mode as opposed to A-Mode due to the subjectivity of image interpretation.

The relationship between ultrasound penetration depth and the soundwave frequency is informed by the penetration depth decreasing as the frequency increases. This is because higher frequencies have shorter wavelengths, leading to more interactions with the medium and thus greater attenuation. Typically, the rule of thumb to calculate the penetration depth of a particular frequency of sound in a given medium is  $500\lambda$  (Johnson & Wales University, 2019). Using the equations below the minimum frequency of ultrasound for the given depth is defined as shown in Equation 5.1).

*Effective Penetration Depth,* 
$$D_P = 500\lambda$$
,

Considering:

$$Wavelength, \lambda = \frac{v_W}{f},$$

Penetration Depth, 
$$D_P = 500 \left(\frac{v_W}{f}\right)$$
,

Equation 5.1: Rule of Thumb for Penetration Depth.

Frequency for Depth, 
$$f_D \leq 500 \left(\frac{v_W}{D_P}\right)$$
,

where:

 $v_W$  = velocity of soundwave through medium  $D_P$  = effective penetration depth (in metres)

Considering a maximum penetration depth of 75 mm (0.075m), and the velocity of soundwave propagation through subcutaneous fat of 1,450 m/s (Johnson & Wales University, 2019) the appropriate frequency is determined as follows:

Frequency for Depth, 
$$f_D \leq 500 \left(\frac{1450}{0.075}\right)$$
,
Frequency for Depth,  $f_D \leq 9.67 \; MHz$ ,

The B-Mode ultrasound probe transmits 1 - 10MHz soundwaves (having a selectable preset of less than 9.67 MHz), and hence was determined to provide the penetration depth required for this application within the chosen configuration.

**Sensor Response Time:** The response of this ultrasound device was measured to be less than 1 second to acquire the measurements of the B-Mode ultrasound into the iPad with only a small amount of latency for connection to a laptop. For machine vision to be applied to acquire a measurement value and provide this to a robot operating system would be a response time of approximately 3 seconds.

Fat Depth Measurements: In general, prior to the selection of B-Mode ultrasound system three systems were evaluated in preliminary trials to confirm that this sensor was the most capable of providing fat depth readings. This was conducted through a number of preliminary trials to test that measurement data was indicative of fat depth measured in beef striploin primals. During these preliminary trials, testing

methodology contained in this chapter was developed and applied for 2 striploins which showed ultrasound measurements aligned with manual ruler-derived measurements. Furthermore, 'calibration cubes' were created by cutting an interface into cubes of beef dripping at known, varying depths to ensure that these interfaces could be seen and to check the penetration depth of the settings used for the experiments (see Figure 5-8, Figure 5-9 & Figure 5-10).



Figure 5-8: Creation of phantom tissue interfaces at known depths within beef fat for preliminary testing.



Figure 5-9: Preliminary experiments validating Butterfly iQ+ tissue depth measurements.

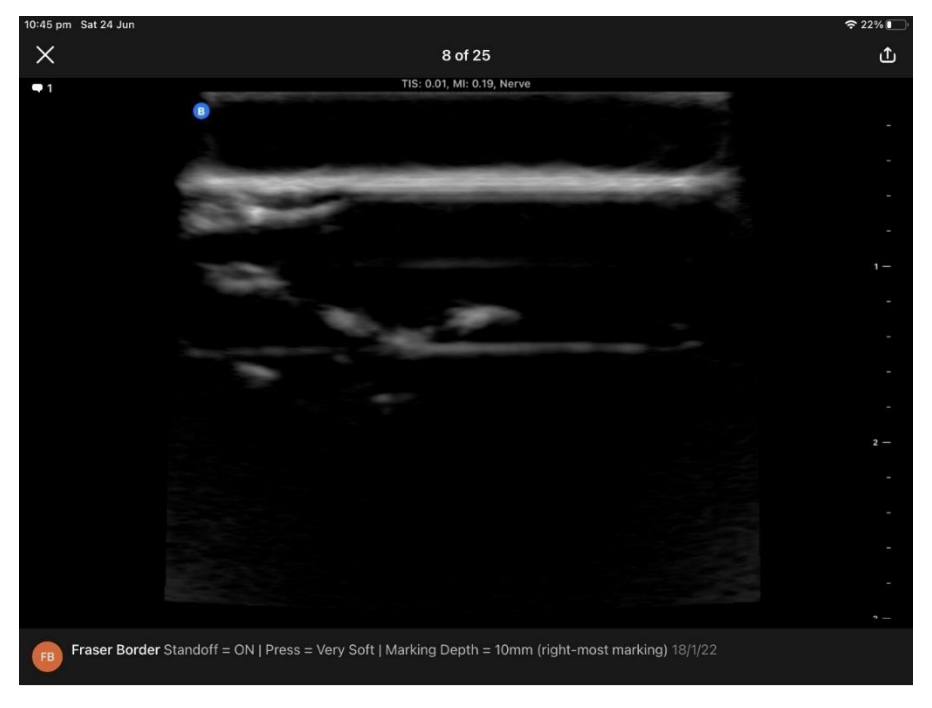


Figure 5-10: A preliminary experiment showing the tissue measurement of a 10 mm deep tissue interface created on side III of the calibration cube showing 15 mm deep (10 mm deep + 5 mm standoff thickness).

## 5.2.2 Experimentation

Experiment Samples: The same samples used in Chapter 4 (striploin 1R, 2R, 3L & 4L) were used in this analysis as well as an additional two striploins that were made available by the collaborating processor. Therefore, a total of six striploins were used in this experiment (LHS: 3 & RHS: 3) which equated to 358 nodes measurements in total. These six striploins deemed to be 'typical' of the untrimmed striploin as their overall characteristics (dimensions and weight) were comparable with those surveyed in Section 3.2.

**Node Marking:** The nodes were marked on the plastic of the striploin fat surface as shown in Chapter 3 before CT imaging. Upon returning the striploins to the refrigerated trailer they had the CT markers on them (see Figure 5-11).



Figure 5-11: Experimental set-up for B-Mode ultrasound sensing experiment.

A stainless-steel was used to poke holes through the plastic to score the node on the surface subcutaneous fat. Upon doing so, the striploin measurement nodes are transferred from the plastic wrapping to the striploin surface. The spacing used for this node mesh was 50 mm in the

X direction (across the length / medial-lateral anatomical plane of the striploin) and 25 mm in the Y direction (across the width / caudal-cranial anatomical plane of the striploin) shown in Figure 5-12.



Figure 5-12: Marking nodes through plastic wrapping using a stainless-steel skewer.

Fat Depth Measurements using B-Mode Ultrasound: Literature suggests the clear link between temperature and soundwave propagation through lean muscle and subcutaneous fat (Diaz-Almanza et al., 2021). To account for this all sensor measurements were taken at a controlled temperature of 8 degrees Celsius in a refrigerated trailer to ensure a similar temperature to that of the processing line.

The probe and the striploins were left in the temperature-controlled room for long enough to ensure that the probe, and hence the temperature adjustment on the probe, was to that of the striploin and environment. After this, the striploin was carefully unwrapped from the plastic wrapping and the Butterfly iQ+ ultrasound probe was placed on each node to acquire ultrasound images. The orientation of the Butterfly iQ+ probe was carefully aligned to ensure that the centre of the probe was aligned to the node so that the centre of the image may be evaluated for precise measurements at the nodes. This was done visually by aligning

both of the blue lines marked on both sides of the probe (indicating the middle of the probe) with the measurement node to acquire images. The image was then analysed on Butterfly Cloud software with measurement tools (see Figure 5-13).

For all of the measurements the standoff and olive oil was used with a single attempt to acquire an image at each node. In some cases the shape of the probe head (with the standoff) and the chasms in the fat surface caused difficulties in acquiring a sound image due to lack of surface contact between the transducer array and the subcutaneous fat (see Figure 5-14). In the case whereby the lack of contact of the ultrasound transducers prevented the acquisition of a discernible image, this node was counted as a 'missed reading'.

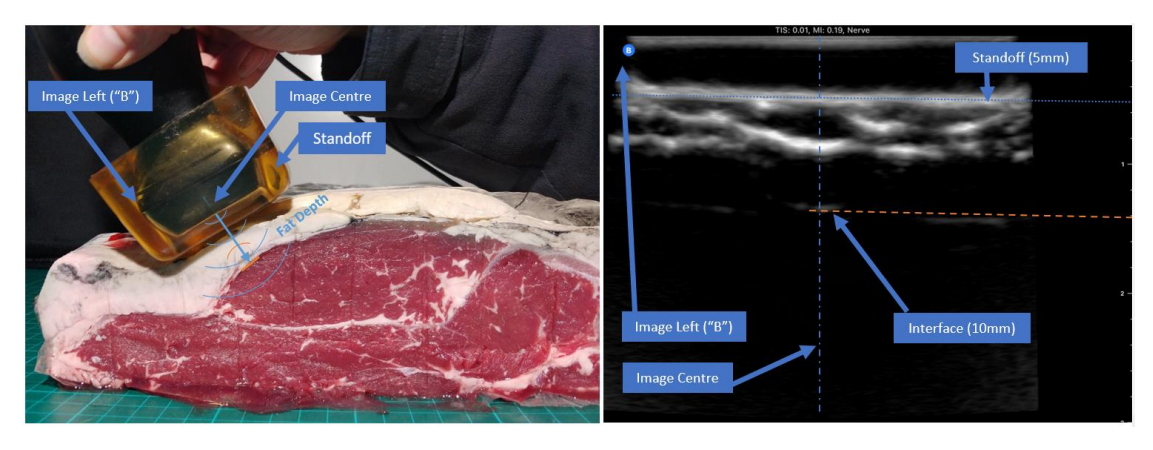


Figure 5-13: Illustration of using B-Mode ultrasound to measure fat depth.

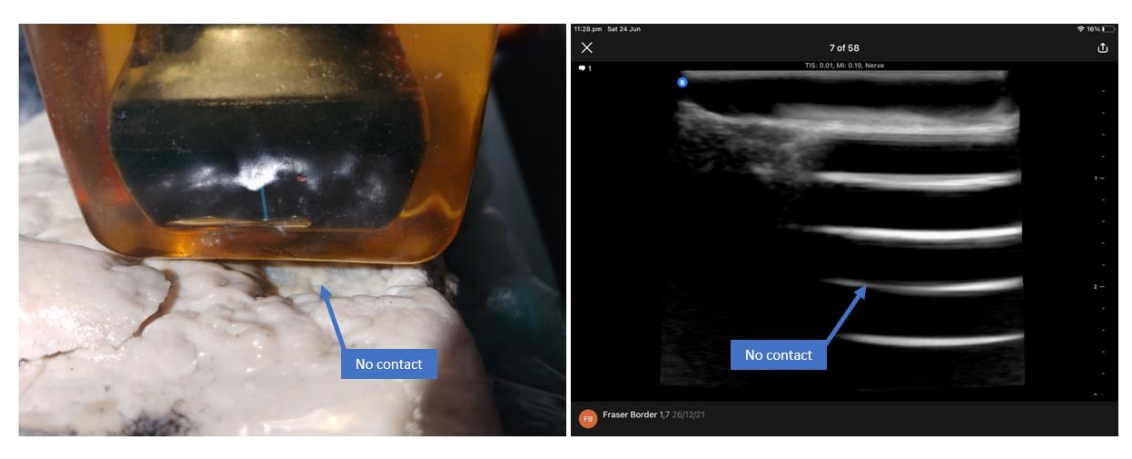


Figure 5-14: An example where the ultrasound could not get a reading due to air gap separation with the surface of the fat.

Fat Depth Measurements using a Ruler: The process of acquiring fat thickness measurements through a manual process using a stainless-steel ruler is outlined in Chapter 3. It is important to note that the B-Mode ultrasound imaging was conducted prior to manual measurements to ensure that there was no deformation causing soundwave backscattering. Upon ultrasound imaging, these nodes were marked with black, food-grade dye, cut into cross-sections and measured at the cross-section face.

A dissection of the striploin was made across the cross-sectional face of the striploin at each 50 mm face. A stainless-steel ruler was then used to record manual fat depth at each node which was recorded in an Excel spreadsheet for later analysis. A photograph of each cross-section, and each node, was acquired to provide a cross-referenceable record and qualitative data of the fat depth measurements (see Figure 5-15).



Figure 5-15: Manual measurements of fat depth at each node: qualitative (left) and quantitative (right)

# **5.3 Experimental Analysis**

This B-Mode ultrasound sensing system was evaluated against the sensor performance evaluation framework developed in Chapter 4 (see Table 4-9). This will be evaluated by considering the error between the manual and B-Mode ultrasound measurements that were interpreted from the greyscale images. As such, the following equation can be considered to calculate error (see Equation 5.2).

Equation 5.2: Error between B-Mode ultrasound and manual fat depth measurements.

Error, 
$$E_{M-US_B} = f_M - f_{US_B}$$

where:

 $f_M$  = the fat thickness measurement acquired manually using a ruler (considered the reference value);

 $f_{US_B}$  = the fat depth measurement acquired using the B-Mode ultrasound sensor (considered the estimated value);

As outlined in Chapter 4 the performance metrics were calculated using the equations specified below:

- Accuracy: Median of Error dataset (see Equation 4.3).
- Precision: IQR of Error dataset (see Equation 4.4).
- Linearity: Coefficient of Determination (see Equation 4.5).
- Reliability: The 'Miss Rate' of the sensor (see Equation 4.7).
- Response Time: The time required to acquire a measurement.

For reliability, the total number of nodes were considered as the number of nodes that there was a measurable lean muscle presented. In some cases, there were nodes where the striploin did not have a lean muscle interface that was measurable. Therefore, at the nodes that there was the capability of ultrasound measurement, and the device provided an error value this was considered a 'missed' instance. Typically, these readings displayed an image without any recognisable tissue interface reflections or predominantly displayed ultrasound reflection errors (see Figure 5-16). In preliminary trials two cases of 'no value' or 'missed' measurements were identified:

- Case 1: No contact between the ultrasound probe head and the subcutaneous fat surface due to surface contours (illustrated in the left image in Figure 5-16).
- Case 2: No interface was discernible in ultrasound image due to the absence of soundwave echo received by the ultrasound transducer (illustrated in the right image in Figure 5-16).

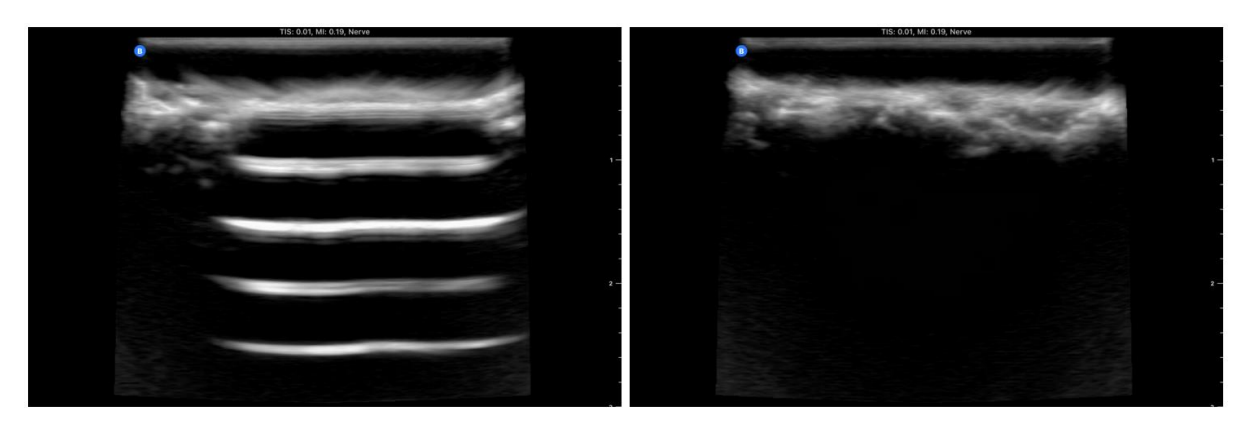


Figure 5-16: Example of the two "No read" / "Missed" measurements for a B-Mode ultrasound.

During the preliminary investigation this sensor was deemed capable to measure at a response time appropriate for this application  $(T_R \leq 15 \, sec)$  and was determined to be less than 3 seconds during measurement observations.

### 5.4 Results

Through evaluating the B-Mode ultrasound and ruler measurements of 6 striploins (RHS: 3, LHS: 3) a total data set of 358 nodes were considered in this investigation.

The error measurement dataset (E) was calculated to create a means of evaluating the distribution of error between the ruler ( $f_R$ ) and B-Mode ultrasound ( $f_{US_B}$ ) fat thickness measurements. Key statistical measures are presented for the unfiltered dataset, and the 1.5 IQR filtered dataset (see Table 5-1).

Table 5-1: Statistical summary of error dataset (E) between ruler and Mode B ultrasound measurements (n = 358)

Statistics	Unfiltered Dataset	Filtered Dataset
Minimum of Error Dataset, $Q_0(E)$	-8.6 mm	-8.6 mm
25th percentile of Error Dataset, $Q_1(E)$	1.0 mm	0.8 mm
Median of Error Dataset, $Q_2(E)$	4.5 mm	4.0 mm
Mean of Error Dataset, $(\bar{E})$	6.5 mm	5.2 mm
75th percentile of Error Dataset, $Q_3(E)$	11.0 mm	10.0 mm
Maximum of Error Dataset, $Q_4(E)$	36.0 mm	19.0 mm
Interquartile Range of Error Dataset, $IQR(E)$	10 mm	9.3 mm
Standard Deviation of Error Dataset, $SD(E)$	7.9 mm	6.3 mm
Range of Error Dataset, $Range(E)$	44.6 mm	27.6 mm
Lower Outlier of Error, $Q_1(E) - 1.5IQR(E)$	-10.5 mm	-9.9 mm
Upper Outlier of Error, $Q_3(E) + 1.5IQR(E)$	19.5 mm	17.9 mm

Zero lower and twenty-five upper bound outliers were identified in this dataset and removed for the creation of the filtered dataset. Filtering the outliers from this dataset, and comparing it to the unfiltered dataset, the general trends and error characteristics were quite similar though these outliers had increased the spread of error at a higher positive value (median, average, IQR). This is shown in Figure 5-17.



Figure 5-17: Statistical Summary of error measurement datasets (unfiltered vs filtered).

Considering the unfiltered dataset is statistically representative the resulting B-Mode ultrasound accuracy and precision metrics were identified as:

Accuracy: Median of Error,  $E_{MDN}$  = +4.5 mm Precision: Interquartile Range of Error, IQR(E) = 10.0 mm

Due to the impact of large, positive outliers a slight decrease in precision of 0.7 mm (larger IQR) and accuracy of 1.3 mm (higher median error). These outliers caused the spread of error to be further towards positive errors (under-estimating the fat depth measurements). For the purposes of evaluating the accuracy (median) and precision (IQR), the effect of outliers was deemed to not to be substantial, though suggested that the sensor or the interpretation of ultrasound images may have been biased.

The unfiltered dataset was plotted on a histogram using bin widths of 4 mm, with excess bins being used to group lower and upper bound outliers (see Figure 5-18).

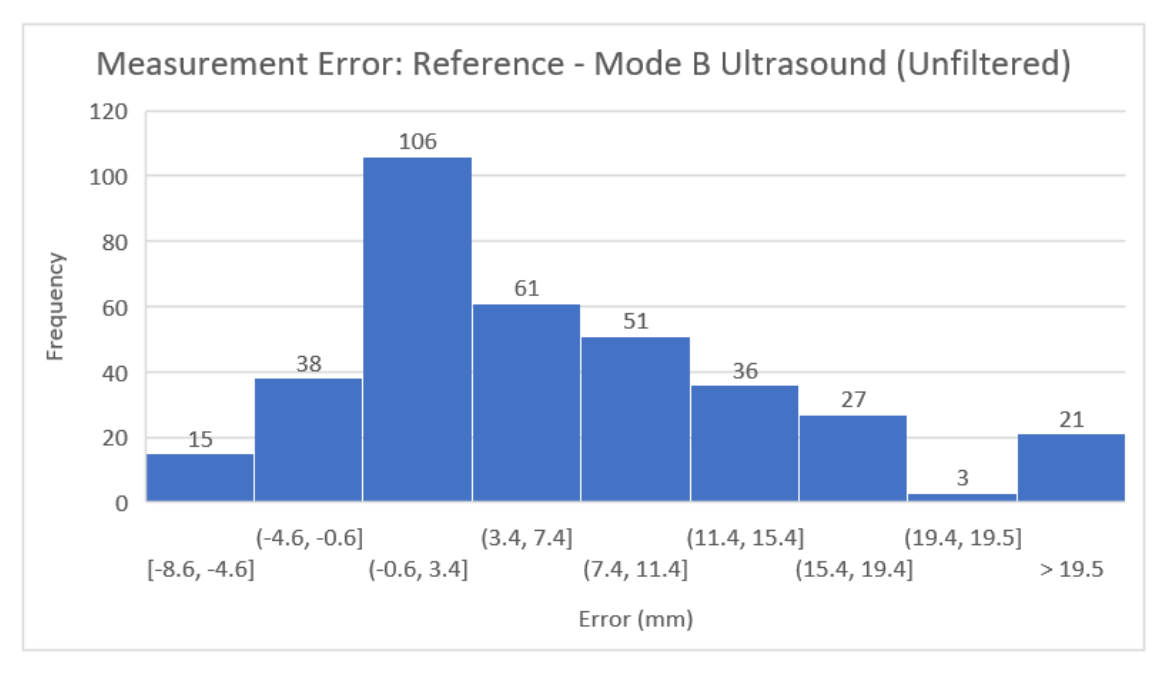


Figure 5-18: Error distribution of unfiltered data showing a non-normal distribution.

This error distribution is not normally distributed, and instead is positively skewed, showing a bias for B-Mode ultrasound to provide an under-estimation of fat depth. The central peak at -0.6 to 3.4 mm error supports that there are no underlying subgroup trends in the dataset except for the positive outliers highlighted previously.

The measurement error across the range of measurements acquired is described in Figure 5-19. An immediate observation derived from the scatterplot is that whilst B-Mode ultrasound was observed to measure fat depth between the range required (0 - 75 mm) in preliminary testing, it did not provide accurate measurements across the operating range. The value of the correlation of determination  $(R^2)$  indicates that spread of residual errors is wide, and in general, do not depict strong linear correlation. The predicted and actual measurements are quite dissimilar across the entire measurement error dataset (see Figure 5-20 & Figure 5-21). It was observed that this was predominantly occurring at larger measurements of fat depth. A significant bias was observed in measurements between 10 to 20 mm even in the instance where the fat depth was a lot larger. The significant variation of error throughout the range of reference measurements indicates strong heteroscedasticity.

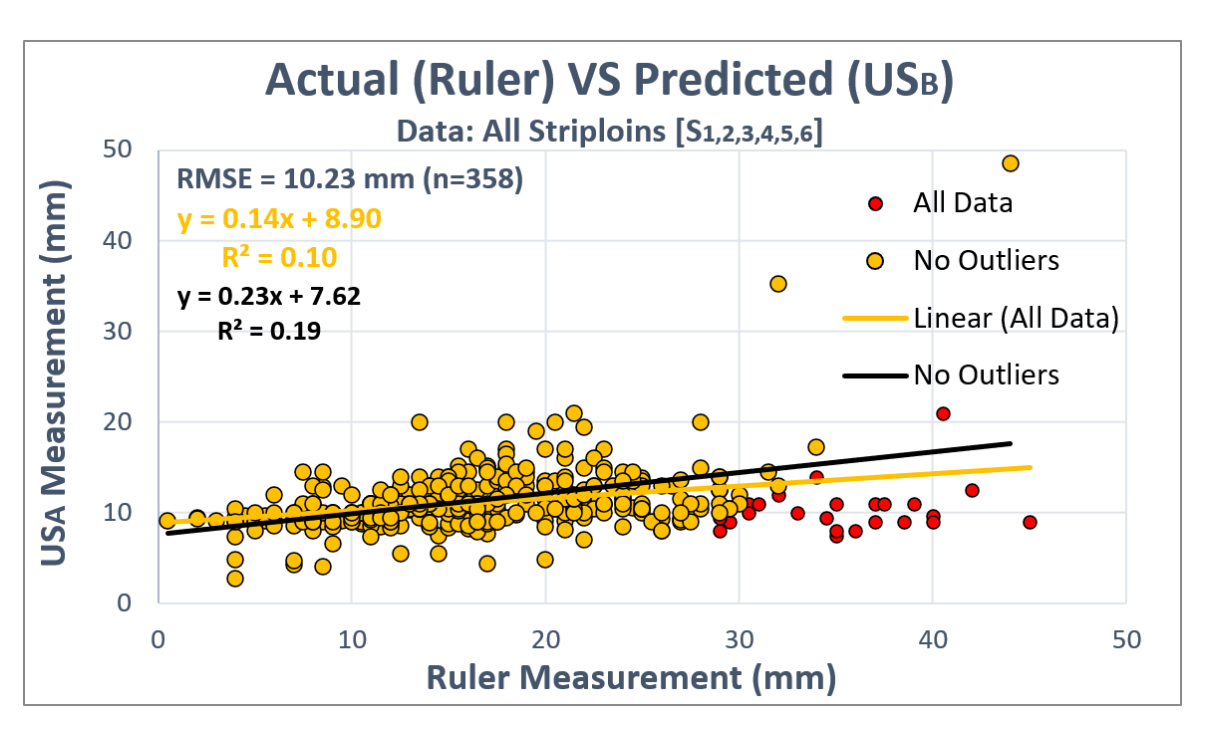


Figure 5-19: The B-Mode ultrasound (USB) vs actual (Ruler) measurement plot.

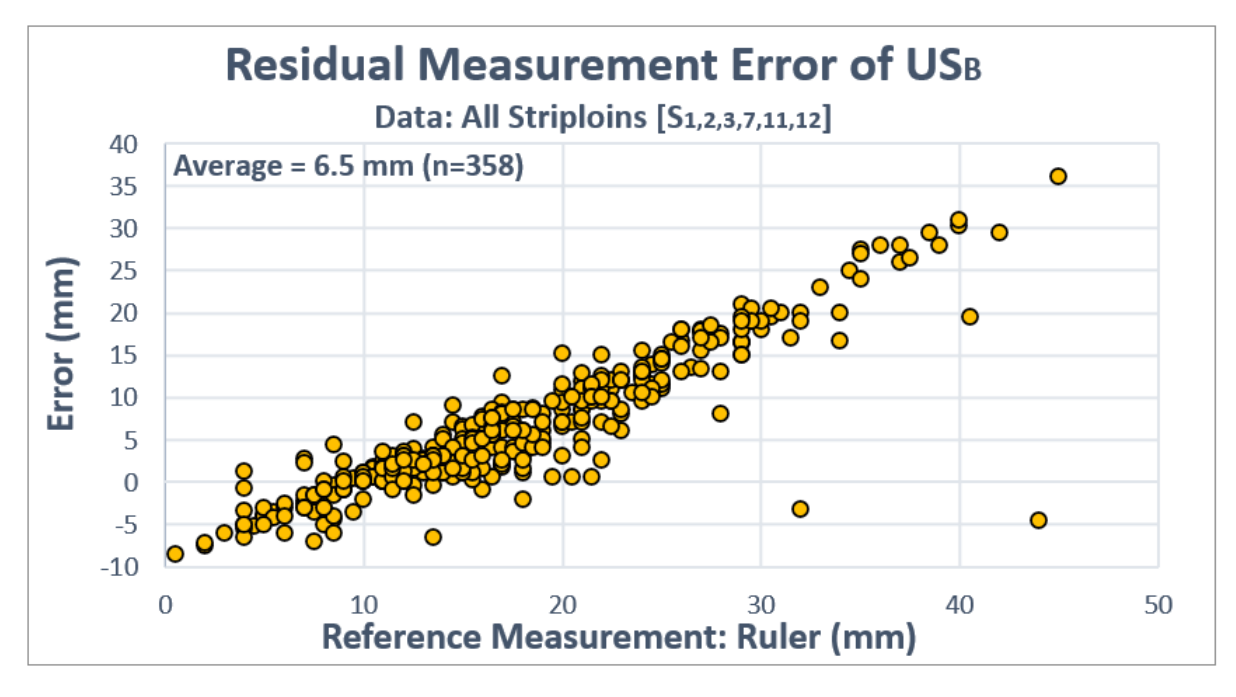


Figure 5-20: Residual error plot of USB-Ruler Dataset (in mm)

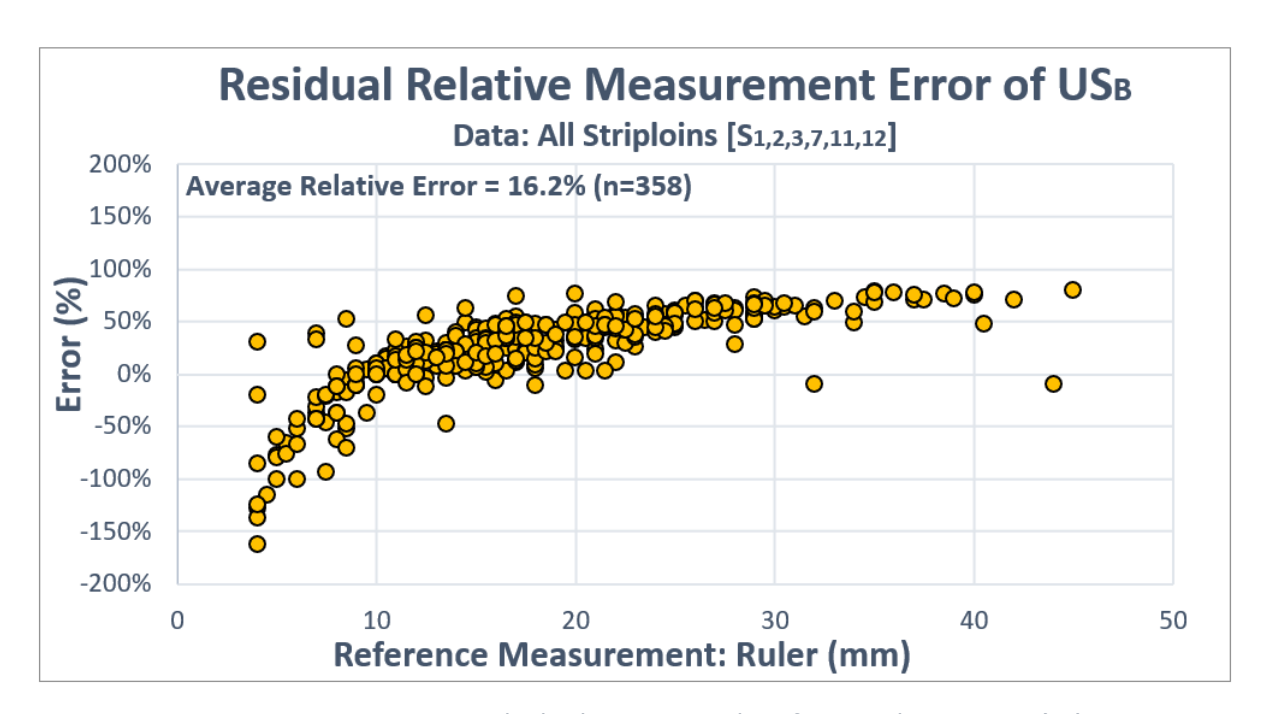


Figure 5-21: Residual relative error plot of USB-Ruler Dataset (%)

As a benchmark of linearity across the operating range, B-Mode ultrasound is concluded upon with the following measures:

## **Range Requirements:**

Found to be feasible in preliminary analyses.

## Linearity:

 $Variance\ over\ Operating\ Range\ \equiv\ R^2=0.10$ 

There were a number of instances whereby the B-Mode ultrasound returned an image that the tissue interface was indiscernible within. From the 410 nodes of potential measurements, 52 nodes did not have a measurement acquired. As such, the miss rate ( $P_M$ ) for B-Mode ultrasound was concluded to be as follows:

# **Reliability:**

Miss Rate, 
$$P_M = \frac{52}{410} * 100\% = 12.7\%$$

It was identified that the response time of the B-Mode ultrasound system to return a measurement to a robotic control system would be approximately less than 3 seconds.

## **Response Time:**

Response Time,  $T_R \leq 3$  second

### 5.5 Discussion

An analysis of B-Mode ultrasound results highlights the predominant distribution of error around zero which indicates that the sensor returned sensible measurements, though skewed with positive error (median error = 4.5 mm). The large spread of error (IQR of error = 10.0 mm) illustrates the imprecision of this sensor to provide measurements that closely represent manual measurements.

The presence of twenty-five, upper-bound outliers (>19.5 mm), in the absence of any lower-bound, negative errors, skewed the data towards higher positive error values. Although the elimination of these outliers did reduce the overall inaccuracy (median error reduced from 4.5 mm to 4.0 mm) and imprecision (IQR of error reduced from 10.0 mm to 9.3 mm), similar overall error trends were observed in both the outlier-filtered (+-1.5IQR) and unfiltered datasets. These outliers were significant enough to illustrate a second peak in the error distribution histogram plot (see Figure 5-18) and highlight systemic bias to underestimate the fat depth at measurement nodes (Note: Error = Manual - Sensor measurement; hence positive error is underestimation of fat depth). The cause for this bias is either due to the sensor to produce clear ultrasound images, the incorrect interpretation of these images, and or, the ultrasound wave reflection of internal tissues within the subcutaneous fat of striploin primal product. Through extensive preliminary

experimentation with the Butterfly iQ+ that included cross-referencing tissue depth measurements with known, artificial interfaces cut into beef lard (melted beef fat) the consistency, quality and depth calibration of these images have been confirmed. The interpretation of images was quite simple, and even though post-examination of looking for a tissue at a known depth (manually measured) many images didn't show any indication of the fat-lean interface tissue. It is probable that a large proportion of positive errors was a measurement to an interface that was significantly shallower than the actual tissue interface due to fat delamination. Whilst delamination of the subcutaneous fat was evaluated in the product survey conducted in Chapter 3 it is suspected that the significance of this phenomenon within the internal product was significantly more than that observed, and perhaps the capability to visually identify delamination phenomena was overestimated (note: a fraction of a millimetre air gap within a fat layer will reflect soundwaves and appear as a tissue interface). This would also explain why this phenomenon was not evident in preliminary trials using beef lard which is rendered (melted) in a way to form a solidified beef fat product that does not contain fat layers. This would also explain a lot of the positive bias of the errors produced by this sensing system (median = 4.5 mm), as well as the poor heteroscedasticity and linearity observed for this sensing system ( $R^2 = 0.1$ ). It should be noted that this error was not due to human misinterpretation error, but the lack of deeper interfaces visibly present in the image due to the inability of soundwaves to pass through the air gap of the fat layer and therefore illustrated to be the deepest interface on the image.

B-Mode ultrasound technology provided more information at each node through the representation of tissue measurements as an image as opposed to A-Mode which provided a numerical value. Though there is a degree of certainty that can be received through an image (e.g., seeing a continuous 'line' that would perhaps represent a tissue interface),

importantly the distinction between the fat-lean interface and an air pocket within the subcutaneous fat layers cannot be easily distinguished. The reliability performance metric (reliability = 12.7%) is likely to have been artificially inflated due to the perceived correctness of the fat-lean tissue interface identifiable within an image, when in reality, this assumption was incorrect due to this tissue interface being air pocket of a fat layer. The perceived attractiveness of this technology to provide more certainty in the information reported at each node was not seen to translate to a better performance.

Though the decision to measure from the surface of the subcutaneous fat was sound based upon known parameters prior to the development of this system, the findings of these results suggest an alternative sensing configuration due to the issues of fat delamination. Instead, this sensing system should be applied measuring from the lean surface of the striploin, at a lower frequency setting, to avoid such biases caused by the delamination of subcutaneous fat layers of the beef striploin. Whilst it is believed that there will be false detections of intramuscular and inter-muscular tissue interfaces, the images collected in this study highlight that these are typically very different, and discrete, when compared to the continuous fat-lean interface (as opposed to air within fat layers mistakenly identified).

The performance of B-Mode ultrasound in comparison to CT imaging is shown in Table 5-2. As expected, B-Mode ultrasound performed significantly worse in all performance metrics when compared to the gold standard of CT imaging except for response time. This comparison highlights that B-Mode ultrasound is approximately a magnitude of four times as inaccurate and imprecise as CT imaging, with a significantly disproportionate performance in linearity and reliability. Despite this, the response time of less than 3 seconds indicates the satisfaction of the response time metric that makes this a feasible technology for the

application of beef striploin fat trimming. In summary, the performance of this sensing system is defined below through applying the performance evaluation framework developed in Chapter 4 (see Table 5-3).

Table 5-2: Comparison of fat measurements using B-Mode ultrasound and medical-CT imaging.

Performance	Sensors for Fat Depth Measurement			
Metric	Medical-CT Imaging	B-Mode Ultrasound		
Accuracy $(E_{MDN})$	+1.2 mm	+4.5 mm		
Precision (IQR(E))	2.5 mm	10 mm		
Linearity (R <sup>2</sup> )	0.93	0.1		
Reliability $(P_M)$	0 %	12.7 %		
Response Time $(T_R)$	10 min	< 3 sec		

Table 5-3: Sensor performance evaluation framework applied to B-Mode ultrasound sensing system.

Performance Metric	Quantity	Performance Rank					Metric Weighting	Metric Score	
		FAIL/POOR 0	FAIR 1	AVERAGE 2	GOOD 3	EXCELLENT 4	EXCEPTIONAL 5		
Accuracy $(E_{MDN})$	4.5 mm	> 10 mm	≤ 10 mm	≤ 7.8 mm	≤ <b>5.6</b> mm	≤ 3.4 mm	≤ 1.2 mm	3	9
Precision $(IQR(E))$	10.0 mm	> 12.5 mm	≤ 12.5 mm	≤ 9.5 mm	≤ 6.5 mm	≤ 4.5 mm	≤ 2.5 mm	5	5
Linearity (R²)	0.1	< 0.5	≥ 0.5	≥ 0.6	≥ 0.71	≥ 0.82	≥ 0.93	2	0
Reliability $(P_M)$	12.7%	> 75%	≤ 75%	≤ 50%	≤ 25%	≤ 10%	≤ 1%	3	9
Response Time $(T_R)$	< 3 sec	> 15 sec	≤ 15 sec	≤ 7.5sec	≤ 3 sec	≤ 2 sec	≤ 1 sec	2	6
B-Mode Ultrasound Sensor Performance Score				29 / 75					

In general, when considering the weightings of these performance metrics, the B-Mode ultrasound sensing system is most significantly penalised for precision (5/25) and linearity (0/10), with "good" scores for accuracy (9/15), reliability (9/15), response time (6/10). The overall score of 29 / 75 will be used in the comparison between B-Mode and A-Mode ultrasound sensing systems in Chapter 7.

In terms of progression towards integration within an automated fat trimming system it is first recommended that the configuration to sense from the lean / medial surface of the striploin is trailed and evaluated using this framework. Pending the results of this evaluation, the ultrasound images acquired by the Butterfly iQ+ device can be sent to a laptop for image analysis to determine the depth of the tissue interface to then communicate this numerical value to a robotic trimming system to inform an automated cut path.

### 5.6 Conclusion

The analyses presented within this chapter provide a means of evaluating the use of B-Mode ultrasound technology as sensing system for automated fat trimming of beef striploin. This system was developed considering insights gained from Chapter 3 and 4 and evaluated using the performance evaluation framework presented in Chapter 4 that considered key performance metrics, weighted by importance, based predominantly upon the gold standard of CT imaging technologies for fat depth measurement. The B-Mode ultrasound sensing system achieved a 29 / 75 performance rating which will be compared to the A-Mode ultrasound system in Chapter 7. The key future recommendation being using the ultrasound sensor to measure from the medial surface of the striploin to avoid measurement issues arising from the delamination of fat layers on the beef striploin.

# CHAPTER 6: ANALYSIS OF A-MODE ULTRASOUND SENSING SYSTEM

This chapter focuses on the development and evaluation of A-Mode ultrasound technology for measuring the fat depth of a beef striploin primal. The objective is to assess the capability of A-Mode ultrasound to be employed in an automated system for uniform fat trimming of beef striploin. By applying the sensor evaluation framework developed in Chapter 4, this chapter concluded upon the effectiveness of A-Mode ultrasound as a sensing modality for this application. The findings presented in this chapter contribute to the understanding of the potential of A-Mode ultrasound technologies and inform the design and optimization of future automated fat trimming systems.

### 6.1 Introduction

This section presents fundamental principles and practical considerations of A-Mode ultrasound, highlights the key design considerations outlined in the analyses of previous chapters (Chapter 3 and 4), and presents the aims for the chapter.

A-mode ultrasound has been the longest used ultrasound technology in the beef industry, used for over 40 years to measure subcutaneous fat depth assisting in automated meat processing systems (Pathak, Singh & Sanjay, 2011). Numerous recent studies comparing A-Mode and B-Mode ultrasound suggest that the difference in accuracy of both modes for subcutaneous fat depth measurements is insignificant in most cases (Wagner et al., 2019; Wagner et al., 2020).

Whilst B-Mode ultrasound can provide clarity through additional information (presented in nearby pixels of an image), the ambiguity of which tissue is being measured cannot be negated completely from A-

Mode. The uncertainty of measuring the correct tissue interface is an inherent risk that accompanies the simplicity of this ultrasonic sensing technology, and the degree of this impact will be highlighted within this analysis.

# 6.1.1 Chapter Aims

The aims of this chapter were to develop and evaluate an A-Mode ultrasound system capable of measuring fat thickness and implemented within the context of an automated system.

Key design considerations that were highlighted in previous explorative work presented in Chapter 3 & 4 will be implemented in the design of this system to provide insights towards how a A-Mode ultrasound sensing system may be developed. The performance of this system was evaluated through applying the sensor performance evaluation framework to conclude on its performance and compare with another sensing technology (B-Mode).

### **6.2 Experimental Setup**

This section presents the preliminary analysis of the selected ultrasound sensor to demonstrate the feasibility of the chosen A-Mode ultrasound sensor considering insights from past analyses. This section outlines the methods employed for the data collection of acquiring sensor and manual fat depth measurements as well as the data analysis method implemented to evaluate the performance of the sensor according to the sensor evaluation framework developed in Chapter 4.

## 6.2.1 Preliminary Investigation into Sensor Feasibility

According to analyses summarised in previous chapters (Chapter 3 & 4), it has been identified that the following parameters define a feasible sensor for measurement of fat depth for the context of automated beef striploin trimming:

- The sensor range / penetration depth of the ultrasound
- Sensor Response Time
- Fat Depth Measurements (in practice)

As such, preliminary analyses within this section were conducted to confirm the feasibility of the chosen sensor prior to the development of a fat depth measurement system.

As outlined in Chapter 3, the work conducted alongside industry was using ultrasound to measure from the lean muscle surface of the striploin (Khodabandehloo, 2018). The A-Mode ultrasound system evaluated utilised a 1 MHz A-Mode ultrasonic probe (classified) as shown in Figure 6-1.



Figure 6-1: A-Mode ultrasound probe integrated into the fat depth sensing system.

The probe was integrated into a A-Mode measurement system in previous work conducted alongside industry through research into the feasibility of automated striploin fat trimming (AMPC, 2018). The system used hardware to interpret ultrasound signals into measurements to be serially communicated into a laptop application that provides a graphical

interface for presenting A-Mode measurement information (see Figure 6-2 & Figure 6-3).

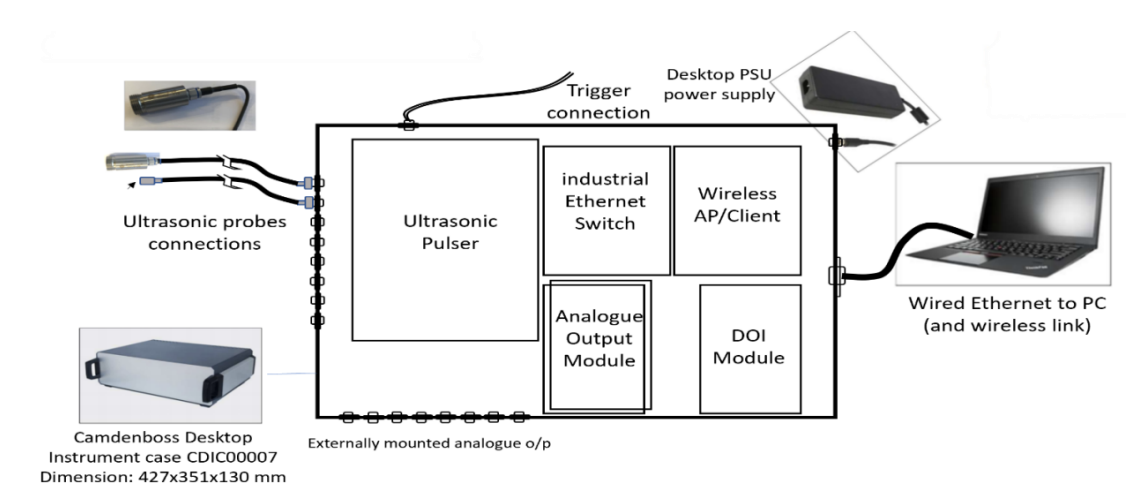


Figure 6-2: A diagram illustrating the A-Mode ultrasound system hardware. Source: Khodabandehloo, 2021).

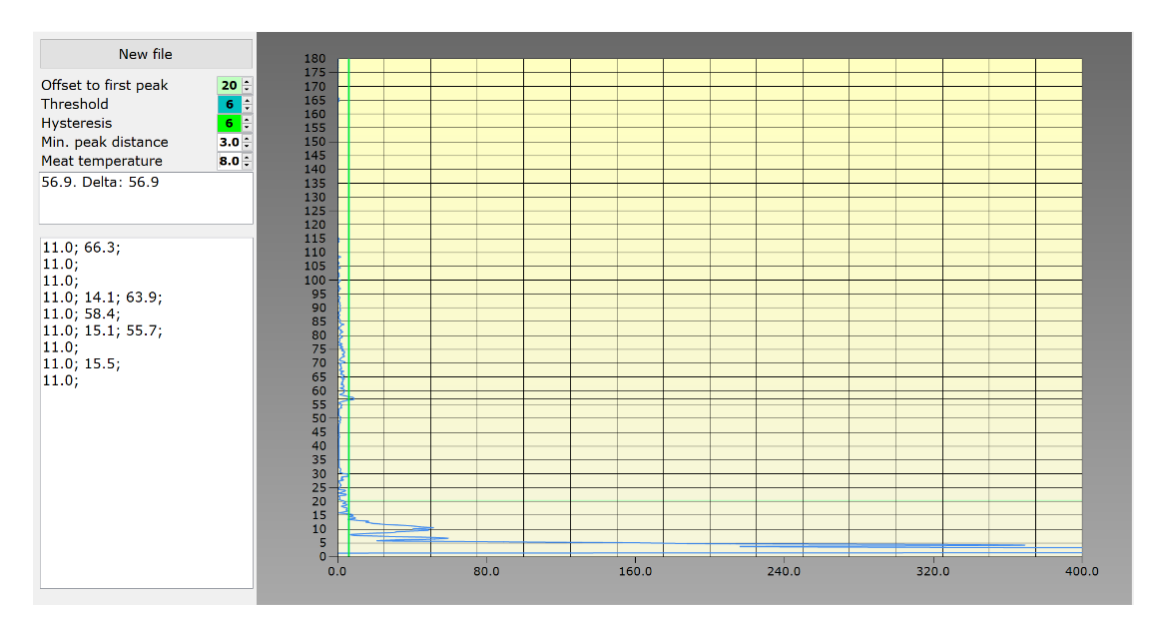


Figure 6-3: The software interface of the A-Mode ultrasound system.

The system software also enabled the tuning of parameters to ensure that the most likely tissue echo, and its depth, could be measured. These parameters included:

 offset to first peak (an offset used to ignore echoes that are too close to the ultrasonic transducer to be considered the fat-lean interface)

- threshold (a parameter that defines the amplitude of the echo that can be considered a tissue as opposed to signal disturbances)
- hysteresis (an offset used to differentiate between tissues close to each other and produce similarly distanced echoes)
- min. peak distance (an offset used to set the expected distance for which echoes are expected to be measured with the ultrasonic transducer)
- meat temperature (temperature is considered to more accurately estimate tissue depth based upon slight variations in soundwave speed through the lean muscle)

Sensing Range: The sensing orientation chosen for this experiment was from the lean surface to the fat lean interface. This decision was based upon the decision of industry research and development due to the presence of delamination in fat layers within the subcutaneous fat tissues that would introduce measurement error due to air bubbles disrupting ultrasound wave propagation (AMPC, 2018). The A-Mode ultrasound measurement was taken upon locating the probe onto the lean meat surface at each measurement node. From the striploins surveyed the maximum height of the striploin primals was seen to be 103 mm (within 97.5% confidence interval). As previously outlined in Chapter 5, the relationship between ultrasound penetration depth and the soundwave frequency can be described below.

Frequency for Depth, 
$$f_D \leq 500 \left(\frac{v_W}{D_P}\right)$$
,

Considering the maximum depth of penetration as 103 mm (0.103m), and the velocity of soundwave propagation through subcutaneous fat as 1,450 m/s (Johnson & Wales University, 2019):

Frequency for Depth, 
$$f_D \leq 500 \left(\frac{1450}{0.103}\right)$$
,  
Frequency for Depth,  $f_D \leq 7.04 \; MHz$ ,

The A-Mode ultrasound probe transmits 1 MHz soundwaves (less than 7.04 MHz), and hence was determined to provide the penetration depth required for this application within the chosen configuration.

**Sensor Response Time:** The response of this ultrasound device was measured to be less than 1 second to acquire the measurements of the A-Mode ultrasound into a laptop (and robot operating system), and so this was considered feasible for this consideration.

Fat Depth Measurements: In general, prior to development all sensors were evaluated in preliminary trials to confirm that the sensor was able to provide fat depth readings. This was conducted through a number of preliminary trials at the premises of the University of Southern Queensland to test that measurement data was indicative of fat depth measured in beef striploin primals. During these preliminary trials the methodology of this chapter was formed and applied for 4 striploins which showed ultrasound measurements aligned with manual ruler-derived measurements.

### 6.2.2 Experimentation

**Experiment Samples:** A random selection of sixteen LHS and four RHS striploin primals (#1 - 16) deemed to be 'typical' of the collaborating processor untrimmed striploins were chosen for this experiment (see Table 6-1). These were taken from the processing line on a typical production run of the collaborating processor and temporarily stored on a bench prior to sensing.

Table 6-1: Striploin dataset for the analysis of A-Mode ultrasound sensing.

Measurement Nodes of Striploin Dataset (Mode-A)				
Striploin #	L/R	Faces (X)	Markings (Y)	Nodes
1	L	8	4	32
2	L	9	4	36
3	R	8	4	32
4	R	8	4	32
5	L	7	4	28
6	R	7	4	28
7	R	9	4	36
8	L	9	4	36
9	L	8	3.5*	28
10	L	8	3.1*	25
11	L	8	3.5*	28
12	L	8	4	32
13	L	8	3.6*	29
14	L	7	3.0*	21
15	L	9	3.6*	32
16	L	8	4	32
Averages Number of Measurement Nodes			30	

Node Marking: A stainless steel plate, referred to as the 'striploin plate', was designed and manufactured from 5 mm thick 316L stainless steel plate to be integrated with a food-grade compatible robotic system (see Figure 6-4). The striploin plate was designed with 22 mm slots to ensure the ultrasonic probe (20 mm in diameter) could be protruded through the plate and into the lean (medial) surface of the striploin. These slots were spaced at 37 mm (centre-to-centre) which was found to provide measurement nodes at a close proximity whilst restricting plate deflection under the striploin weight which would complicate programming precise positioning of the ultrasound probe. The first iteration of this 'striploin plate' was made with holes, though the use of slots enabled adjustment of measurement nodes lengthwise if needed during prototyping.

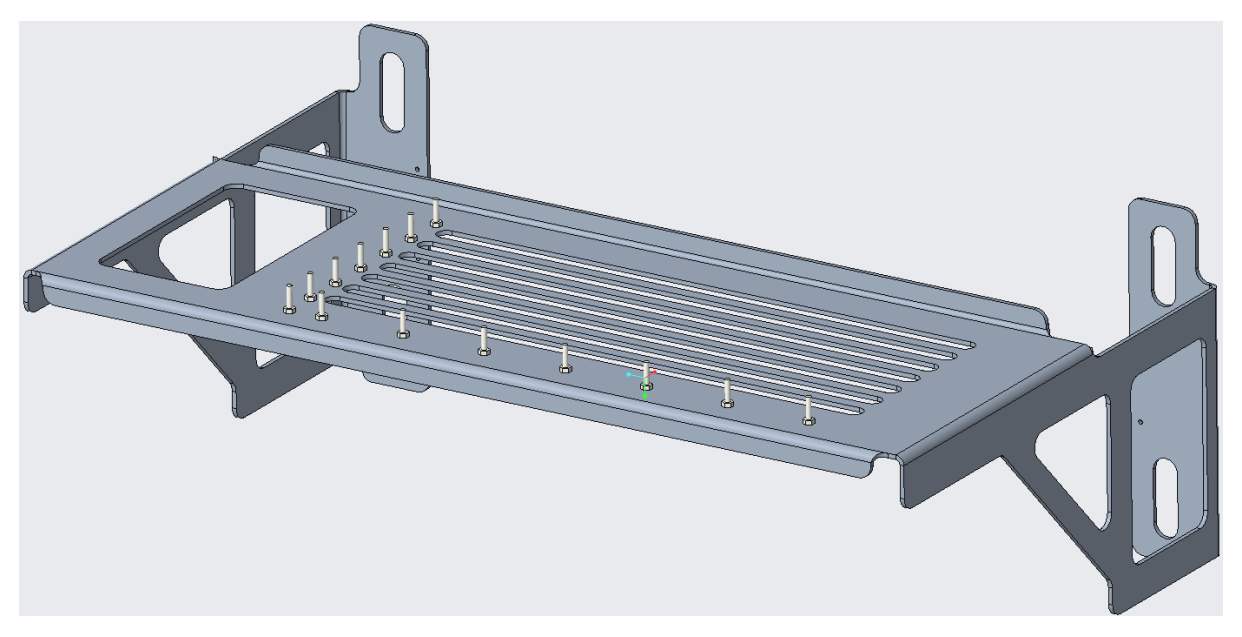


Figure 6-4: The 'striploin plate' developed for locating the striploin in the workspace of the robot arm.

The measurement node spacing lengthwise was chosen to be 50 mm to balance cycle time and measurement node mesh resolution. The spacing for this node mesh was 50 mm in the X direction (across the length / medial-lateral anatomical plane of the striploin) and 37 mm in the Y direction (across the width / caudal-cranial anatomical plane of the striploin). The origin of the measurement node mesh was determined by the first nylon bolt hole (in the X direction) and the first slot (in the Y direction) with reference to the striploin located against the nylon bolts that were assembled on the striploin plate. The position of these measurement nodes is shown in Figure 6-5. The robotic system that was used to position the sensors to acquire measurements at the measurement nodes is shown in Figure 6-6.

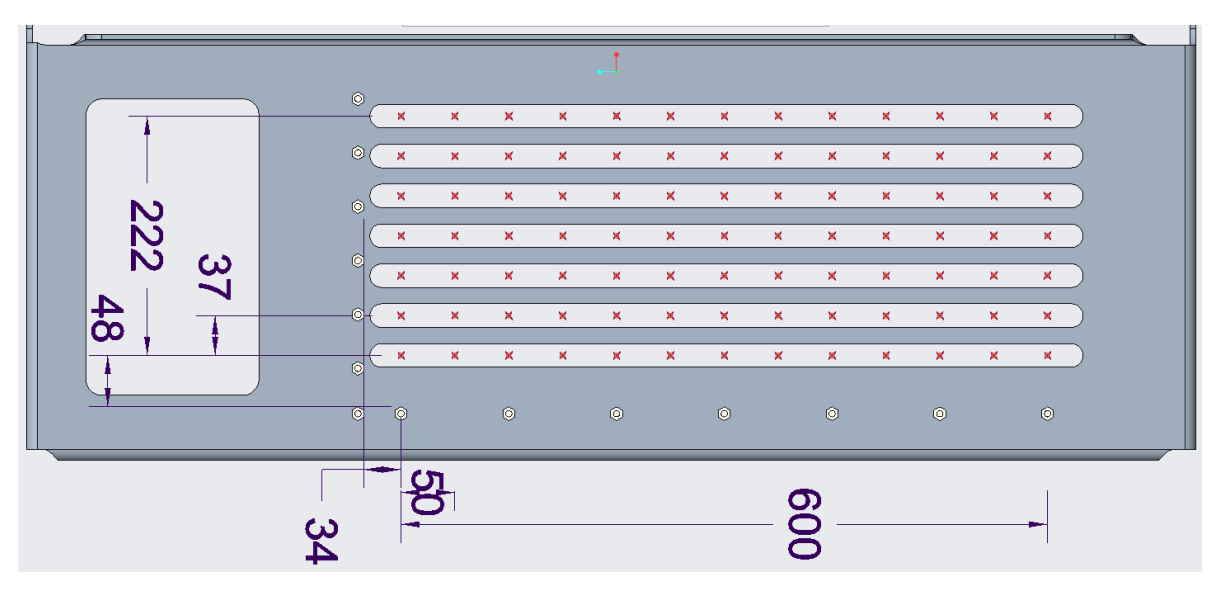


Figure 6-5: The measurement node locations in reference to the nylon bolts used for locating the striploin on the 'striploin plate'.



Figure 6-6: The experimental setup inside the collaborating processor's facility using a manipulator arm robot to position sensors at measurement nodes.

In addition to numbering each node (i, j), based upon its x and y coordinate the terminology of "point" (y) and "face" (x) was used. Due to the large fat deposits along the tail of the striploin (flank / ventral edge) it was decided that measurement nodes at these locations were not too important or crucial. As such, this edge was aligned to the nylon bolts running lengthwise along the plate which had a 48 mm distance from this edge to the first row of measurement nodes. No cross-sectional face (rump / rib) was prescribed to be aligned to the nylon bolts running widthwise along this plate. For this measurement node mesh a 'typical' striploin of 388 - 456 mm in length and 221 - 309 mm in width (as defined in Chapter 3) would have approximately a measurement node mesh of  $4 \times 7$  (28 nodes) and  $7 \times 8$  (56 nodes) respectively.

Literature suggests the clear link between temperature and soundwave propagation through lean muscle and subcutaneous fat (Diaz-Almanza, 2021). Therefore, the experiments were conducted within the processor's facility (near the processing line), which ensured that a temperature-controlled environment was adhered to. In addition to this, there was no need for plastic wrapping of the striploins which were sourced minutes before the trial from the processing line and would not be susceptible to moulding the shape of the vacuum bag.

During the fat depth measurement process the red dot of the LiDAR (Light Detection and Ranging) sensor mounted above the striploin was used to mark the location of the node measurement on the subcutaneous fat using black, food-grade gel. These markings were used later to align the node location of the A-Mode ultrasound measurements with manual measurements (see Figure 6-7).

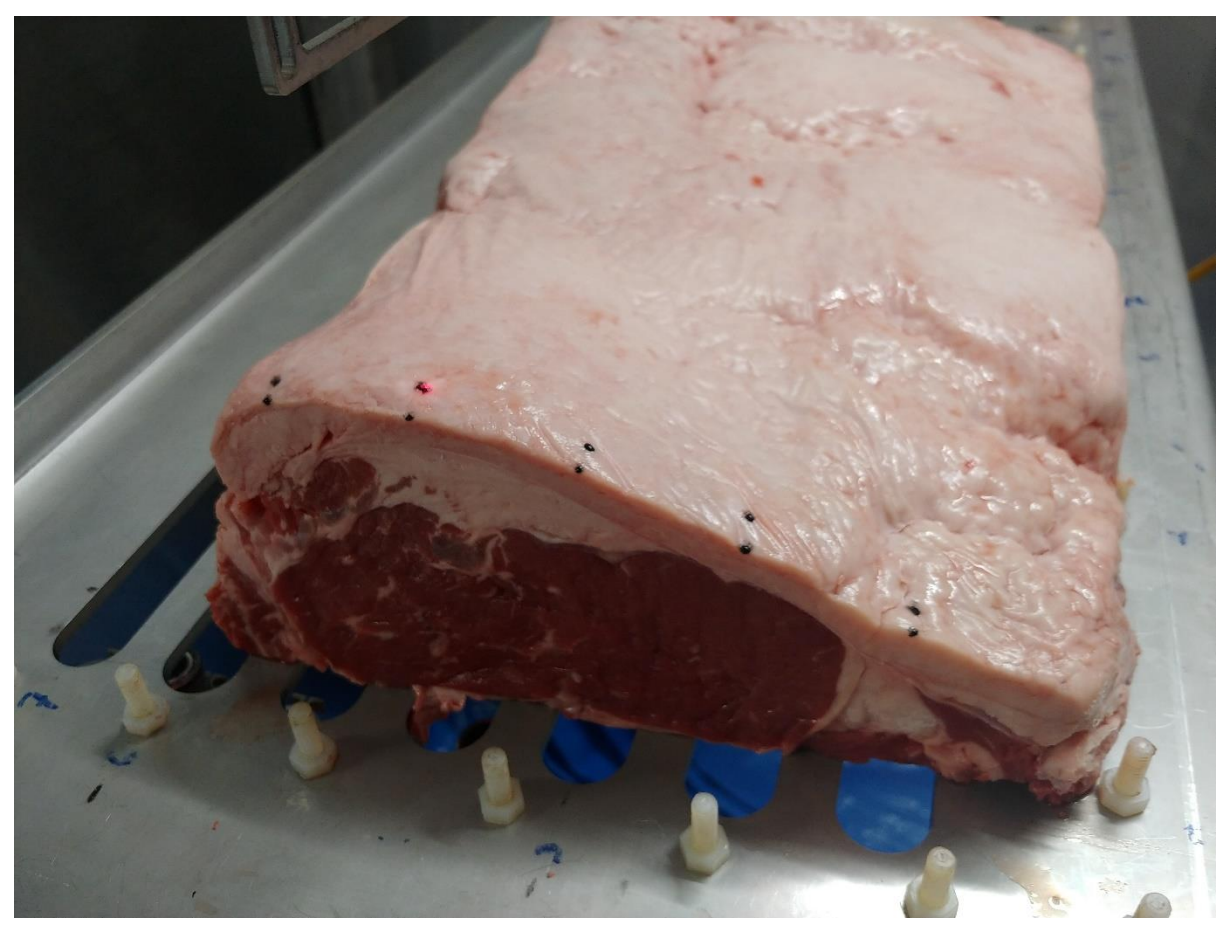


Figure 6-7: Marking measurement nodes using laser dot to cross-reference manual and ultrasound (A-Mode) measurements.

Fat Depth Measurements using A-Mode Ultrasound: A 304 stainless steel bracket assembly was designed with CAD software and manufactured to locate the A-Mode ultrasound probe and a LiDAR distance measurement sensor along the same axis using a manipulator arm robot. Of this assembly, the key bracket referred to the 'C-Arm', was designed to enable both sensors (A-Mode ultrasound and LiDAR) to align measurement axes to ascertain the fat depth at the particular node (see Figure 6-8 & Figure 6-9). This was manufactured from 5 mm stainless steel 304 plate.

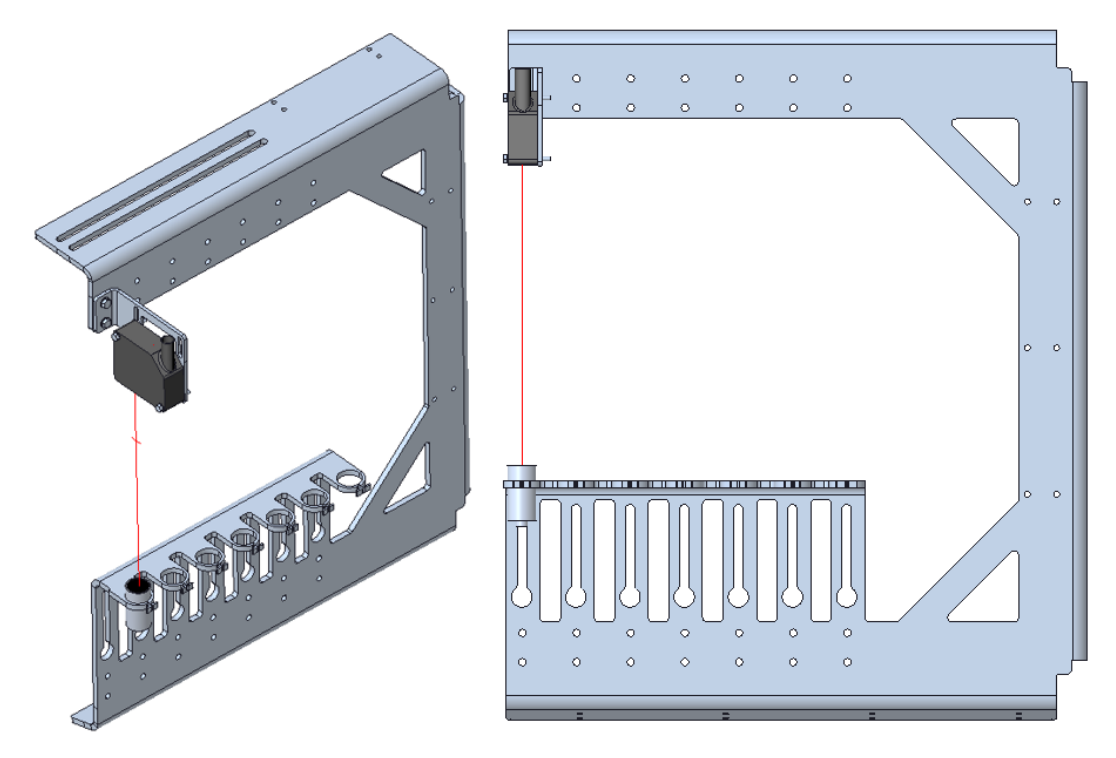


Figure 6-8: C-Arm bracket designed for positioning ultrasound sensor at nodes on the striploin plate.



Figure 6-9: LiDAR and ultrasound sensors assembled onto the C-Arm bracket.

Two sets of sensor pairs (LiDAR and ultrasound probe) were attached to the C-Arm and used simultaneously to enable a larger amount of measurement nodes to be measured within the constraints of the robot reach. These were mounted on positions on the C-Arm to measure the following simultaneously as shown in Figure 6-10.

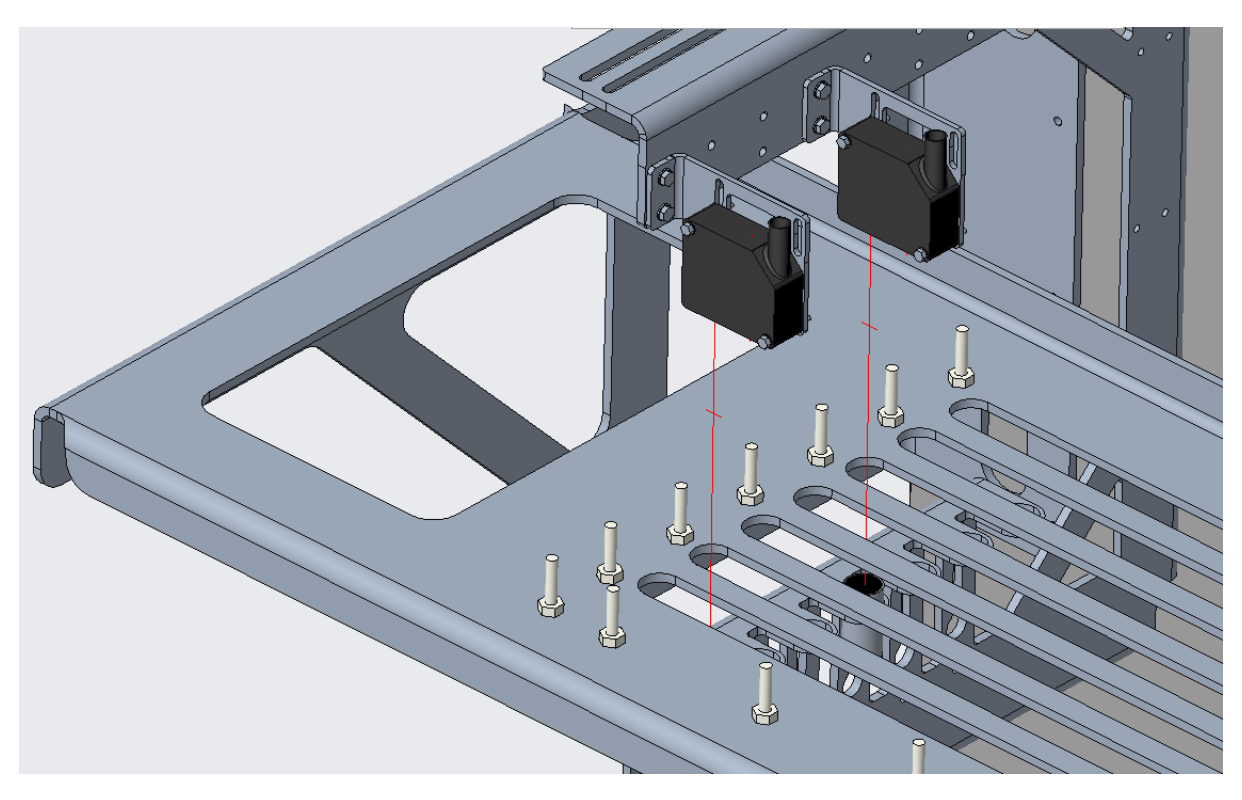


Figure 6-10: Sensing configuration using 2 sets of ultrasound probes (A-Mode) and LiDAR to ascertain fat thickness.

Using this configuration, at each node the position of the surface of the subcutaneous fat (referred to as 'fat height') was calculated by considering the distance measurement from the LiDAR sensor to the subcutaneous fat and the known height of the LiDAR sensor above the striploin plate when the measurement was acquired (illustrated in Figure 6-11). This method provided a simple means of ascertaining the fat height at each node with the LiDAR sensor. The ultrasound measurement provided the measurement from the lean surface of the striploin to the fat-lean interface of the striploin (referred to as 'meat height'). Through calculating the differential distance between the meat height and fat height the fat depth, or fat thickness, could be ascertained. This is illustrated in Figure 6-12.

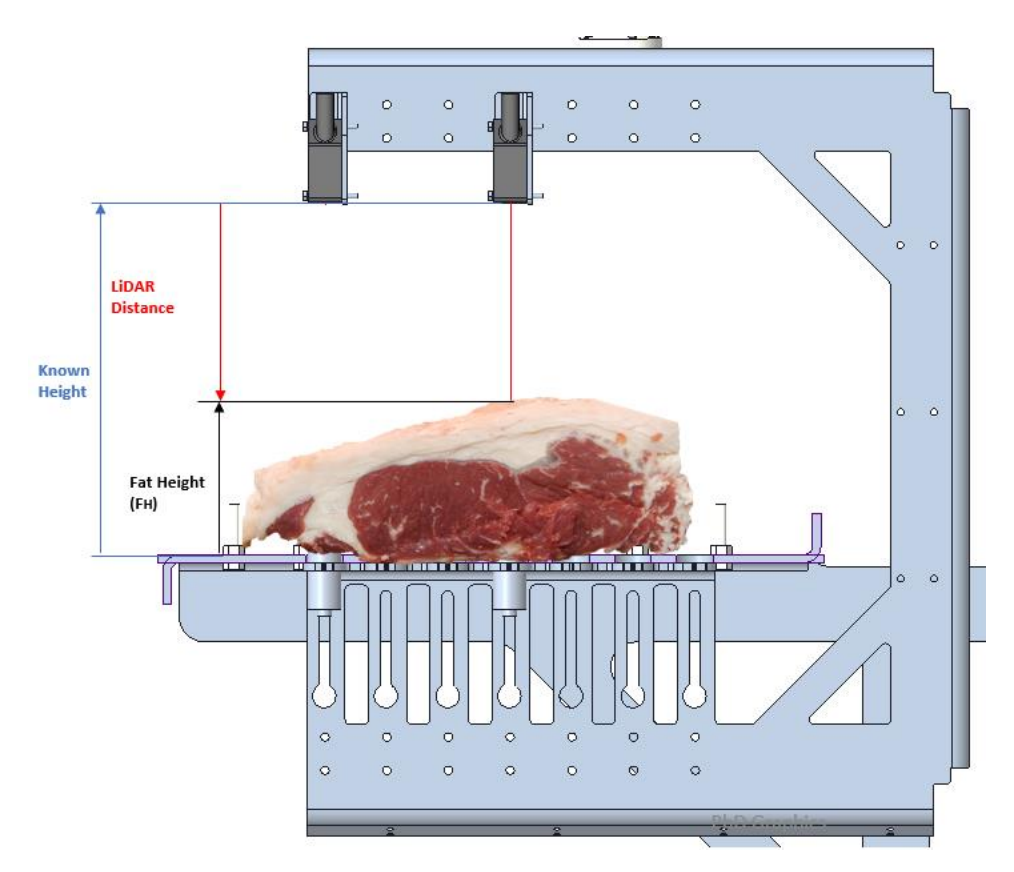


Figure 6-11: An illustration of the calculation of fat height (FH) using the LiDAR sensor.

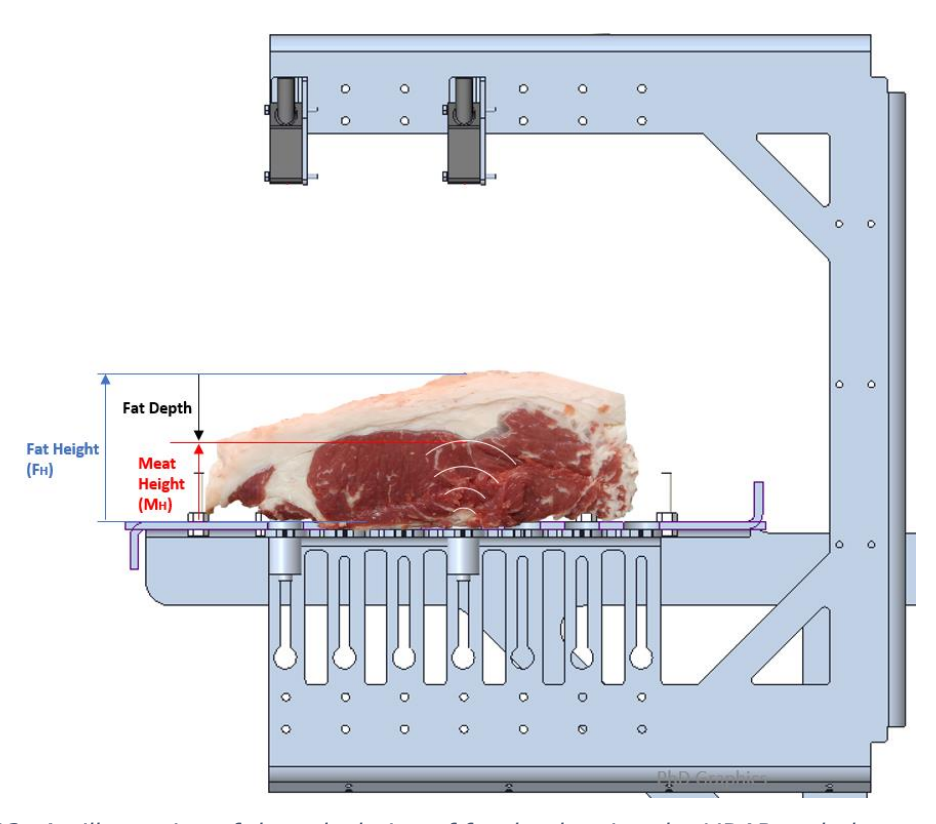


Figure 6-12: An illustration of the calculation of fat depth using the LiDAR and ultrasound sensors in this configuration.

The precise positioning of the sensing axes of the sensors mounted on the C-Arm was conducted through defining node positions in 3-dimensional space with a 6-axis manipulator arm robot (ABB IRB140). These node points were taught within the robot program precisely in 3D space using stainless steel rulers, laser sights and spirit levels to ensure alignment errors were not introduced in measurements (see Figure 6-13).

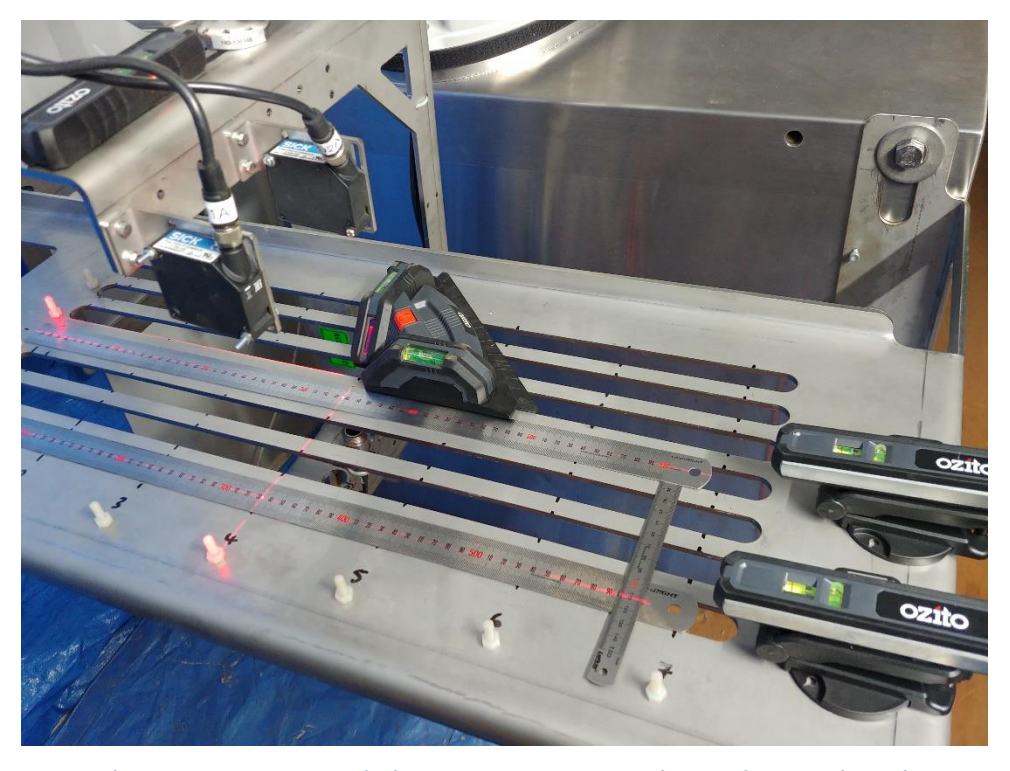


Figure 6-13: The measurement node locations were precisely taught into the robot coordinate system in 3D space using laser levels.

Upon a programmatic trigger, the ultrasound measurements were acquired within the device software and displayed graphically on a laptop application. Preliminary trials using the ultrasound sensor with numerous striploin samples identified the following parameter settings enabled this sensor to work most consistently and accurately:

- offset to first peak: 20

threshold: 6hysteresis: 6

min. peak distance: 3meat temperature: 8

The software filtered for the largest measurement result and returned this measurement as this would provide a means of filtering for reflections caused by tissue variances within the lean muscle. It is assumed that the largest measurement result links to the echo reflection of ultrasound wave at the fat-lean interface. As illustrated in Figure 6-14, this method has the possibility to introduce errors to fat depth estimations when a delamination in the subcutaneous fat of the striploin returns a strong echo (due to an air gap). As highlighted in Chapter 3, the phenomenon of air gaps within the subcutaneous fat layers were found to be uncommon in the striploins surveyed in this experiment.

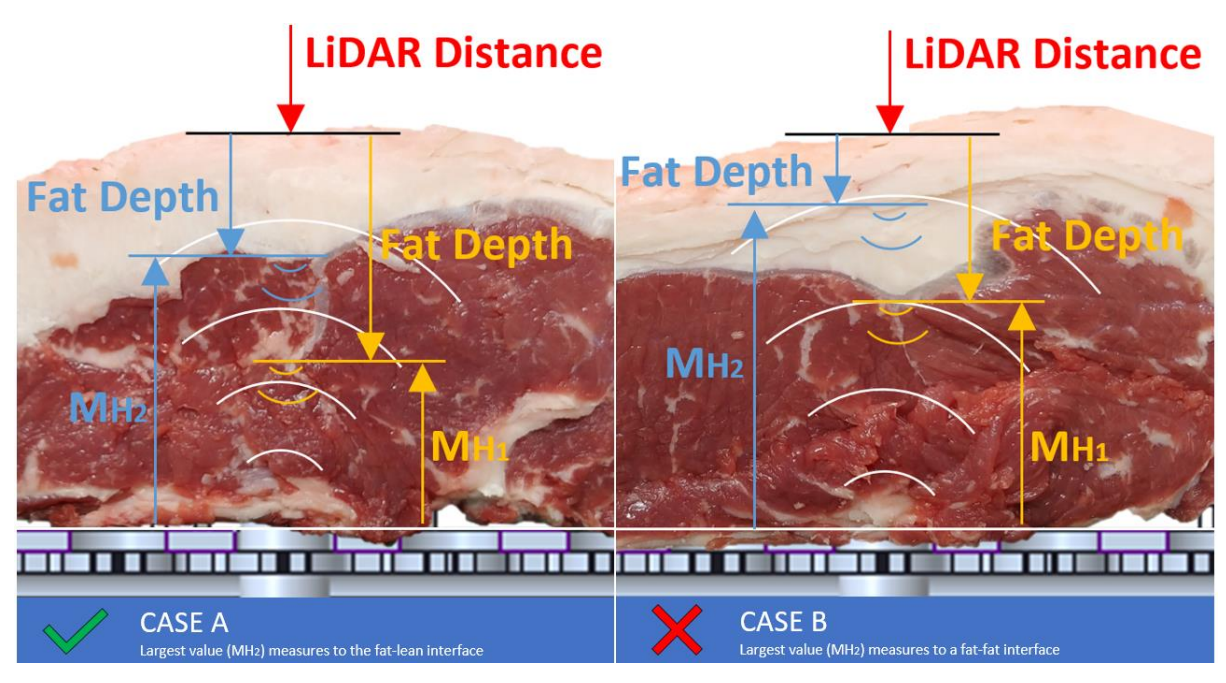


Figure 6-14: An illustration of the scenario whereby the chosen filtering method of the A-Mode ultrasound measurements would, and would not, work to accurately estimate fat depth.

This distance measurement ( $M_H$ ), as well as the calculated fat height measurement derived using the LiDAR sensor measurement ( $F_H$ ), was recorded within a sensing matrix of the robot indexed to store these measurements in2-dimensional matrices corresponding to the physical node position (i, j). Each measurement was returned to the TeachPendant

as the robot was progressed through each measurement node (see Figure 6-15).

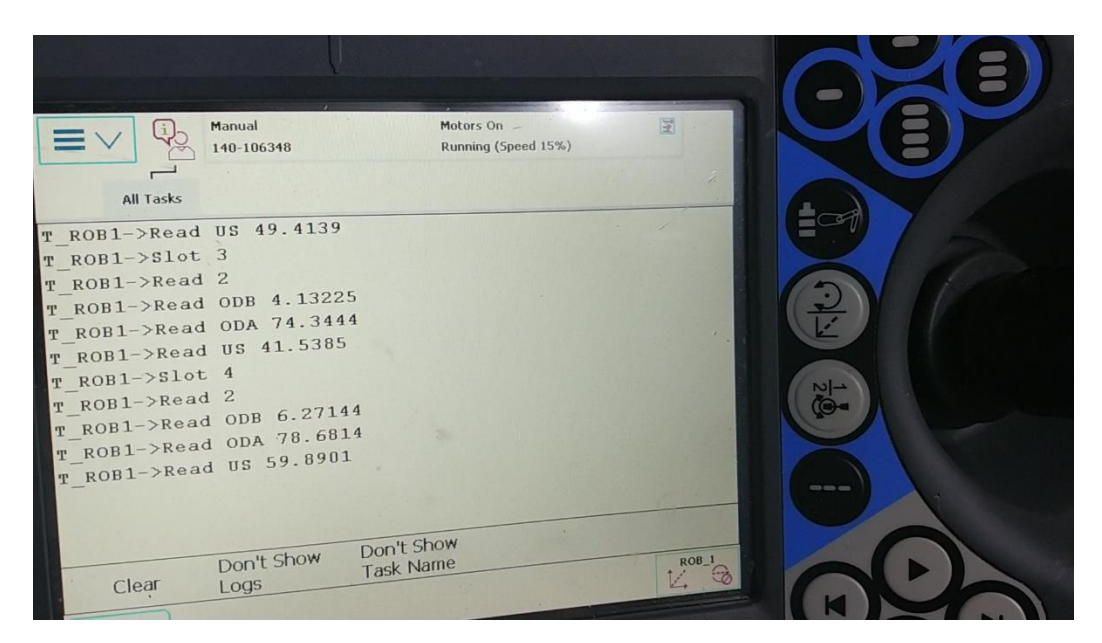


Figure 6-15: Measurements displayed using the robot movement program.

At the conclusion of each sensing cycle, the fat thickness (FTH) matrix was calculated using values stored within the meat height (MH) and fat height (FH) matrices before these matrices were exported as a comma-separated-value (".csv") file that was transferred to a laptop through a wired ethernet connection.

**Fat Depth Measurements using a Ruler:** The process of acquiring fat thickness measurements through a manual process using a stainless-steel ruler was similar to that outlined in Chapter 3.

After A-Mode ultrasound measurements were acquired and saved in a file a dissection of the striploin was made across the cross-sectional face of the striploin at each 50 mm face. A stainless-steel ruler was then used to record manual fat depth at each node which was recorded in an Excel spreadsheet for post-experiment analysis. A plastic  $10 \times 10 \text{ mm}$  grid was placed against each of these cross-sectional faces to provide a cross-

referenceable record of the fat depth at each node and photographed for each face (see Figure 6-16).

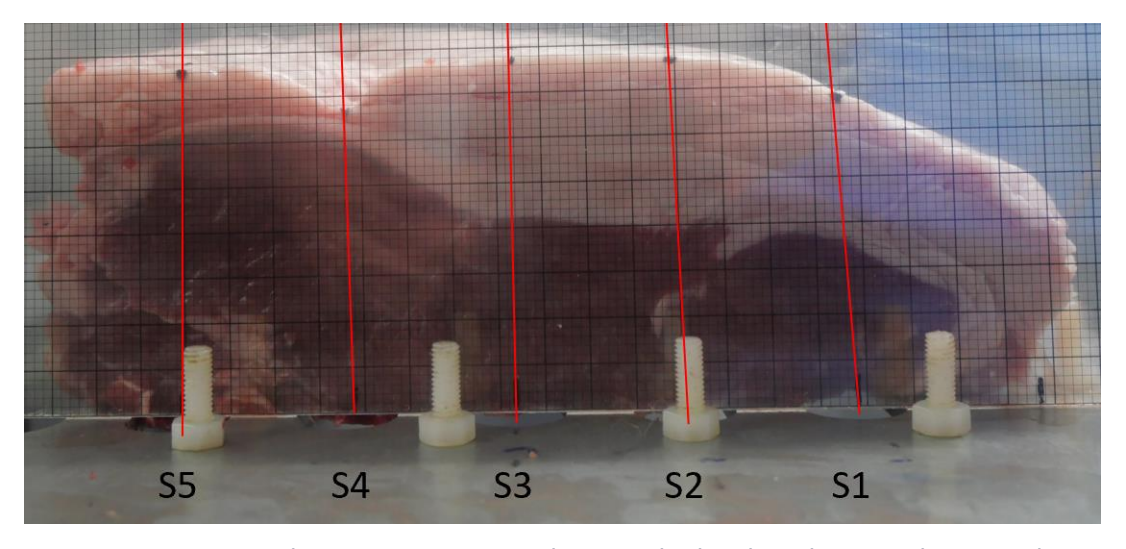


Figure 6-16: Each cross-section was photographed with a plastic grid to provide cross-referenceable measurements.

# **6.3 Experimental Analysis**

This A-Mode ultrasound sensing system was evaluated against the sensor performance evaluation framework developed in Chapter 4 (see Table 4-9). Though, due to the configuration of the ultrasound providing meat height (MH) values, which were then used to calculate fat depth, the error between manual and ultrasound measurements of meat height (MH) were considered. In preliminary trials LiDAR was seen to be highly consistent and a well-proven technology. Hence the following equation was used to calculate error for this analysis (see Equation 6.1).

Equation 6.1: Calculation of Error for A-Mode ultrasound considering meat height.

Error, 
$$E_{M-US_A} = MH_M - MH_{US_A}$$

where:

 $MH_M$  = the height of the fat-lean interface measurement acquired manually using a ruler (considered the reference value)

 $MH_{US_A}$  = the depth measurement acquired using the A-Mode ultrasound sensor (considered the estimated value)

As outlined in Chapter 4 the performance metrics were calculated using the equations specified below:

- Accuracy: Median of Error dataset (see Equation 4.3).
- Precision: IQR of Error dataset (see Equation 4.4).
- Linearity: Coefficient of Determination (see Equation 4.5).
- Reliability: The 'Miss Rate' of the sensor (see Equation 4.7).
- Response Time: The time required to acquire a measurement.

For reliability, the total number of nodes were considered as the number of nodes that lean muscle was measured. In some cases, there were no parts of the striploin over a node, where the striploin did not have a lean muscle interface measurable. Therefore, at the nodes that there was the capability of ultrasound measurement, and the device provided an error value this was considered a 'missed' instance. In preliminary trials it was identified that the following values that were returned by the ultrasound system were typically error values (11-12, 13-17, 24-28). As such, these values will be defined as 'no value' missed measurements.

During the preliminary investigation this sensor was deemed capable to measure at a response time less than 3 seconds, appropriate for this application ( $T_R \leq 15 \ sec$ ).

### 6.4 Results

Through evaluating the A-Mode ultrasound and ruler measurements of 16 striploins (RHS: 4, LHS: 12) a total data set of 477 nodes were measured.

The error measurement dataset (E) was calculated to create a means of evaluating the distribution of error between the ruler ( $f_R$ ) and A-Mode ultrasound ( $f_{US-A}$ ) fat thickness measurements. Key statistical measures are presented for the unfiltered dataset, and the 1.5 IQR filtered dataset (see Table 6-2).

Table 6-2: Statistical summary of error dataset (E) between ruler and USA measurements (n = 216)

Statistics	Unfiltered Dataset	Filtered Dataset
Minimum of Error Dataset, $Q_0(E)$	-21.7 mm	-21.7 mm
25th percentile of Error Dataset, $Q_1(E)$	-0.8 mm	-0.8 mm
Median of Error Dataset, $Q_2(E)$	1.7 mm	1.6 mm
Mean of Error Dataset, $(\bar{E})$	3.6 mm	1.8 mm
75th percentile of Error Dataset, $Q_3(E)$	3.2 mm	2.9 mm
Maximum of Error Dataset, $Q_4(E)$	62.8 mm	30.9 mm
Interquartile Range of Error Dataset, $IQR(E)$	3.9 mm	3.7 mm
Standard Deviation of Error Dataset, $SD(E)$	10.6 mm	6.1 mm
Range of Error Dataset, $Range(E)$	84.5 mm	52.6 mm
Lower Outlier of Error, $Q_1(E) - 1.5IQR(E)$	-6.7 mm	-6.5 mm
Upper Outlier of Error, $Q_3(E) + 1.5IQR(E)$	9.1 mm	8.8 mm

Seven lower bound and 19 upper bound outliers were identified in this dataset and removed for the creation of the filtered dataset: Lower Outliers ( $\leq -6.7 \, mm$ ): -7.7, -12.4, -21.7, -17.1, -11.5, -7.2, -13.4 Upper Outliers ( $\geq 9.1 \, mm$ ): 62.8, 43.8, 30.9, 41.4, 38.5, 37.1, 29.7, 17.0, 46.3, 21.5, 46.3, 28.9, 12.8, 10.9, 28.4, 20.7, 28.8, 9.5, 49.1,

Filtering the outliers from this dataset, and comparing it to the unfiltered dataset, the general trends and error characteristics differed

significantly around the mean, though were similarly around the median (see Figure 6-17).



Figure 6-17: Statistical summary of error measurement datasets (unfiltered vs filtered)

With only a very slight reduction of IQR (precision) of 0.4 mm due to the impact of outliers (mostly upper-bound outliers) causing the spread to be further towards positive errors (A-Mode ultrasound underestimating the meat height, and therefore through calculations, overestimating fat depth measurements). For the purposes of evaluating the accuracy (median) and precision (IQR), the effect of outliers was deemed negligible. As such, the unfiltered dataset was concluded to be representative of the fat depth measurements and therefore used for further analysis. Though, for optimisation of the use of A-Mode ultrasound this should be considered further. This reiterates the decision of using median error as opposed to average error to compare sensors for this thesis.

The unfiltered dataset was plotted on a histogram using bin widths of 1.5 mm, with excess bins being used to group lower and upper bound outliers (see Figure 6-18).

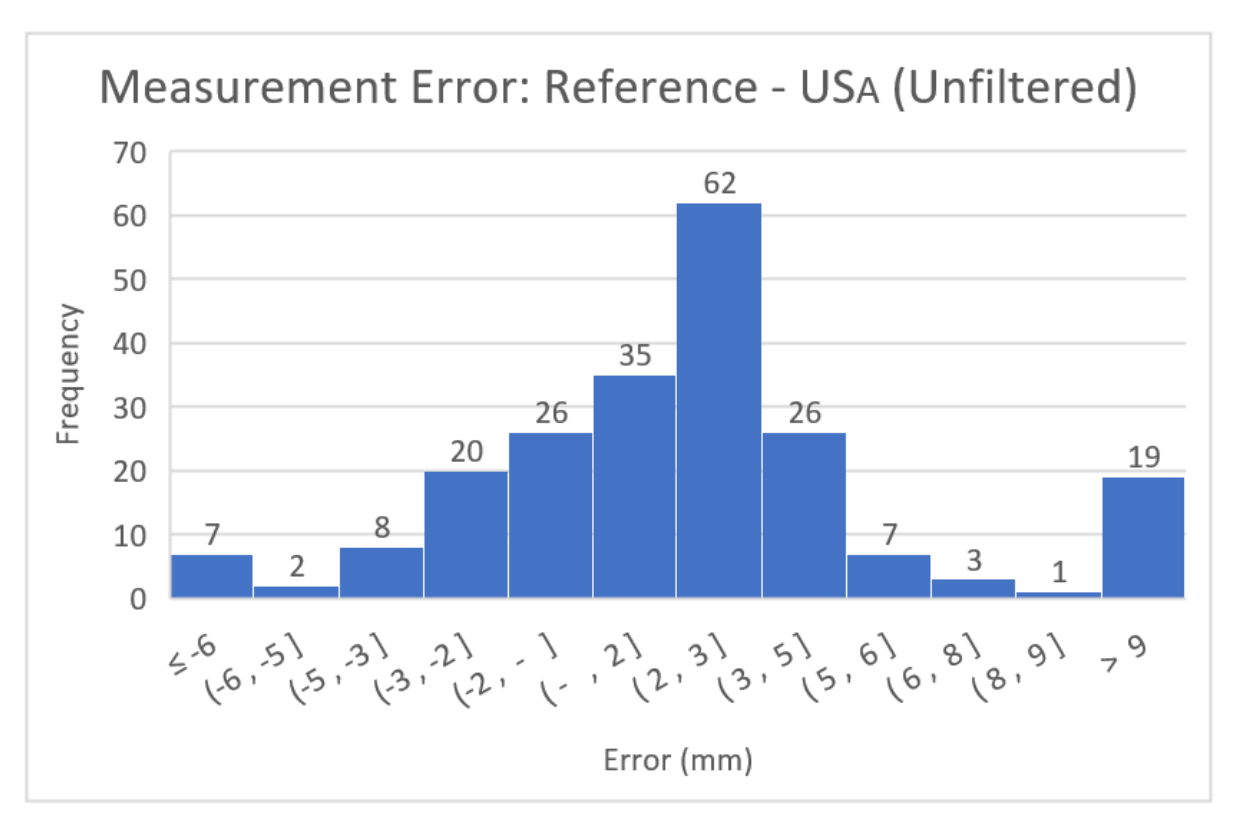


Figure 6-18: Error distribution of unfiltered data showing a non-normal distribution.

As supported within literature, this error distribution is not normally distributed, and is negatively skewed, showing a bias for A-Mode ultrasound to measure meat height less than the ruler quite consistently, and thus would provide an over-estimation of fat depth. The central peak at +2 to 3 mm error supports that there are no underlying subgroups trends in the dataset except for the positive outliers highlighted previously.

For this dataset the error of the A-Mode ultrasound measurements compared to the manual measurements ( $E_{R-US_A}$ ) was calculated to be 3.6 mm and 1.7 mm for the average and median error respectively. The large

change in the average of error from 3.6 to 1.7 mm (change of 1.9 mm) in comparison to the median from 1.7 to 1.6 mm identifies the large amount of bias created by the sensor, or the filtering applied to acquire a measurement from the A-Mode ultrasound system.

As a benchmark of accuracy and precision, A-Mode ultrasound is concluded upon with the following measures:

Accuracy: Median of Error,  $E_{MDN}$  = +1.7 mm

Precision: Interquartile Range of Error, IQR(E) = 3.9 mm

The measurement error across the range of measurements acquired is illustrated in Figure 6-19. Firstly, it can be seen that A-Mode ultrasound was able to measure at any depth required within this analysis. For this subset of striploins, the minimum range and maximum ranges were found to be 18 mm and 83 mm respectively.

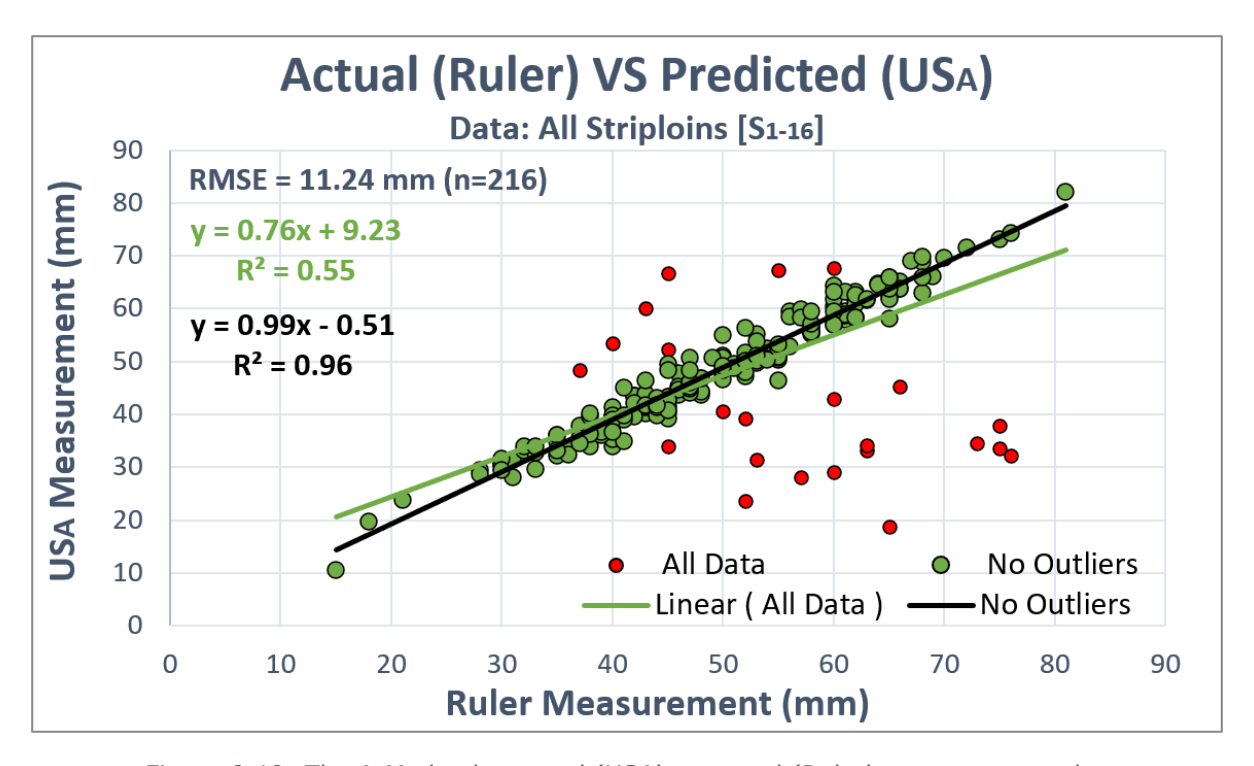


Figure 6-19: The A-Mode ultrasound (USA) vs actual (Ruler) measurement plot.

The correlation of determination  $(R^2)$  value of this linear regression for the error dataset is vastly different when error outliers are removed: 0.55 to 0.96 (see Figure 6-19). This illustrates that the majority of the A-Mode measurements closely align with the manual measurements, though the few outliers significantly weight the trendline towards underestimation. Additionally, that there are a few clusters of datapoints that have a high modality in the sensor measurement that are significantly dissimilar to the reference (manual) measurement. This occurs when A-Mode ultrasound measurements are at approximately 20 mm, and 33 to 38 mm.

A further analysis of heteroscedasticity is visualised within Figure 6-20 & Figure 6-21 which both show a slight to moderate increase in variation of error across the range of reference measurements. Though error in general does not substantially increase, the error magnifies with a positive linear correlation the larger the measurement for outlier error measurements. These are trends that indicate a systemic underestimation of measurements and will be further discussed in the following subsection.

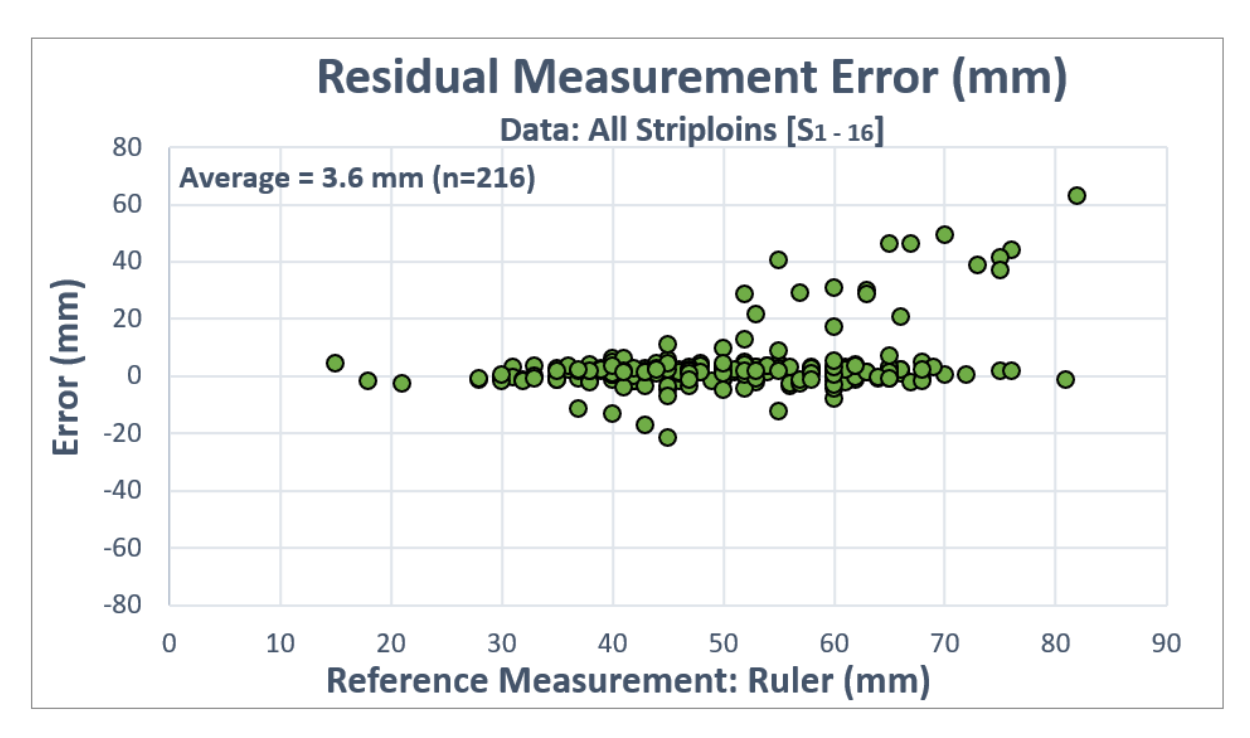


Figure 6-20: Residual Error Plot of USA-Ruler Dataset (in mm)

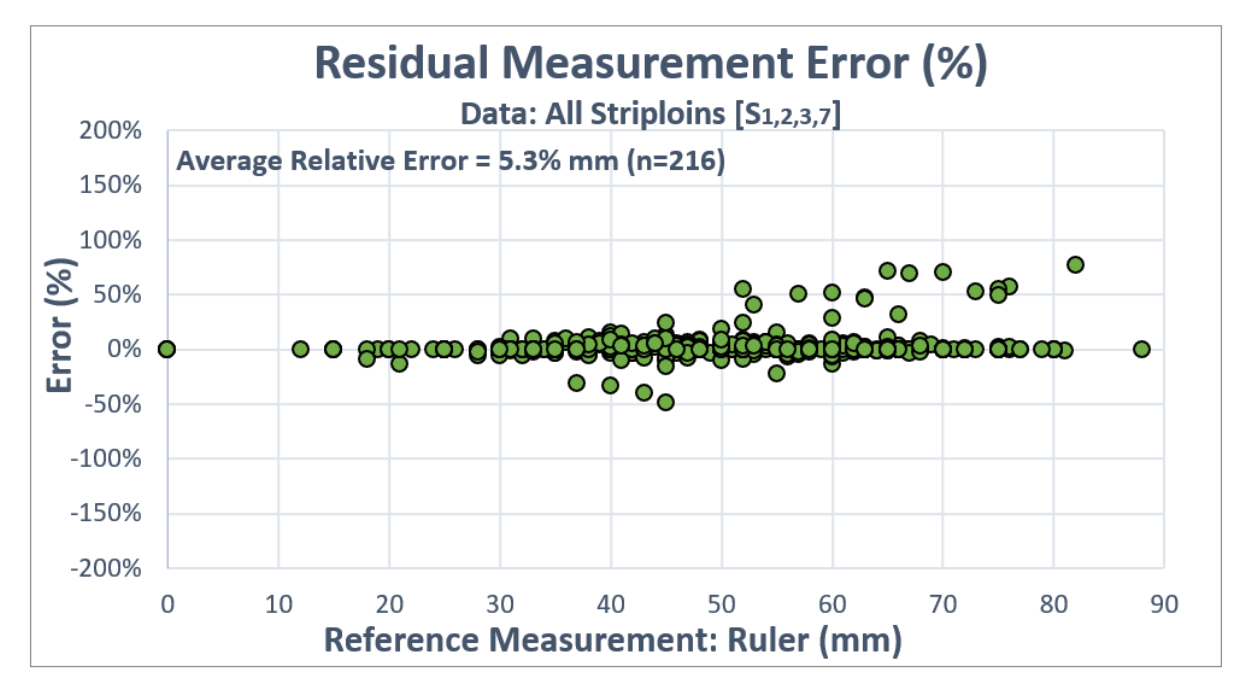


Figure 6-21: Residual Relative Error Plot of USA-Ruler Dataset (%)

As a benchmark of linearity in the measurement range, A-Mode ultrasound was found to exhibit the following performance:

## **Range Requirements:**

Found to be feasible in preliminary analyses.

### **Linearity:**

*Variance over Operating Range*  $\equiv R^2 = 0.55$ 

There were a number of instances whereby the A-Mode ultrasound returned an error value identified in preliminary trials as 11-12, 13-17, 24-28. From the 477 nodes of potential measurements, 261 nodes did not have a measurement acquired. As such, the miss rate ( $P_M$ ) for A-Mode ultrasound was concluded to be as follows:

As a benchmark of reliability, A-Mode ultrasound is concluded upon with the following measures:

# **Reliability:**

Miss Rate, 
$$P_M = \frac{261}{477} * 100\% = 55\%$$

As previously presented, it was identified that the response time of the A-Mode ultrasound system was approximately less than 1 second.

Response Time, 
$$T_R \leq 1$$
 second

#### 6.5 Discussion

An analysis of A-Mode ultrasound results highlight the narrow distribution of error around zero which indicates that the sensor returned accurate measurements on average, though slightly skewed with positive error (median error = 1.7 mm). The narrow spread of error (IQR of error = 3.9 mm) illustrates the quite high precision of this sensor to provide measurements that closely represent manual measurements.

The presence of nineteen upper-bound outliers (>9.1 mm), with only seven lower-bound outliers (-6.7 mm), insignificantly skewed the data towards higher positive error values. Although the elimination of these outliers did very slightly reduce the overall inaccuracy (median error reduced from 1.7 mm to 1.6 mm) and imprecision (IQR of error reduced from 3.9 mm to 3.7 mm), the difference in overall trends were between outlier-filtered (+-1.5 IQR) and unfiltered datasets was negligible. Upon further analysis of these outliers, it was identified that there were likely 'error' values returned by the A-Mode ultrasound labelled at approximately 20 mm, and 33 to 38 mm. Though the further optimisation of these prototype systems is out of scope for this work it may be that by classifying any A-Mode ultrasound measurement less than 24 mm as an "error value" would remove 5 of the 19 upper-bound outliers and increase the accuracy, precision, and linearity ( $R^2 = 0.55$ ), though decrease the reliability (reliability = 55%) of this A-Mode ultrasound system. It is possible that the significant, though few, outliers were either stray measurements that incidentally measured intramuscular fat tissue or even error codes of the device (due to the high modality of few readings).

The A-Mode ultrasound technology provided less information at each node (a single numerical value), though with a significantly faster response time is likely to provide measurements at more node locations. This is advantageous for a fat trimming system as it provides a capability to better represent the fat depth in finer resolution across the striploin with high fat depth variability. Though less information is provided at each node using A-Mode ultrasound, there is a degree of certainty that can be ascertained through considering the spatial and biological relationships of fat depth across the beef striploin. The implementation of interpolation to estimate fat depth at various "missed" measurement nodes is a powerful technique that is recommended for further investigation.

It is important to recognise that these performance metrics should not be considered in absolute terms, but relatively to the performance of the gold standard (medical-CT imaging) considered for this application. A comparison of the A-mode ultrasound results against the gold standard is shown in Table 6-3. A-Mode ultrasound performed comparatively similar to the gold standard in a number of performance metrics. This comparison highlights that A-Mode ultrasound is approximately 42% less accurate and 56% less precise as CT imaging, with a significantly disproportionate performance in linearity and reliability. Despite this, the response time of less than 1 second indicates the satisfaction of the response time metric that makes this a feasible technology for the application of beef striploin fat trimming. In summary, the performance of this sensing system is defined below through applying the performance evaluation framework developed in Chapter 4 (see Table 6-4).

Table 6-3: Comparison of fat measurements using A-Mode ultrasound and medical-CT imaging.

Performance	Sensors for Fat Depth Measurement			
Metric	Medical-CT Imaging	A-Mode Ultrasound		
Accuracy $(E_{MDN})$	+1.2 mm	+1.7 mm		
Precision ( <i>IQR(E)</i> )	2.5 mm	3.9 mm		
Linearity ( R <sup>2</sup> )	0.93	0.55		
Reliability $(P_M)$	0 %	55 %		
Response Time $(T_R)$	10 min	< 1 sec		

Table 6-4: Sensor performance evaluation framework applied to A-Mode ultrasound sensing system.

Performance Metric	Quantity	Performance Rank					Metric Weighting	Metric Score	
		FAIL/POOR 0	FAIR 1	AVERAGE 2	GOOD 3	EXCELLENT 4	EXCEPTIONAL 5		
Accuracy $(E_{MDN})$	1.7 mm	> 10 mm	≤ 10 mm	≤ 7.8 mm	≤ 5.6 mm	≤ <b>3.4</b> mm	≤ 1.2 mm	3	12
Precision $(IQR(E))$	3.9 mm	> 12.5 mm	≤ 12.5 mm	≤ 9.5 mm	≤ 6.5 mm	≤ 4.5 mm	≤ 2.5 mm	5	20
Linearity (R²)	0.55	< 0.5	≥ 0.5	≥ 0.6	≥ 0.7	≥ 0.8	≥ 0.93	2	2
Reliability $(P_M)$	55%	> 75%	≤ 75%	≤ 50%	≤ 25%	≤ 10%	≤ 1%	3	3
Response Time $(T_R)$	< 1 sec	> 15 sec	≤ 15 sec	≤ 7.5sec	≤3 sec	≤ 2 sec	≤ 1 sec	2	10
A-Mode Ultrasound Sensor Performance Score							47 / 75		

In general, when considering the weightings of these performance metrics, the A-Mode ultrasound sensing system is most significantly penalised for reliability (3/15) and linearity (2/10), with "excellent" scores for accuracy (12/15), precision (20/25), and "exceptional" for response time (10/10). The overall score of 45/75 will be used in the comparison between B-Mode and A-Mode ultrasound sensing systems in Chapter 7.

In terms of progression towards integration within an automated fat trimming system it is concluded that this sensing system is capable for fat depth measurement to a high degree of accuracy and precision, and this chapter has outlined a means of integrating this sensing system into an automated trimming system (see Section 6.2).

#### 6.6 Conclusion

The analyses presented within this chapter provide a means of evaluating the use of A-Mode ultrasound technology as sensing system for automated fat trimming of beef striploin. This system was developed considering insights gained from Chapter 3 and 4 and evaluated using the performance evaluation framework presented in Chapter 4 that considered key performance metrics, weighted by importance, based predominantly upon the gold standard of CT imaging technologies for fat depth measurement. The A-Mode ultrasound sensing system achieved a 49 / 75 performance rating which will be compared to the B-Mode ultrasound system in Chapter 7. The key future recommendation being the implementation of filtering and fat depth interpolation based upon spatial and biological relationships of tissues within the beef striploin.

## **CHAPTER 7: CONCLUSION**

This chapter concludes upon the processes and methodologies employed to develop, evaluate and implement a system to measure or estimate the fat depth of a beef striploin primal. The results of each system are compared and recommendations upon the most promising technology and technique for implementation upon automated beef striploin fat trimming is provided. A reflection is provided upon further work, both particular to beef striploin fat trimming and alternative tasks in the red meat processing industry.

### 7.1 Achievement Against Research Objectives

The research presented in this thesis provided the following insights and conclusions upon the research objectives.

### 7.1.1 Review of Sensing Technologies for Uniform in Fat Trimming.

**Objective 1:** To identify the most feasible sensing technologies for the application of automated uniform fat trimming of beef striploin through conducting a literature review (see Chapter 2).

The objective of identifying the most feasible sensing technologies for the application of automated uniform fat trimming of beef striploin is met through a literature review that recommends ultrasound as the most promising technology for this task. The recommendations were based on criteria considered fundamental to the automated fat trimming system with assigned weightings.

The literature review identified two ultrasound-derived sensing systems (B-Mode and A-Mode) to be tested for measuring fat depth. The literature review also identified gaps in knowledge related to the

benchmarking and evaluation of sensing technologies for this application and the key processing requirements and product considerations of the uniform fat trimming process. This review emphasizes the need for further examination of the process and the beef striploin primal to define the performance requirements at a more detailed level. This understanding will guide the development of a methodology to assess and compare the performance of these ultrasound sensors, which are outlined in detail in Chapter 4.

Furthermore, the review establishes medical CT, as shown in the research assessing X-ray technologies for red meat processing, as the 'gold standard' in sensing systems. This provides a benchmark for the optimal sensing performance and a basis for evaluating the performance of practical technologies like ultrasound. Therefore, the literature review effectively answers the objective by identifying ultrasound as the most feasible technology and outlining steps for its development and evaluation in the context of automated uniform fat trimming of beef striploin.

# 7.1.2 Provide insights from the analysis of striploin characteristics and trimming task.

**Objective 2:** To define the key parameters that inform the system capabilities for the task of uniform fat trimming of beef striploin through analysing fat characteristics and industry standards.

The striploin primal's dimensions, particularly width and weight, vary considerably due to human error in approximation and the cranial/rib face curvature, impacting the system's sensing capabilities. Moreover, the condition of the fat cover also varies, but with a 10% probability of fat tears affecting system measurements, this factor is considered insignificant.

The average processing time for fat trimming is 27 seconds, serving as a critical benchmark for an automated system's response time. Furthermore, the analysis identifies that non-real-time 'bridging' and 'planing' techniques are required, suggesting that sensing is required for path planning the trajectory of the trimming blade.

Analysis of the subcutaneous fat depth uncovers important characteristics for developing a suitable sensing system. The mean fat depth is 16 mm, with most measurements falling between 0 - 32 mm. These insights help to define the penetration depth range of an ultrasound sensor.

Spatial relationships of fat depth distribution across the striploin could assist in the optimization of node locations, indicating that many nodes could be omitted from the automated system's sensing and trimming processes. Key spatial insights presented in Chapter 3 show that there are various locations that have very little fat thickness (typically up to 50 – 75 mm along the spine edge) that likely don't require as high a sensing resolution than other areas (or sensing in general). There are other areas of the striploin that show high fat variability (50 – 200 mm from the caudal face and from past 75 mm from the spine edge to the flank edge) that suggest a small node mesh spacing for a higher resolution to trim closer to the fat-lean interface. The fat distribution's normality and observed spatial patterns suggest spatial modelling could enhance fat depth estimations and apply generalised cut path and fat depth learnings across processors. Finally, due to the gradient of fat thickness on the striploin it was identified that the least complex orientation for trimming is along length of the striploin.

This foundation aids the description of parameters for a sensor performance metric, ultimately informing the development of feasible ultrasonic sensors within sensing systems.

# 7.1.3 Establishment of sensor performance evaluation metric specific to uniform fat trimming automation.

**Objective 3:** To establish a framework for evaluating sensor performance that outlines the process of ranking sensors against metrics important for the automation of beef striploin fat trimming (see Chapter 4).

The section presents a clear framework to evaluate sensor performance for automated beef striploin fat trimming. This framework outlines a set of key metrics - Accuracy, Precision, Linearity, Reliability, and Response Time - each with specific weightings reflecting their importance to the system's performance.

Accuracy and Precision, both with a weighting of 3, assess the deviation between the sensor's measurements and the manual measurements, while Linearity, with a weighting of 2, examines the degree to which the sensor's measurements correspond with the reference measurements. Reliability, also weighted at 3, evaluates the proportion of measurements missed by the sensor. Finally, Response Time, weighted at 2, gauges the sensor's speed by observing the developed sensing system. These metrics and their corresponding weightings collectively provide a comprehensive set of criteria to measure the performance of sensors in an automated beef striploin fat trimming system. Using medical-CT imaging as the gold standard, this framework sets the thresholds for each metric.

The framework was applied to evaluate the candidate sensing technologies with reference to this gold standard. This consistent application of the evaluation framework facilitated the means of a direct comparison between the sensors, guiding the selection of the most suitable sensor for this specific application.

# 7.1.4 Development of ultrasound systems to evaluate performance for automation implementation.

**Objective 4:** To develop, implement and evaluate novel ultrasound sensing systems capable of integration into an automated system to measure fat depth across an untrimmed beef striploin.

Insights gained from analysing the untrimmed beef striploin primal, the final specifications of the striploin product and the trimming sub-tasks and timing were used to define a means of ascertaining the feasibility of a sensor prior to development. Preliminary experiments were performed with each sensor to determine the best configuration for the sensor with respect to the striploin to achieve their best against the evaluation criteria.

# 7.1.5 Evaluation of systems to conclude upon the technologies' appropriateness for this application.

**Objective 5:** To conclude upon evaluations of sensing systems and provide recommendations to inform the development of practical sensing systems for integration into an automated system capable of uniform fat trimming of beef striploin.

The preceding chapters of this dissertation have provided a comprehensive and in-depth analysis of two distinct ultrasound technologies, A-Mode and B-Mode, and their viability as sensors for automated fat trimming in bovine striploin using the developed performance evaluation framework (see Table 7-1).

Table 7-1: Comparative evaluation of A-Mode & B-Mode ultrasound systems.

Performance	Importance	Sensors Evaluated		
Metric	Weighting	B-Mode Ultrasound	A-Mode Ultrasound	
Accuracy $(E_{MDN})$	3	+4.5 mm	+1.7 mm	
(L <sub>MDN</sub> )	3	[SCORE = 9]	[SCORE = 12]	
Precision (IQR(E))	E	10 mm	3.9 mm	
	5	[SCORE = 5]	[SCORE = 20]	
Linearity ( R <sup>2</sup> )	2	0.1	0.55	
		[SCORE = 0]	[SCORE = 2]	
Reliability	2	12.7 %	55 %	
$(P_M)$	3	[SCORE = 9]	[SCORE = 3]	
Response Time $(T_R)$	2	< 3 sec	< 1 sec	
		[SCORE = 6]	[SCORE = 10]	
Sensor Score ( / 75)		29	47	

Through this comparison it was identified that A-Mode was performed better than the B-Mode ultrasound sensing system overall with an overall score of 47 as opposed to 29. In comparison to B-Mode, A-Mode performed 2 ranks better in precision, and response time, one rank better in accuracy and linearity, but 2 ranks worse in reliability. Whilst both error datasets showed positive error compared to reference measurements to underestimate fat depth, B-Mode had significantly higher median and IQR in addition to indications of systemic error due likely to fat delamination within the striploin.

In principle, B-Mode ultrasound was hypothesised to perform better than A-Mode due to the capability to provide certainty through providing greyscale images to discern tissue interfaces for measurement. Whilst B-Mode ultrasound did perform significantly better in the reliability performance metric, 55% in comparison to 12.7%, due to the imitation of delaminated fat layers as the fat-lean interface, this did not assist. It is very likely that the false confidence of tissue discernment deflated the actual number of "missed" measurements, and therefore inflated the reliability performance and deflated the accuracy and precision performance of B-Mode ultrasound. This was not due to human misinterpretation error, but the lack of deeper interfaces visibly present in the image due to the inability of soundwaves to pass through the air gap of the fat layer and therefore illustrated to be the deepest interface on the image.

Despite yielding less information at each node, though this analysis found this not to be useful, the significantly faster response time and the ability to provide measurements at more node locations present a distinct advantage. The fat variability identified in Chapter 3 supports the notion that the increased number of nodes is valuable, if possible, for representing the fat depth contour across the untrimmed beef striploin.

In terms of integration into an automated fat trimming system, both technologies present unique challenges and opportunities. For B-Mode the recommendation is to trial a configuration sensing from the lean surface of the striploin, aiming to circumvent issues related to fat delamination. Conversely, A-Mode shows promise for immediate integration given its high degree of accuracy, precision, and response time.

The two sensing technologies represent different strategies in the trade-off between providing richer data (B-Mode) and speedier, more precise measurements (A-Mode). With a different measurement

configuration to that employed in this research (from the lean surface), B-Mode offers potential for more detailed understanding of the fat layer. Though, this could be at the expense of efficiency and overall effectiveness in a real-world, fast-paced meat processing environment. Furthermore, the data complexity may increase the probability of measurement errors and the difficulty of interpretation. On the contrary, A-Mode, despite providing less information at each node, delivers measurements with higher speed and precision. The capacity of this technology to effectively capture the fat depth variability across the striploin, combined with its quick response time, make it particularly suited for an environment where high-throughput and precision are paramount. In addition, the relatively straightforward data produced by A-Mode could be more readily utilized with less need for complex interpretation or high computational resources.

It can be concluded that A-Mode ultrasound technology exhibits superior potential for the application of automated fat trimming. Its inherent strengths in accuracy, precision, and response time, coupled with the relative simplicity of data interpretation, provide a robust basis for its integration into an automated system. While it may not offer the richness of data inherent to B-Mode, it decisively compensates by delivering high-performance metrics where they matter most in this specific application - speed, accuracy, and precision. Thus, as we progress towards more efficient and precise meat processing methods, A-Mode ultrasound technology indeed stands as a promising tool for automated fat trimming.

Future research for further development of an automated fat trimming system should focus on further enhancing the efficiency of A-Mode technology, with potential avenues of exploration including the implementation of advanced filtering techniques and fat depth interpolation based on spatial and biological tissue relationships within the beef striploin.

#### 7.2 Recommendations for Future Work

A number of recommendations are provided to further investigate the development of an automated striploin fat trimming system. These recommendations are centred around two areas: sensing and automation implementation insights.

### 7.2.1 Sensing of Subcutaneous Fat Depth Measurements

The recommendations for future work regarding the evaluation and development of the sensing technologies to measure the subcutaneous fat depth of beef striploin are:

**B-Mode Ultrasound**: An independent evaluation was conducted in Chapter 3 to evaluate the claim made by Khodabandehloo (2018) that fat cover damage caused by processors' downward hide puller mechanism would yield measuring from the fat surface with ultrasound unfeasible. This evaluation found that fat cover damage affected only 10% of striploins, and of those affected, the location of damage was at a location not critical for measurement (on the flank edge / tail). Despite this, findings presented in Chapter 5 show that B-Mode ultrasound struggled to acquire images with discernible fat-lean interface locations that accurate measurement could be taken from. It was identified that delamination of the subcutaneous fat layers of the striploin may have introduced ultrasound barriers (air gaps) that prevented penetration of soundwaves to acquire discernible images to be acquired. Through this research it has been suggested that B-Mode ultrasound will likely yield better results through sensing from the lean meat/muscle surface of the striploin and therefore a different orientation to that considered in this research is recommended.

**Evaluating other Sensing Technologies**: It is considered that force, spectroscopy, and rapid-CT imaging would be potential candidates for this application. These technologies were out of scope for this research

and, as with all conclusions devised considering only every desktop research, it is suggested they be developed using insights from this thesis (particularly Chapter 3) and evaluated in practice using the performance evaluation framework developed in this research. It is recommended that future work should be undertaken to developed other sensing systems for this application to be evaluated with the performance evaluation metric developed within this research.

Rapid CT imaging (such as systems offered by DMRI and RapiScan) should be investigated further. Whilst research has been conducted to identify subcutaneous fat depth using CT imaging, for the application to be feasible for beef striploin fat trimming a focus on integrating into automation systems and operating this machine safely in a configuration that is capable of sensing at line speed is required. Throughout this research access to these machines was tried but unsuccessful, therefore only medical-grade CT was considered for evaluation.

Since beginning this research substantial more research has been conducted in the field of spectroscopy for fat depth measurements. It is suggested that further desktop research should be conducted on this technology and perhaps a prototype system be developed and assessed using the performance evaluation metric develop and applied within this research.

### 7.2.2 Automation of Uniform Fat Trimming of Beef Striploin

Further work is recommended to be undertaken to further progress the capabilities of an automated system for uniform fat trimming using A-Mode ultrasound sensing.

**A-Mode Ultrasound Sensing Parameter Optimisation:** With further development both ultrasound sensing systems can perform better than that shown in this research. The constraint of time and budget within

the PhD was the limiting factor, hence the scope of development was for a proof-of-concept system without focusing on optimisation of the performance. Post-trials of results presented in Chapter 6 a better parameter setting within the laptop software settings was identified that would enable more reliable node measurements (e.g. less "missed" nodes). These settings will be implemented to improve the reliability of the sensor, likely to the magnitude of approximately 10 - 20% improvement (40% – 50% reliability).

In addition to this, the insight from Chapter 3 and Chapter 6 highlighted the optimisation of thresholds to remove error outliers of meat height measurements (used to calculate fat depth), and improve accuracy and precision at the cost of reliability. For example, applying the filter to ignore all sensor values less than 25 mm would remove 5 outliers and 1 correctly measured datapoint. It is likely that there is a balance for this filter threshold that will be most ideal for an automated system with commercial constraints.

Path Planning Optimisation: Further work will be conducted considering the findings of Chapter 3 and Chapter 6 to provide a means of optimising the path for both the sensing path and cutting path of the automated system. The spatial patterns of the "missed" measurement nodes provide an insight into the nodes which are least likely to yield an informative result, and therefore, may be omitted from the cycle to reduce time spend on locations that have a low probability of receiving a measurement. Additionally, the spatial patterns of fat height, meat height and fat depth will be considered to tweak the filters applied to determine erroneous values as well as the interpolation of the measurements at these nodes. For example, applying the filter to ignore all sensor values less than 25 mm would remove 5 outliers and 1 correctly measured datapoint. It is likely that there is a balance for this filter threshold that will be most ideal for an automated system with commercial constraints.

Integration for Cutting: For a practical application it is vital to consider the integration of this sensing technique with an automated cutting control system. The scope of this research was on the sensing with only general evaluation and consideration given for how these sensors would lend themselves for integration within an automated system. Whilst identifying and planning a cut path is the initial step, the actuation of the cut path is another challenge that needs to be considered as characteristics of flex, forces and fixation will affect the trimming accuracy and the final fat trim remaining on the striploin. The deviations during this process may also assist to further inform and refine the thresholds of the performance evaluation framework developed in this work.

Methods to Restraining Fat During Trimming: As previously mentioned, the cut path is only a part of the issue for automated fat trimming. As such, work is currently being conducted to develop a restrainer to prevent the trimming tool to deviate from the cut path due to reaction, shearing forces at the point of cutting and flexion of the fat during trimming. The automated system presented in Chapter 6 is being further developed within industry-sponsored R&D provided by AMPC.

## REFERENCES

ABARES 2023, Snapshot of Australian Agriculture, accessed 17 June 2023,

<a href="https://www.agriculture.gov.au/abares/products/insights/snapshot-of-australian-agriculture">https://www.agriculture.gov.au/abares/products/insights/snapshot-of-australian-agriculture</a>

Abolhassani N, Patel R, & Moallem M, Needle insertion into soft tissue: a survey. Med Eng Phys 2007; 29(4): 413-431.

Abolhassani N, Patel R, & Moallem M, Needle insertion into soft tissue: a survey. Med Eng Phys 2007; 29(4): 413-431.

Adobe 2021, Meat Factory, accessed 10 November 2020,

<a href="https://stock.adobe.com/au/search?k=meat+factoryhttps://meat.tamu.">https://stock.adobe.com/au/search?k=meat+factoryhttps://meat.tamu.</a> edu/2015/07/20/bloomin-brands-beef-101/img 1577/>

Agri-Food and Biosciences Institute. The evaluation of ultrasonic instruments used to measure the depth of back fat a P2 in live pigs. Available at:

https://pdfs.semanticscholar.org/b9e1/fa7da6e9b3456bbc543f972f9f4caf 314d8c.pdf. Accessed 26 June 2020.

Al-Naif Group 2013, *Madina Factory*, accessed 12 July 2019, <a href="https://naifgroup.me/madinafactory.php?fbclid=IwAR1FznsxV8g1NDW8">https://naifgroup.me/madinafactory.php?fbclid=IwAR1FznsxV8g1NDW8</a> L0p5f7a6Lly5qnOediRDQ0RL3juiFoA8DyaXv5d2FZw>

Álvarez, R., Díez-González, J., Alonso, E., Fernández-Robles, L. et al. (2019), 'Accuracy Analysis in Sensor Networks for Asynchronous Positioning Methods', Sensors (Basel), 19(13), 3024 (2019). Available at: https://www.ncbi.nlm.nih.gov/pmc/articles/PMC6651124/

Aly, B. A., Low, T., Long, D., Baillie, C., Brett, P., et al. (2023), 'Robotics and sensing technologies in red meat processing: A review', Trends in Food Science & Technology, 137, 142-155, doi: 10.1016/j.tifs.2023.05.015.

Anderson, B. S., Moore, A. W., & Cohn, D. (2000), 'A Nonparametric Approach to Noisy and Costly Optimization', Retrieved from Robotics Institute, Carnegie Mellon University website:

http://www.cs.cmu.edu/~brigham/papers/icml2000.pdf

Attec Denmark A/S 2014, ATTEC Danmark A/S - 3D loin trimmer [Video file], accessed 12 February 2020,

<a href="https://www.youtube.com/watch?v=wOdua1jk9F8">https://www.youtube.com/watch?v=wOdua1jk9F8</a>

Attec. 3D loin trimmer. Available at:

https://www.youtube.com/watch?v=wOdua1jk9F8.

AUS-MEAT Limited 2005, Handbook of Australian Meat 7th Edition
(International Red Meat Manual), accessed 12 September 2020,

<a href="https://lambandbeef.com/downloads/Handbook">https://lambandbeef.com/downloads/Handbook</a> of Australian Meat 7th

Edition-English.pdf>

Australian Meat Processor Corporation 2017, Cost to Operate and Processing Cost Competitiveness, accessed 21 January 2019,

<a href="https://www.ampc.com.au/getmedia/cddf3a65-fac3-49a9-a0db-986bd25dfd1b/AMPC">https://www.ampc.com.au/getmedia/cddf3a65-fac3-49a9-a0db-986bd25dfd1b/AMPC</a> CostToOperateAndProcessingCostCompetetitivness

FinalReport.pdf?ext=.pdf>

Australian Meat Processor Corporation 2017, Cost to Operate and Processing Cost Competitiveness, accessed 21 January 2019, <a href="https://www.ampc.com.au/getmedia/cddf3a65-fac3-49a9-a0db-986bd25dfd1b/AMPC">https://www.ampc.com.au/getmedia/cddf3a65-fac3-49a9-a0db-986bd25dfd1b/AMPC</a> CostToOperateAndProcessingCostCompetetitivness FinalReport.pdf?ext=.pdf>

Australian Meat Processor Corporation 2018a, *Analysis of regulatory and related costs in red meat processing*, date accessed 26 June 2020, <a href="https://www.ampc.com.au/uploads/cgblog/id410/FINAL Cost to Operate Report Oct 2018.pdf">https://www.ampc.com.au/uploads/cgblog/id410/FINAL Cost to Operate Report Oct 2018.pdf</a>

Australian Meat Processor Corporation 2018b, *Strategic plan 2018-2022* and beyond, date accessed 18 January 2019, <a href="https://www.ampc.com.au/uploads/pdf/strategic-plans/2018-22-Strategic-Plan.pdf">https://www.ampc.com.au/uploads/pdf/strategic-plans/2018-22-Strategic-Plan.pdf</a>>

Australian Meat Processor Corporation 2019, Strategic risks facing the Australian red meat industry, date accessed 20 January 2019, <a href="https://www.ampc.com.au/uploads/pdf/strategic-plans/42161">https://www.ampc.com.au/uploads/pdf/strategic-plans/42161</a> AMPC RiskDocumentvLR.pdf>

Australian Meat Processor Corporation 2020, *Strategic Plan 2020-2025*, accessed 2 May 2021, <a href="https://www.ampc.com.au/getmedia/4832a7b0-def8-4af4-8762-d91bb4cbac42/AMPC">https://www.ampc.com.au/getmedia/4832a7b0-def8-4af4-8762-d91bb4cbac42/AMPC</a> StrategicPlan 2020 2025.pdf>

Australian Meat Processor Corporation. Desk Top Review in to Collaborative Robot Applications in the Red Meat Industry. Available at: https://www.ampc.com.au/uploads/cgblog/id7/Desk-Top-Review-in-to-Collaborative-Robot-Applications-in-the-Red-Meat-Industry.pdf. Accessed 19 April 2020c.

Australian Meat Processor Corporation. Final report first feasibility of shoulder de-boning. Available at:

https://www.ampc.com.au/uploads/pdf/Processing%20Technologies/Final-Report-2017-1050-Shoulder-Deboning-Feasibility.pdf. Accessed 26 June 2020b.

Australian Radiation Protection and Nuclear Safety Agency 2008,

Radiation Protection in Diagnostic and Interventional Radiology, Australian
Government, Attorney-General's Department, Robert Garran Offices,

National Circuit Barton ACT 2600, accessed 17 August 2020,

<a href="https://www.arpansa.gov.au/sites/default/files/legacy/pubs/rps/rps14">https://www.arpansa.gov.au/sites/default/files/legacy/pubs/rps/rps14</a>
1.pdf>

Bacci M, Porcinai S, Radicati B. Principal component analysis of near-infrared spectra of alteration products in calcareous samples. Appl Spectrosc 1997; 51(5): 700-706.

beef carcases, Meat & Livestock Australia Limited, Locked Bag 991 NORTH SYDNEY NSW 2059, accessed 3 July 2021,

<a href="https://www.mla.com.au/contentassets/7f0bc41ce28e4082ac2758f77f7">https://www.mla.com.au/contentassets/7f0bc41ce28e4082ac2758f77f7</a>
<a href="mailto:5be91/v.tec.1722---rapiscan-rtt-110-system-upgrade-accuracy-validation-final-report.pdf">be91/v.tec.1722---rapiscan-rtt-110-system-upgrade-accuracy-validation-final-report.pdf</a>

Beef It's What's For Dinner 2023, *Slice and Save: Ribeye*, accessed 12 December 2021, <a href="https://www.beefitswhatsfordinner.com/cuts/slice-and-save/slice-and-save-ribeye">https://www.beefitswhatsfordinner.com/cuts/slice-and-save-ribeye</a>>

Bellmer D, Morgan M, Forrest J et al. Modeling of back fat on untrimmed pork loins. Appl Eng Agric 1996; 12(5): 579-584.

Bergen R, McKinnon J, Christensen D et al. Use of real-time ultrasound to evaluate live animal carcass traits in young performance-tested beef bulls. J Anim Sci 1997; 75(9): 2300-2307.

Betancourt, M. 2019, *Advantages of Buying A Whole Side of Beef*, Holy Smoked Sausage, accessed 10 November 2020,

<a href="https://holysmokedsausage.com/why-buy-a-whole-side-of-beef/https://meat.tamu.edu/2015/07/20/bloomin-brands-beef-101/img\_1577/">https://holysmokedsausage.com/why-buy-a-whole-side-of-beef/https://meat.tamu.edu/2015/07/20/bloomin-brands-beef-101/img\_1577/>

Border, F. (2016), 'Design methodology evaluation: an investigation into the 'right' data for situational awareness of RTS-based tele-robotic systems in limited network environments', [UniSQ Honours Project], Available at: <a href="https://sear.unisq.edu.au/31376/">https://sear.unisq.edu.au/31376/</a>

Brett P, Du X, Zoka-Assadi M et al. Feasibility study of a hand guided robotic drill for cochleostomy. BioMed Res Int 2014; 2014: 1-7.

Brett, P. et al. 2014, *Feasibility Study of a Hand Guided Robotic Drill for Cochleostomy*, Hindawi, accessed 17 September 2019, <a href="https://www.hindawi.com/journals/bmri/2014/656325/">https://www.hindawi.com/journals/bmri/2014/656325/</a>

Brondum J. New sensors and techniques for meat quality measurements. AMSA 1998; 51: 13-18.

Brøndum J. New sensors and techniques for meat quality measurements. 52st annual RCM 1998: 51: 13-18.

Brooke, J. (2016) 'SUS: A 'Quick and Dirty' Usability Scale', in Jordan, P.W., Thomas, B.A., Weerdmeester, B.A. and McClelland, I.L. (eds.) Usability Evaluation in Industry, pp.189-194. Boca Raton: CRC Press. Available at:

https://www.taylorfrancis.com/chapters/edit/10.1201/9781498710411-35/sus-quick-dirty-usability-scale-john-brooke.

Brumby, O. Shirazi, M. Starling, S. 2016, *Line Scan CT for Beef & Lamb by Rotating Carcass*, Meat & Livestock Australia Limited, Locked Bag 991 NORTH SYDNEY NSW 2059, accessed 12 August 2020, <a href="https://www.mla.com.au/contentassets/413fa62cc9284ba78dcdec60832">https://www.mla.com.au/contentassets/413fa62cc9284ba78dcdec60832</a> ac288/a.mqa.0016 final report.pdf>

Busch D, Dinkel C, Minyard J. Body measurements, subjective scores and estimates of certain carcass traits as predictors of edible portion in beef cattle. J Anim Sci 1969; 29(4): 557-566.

Butterfly, 2023a, *User Manual*, accessed 22 April 2023, <a href="https://support.butterflynetwork.com/hc/en-us/articles/16906028518939-User-Manual">https://support.butterflynetwork.com/hc/en-us/articles/16906028518939-User-Manual</a>

Butterfly, 2023b, *Butterfly iQ Personal Ultrasound System User Manual*, accessed 22 July 2021,

<a href="https://manual.butterflynetwork.com/butterfly-iq-user-manual rev-s-en.pdf">https://manual.butterflynetwork.com/butterfly-iq-user-manual rev-s-en.pdf</a>>

Cai, L., Shi, W., Miao, Z. et al. (2018), 'Accuracy Assessment Measures for Object Extraction from Remote Sensing Images', Remote Sensing, Volume 10, Issue 2, 303 (2018). Available at: <a href="https://doi.org/10.3390/rs10020303">https://doi.org/10.3390/rs10020303</a>.

Calnan, H. Corlett, M. Connaughton, S & Gardner, G. 2021, *Rapiscan RTT-110 system upgrade accuracy validation*, Meat & Livestock Australia Limited, Locked Bag 991 NORTH SYDNEY NSW 2059, accessed 21 May 2021,

<a href="https://www.mla.com.au/contentassets/7f0bc41ce28e4082ac2758f77f7">https://www.mla.com.au/contentassets/7f0bc41ce28e4082ac2758f77f7</a>
<a href="mailto:5be91/v.tec.1722---rapiscan-rtt-110-system-upgrade-accuracy-validation-final-report.pdf">be91/v.tec.1722---rapiscan-rtt-110-system-upgrade-accuracy-validation-final-report.pdf</a>

Canadian Food Inspection Agency 2023, *Beef – Meat cuts manual*, date accessed 7 June 2019, <a href="https://www.inspection.gc.ca/food-label-requirements/labelling/industry/meat-and-poultry-products/meat-cuts/beef/eng/1348582373896/1348589471777">https://www.inspection.gc.ca/food-label-requirements/labelling/industry/meat-and-poultry-products/meat-cuts/beef/eng/1348582373896/1348589471777>

Canadian Food Inspection Agency 2023, *Beef – Meat cuts manual*,

Government of Canada, accessed 10 November 2020,

<a href="https://inspection.canada.ca/food-labels/labelling/industry/meat-and-poultry-products/meat-cuts/beef/eng/1348582373896/1348589471777">https://inspection.canada.ca/food-labels/labelling/industry/meat-and-poultry-products/meat-cuts/beef/eng/1348582373896/1348589471777</a>>

Carling, K. (2000), 'Resistant outlier rules and the non-Gaussian case', Computational Statistics & Data Analysis, Volume 33, Issue 3, pp 249-258 (2000). Available at:

https://www.sciencedirect.com/science/article/pii/S0167947399000572

Carter A. 2022, Key Address for WHS Issues in the Australian Red Meat industry [PowerPoint Presentation]. Australian Meat Processor Corporation WHS Conference, June 2, Brisbane, QLD, Australia.

Cook J. & Anderson, F 2017, *Beef and lamb OCM with CT in situ further development*, Meat & Livestock Australia Limited, Locked Bag 991 NORTH SYDNEY NSW 2059, accessed 7 August 2020,

<a href="https://www.mla.com.au/research-and-development/reports/2017/beef-and-lamb-ocm-with-ct-in-situ-further-development/">https://www.mla.com.au/research-and-development/reports/2017/beef-and-lamb-ocm-with-ct-in-situ-further-development/</a>

Cook, J. Shirazi, M. Gardner, G. 2016, *X-Ray OCM Bone, Fat and Muscle Trials Final Report*, Meat & Livestock Australia Limited, Locked Bag 991

NORTH SYDNEY NSW 2059, accessed 12 August 2020, <
<a href="https://www.mla.com.au/contentassets/cea54d9bbb744077b6d3c3fac6dccf9e/a.tec.0124">https://www.mla.com.au/contentassets/cea54d9bbb744077b6d3c3fac6dccf9e/a.tec.0124</a> final report .pdf>

Coravos, A., Doerr, M., Goldsack, J. et al. (2020), 'Modernizing and designing evaluation frameworks for connected sensor technologies in medicine'. npj Digit. Med. 3, 37 (2020). Available at: <a href="https://doi.org/10.1038/s41746-020-0237-3">https://doi.org/10.1038/s41746-020-0237-3</a>

Cross M 2011a, Part 1 - How to bone a Forequarter of beef demonstration by Master Butcher Michael Cross [Video file], YouTube, accessed 10

November 2020, <a href="https://www.youtube.com/watch?v=yh94UwlhJuY">https://www.youtube.com/watch?v=yh94UwlhJuY</a>

Cross M 2011b, Part 2 - How to bone a hind quarter of beef demonstration by Master Butcher Michael Cross [Video file], YouTube, accessed 10 November 2020, <a href="https://www.youtube.com/watch?v=U-89ls7srE0&t=3s">https://www.youtube.com/watch?v=U-89ls7srE0&t=3s</a>>

Cross M 2011c, Part 3 - How to bone a hind quarter of beef demonstration by Master Butcher Michael Cross [Video file], YouTube, accessed 10 November 2020, <a href="https://www.youtube.com/watch?v=HXTHKXqXATs">https://www.youtube.com/watch?v=HXTHKXqXATs</a>

D'Amico, B., Park, S. and Lee, S. (2022) 'A Case Study of the Effect of the Internet of Things on the Smart City', Telematics and Informatics, 65, 101716. Available at:

https://www.sciencedirect.com/science/article/pii/S0951832022001351.

Dash, C. S. K., Behera, A. K., Dehuri, S. et al., (2023), 'An outliers detection and elimination framework in classification task of data mining', Decision Analytics Journal, Volume 6, 100164 (2023). Available at: <a href="https://www.sciencedirect.com/science/article/pii/S2772662223000048">https://www.sciencedirect.com/science/article/pii/S2772662223000048</a>

De Ponte Müller, F. (2017), 'Survey on Ranging Sensors and Cooperative Techniques for Relative Positioning of Vehicles', Sensors, Volume 17, Issue 2, 271 (2017). Available at: <a href="https://doi.org/10.3390/s17020271">https://doi.org/10.3390/s17020271</a>.

den Boer KT, Herder JL, Sjoerdsma W et al. Sensitivity of laparoscopic dissectors: what can you feel. Surg Endosc 2014; 13: 869-873.

Department of Primary Industries. The value of online measures - a processor perspective. Available at: https://www.mla.com.au/download/finalreports?itemId=3033. Accessed 9 May 2019.

Diabetes Research in Children Network (DIRECNET) Study Group, (2003). 'The accuracy of the CGMS in children with type 1 diabetes: results of the diabetes research in children network (DirecNet) accuracy study', Diabetes Technol Ther, 5(5), 781-9. doi: 10.1089/152091503322526987.

Diaz-Almanza, S., García-Galicia, I. A., Rentería-Monterrubio, A. L. et al. (2021), 'Analysis of the simultaneous measurement of acoustic phase velocity and stress-strain relationship in beef: An approach to Young's modulus', Applied Acoustics, 182, 108237, doi: 10.1016/j.apacoust.2021.108237.

Drury, C.G., Kliever, K. and Da Costa, J.B. (2022) 'Investigating the Effectiveness of a Remote Mindfulness-Based Stress Reduction Program on Stress Reduction and Well-being among Undergraduates: A Randomized Controlled Trial', Mindfulness, pp.1-12. Available at: <a href="https://www.ncbi.nlm.nih.gov/pmc/articles/PMC8839404/">https://www.ncbi.nlm.nih.gov/pmc/articles/PMC8839404/</a>.

Du X, Brett PN, Zhang Y et al. A hand-guided robotic drill for cochleostomy on human cadavers. Journal of Robotic Surgey 2018; 2018(5): 13-18.

Durai, S. K. S. & Shamili, M. D. (2022), 'Smart farming using Machine Learning and Deep Learning techniques', Decision Analytics Journal, Volume 3, 100041 (2022). Available at:

https://www.sciencedirect.com/science/article/pii/S277266222200011X

e-Echocardiolography, 2023, *Ultrasound Beam Shape & Focusing*, JLS Interactive, LLC, accessed 22 February 2023, <a href="https://e-echocardiography.com/page/page.php?UID=1429454181">https://e-echocardiography.com/page/page.php?UID=1429454181</a>>

Eltaib MEH, Hewit JR. Tactile sensing technology for minimal access surgery - a review. Mechatronics 2003; 13: 1163-1177.

Ernest & Young 2017, State of the Industry Report: The Australian Red Meat and Livestock Industry, Meat & Livestock Australia, 200 George Street, Sydney NSW 2000 Australia, GPO Box 2646 Sydney NSW 2001, accessed 18 January 2019, <a href="https://www.mla.com.au/globalassets/mla-corporate/research-and-development/documents/industry-issues/state-of-the-industry-v-1.2-final.pdf">https://www.mla.com.au/globalassets/mla-corporate/research-and-development/documents/industry-issues/state-of-the-industry-v-1.2-final.pdf</a>>

Ernest & Young 2017b, Independent review of the proposed installation of DEXA in AUS-MEAT registered processing facilities: Issues Paper #2,

Australian Meat processor Corporation, Accessed 10 May 2019,

<a href="https://cdn2.hubspot.net/hubfs/3317097/%20Ampc%20July2017/Pdf/D">https://cdn2.hubspot.net/hubfs/3317097/%20Ampc%20July2017/Pdf/D</a>
EXA-Independent-Review-Issues-Paper-2-FINAL.pdf>

Ernest & Young 2021, State of the Industry Report 2021: The Australian Red Meat and Livestock Industry, Meat & Livestock Australia, 200 George Street, Sydney NSW 2000 Australia, GPO Box 2646 Sydney NSW 2001, accessed 17 July 2021, <a href="https://www.mla.com.au/globalassets/mla-corporate/prices--markets/documents/trends--analysis/soti-report/2789-mla-state-of-industry-report-2021\_d11\_single.pdf">https://www.mla.com.au/globalassets/mla-corporate/prices--markets/documents/trends--analysis/soti-report/2789-mla-state-of-industry-report-2021\_d11\_single.pdf</a>>

Falbriard, M., Meyer, F., Mariani, B. et al. (2018), 'Accurate Estimation of Running Temporal Parameters Using Foot-Worn Inertial Sensors', Frontiers in Physiology, Volume 9, Article 610 (2018). Available at: <a href="https://www.frontiersin.org/articles/10.3389/fphys.2018.00610">https://www.frontiersin.org/articles/10.3389/fphys.2018.00610</a>

Farmers Weekly 2018, Behind the scenes look at new high-tech beef abattoir, accessed 12 July 2019,

<a href="https://www.fwi.co.uk/livestock/beef/pictures-behind-scenes-look-new-high-tech-beef-abattoir">https://www.fwi.co.uk/livestock/beef/pictures-behind-scenes-look-new-high-tech-beef-abattoir</a>

Feiner G. The Protein and Fat Content of Meat, Chapter 1, in Meat product handbook: Practical science and technology, North America, Woodhead Publishing Limited, 2006

Fischer, P., Dietrich, P., Achterberg, E. P. et al., (2021). Effects of Measuring Devices and Sampling Strategies on the Interpretation of Monitoring Data for Long-Term Trend Analysis. Front. Mar. Sci., 8. doi:10.3389/fmars.2021.770977

Fong, K. Y., Tan, A. Sulaiman, M. wt al., (2022), 'Phantom and Animal Study of a Robot-Assisted, CT-Guided Targeting System using Image-Only Navigation for Stereotactic Needle Insertion without Positional Sensors', Journal of Vascular and Interventional Radiology, Volume 33, Issue 11, pp 1416-1423.e4 (2022). Available at: https://www.sciencedirect.com/science/article/pii/S1051044322011253

Four Dimensional Digital Imaging Inc 2021, *Cone Beam X-ray Livestock Imaging*, Meat & Livestock Australia Limited, Locked Bag 991 NORTH SYDNEY NSW 2059, accessed 21 May 2021,

<a href="https://www.mla.com.au/globalassets/mla-corporate/research-and-development/final-reports/2021/p.psh.0915-final-report.pdf">https://www.mla.com.au/globalassets/mla-corporate/research-and-development/final-reports/2021/p.psh.0915-final-report.pdf</a>

Frontmatec 2020a, *ALTL 1100 Automatic Loin Trimmer V3.3*, accessed 12 February 2020, <a href="https://www.frontmatec.com/media/6493/altl-1100-automatic-loin-trimmer-v3-3-gb\_spread.pdf">https://www.frontmatec.com/media/6493/altl-1100-automatic-loin-trimmer-v3-3-gb\_spread.pdf</a>>

Frontmatec 2020b, ALTD 450 Frontmatec 3D Loin Trimmer GB V1.3, accessed 12 February 2020,

<a href="https://www.frontmatec.com/media/3290/altd-450-frontmatec-3d-loin-trimmer-gb-v1-3">https://www.frontmatec.com/media/3290/altd-450-frontmatec-3d-loin-trimmer-gb-v1-3</a> spread.pdf>

Frontmatec. 3D line trimmer type ALTD-450. Available at: https://www.frontmatec.com/media/3890/altd-450-frontmatec-3d-loin-trimmer.pdf. Accessed 25 June 2020b.

Frontmatec. Automatic loin trimmer type ALTL-1100. Available at: <a href="https://www.frontmatec.com/media/3891/altl-1100-automatic-loin-trimmer.pdf">https://www.frontmatec.com/media/3891/altl-1100-automatic-loin-trimmer.pdf</a>. Accessed 25 June 2020a.

Fumagalli M, Gijsberts A, Ivaldi S et al. Learning to exploit proximal force sensing: A comparison approach, in Studies in Computational Intelligence, Berlin, Springer, 2010.

Garcia, D. 2023, *PFIELD RMS acoustic pressure field of a linear or convex array*, University of Lyon, France, accessed 22 February 2023, <a href="https://www.biomecardio.com/MUST/functions/html/pfield\_doc.html">https://www.biomecardio.com/MUST/functions/html/pfield\_doc.html</a>

Godfrey, A., Del Din, S., Barry, G. et al. (2015), 'Instrumenting gait with an accelerometer: A system and algorithm examination', Medical Engineering & Physics, Volume 37, Issue 4, pp 400-407 (2015). Available at: <a href="https://doi.org/10.1016/j.medengphy.2015.02.003">https://doi.org/10.1016/j.medengphy.2015.02.003</a>.

Goldsack, J.C., Coravos, A., Bakker, J.P. et al. (2020), 'Verification, analytical validation, and clinical validation (V3): the foundation of determining fit-for-purpose for Biometric Monitoring Technologies (BioMeTs)', npj Digit. Med. 3(55), Available at: <a href="https://doi.org/10.1038/s41746-020-0260-4">https://doi.org/10.1038/s41746-020-0260-4</a>

Goodwin, S. 2018, *Beef City rides out fickle markets, seasons*, Farm Online National, date accessed 23 March 2023, <a href="https://www.farmonline.com.au/story/5740224/beef-city-rides-out-fickle-markets-seasons/">https://www.farmonline.com.au/story/5740224/beef-city-rides-out-fickle-markets-seasons/</a>>

Guo S., Wang Y., Xiao N. et al. Study on real-time force feedback for a master–slave interventional surgical robotic system. Biomed Microdevices 2018; 20(3). <a href="https://doi.org/10.1007/s10544-018-0278-4">https://doi.org/10.1007/s10544-018-0278-4</a>

Halim MHA, Buniyamin N, Shari MAM et al. The use of ultrasound as a fat measurement sensor for the food industry: A review. Int conf smart Instrumentation measurement applications, Kuala Lumpur, Malaysia, 26-26 November, 2013, https://doi.org/10.1109/ICSIMA.2103.6717974.

Halim MHA, Buniyamin N, Shari MAM et al. The use of ultrasound as a fat measurement sensor for the food industry: A review. Int conf smart Instrumentation measurement applications, Kuala Lumpur, Malaysia, 26-26 November, 2013, https://doi.org/10.1109/ICSIMA.2103.6717974.

Halim MHA, Buniyamin N, Shari MAM et al. The use of ultrasound as a fat measurement sensor for the food industry: A review. Res. Gate, 2013; 1(1): 315-320. https://doi.org/10.1109/ICSIMA.2013.6717974.

Hambrock BW. Linear fat measurements to predict pig carcass composition. Available at:

http://citeseerx.ist.psu.edu/viewdoc/download?doi=10.1.1.598.6364&rep =rep1&type=pdf. Accessed 26 June 2020.

Hamed A, Tang SC, Ren H et al. Advances in haptics, tactile sensing, and manipulation for robot-assisted minimally invasive surgery, noninvasive surgery, and diagnosis. J Robot 2012; 2012: 1-14.

https://www.doi.org/10.1155/2012/412816.

Hedrick HB. Methods of estimating live animal and carcass composition. J Anim Sci 1983; 57(5): 1316-1327.

Hoaglin, D. C., Iglewicz, B. & Tukey, J. W. (1986), 'Performance of Some Resistant Rules for Outlier Labeling', Journal of the American Statistical Association, Volume 81, Issue 396, pp 991-999 (1986). Available at: <a href="https://www.jstor.org/stable/2289073">https://www.jstor.org/stable/2289073</a>

Hodan, T., Michel, F., Brachmann, E., et al., (2018), 'BOP: Benchmark for 6D Object Pose Estimation', ECCV Journal. Available at:

<a href="https://openaccess.thecvf.com/content">https://openaccess.thecvf.com/content</a> ECCV 2018/papers/Tomas Hoda

<a href="https://openaccess.thecvf.com/content">n PESTO 6D Object ECCV 2018 paper.pdf</a>

Houghton P, Turlington L. Application of ultrasound for feeding and finishing animals: A review. J Anim Sci 1992; 70(3): 930-941.

Husband, PM 1993, 'Carcass chilling - principles. In: Chilling of Sides and Carcasses & Subsequent Chilled Holdings', CSIRO Workshop Proceedings, March 1993, Australia, pp. 3-20

<a href="https://publications.csiro.au/publications/publication/PIprocite:62b9ac2">https://publications.csiro.au/publications/publication/PIprocite:62b9ac2</a>
6-d4fc-44d4-a249-b5a33db553fc>

IMV imaging, 2023, *The A, B, M's – Ultrasound Modes Explained*, accessed 20 April 2023, <a href="https://blog.imv-imaging.co.uk/blog/the-a-b-ms-ultrasound-modes-explained?fbclid=IwAR3rm4TaljDsn8Lk9">https://blog.imv-imaging.co.uk/blog/the-a-b-ms-ultrasound-modes-explained?fbclid=IwAR3rm4TaljDsn8Lk9</a> NFkTS4hp4bXCkvFEh2wZOoErvZ 3Gqo0u2ssDJzTRI>

Islam, T. & Mukhopadhyay, S. C. (2019), 'Linearization of the sensors characteristics: a review', Volume 12, Issue 1, pp 1-21 (2019). Available at: <a href="https://doi.org/10.21307/ijssis-2019-007">https://doi.org/10.21307/ijssis-2019-007</a>.

Jakob, V.; Küderle, A.; Kluge, F.; Klucken, J.; Eskofier, B.M.; Winkler, J.; Winterholler, M.; Gassner, H. Validation of a Sensor-Based Gait Analysis System with a Gold-Standard Motion Capture System in Patients with Parkinson's Disease. Sensors 2021, 21, 7680.

https://doi.org/10.3390/s21227680

Jespersen BM & Munch L. Chapter 11 - Cereals and Cereal Products. Infrared Spectroscopy for Food Quality Analysis and Control 2009; 275-319.

John the Butcher 2018, *Hindquarter Beef Primal Breakdown*, accessed 10 November 2020, <a href="https://askjohnthebutcher.com/hindquarter-beef-primal-breakdownhttps://meat.tamu.edu/2015/07/20/bloomin-brands-beef-101/img\_1577/">https://askjohnthebutcher.com/hindquarter-beef-primal-breakdownhttps://meat.tamu.edu/2015/07/20/bloomin-brands-beef-101/img\_1577/</a>

Johnson & Wales University, 2019, '17.7 Ultrasound', in College Physics, accessed 20 December 2021,

<a href="https://jwu.pressbooks.pub/collegephysics/chapter/ultrasound/#import-auto-id2672118">https://jwu.pressbooks.pub/collegephysics/chapter/ultrasound/#import-auto-id2672118>

Jones SDM, Allen OB, Haworth CR. The accuracy of two recording instruments in the measurement of subcutaneous fat thickness in pork carcasses. Can J Anim Sci 1982; 62: 731-738.

Jung JH, Shim KS, Na CS et al. Studies on intramuscular fat percentage in live swine using real-time ultrasound to determine pork quality. Asian Austral J Anim 2015; 28(3): 318-322.

Kempster AJ, Chadwick JP, & Jones DW. An evaluation of the hennessy grading probe and the SFK fat-o-meater for use in pig carcass classification and grading. CUP 1985; 40(2): 323-329.

Kettenbach J, Kacher DF, Kanan AR et al. Intraoperative and interventional MRI: recommendations for a safe environment. Minim Invasiv Ther 2006; 15(2): 53-64.

Kettenbach J, Kacher DF, Kanan AR et al. Intraoperative and interventional MRI: recommendations for a safe environment. Minim Invasiv Ther 2006; 15(2): 53-64.

Khaled, W. (2023), 'Displacement estimation analyses for reconstructive ultrasound elastography using finite-amplitude deformations'. Available at: <a href="http://www-brs.ub.ruhr-uni-bochum.de/netahtml/HSS/Diss/KhaledWalaaAM/diss.pdf">http://www-brs.ub.ruhr-uni-bochum.de/netahtml/HSS/Diss/KhaledWalaaAM/diss.pdf</a>

Khodabandehloo, K. 2018, *Technology evaluation for fat removal for beef striploins*, Australian Meat Processor Corporation, accessed 24 August 2018, <a href="https://www.ampc.com.au/getmedia/1785d85f-7abb-4c07-a73b-72f02eb1b161/AMPC">https://www.ampc.com.au/getmedia/1785d85f-7abb-4c07-a73b-72f02eb1b161/AMPC</a> technologyEvaluationForFatRemoval FinalReport.pd f?ext=.pdf>

Khodabandehloo, K. 2019, Prototype development of machine to remove fat from beef striploins leaving a uniform thickness behind - Stage 2,

Australian Meat Processor Corporation, accessed 10 June 2019,

<a href="https://www.ampc.com.au/research-development/advanced-manufacturing/prototype-development-of-machine-to-remove-fat-from-beef-striploins-leaving-a-uniform-thickness">https://www.ampc.com.au/research-development/advanced-manufacturing/prototype-development-of-machine-to-remove-fat-from-beef-striploins-leaving-a-uniform-thickness></a>

Khodabandehloo, K. 2021, *Beef striploin fat removal - Stage 2A): Twin-head laser and ultrasonic 3D fat-lean boundary profiling sub-system*,

Australian Meat Processor Corporation, accessed 20 June 2021,

<a href="https://www.ampc.com.au/getmedia/b1b5654f-e18e-47b7-97a3-52b36e2bc8ed/2021-1077-Stage-2A-FINAL-Open-Report.pdf?ext=.pdf">https://www.ampc.com.au/getmedia/b1b5654f-e18e-47b7-97a3-52b36e2bc8ed/2021-1077-Stage-2A-FINAL-Open-Report.pdf?ext=.pdf</a>

Kim, Y. et al. 2016, Improvement of Depth Profiling into Biotissues Using Micro Electrical Impedance Spectroscopy on a Needle with Selective Passivation, MDPI, accessed 17 September 2019, <a href="https://www.mdpi.com/1424-8220/16/12/2207">https://www.mdpi.com/1424-8220/16/12/2207</a>

Kirton AH, Feist CL, Duganzich DM et al. Use of the Hennessy grading probe (GP) for predicting the meat, fat and bone yields of beef carcasses. Int J Meat Sci 1987; 20(1): 52-63.

Klonoff, D. C. (2004), 'The Need for Separate Performance Goals for Glucose Sensors in the Hypoglycemic, Normoglycemic, and Hyperglycemic Ranges', Diabetes Care, 27(3), 834–836 (2004). Available at: <a href="https://doi.org/10.2337/diacare.27.3.834">https://doi.org/10.2337/diacare.27.3.834</a>

Kollman, C., Wilson, D. M., Wysocki, T. et al., (2005). Limitations of Statistical Measures of Error in Assessing the Accuracy of Continuous Glucose Sensors. Diabetes Technol Ther, 7(5), 665-674. Available at: doi:10.1089/dia.2005.7.665

Konopacki, M. 2006, Freshly slaughtered beef carcasses hanging in a refrigerated cooler of the meat processing plant. The loin eye is exposed to determine the quality, Alamy, accessed 12 November 2020, <a href="https://www.alamy.com/freshly-slaughtered-beef-carcasses-hanging-in-a-refrigerated-cooler-of-the-meat-processing-plant-the-loin-eye-is-exposed-to-determine-the-quality-image355655210.html?imageid=582E01C1-62A5-437C-8D81-EF5525AA540A&p=554987&pn=1&searchId=986444b9194b9972604ae26b02155bd8&searchtype=0https://meat.tamu.edu/2015/07/20/bloomin-brands-beef-101/img 1577/>

Kuorilehto, M. Hännikäinen, M & Hämäläinen, T. (2008), 'Rapid design and evaluation framework for wireless sensor networks', Ad Hoc Networks, Volume 6, Issue 6, pp 909-935 (2008), Available at: <a href="https://doi.org/10.1016/j.adhoc.2007.08.003">https://doi.org/10.1016/j.adhoc.2007.08.003</a>.

Lain, A., Garcia, L., Gine, C. et al., (2017), 'New Methods for Imaging Evaluation of Chest Wall Deformities', Frontiers in Pediatrics, Volume 5. Available at: https://doi.org/10.3389/fped.2017.00257

Lall, A., Data streaming algorithms for the Kolmogorov-Smirnov test, 2015 IEEE International Conference on Big Data (Big Data), Santa Clara, CA, USA, 2015, pp. 95-104, doi: 10.1109/BigData.2015.7363746.

Leaflet, A. (1997), 'USOFT: An Ultrasound Image Analysis Software for Beef Quality Research', Computer Science, Published. [Online]. Available: <a href="https://www.semanticscholar.org/paper/USOFT-%3A-An-Ultrasound-Image-Analysis-Software-for-Leaflet/f2a21c14a34c0f4ee679e3f048a731b1938186b6">https://www.semanticscholar.org/paper/USOFT-%3A-An-Ultrasound-Image-Analysis-Software-for-Leaflet/f2a21c14a34c0f4ee679e3f048a731b1938186b6</a>

Leblanc, G. (1990), Apparatus for trimming back fat off a pork loin, United States of America US5090939A,

Lewis, A. D. & Groth, K. M. (2022), 'Metrics for evaluating the performance of complex engineering system health monitoring models', Reliability Engineering & System Safety, Volume 223, 108473 (2022). Available at: <a href="https://doi.org/10.1016/j.ress.2022.108473">https://doi.org/10.1016/j.ress.2022.108473</a>.

Liu, H., Schneider, P., Haugen, R. et al. (2019). 'Performance Assessment of a Low-Cost PM2.5 Sensor for a near Four-Month Period in Oslo, Norway', Atmosphere, Volume 10, Issue 2, 41. Available at: <a href="https://doi.org/10.3390/atmos10020041">https://doi.org/10.3390/atmos10020041</a>

Liu, X., Jayaratne, R., Thai, P., Kuhn, T., Zing, I., Christensen, B., Lamont, R., Dunbabin, M., Zhu, S., Gao, J., Wainwright, D., Neale, D., Kan, R., Kirkwood, J., & Morawska, L. (2020), 'Low-cost sensors as an alternative for long-term air quality monitoring', Environmental Research, Volume 185, 109438 (2020). Available at:

https://www.sciencedirect.com/science/article/pii/S0013935120303315

Long, J & Thiede, D 1994, *Inclined automatic meat trimmer apparatus and method*, United States of America US5399118A.

Maguire T. 2018. *Industry Problems Presented by Industry [PowerPoint Presentation]*. International Food and Automation Networking Conference (IFAN), April 20, Georgia, Atlanta, United States of America.

Marel 2018, Bone-in Loin Trimmer – Increase yield, reduce labor and improve quality [Video file], accessed 15 February 2020, <a href="https://www.youtube.com/watch?v=Pr-Bc5xyPZY">https://www.youtube.com/watch?v=Pr-Bc5xyPZY</a>

Marel 2020a, 6000DHT Loin Trimmer, accessed 15 February 2020, <a href="https://marel.com/en/products/6000dht-loin-trimmer">https://marel.com/en/products/6000dht-loin-trimmer</a> Accessed 25 June 2020.

Marel 2020b, *Townsend AT 21-620 Autotrimmer*, accessed 15 February 2020, <a href="https://marel.com/en/products/townsend-at-21-620-autotrimmer">https://marel.com/en/products/townsend-at-21-620-autotrimmer</a>>

Marel. 6000DHT loin trimmer. Available at: https://marel.com/products-solutions/6000dht-loin-trimmer/#tab\_publications. Accessed 24 June 2020a.

Marel. AT 21-620 auto trimmer. Available at:

https://marel.com/products-solutions/at-21-620-auto-trimmer/. Accessed 25 June 2020b.

Marel. SK 15-350 auto shoe adjust skinner. Available at: https://marel.com/products-solutions/sk-15-350-auto-shoe-adjust-skinner/.

Masters Dissertation: Tshwane University of Technology. Linear fat measurements to predict pig carcass composition. Available at: http://citeseerx.ist.psu.edu/viewdoc/download?doi=10.1.1.598.6364&rep=rep1&type=pdf. Accessed 26 June 2020.

Mata, K. Jose, C. Williams, A & Gardner, G. 2021, Effect of machine and carcase factors on CT prediction of carcase composition in lamb and beef carcases, Meat & Livestock Australia Limited, Locked Bag 991 NORTH SYDNEY NSW 2059, accessed 3 July 2021,

<a href="https://www.mla.com.au/contentassets/7f0bc41ce28e4082ac2758f77f7">https://www.mla.com.au/contentassets/7f0bc41ce28e4082ac2758f77f7</a>
<a href="mailto:5be91/v.tec.1722---rapiscan-rtt-110-system-upgrade-accuracy-validation-final-report.pdf">be91/v.tec.1722---rapiscan-rtt-110-system-upgrade-accuracy-validation-final-report.pdf</a>

Matthews, B Joll, D Ziauddin, H & Wilson, D 1976, *Apparatus for making a simulated natural cut of meat*, United States of America US4731906A.

McLaren DG, McKeith FM, Novakofski J. Prediction of carcass characteristics at market weight from serial real-time ultrasound measures of backfat and loin eye area in the growing pig. J Anim Sci 1998; 67(7): 1657-1667.

McPhee M. 2014a, Quantifying the benefits of developing a CT marbling solution (Phase 1), Meat & Livestock Australia Limited, Locked Bag 991 NORTH SYDNEY NSW 2059, accessed 7 August 2020,

<a href="https://www.mla.com.au/contentassets/80babdfbaee546eb9b84124f75f">https://www.mla.com.au/contentassets/80babdfbaee546eb9b84124f75f</a> bc719/a.tec.0100 phase 1 final report.pdf>

McPhee M. 2014b, Quantifying the benefits of developing a CT marbling solution (Phase 2), Meat & Livestock Australia Limited, Locked Bag 991 NORTH SYDNEY NSW 2059, accessed 7 August 2020,

<a href="https://www.mla.com.au/contentassets/0fbb57abda734131bfa60559de">https://www.mla.com.au/contentassets/0fbb57abda734131bfa60559de</a>
<a href="https://www.mla.com.au/contentassets/0fbb57abda734131bfa60559de">https://www.mla.com.au/contentassets/0fbb57abda734131bfa60559de</a>
<a href="https://www.mla.com.au/contentassets/0fbb57abda734131bfa60559de">https://www.mla.com.au/contentassets/0fbb57abda734131bfa60559de</a>
<a href="https://www.mla.com.au/contentassets/0fbb57abda734131bfa60559de">https://www.mla.com.au/contentassets/0fbb57abda734131bfa60559de</a>

Meat & Livestock Australia 2014, A.SCT.0029 39 42 44 47 49 50 51 56 58 Supply Chain Objective Carcase Measurement - supporting activities, Meat & Livestock Australia Limited, Locked Bag 991 NORTH SYDNEY NSW 2059, accessed 7 August 2020,

<a href="https://www.mla.com.au/contentassets/57e7d0b5c13643adb4008c92e9">https://www.mla.com.au/contentassets/57e7d0b5c13643adb4008c92e9</a>
<a href="mailto:735372/a.sct.0029">735372/a.sct.0029</a> final report.pdf>

Meat & Livestock Australia 2018a, *Market Snapshot* | *Goatmeat Global Summary*, accessed 19 January 2019,

<a href="https://www.mla.com.au/globalassets/mla-corporate/prices--">https://www.mla.com.au/globalassets/mla-corporate/prices--</a>
<a href="markets/documents/os-markets/red-meat-market-snapshots/2018-mla-ms\_global-goatmeat.pdf">ms\_global-goatmeat.pdf</a>

Meat & Livestock Australia 2018b, *Global Market Snapshot*| *Sheepmeat*, accessed 20 January 2019, <a href="https://www.mla.com.au/globalassets/mla-corporate/prices--markets/documents/os-markets/export-statistics/oct-2018-snapshots/mla-sheepmeat-market-snapshot---global---oct-2018-v2.pdf">
v2.pdf</a>

Meat & Livestock Australia 2018c, Fast Facts: Australia's Beef Industry, accessed 20 January 2019, <a href="https://www.mla.com.au/globalassets/mla-corporate/prices--markets/documents/trends--analysis/fast-facts--maps/mla\_beef-fast-facts-2018.pdf">https://www.mla.com.au/globalassets/mla-corporate/prices--markets/documents/trends--analysis/fast-facts--maps/mla\_beef-fast-facts-2018.pdf</a>>

Meat & Livestock Australia 2018d, *Global Market Snapshot*| *Beef*, accessed 20 January 2019, <a href="https://www.mla.com.au/globalassets/mla-corporate/prices--markets/documents/os-markets/export-statistics/oct-2018-snapshots/mla-beef-market-snapshot---global---oct-2018-v2.pdf">https://www.mla.com.au/globalassets/mla-corporate/prices--markets/documents/os-markets/export-statistics/oct-2018-snapshots/mla-beef-market-snapshot---global---oct-2018-v2.pdf</a>

Meat & Livestock Australia 2018e, MSA-Graded Beef Primal and Sub-Primal Cuts, accessed 11 November 2019,

<a href="https://www.mla.com.au/globalassets/mla-corporate/marketing-beef-and-lamb/documents/meat-standards-australia/beef-cuts-poster-a3-1.pdf">https://www.mla.com.au/globalassets/mla-corporate/marketing-beef-and-lamb/documents/meat-standards-australia/beef-cuts-poster-a3-1.pdf</a>

Meat & Livestock Australia, 2011, *3D X-Ray Developments*, accessed 7 August 2020, <a href="https://www.mla.com.au/research-and-development/reports/2011/3d-x-ray-developments/">https://www.mla.com.au/research-and-development/reports/2011/3d-x-ray-developments/</a> Accessed 14 May 2019b.

Meat & Livestock Australia, 2020c, *Tallow prices performing well*, date accessed 23 March 2023, < <a href="https://www.mla.com.au/prices-markets/market-news/2020/tallow-prices-performing-well/">https://www.mla.com.au/prices-markets/market-news/2020/tallow-prices-performing-well/</a>>

Meat & Livestock Australia, 2022c, *Cattle market in 2022: a year in review*, date accessed 23 March 2023, <a href="https://www.mla.com.au/news-and-events/industry-news/cattle-market-in-2022-a-year-in-review/#:~:text=So%20far%20in%202022%2C%20grainfed,above%20the%2010%2Dyear%20average.&text=In%202022%2C%20national%20cattle%20slaughter,rates%20consistently%20lower%20than%202021>

Meat and Livestock Australia (2022) 'Rapiscan RTT 110 System Upgrade Accuracy Validation', Meat and Livestock Australia. Available at: <a href="https://www.mla.com.au/research-and-development/reports/2022/rapiscan-rtt-110-system-upgrade-accuracy-validation/">https://www.mla.com.au/research-and-development/reports/2022/rapiscan-rtt-110-system-upgrade-accuracy-validation/</a>.

Meat and Livestock Australia (2022), 'Fat distribution and eating quality', Meat and Livestock Australia, Level 1, 40 Mount Street North Sydney NSW 2059, accessed 20 January 2021,

<a href="https://www.mla.com.au/globalassets/mla-corporate/marketing-beef-and-lamb/documents/meat-standards-australia/msa14-beef-tt\_fat-distribution-and-eating-quality-lr.pdf">https://www.mla.com.au/globalassets/mla-corporate/marketing-beef-and-lamb/documents/meat-standards-australia/msa14-beef-tt\_fat-distribution-and-eating-quality-lr.pdf</a>

Meat and Livestock Australia Limited. Electrical conductivity instrument for beef carcass fat thickness measurement. Available at https://www.mla.com.au/research-and-development/search-rd-reports/final-report-details/Eating-Quality/Electrical-conductivity-instrument-for-beef-carcass-fat-thickness-measurment/2819. Accessed 26 June 2020.

Meat and Livestock Australia. Beef and Lamb OCM with CT in situ further development. Available at: https://www.mla.com.au/Research-and-development/Search-RD-reports/RD-report-details/Eating-Quality/2D-3D-and-CT-x-ray-based-scanning-for-measuring-meat-parameters/2424.

Meat and Livestock Australia. Objective primal measurement (OPM) pack-off primal pick and pack: Fundamental vision and sensing evaluation. Available at: https://www.mla.com.au/research-and-development/search-rd-reports/final-report-details/Objective-Primal-Measurement-OPM-Pack-off-Primal-Pick-and-Pack-Fundamental-Vision-and-Sensing-Evaluation/3618#. Accessed 12 May 2019a.

Medical Radiation Resources, 2012, *Briefly describe the major parts of an ultrasound transducer?*, accessed 20 April 2023,

<a href="http://medradresource.blogspot.com/2012/11/briefly-describe-major-parts-of.html">http://medradresource.blogspot.com/2012/11/briefly-describe-major-parts-of.html</a>

Merriam, S.B. (2005), 'What Can You Tell from an N of 1?: Issues of Validity and Reliability in Qualitative Research', PAACE Journal of Lifelong Learning, 14, pp.57-62. Available at:

https://www.tandfonline.com/doi/pdf/10.3109/10929080500097687.

Moco Food Services, 2023, *Beef City: Platinum Beef Striploin Grain Fed MSA MB 1*+, date accessed 23 March 2023,

<a href="https://www.mocofoodservices.com.au/meat-and-poultry/beef/beef-striploin-yp-gf-msa-ms-platinum/">https://www.mocofoodservices.com.au/meat-and-poultry/beef/beef-striploin-yp-gf-msa-ms-platinum/</a>

Morlein D, Rosner F, Brand S et al. Non-destructive estimation of the intramuscular fat content of the Longissimus muscle of pigs by means of spectral analysis of ultrasound echo signals. Meat Sci 2005; 69(2): 187-199.

Morton, E. 2020, *Investigating aviation security screening equipment in the meat industry*, Meat & Livestock Australia Limited, Locked Bag 991 NORTH SYDNEY NSW 2059, accessed 15 August 2020,

<a href="https://www.mla.com.au/contentassets/97333b65e9184f03a115df0b3cc">https://www.mla.com.au/contentassets/97333b65e9184f03a115df0b3cc</a>
4b513/p.psh.0930 final report .pdf>

Mueller K. Feasibility analysis of a novel method for bovine carcass fat thickness estimation. Honours dissertation 2018, University of Southern Queensland.

Müller, B., Ilg, W., Giese, M. A. et al., (2017), 'Validation of enhanced kinect sensor based motion capturing for gait assessment', PLoS ONE. Available at: <a href="https://doi.org/10.1371/journal.pone.0175813">https://doi.org/10.1371/journal.pone.0175813</a>.

Nam, Y., Kong, Y., Reyes, B. et al., (2016), 'Monitoring of Heart and Breathing Rates Using Dual Cameras on a Smartphone'. PLOS ONE, 11, e0151013. doi: 10.1371/journal.pone.0151013.

Narsaiah K, & Jha S. Nondestructive methods for quality evaluation of livestock products. Int J Food Sci Tech 2012; 49(3): 342-348.

Ng, A. & Swanevelder, J. (2011), 'Resolution in ultrasound imaging', Continuing Education in Anaesthesia, Critical Care and Pain, 11(5), 186-192. DOI: 10.1093/bjaceaccp/mkr030.

Niesten, M.E., van der Lubbe, R.H.J., Talamini, L.M. et al. (2019), 'A Review of Methods for Assessing Usability (Effectiveness, Efficiency, and Satisfaction) in Mobile Health Applications', npj Digital Medicine, 2, pp.1-12. Available at: <a href="https://www.nature.com/articles/s41746-019-0082-4">https://www.nature.com/articles/s41746-019-0082-4</a>.

Okamura AM. Haptic feedback in robot-assisted minimally invasive surgery. Curr Opin Urol 2009; 19(1): 102-107.

Ortmaier T, Deml B, Kübler B et al. Robot assisted force feedback surgery. Chapter 10, in Springer Tracts in Advanced Robotics, Berlin, Springer, 2007. Available at:

https://link.springer.com/chapter/10.1007/978-3-540-71364-7\_22 Accessed 26 June 2020. Palmer, G. 2015, *A.TEC.0110 Final Report*, Meat and Livestock Australia Limited, accessed 6 August 2020,

<a href="https://www.mla.com.au/contentassets/5b27417e8115450183ed22abe">https://www.mla.com.au/contentassets/5b27417e8115450183ed22abe</a>
<a href="https://www.mla.com.au/contentassets/5b27417e8115450183ed22abe">0f87907/a.tec.0110</a> final report.pdf>

Pan, Z. & Singh, R. P. (2001), 'Physical and Thermal Properties of Ground Beef During Cooking', LWT - Food Science and Technology, Volume 34, Issue 7, Pages 437-444 (2001). Available at:

https://www.sciencedirect.com/science/article/pii/S0023643801907625

Park B, Whittaker AD, Miller RK et al. Measuring intramuscular fat in beef with ultrasonic frequency analysis. J Anim Sci 1994; 72: 117-125.

Pathak V, Singh V, Sanjay Y. Ultrasound as a modern tool for carcass evaluation and meat processing: A review. Int j Meat Sci 2011; 1(2): 83-92.

Petra I, Holding DJ, Ma X et al. Fast and accurate tactile sense feedback estimation for innovative flexible digit for clinical applications. Electron Lett 2006; 42(14): 790-792.

Plus Maths 2021, Saving lives: the mathematics of tomography, accessed 7 August 2020, <a href="https://plus.maths.org/content/saving-lives-mathematics-tomography">https://plus.maths.org/content/saving-lives-mathematics-tomography</a>>

Prieto N, Pawluczyk O, Dugan MER et al. A review of the principles and application of near-infrared spectroscopy to characterize meat, fat, and meat products. Appl Spectrosc 2017; 71(7): 1403-1426.

Purnell G, Maddock N, Khodabandehloo K. Robot deboning for beef forequarters. Robotica 1990; 8(4): 303-310.

Radiology Key, 2021, *Chapter 16: Computed Tomography*, accessed 26 June 2021, <a href="https://radiologykey.com/computed-tomography-3/">https://radiologykey.com/computed-tomography-3/</a>>

Red Meat Advisory Council 2020, *Meat industry strategic plan MISP 2020 including outlook to 2030*, date accessed 18 January 2019, <a href="https://www.mla.com.au/globalassets/mla-corporate/generic/about-mla/misp-2020.pdf">https://www.mla.com.au/globalassets/mla-corporate/generic/about-mla/misp-2020.pdf</a>>

Red Meat Advisory Council 2020, *Meat Industry Strategic Plan*, accessed 21 January 2019, <a href="https://www.mla.com.au/globalassets/mla-corporate/generic/about-mla/misp-2020.pdf">https://www.mla.com.au/globalassets/mla-corporate/generic/about-mla/misp-2020.pdf</a>

Reina-Tosina, J., Rönnberg, N., González, R. et al. (2015) 'An Experimental Study on the Design of a Tablet Application for Individuals with Alzheimer's Disease', Technology and Disability, 27, pp.69-81. Available at:

https://www.sciencedirect.com/science/article/pii/S1350453315000375.

Reproscan, 2023, *Flexx*, accessed 22 January 2020, < <a href="https://reproscan.com/products/flexx/">https://reproscan.com/products/flexx/</a>>

Rieger, C. & Majchrzak, T. (2016), 'Weighted Evaluation Framework for Cross-Platform App Development Approaches', Information Systems: Development, Research, Applications, Education, Volume 264, pp 1510-1517, Available at: <a href="https://link.springer.com/chapter/10.1007/978-3-319-46642-2">https://link.springer.com/chapter/10.1007/978-3-319-46642-2</a> 2.

Roberts JJ, Motin JC, Swain D et al. 2017, A feasibility study on the potential use of near infrared reflectance spectroscopy to analyze meat in live animals: Discrimination of muscles. J Spectrosc 2017; https://www.doi.org/10.1155/2017/3948708.

Rodbard, D. (2014). Characterizing Accuracy and Precision of Glucose Sensors and Meters. Journal of Diabetes Science and Technology, 8(5), 980–985. doi: 10.1177/1932296814541810. Available at: https://www.ncbi.nlm.nih.gov/pmc/articles/PMC4455380/

Rosen J, Brown JD, Chang L et al. Generalized approach for modelling minimally invasive surgery as a stochastic process using a discrete Markov model. IEEE Trans Biomed Eng 2006; 53(3): 399-413.

S.G. Heilbron Economic & Policy Consulting 2018, *Analysis of Regulatory and Related Costs in Red Meat*, Australian Meat Processor Corporation, Level 1, 181 Bay Street Brighton, VIC, 3186, accessed 21 January 2019, <a href="https://www.ampc.com.au/uploads/cgblog/id410/FINAL Cost to Operate Report Oct 2018.pdf">https://www.ampc.com.au/uploads/cgblog/id410/FINAL Cost to Operate Report Oct 2018.pdf</a>

Sahin et al. 2008, The use of ultrasound to predict the carcass composition of live Akkaraman lambs, Hindawi, accessed 17 September 2019,

<a href="https://www.researchgate.net/publication/277475863">https://www.researchgate.net/publication/277475863</a> The use of ultra sound to predict the carcass composition of live Akkaraman lambs>

Savell, J. 2015, *Drew Cassens splitting beef carcass*, Texas A&M University, accessed 10 November 2020, <a href="https://meat.tamu.edu/2015/07/20/bloomin-brands-beef-101/img-1577/">https://meat.tamu.edu/2015/07/20/bloomin-brands-beef-101/img-1577/></a>

Scheffel, R. M. & Fröhlich, A. A. (2019), 'Increasing sensor reliability through confidence attribution', Journal of the Brazilian Computer Society, Volume 25, Article number: 13 (2019). Available at: https://doi.org/10.1186/s13173-019-0094-6

Scholz AM, Bunger L, Kongsro J et al. Non-invasive methods for the determination of body and carcass composition in livestock: Dual-energy x-ray absorptiometry, computed tomography, magnetic resonance imaging and ultrasound: Invited review. Anim 2015; https://www.doi.org/10.1017/S17517311150000336.

Schulze RKW, Curic D, d'Hoedt B. B-mode versus A-mode ultrasonographic measurements of mucosal thickness in vivo. Oral Surg Oral Med Oral Radiol Endod 2002; 93(1): 110-117.

Science ABC, 2022, *How Does An Ultrasound Machine Work?*, accessed 22 April 2023, <a href="https://www.scienceabc.com/innovation/how-ultrasound-scanning-sonography-3d-sonogram-work-pregnancy-due-date.html">https://www.scienceabc.com/innovation/how-ultrasound-scanning-sonography-3d-sonogram-work-pregnancy-due-date.html</a>

Shcherbina, A., Mattsson, C. M., Waggott, et al. (2016), 'Accuracy in wrist-worn, sensor-based measurements of heart rate and energy expenditure in a diverse cohort', [ResearchGate], Available at: DOI:10.1101/094862

Shepard H, Green R, Golden B et al. Genetic parameter estimates of live animal ultrasound measures of retail yield indicators in yearling breeding cattle. J Anim Sci 1996; 74(4): 761-768.

Silva SR, Cadavez VP. Real-time ultrasound (RTU) imaging methods for quality control of meats. Chapter 11, in Computer vision technology in the food and beverage industries, Cambridge, Woodhead Publishing, 2012

Simianer H, Lindberg JE, Fourichon C et al. The use of artificial neural networks for predicting meat content in pig carcasses, chapter 2, in Book of Abstracts of the 64th Annual Meeting of the European Federation of Animal Science, Nantes, Wageningen Academic Publishers, 2013

Slaughter Floor Operations, Woolwise, accessed 10 November 2020, <a href="https://www.woolwise.com/wp-content/uploads/2017/07/Meat-418-518-07-T-11.docx">https://www.woolwise.com/wp-content/uploads/2017/07/Meat-418-518-07-T-11.docx</a>

Song, Y. Hu, Z. Li, T. et al. (2022), 'Performance Evaluation Metrics and Approaches for Target Tracking: A Survey', Sensors (Basel), 22(3), pp.793. Available at:

https://www.ncbi.nlm.nih.gov/pmc/articles/PMC8839404/.

Specht M, Statistical Distribution Analysis of Navigation Positioning
System Errors—Issue of the Empirical Sample Size. MDPI, 2020; 20(24):
7144. https://doi.org/10.3390/s20247144

Statistics Kingdom 2022, *Kolmogorov-Smirnov Test Calculator*, accessed 10 November 2022, <a href="https://www.statskingdom.com/kolmogorov-smirnov-test-calculator.htmlhttps://meat.tamu.edu/2015/07/20/bloomin-brands-beef-101/img\_1577/">https://www.statskingdom.com/kolmogorov-smirnov-test-calculator.htmlhttps://meat.tamu.edu/2015/07/20/bloomin-brands-beef-101/img\_1577/</a>

Stavrev, P 1997, Methods for fat depth measurements., accessed 22 August 2023,

<a href="https://www.researchgate.net/profile/Pavel-">https://www.researchgate.net/profile/Pavel-</a>

Stavrev/publication/260654600\_Methods\_of\_Fat\_Depth\_Measurement\_P\_V\_Stavrev\_Mark\_Peter\_F\_Loeffen\_1998\_Volume\_682\_MIRINZ\_Confidential\_Report/links/0c960531edc7b1299e000000/Methods-of-Fat-Depth-Measurement-P-V-Stavrev-Mark-Peter-F-Loeffen-1998-Volume-682-MIRINZ-Confidential-Report.pdf>

Talasaz A, Trejos AL, Patel RV. Effect of force feedback on performance of robotics-assisted suturing. 4th IEEE RAS EMBS Int Conf Biomed robot Biomechatron 2012;

Tan J. Meat quality evaluation by computer vision. J Food Eng 2004; 61(1): 27-35.

Teira GA, Tinois E, Lotufo RDA et al. Digital-image analysis to predict weight and yields of boneless subprimal beef cuts. Sci Agr 2003; 60(2): 403-408.

The Diabetes Research in Children Network (DirecNet) Study Group, (2004), 'Accuracy of the GlucoWatch G2 Biographer and the Continuous Glucose Monitoring System During Hypoglycemia: Experience of the Diabetes Research in Children Network', Diabetes Care, 27(3), 722–726. doi: 10.2337/diacare.27.3.722.

Thompson, J 2009, *Animal Welfare, Ritual Slaughter and Slaughter Floor Operations*, Woolwise, accessed 10 November 2020, <a href="https://www.woolwise.com/wp-content/uploads/2017/07/Meat-418-518-07-T-11.docx">https://www.woolwise.com/wp-content/uploads/2017/07/Meat-418-518-07-T-11.docx</a>

Tiwana MI, Redmond SJ, Lovell NH. A review of tactile sensing technologies with applications in biomedical engineering. Elsevier 2012; 179(2012): 17-31.

Tomazevic, D., Likar, B. & Pernus, F. (2004), "Gold standard" data for evaluation and comparison of 3D/2D registration methods', Computer Aided Surgery, Volume 9, Issue 4, pp 137-144 (2004). Available at: <a href="https://www.tandfonline.com/doi/pdf/10.3109/10929080500097687">https://www.tandfonline.com/doi/pdf/10.3109/10929080500097687</a>

UNECE Standard. Bovine meat carcases and cuts, 2015 ed., New York & Geneva, United Nations Economic Commission for Europe, 2016

United Nations Economic Commission for Europe 2007, UNECE Standard
Bovine Meat - Carcases and Cuts, accessed 12 January 2021,

<a href="https://unece.org/fileadmin/DAM/trade/agr/meetings/ge.11/2007/2007">https://unece.org/fileadmin/DAM/trade/agr/meetings/ge.11/2007/2007</a>
i01 e Bovine.pdf>

University of Gelph, Animal Biosciences. Fat depth measurement. Available at:

http://animalbiosciences.uoguelph.ca/~swatland/rep242nr.html. Accessed 24 June 2020.

University of Washington, 2017, *Ultrasound*, accessed 20 December 2021, <a href="https://courses.washington.edu/bioen508/Lecture6-US.pdf">https://courses.washington.edu/bioen508/Lecture6-US.pdf</a>>

User Manual, accessed 22 July 2021,
< https://manual.butterflynetwork.com/butterfly-iq-user-manual rev-sen.pdf>

van den Gobbelsteen JJ, Lee RA, van Noorden M et al. Indirect measurement of pinch and pull forces at the shaft of laparoscopic graspers. Med Biol Eng Comput 2012; 50: 215-221.

Versi E. (1992), "Gold Standard" is an appropriate term, (BioMeTs), BMJ; 305(6846): 187, Available at: doi: 10.1136/bmj.305.6846.187-b

Vetscraft 2023, *Basics of Anatomy*, accessed 12 September 2020, <a href="https://www.vetscraft.com/basics-of-anatomy/">https://www.vetscraft.com/basics-of-anatomy/</a>>

Wagner CR, Howe RD. Force feedback benefit depends on experience in multiple degree of freedom robotic surgery task. IEEE T Robot 2007; 23(6): 1253-1240.

Wagner, D. R., Teramoto, M., Judd, T. et al. (2020), 'Comparison of Amode and B-mode Ultrasound for Measurement of Subcutaneous Fat', Ultrasound Med Biol, 46(4), 944-951, doi: 10.1016/j.ultrasmedbio.2019.11.018.

Wagner, D. R., Thompson, B. J., Anderson, D. A. et al. (2019). 'A-mode and B-mode ultrasound measurement of fat thickness: a cadaver validation study', Eur J Clin Nutr, 73(4), 518-523. doi: 10.1038/s41430-018-0085-2

Watzlaf, V.J., McInerney, J., Mai, T. et al. (2017) 'Usability Testing of Two eHealth Mobile Applications: A 2×2 Crossover Design Study', Journal of Medical Internet Research, 19(6), e204. Available at: <a href="https://journals.plos.org/plosone/article?id=10.1371/journal.pone.01758">https://journals.plos.org/plosone/article?id=10.1371/journal.pone.01758</a> 13.

Wen, Y., Guo, D., Zhang, J. et al., (2022), 'Clinical photoacoustic/ultrasound dual-modal imaging: Current status and future trends', Frontiers in Physiology, 13. DOI: 10.3389/fphys.2022.1036621. License: CC BY 4.0.

Whitman TA, Forrest JC, Morgan M et al. Electrical measurement for detecting early postmortem changes in porcine muscle. J Anim Sci 1996; 74(1): 80-90.

Wnek K, Golebiewski M, Przysucha T. Validation of the first objective evaluation system for beef carcasses. Can J Anim 2017; 98(1): 53-60.

Xin H, Zelek JS, Carnahan H. Laparoscopic surgery, perceptual limitations and force: A review. CSCBC 2014. Available at:

https://www.researchgate.net/profile/John\_Zelek2/publication/23777496 7\_Laparoscopic\_surgery\_perceptual\_limitations\_and\_force\_A\_review/link s/0f31752dd5bf019665000000.pdf. Accessed 26 June 2020.

Zhang, S., Bergner, Y., DiTrapani, J., et al., (2021), 'Modeling the interaction between resilience and ability in assessments with allowances for multiple attempts', Computers in Human Behavior, Volume 122, 106847 (2021). Available at:

https://www.sciencedirect.com/science/article/pii/S0747563221001709

Zhao, Y. Song, M. & Xin, C. (2011), 'A weighted cooperative spectrum sensing framework for infrastructure-based cognitive radio networks', Computer Communications, Volume 34, Issue 12 (2011), pp 1510-1517, Available at: <a href="https://doi.org/10.1016/j.comcom.2011.02.007">https://doi.org/10.1016/j.comcom.2011.02.007</a>.

Zhou T, Peng Y, Lui Y. Detection of pork backfat thickness based on nearest neighbor clustering and improved hough algorithm. CSAE 2014; 30(5). https://doi.org/10.3969/j.issn.1002-6819.2014.05.031.

## **APPENDICES**

## **Appendix A: Product & Process Analysis**

#### A.1: Cavities Created by Table Boning

This appendix includes a summary of the analysis conducted to ascertain the typical cavities that are created in the boning of a 100-day grain-fed beef striploin primals at the collaborating processor's facility.

A beef striploin was taken from the processing line immediately after chine sawing to evaluate the cavities of the bones that needed to be removed during the table boning process prior to fat trimming. A boning knife was used to carefully remove all bones (button bones and flat bones) from the lean muscle surface of the striploin whilst leaving as much lean muscle on the striploin as possible (see Figure A- 1: Location of button bones (B1, B2, ..., B6) and flat bones (F1, F2, ..., F6) in a boneless striploin & Figure A- 2: Removal of button bones (B1, B2, ..., B6) and flat bones (F1, F2, ..., F6) from a boneless striploin).

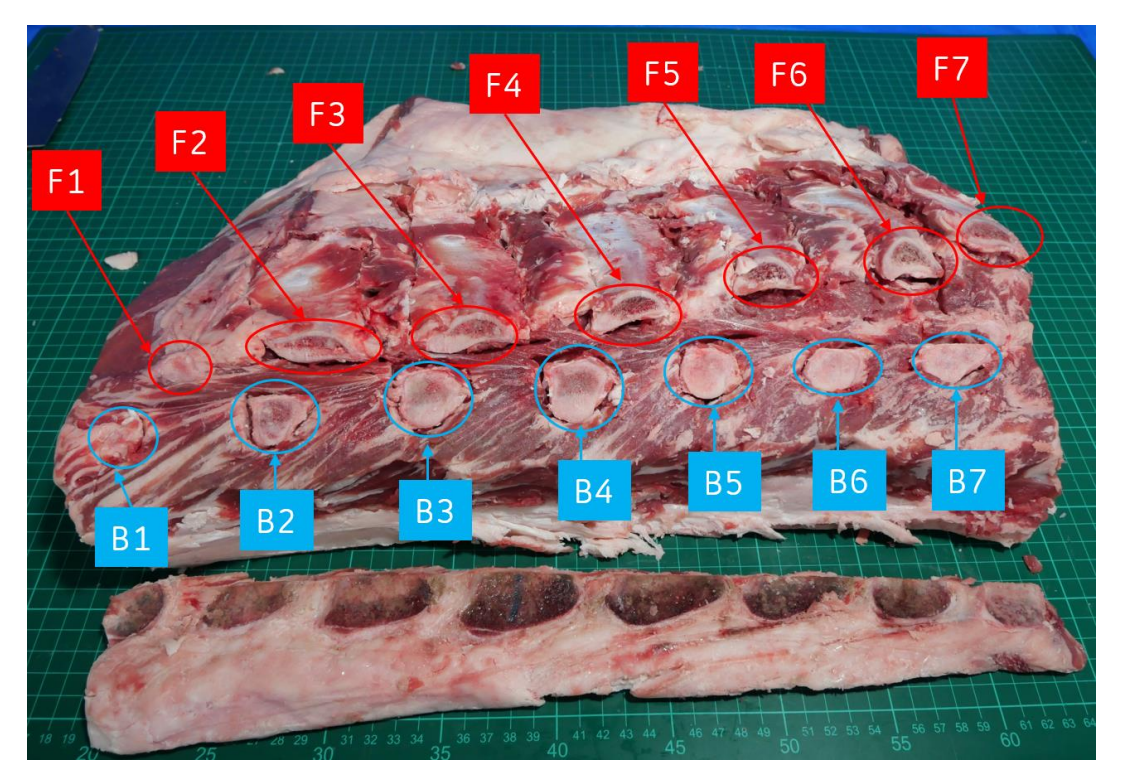


Figure A- 1: Location of button bones (B1, B2, ..., B6) and flat bones (F1, F2, ..., F6) in a boneless striploin

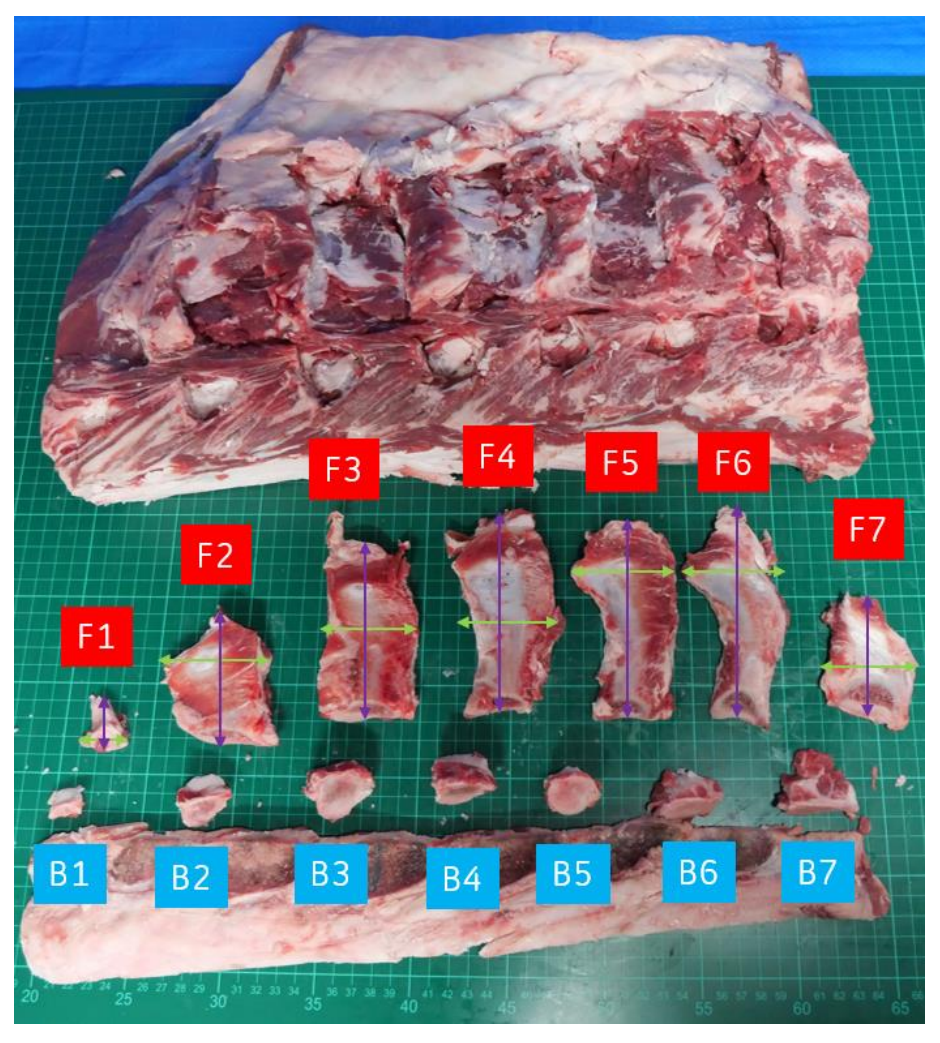


Figure A- 2: Removal of button bones (B1, B2, ..., B6) and flat bones (F1, F2, ..., F6) from a boneless striploin

The seven button bones (B1, B2, B3, B4, B5, B6, B7) and flat bones (F1, F2, F3, F4, F5, F6, F7) were removed were photographed and measured for maximum length and width to approximate the area of the cavity (see Figure A- 3: Close-Up images of button bones & flat bones.). The depth of each cavity that remained after deboning the striploin was also measured with a stainless steel ruler (see Figure A- 4: Measurement of Cavities after removing Button Bones & Flat Bones.).

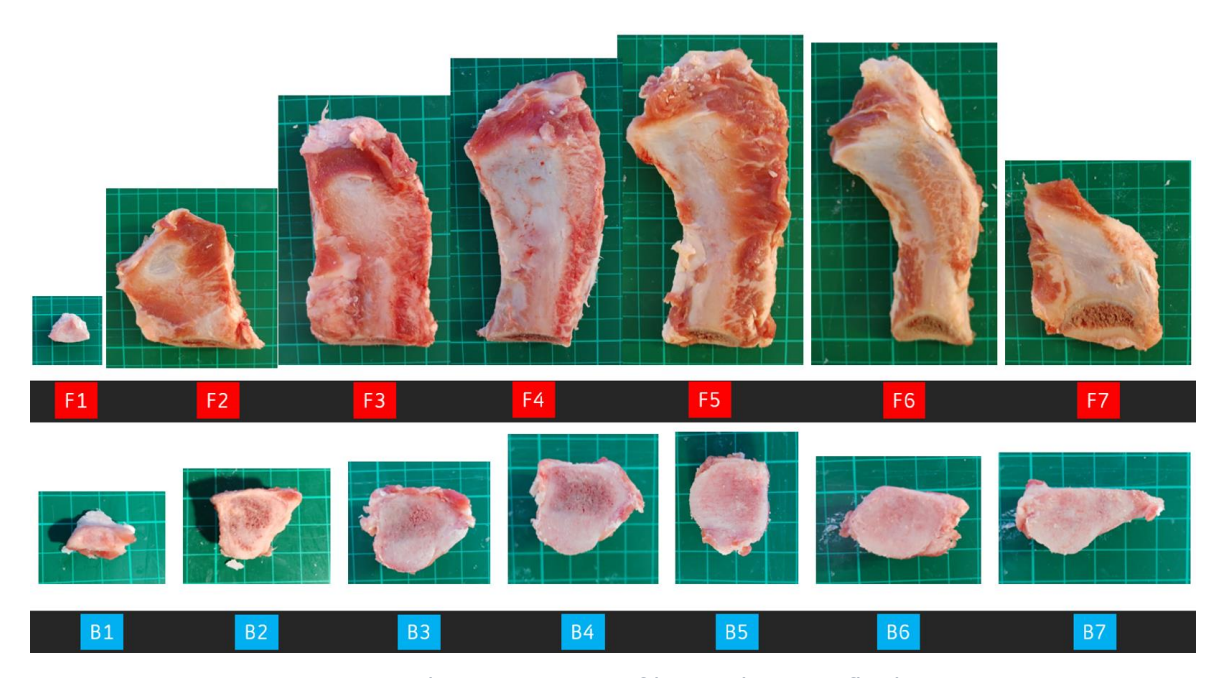


Figure A- 3: Close-Up images of button bones & flat bones.



Figure A- 4: Measurement of Cavities after removing Button Bones & Flat Bones.

Table A- 1: Measurement of Flat Bone Dimensions & Table A- 2: Measurement of Button Bone Dimensions outline the area of the bone

cavities in the striploin for flat bones and button bones respectively. The depth of the cavities ranged from 10 – 20 mm with the average depth being 15 mm.

Table A- 1: Measurement of Flat Bone Dimensions

Flat Bone #	Max Width (mm)	Max Length (mm)
1	25	15
2	62	56
3	56	92
4	60	105
5	62	105
6	63	100
7	48	50

Table A- 2: Measurement of Button Bone Dimensions

Button Bone #	Max Width (mm)	Max Length (mm)
1	22	15
2	30	22
3	36	30
4	35	32
5	25	30
6	37	21
7	42	20

### A.2: Dataset for Product Variability of Untrimmed Striploins

This appendix includes a summary of the analysis conducted to ascertain the typical dimensions and weights of an untrimmed 100-day grain-fed beef striploin primals at the collaborating processor's facility.

Twenty striploins were taken from the processing line conveyor of a typical processing run immediately before fat trimming on the 28<sup>th</sup> of April, 2021. The following table shows the carcase characteristics of the striploins that were surveyed in this analysis. The following descriptions apply to the striploins that were reported on in Table A- 3: Striploin dataset characteristics captured by processor. (C Anderson 2021, pers. comm., 29 April).:

- All carcases were from the same lot (approximately a 200km radius in geographical location), slaughtered the day prior (27/04/2021), were RFID labelled, assigned a body number and these carcases entered the boning room between 11:23AM 11:51AM on the experimentation date (28/04/2021).
- All carcases were declared to have conformed to standards (this column has been removed from dataset)
- The steers were 139-day grain-fed steers (nominally termed '100-day' grain-fed) slaughtered on the 27th of April, 2021.
- The feedlot fed steers a mixture of vegetable oil, molasses,
   forage silage, cereal hay, barley (C Anderson 2021, pers. comm.,
   29 April).
- All carcasses were from male bovine and determined to be:
  - o mostly <18 months old (dentition = 0, n = 14)
  - $\circ$  some <30 months old (dentition = 2, n = 5)
  - o one > 42 months old (dentition = 4, n = 1)
- The following codes were used to classify the cattle breed of the carcase:
  - o CHAR Charolais
  - SG Santa Gertrudis

- o MANSP Mandalong Special
- o BRAFD Braford
- o BRANG Brangus
- o HFD Hereford
- o SIM Simmental
- o ANG Angus
- o LIM Limousin
- Striploin primals were collected from the processor's conveyor prior to 'finishing' by a slicer and returned to the line after measurements were acquired.

Table A- 3: Striploin dataset characteristics captured by processor.

	Live Weight	Left Hot Weight	Right Hot	Right Fat Depth			Meat	Fat		Eye Muscle		
Body # ▼	(kg) ▼	(kg) ▼	_		Dentitic •	Marbl 🔻	Colou •	Colou -	Rib Sit ▼	(mm)	Sire 💌	Dam <b>▼</b>
524	737.6	209.5	205.5	32	2	1.2	1C	0	12	90	CHAR	CHAR
526	767.5	218	211.5	28.1	0	1.6	2	0	12	92	MANSP	MANSP
528	721.0	200	197.5	20.9	0	1	1C	0	12	87	BRAFORD	BRANGUS
450	660.1	193	191.5	21.4	0	1.6	2	0	12	101	CHAR	HFD
452	712.8	199.5	202.5	11.2	0	1.6	2	0	12	116	CHAR	CHAR
454	682.8	179	181	26.6	2	1.4	2	0	12	64	BRANG	HFD
457	707.6	198	202.5	23.5	0	1.4	2	0	12	89	HFD	SIM
459	695.2	190	193.5	28.1	2	1.4	2	0	12	104	CHAR	CHAR
462	669.4	186.5	188.5	14.7	0	1.4	2	0	12	74	CHAR	CHAR
465	650.8	182	182.5	31.5	0	1.4	2	0	12	78	HFD	HFD
463	708.6	200.5	201	29.1	0	1.4	2	0	12	94	ANG	HFD
468	697.3	197	199	17	2	1.2	2	0	12	108	ANG	LIM
566	673.5	197.5	193.5	11.2	0	1	1B	0	12	74	CHAR	HFD
567	744.8	197.5	197.5	18.7	4	1.6	2	0	12	72	ANG	HFD
569	722.1	194.5	195	32.9	0	1.2	1B	0	12	86	HFD	HFD
572	637.4	184.5	185.5	14.7	0	1.4	2	0	12	95	LIM	LIM
574	703.5	198	193	25.1	0	1.4	2	0	12	100	CHAR	HFD
576	657.0	193.5	192	17	2	1.4	1C	0	12	90	MANSP	MANSP
578	729.3	209	207	23	0	1.4	2	0	12	80	HFD	HFD
547	640.5	186	185	20.3	0	1.6	2	0	12	94	ANG	LIM
Average	695.9	195.7	195.3	22.4						89.4		
SD	35.4	9.4	8.1	6.6						12.8		

The photographs in Figure A- 5: Striploin dataset (n=20) observed for fat cover damage. were used to observations of fat cover. Of the observed striploin dataset (n=20), two striploins exhibited a 10cm x 10cm area of fat cover damage.

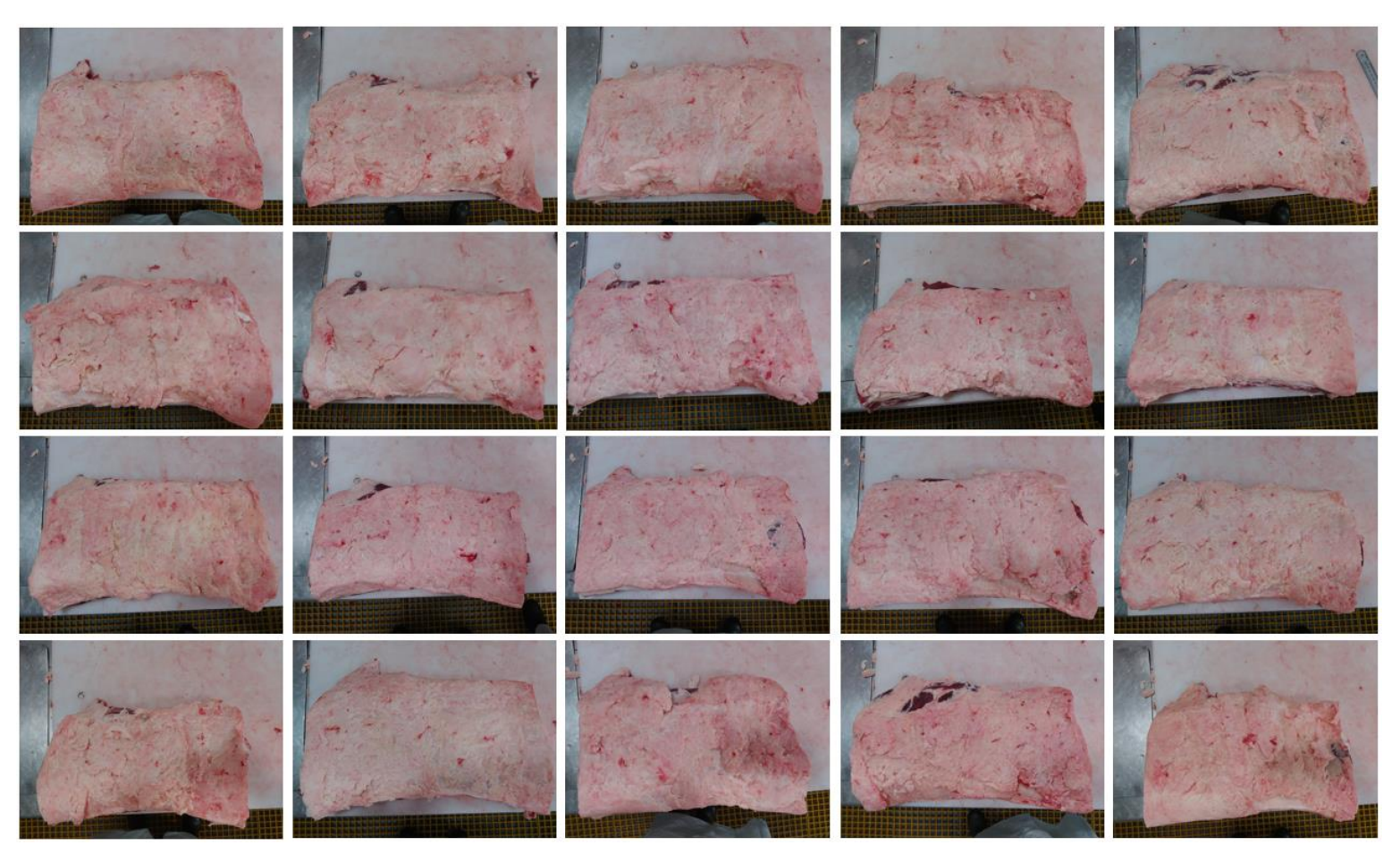


Figure A- 5: Striploin dataset (n=20) observed for fat cover damage.

#### A.3: Time-Motion Analysis of Striploin Fat Trimming

This appendix includes the results of the time-motion analysis conducted on the afternoon shift of the 5<sup>th</sup> of June 2023 at the collaborating processor's facility. The time to trim the entire striploin, separated into trimming the lean (medial) side and fat components, for 4 unidentified slicers over 25 observations. The raw data recorded in this Time-Motion study is presented in Table A- 4: Slicers' times for fat trimming as recorded in the Time-Motion Study. Only the 'Trimming Fat' component was considered for the analysis presented in the main body of the thesis.

Table A- 4: Slicers' times for fat trimming as recorded in the Time-Motion Study

Tin	ne-Mo	tion Mea	suremer	nts of Fat	Trimming
Striploin		Trimming	Trimming	Total	Fat Trimming Slicer
#	Label	Lean (s)	Fat (s)	Trimming (s)	Average (s)
1		29	30	59	
2		22	22	44	
3	Δ.	17	36	53	20.0
4	Α	15	31	46	30.0
5		21	30	51	
6		21	31	52	
7		23	23	46	
8		21	16	37	
9	В	21	31	52	25.5
10	В	26	22	48	20.0
11		27	32	59	
12		25	29	54	
13		18	42	60	
14		11	21	32	
15	С	25	23	48	31.7
16	0	21	32	53	31.7
17		25	35	60	
18		16	37	53	
19		28	20	48	
20		20	38	58	
21		30	21	51	
22	D	14	13	27	22.6
23		15	15	30	
24		26	25	51	
25		20	26	46	
Average		21.5	27.2	48.7	

### **Appendix B: Dataset for Manual Fat Depth Measurements**

This appendix includes the measurements and calculations used in the calculation of results presented in Chapter 3.

# **B.1: Fat Depth Measurements (LHS & RHS)**

The manual (ruler) fat depth measurements of the striploins used in this analysis is tabulated below.

# **Average RHS Striploin Fat Depth Dataset:**

Table B- 1: Average Fat Depth for RHS Striploins (1R & 2R) presents the average fat depth calculated from combining the RHS striploin dataset: 1R & 2R. It should be noted that most of these averages were calculated using 2 measurements in total (one from each striploin). The highlighted nodes in this dataset were calculated with only 1 measurement as shown below:

- Red: 1 measurement to calculate average (1R)

Table B- 1: Average Fat Depth for RHS Striploins (1R & 2R)

	A۱	/erage	Fat De	epth o	f RHS	Striplo	in Dat	aset (F	RHS)	
	F1	F2	F3	F4	F5	F6	F7	F8	F9	F10
P1	10.5	6.0	8.8	6.0	9.0	11.3	15.3	19.8	9.0	-
P2	4.8	10.5	6.5	4.3	5.8	7.5	8.5	17.5	5.0	-
Р3	8.3	12.5	15.0	11.3	11.8	4.5	7.3	11.0	27.5	ı
P4	7.8	11.3	23.0	16.3	17.8	14.5	10.0	12.0	12.0	-
P5	10.3	21.3	23.8	16.5	14.0	14.3	8.0	8.3	11.0	ı
P6	14.8	25.8	23.8	18.5	15.5	12.3	9.5	11.0	12.5	1
P7	22.0	21.5	20.0	14.5	12.3	13.3	15.0	17.0	19.0	-
P8	11.5	20.8	14.8	15.8	21.0	29.5	18.5	19.8	20.0	-
P9	16.0	18.3	18.3	18.0	34.5	33.0	20.5	20.0	25.5	-
P10	-	-	-	-	-	-	-	-	-	-

#### **Average LHS Striploin Fat Depth Dataset:**

Table B- 2: Average Fat Depth for LHS Striploins (3L & 4L) presents the average fat depth calculated from combining the LHS striploin dataset: 3L & 4L. It should be noted that most of these averages were calculated using 2 measurements in total (one from each striploin). The highlighted nodes in this dataset were calculated with only 1 measurement as shown below:

- Red: 1 measurement to calculate average (3L)

- Yellow: 1 measurement to calculate average (4L)

	Α	verage	Fat D	epth o	of LHS S	Striploi	n Data	set (Flh	s <b>)</b>	
	F1	F2	F3	F4	F5	F6	F7	F8	F9	F10
P1	11.3	8.0	7.5	7.5	9.3	12.8	17.5	16.5	-	-
P2	8.8	19.5	14.0	12.0	8.0	8.8	14.8	21.5	-	-
Р3	8.8	23.3	16.5	20.8	20.3	15.0	16.3	18.5	-	-
P4	14.8	24.3	23.0	20.3	20.5	16.3	13.3	15.8	-	-
P5	19.5	21.5	25.0	21.5	18.3	13.3	13.0	13.8	-	-
P6	17.8	26.0	22.5	21.5	21.3	16.3	15.5	16.8	-	-
P7	23.0	20.0	23.5	27.8	28.3	21.8	30.3	23.0	-	-
P8	20.0	18.0	20.0	-	31.0	22.0	21.0	27.0	-	-
P9	-	-	ı	-	-	1	-	-	-	-
P10	_	_		_	_		_	-	_	_

Table B- 2: Average Fat Depth for LHS Striploins (3L & 4L)

# **Average Combined (LHS & RHS) Striploin Fat Depth Dataset:**

Table B- 3: Average Fat Depth for Combined Striploin Dataset (1R, 2R, 3L, 4L) presents the average fat depth calculated from combining all data from the striploin dataset: 1R, 2R, 3L & 4L. It should be noted that most of these averages were calculated using 4 measurements in total (one from each striploin). The highlighted nodes in this dataset were calculated with less than 4 as shown below:

- Red: 1 measurement to calculate average (2R)

- Yellow: 2 measurements to calculate average (1R & 2R)

- Grey: 3 measurements to calculate average (1R, 2R, 4L)
- Green: 3 measurements to calculate average (1R, 2R, 3L)

Table B- 3: Average Fat Depth for Combined Striploin Dataset (1R, 2R, 3L, 4L)

	Avera	ge Fa	t Dep	th of	Comb	ined S	Striplo	in Da	taset (I	Fc)
	F1	F2	F3	F4	F5	F6	F7	F8	F9	F10
P1	10.9	7.0	8.1	6.8	9.1	12.0	16.4	18.1	9.0	-
P2	6.8	15.0	10.3	8.1	6.9	8.1	11.6	19.5	5.0	-
Р3	8.5	17.9	15.8	16.0	16.0	9.8	11.8	14.8	27.5	-
P4	11.3	17.8	23.0	18.3	19.1	15.4	11.6	13.9	12.0	-
P5	14.9	21.4	24.4	19.0	16.1	13.8	10.5	11.0	11.0	-
P6	16.3	25.9	23.1	20.0	18.4	14.3	12.5	13.9	12.5	-
P7	22.5	20.8	21.8	21.1	20.3	17.5	22.6	20.0	19.0	-
P8	15.8	19.4	17.4	15.8	26.0	25.8	19.8	23.4	20.0	-
P9	16.0	18.3	18.3	18.0	34.5	33.0	20.5	20.0	25.5	-
P10	1	-	-	-	•	ı	-	1	1	-

# B.2: Trim Cut Path for Combined (LHS & RHS) Striploin Dataset

Table B- 4: Cut Path Position for Combined Striploin Dataset (1R, 2R, 3L, 4L) presents the average fat depth of the combined striploin dataset filtered to make the minimum coordinate the fat specification of 12 mm (highlighted in green).

Table B- 4: Cut Path Position for Combined Striploin Dataset (1R, 2R, 3L, 4L)

	Tr	im Cut	Path	of Con	nbined	Strip	loin Da	ataset	(Tc)	
	F1	F2	F3	F4	F5	F6	F7	F8	F9	F10
P1	12.0	12.0	12.0	12.0	12.0	12.0	16.4	18.1	12.0	-
P2	12.0	15.0	12.0	12.0	12.0	12.0	12.0	19.5	12.0	-
Р3	12.0	17.9	15.8	16.0	16.0	12.0	12.0	14.8	27.5	-
P4	12.0	17.8	23.0	18.3	19.1	15.4	12.0	13.9	12.0	-
P5	14.9	21.4	24.4	19.0	16.1	13.8	12.0	12.0	12.0	-
P6	16.3	25.9	23.1	20.0	18.4	14.3	12.5	13.9	12.5	-
P7	22.5	20.8	21.8	21.1	20.3	17.5	22.6	20.0	19.0	-
P8	15.8	19.4	17.4	15.8	26.0	25.8	19.8	23.4	20.0	-
P9	16.0	18.3	18.3	18.0	34.5	33.0	20.5	20.0	25.5	-
P10	-	-	-	-	-	-	-	-	-	-

# **B.3: Gradient of Fat Depth Measurements**

The forward gradient calculated using the raw manual (ruler) fat depth measurements of the striploins used in this analysis is tabulated in Table B- 5: Gradient in the Y Direction (along striploin width) of the trimming cut path. & Table B- 6: Gradient in the X Direction (along striploin length) of the trimming cut path. and visualised in Figure B- 1: The average fat depth of the striploin dataset (Fc) illustrating the gradient across the length (Faces) in the 'X' direction. & Figure B- 2: The average fat depth of the striploin dataset (Fc) illustrating the gradient across the width (points) in the 'Y' direction..

Table B- 5: Gradient in the Y Direction (along striploin width) of the trimming cut path.

	Gra	dient i	n Y Dir	ection	of Trin	n Cut P	ath (To	c)		
	F1	F2	F3	F4	F5	F6	F7	F8	F9	F10
P1	-	-	-	-	-	-	-	-	-	-
P1 > P2	1	6.9	1	-	1	1	- 10.0	3.2	-	-
P2 > P3	ı	6.6	8.6	9.2	9.2	ı	-	- 10.9	35.5	-
P3 > P4	1	- 0.3	16.6	5.2	7.2	7.7	-	- 2.0	- 35.5	-
P4 > P5	6.6	8.3	3.2	1.7	- 6.9	- 3.7	-	- 4.3	-	-
P5 > P6	3.2	10.3	- 2.9	2.3	5.2	1.1	1.1	4.3	1.1	-
P6 > P7	14.3	- 11.7	- 3.2	2.6	4.3	7.4	23.2	14.0	14.9	-
P7 > P8	- 15.5	- 3.2	- 10.0	- 12.3	13.2	18.9	- 6.6	7.7	2.3	-
P8 > P9	0.6	- 2.6	2.0	5.2	19.5	16.6	1.7	- 7.7	12.6	-
P10	1	-	1	-	1	1	-	1	-	-
Absolute Average (deg)	5.0	6.2	5.8	4.8	8.2	6.9	5.3	6.8	12.7	6.9
Absolute Maximum (deg)	15.5	11.7	16.6	12.3	19.5	18.9	23.2	14.0	35.5	35.5
Maximum Positive (deg)	14.3	10.3	16.6	9.2	19.5	18.9	23.2	14.0	35.5	35.5

Table B- 6: Gradient in the X Direction (along striploin length) of the trimming cut path.

			Gı	radient	t in X D	irectio	n of T	rim Cu	t Path	(Tc)			
											(	Gradient (d	eg)
	F1	F1 > F2	F2 > F3	F3 > F4	F4 > F5	F5 > F6	F6 > F7	F7 > F8	F8 > F9	F10	Absolute Average	Absolute Maximum	Maximum (Positive)
P1	-	-	-	-	-	1	5.0	2.0	- 7.0	-	1.8	7.0	5.0
P2	-	3.4	- 3.4	-	-	-	•	8.6	- 8.6	-	3.0	8.6	8.6
Р3	-	6.7	- 2.4	0.3	-	- 4.6	-	3.2	14.6	-	4.0	14.6	14.6
P4	-	6.6	6.0	- 5.4	1.0	- 4.3	- 3.9	2.1	- 2.1	-	3.9	6.6	6.6
P5	-	7.4	3.4	- 6.2	- 3.3	- 2.7	- 2.0	-	-	-	3.1	7.4	7.4
P6	-	11.0	- 3.2	- 3.6	- 1.9	- 4.7	- 2.0	1.6	- 1.6	-	3.7	11.0	11.0
P7	-	- 2.0	1.1	- 0.7	- 1.0	- 3.2	5.9	- 3.0	- 1.1	-	2.3	5.9	5.9
P8	-	4.2	- 2.3	- 1.9	11.7	- 0.3	- 6.9	4.2	- 3.9	-	4.4	11.7	11.7
P9	-	2.6	-	- 0.3	18.9	- 1.7	- 14.3	- 0.6	6.3	-	5.6	18.9	18.9
P10	-	-	-	-	-	-	-	-	-	-	3.5	18.9	18.9

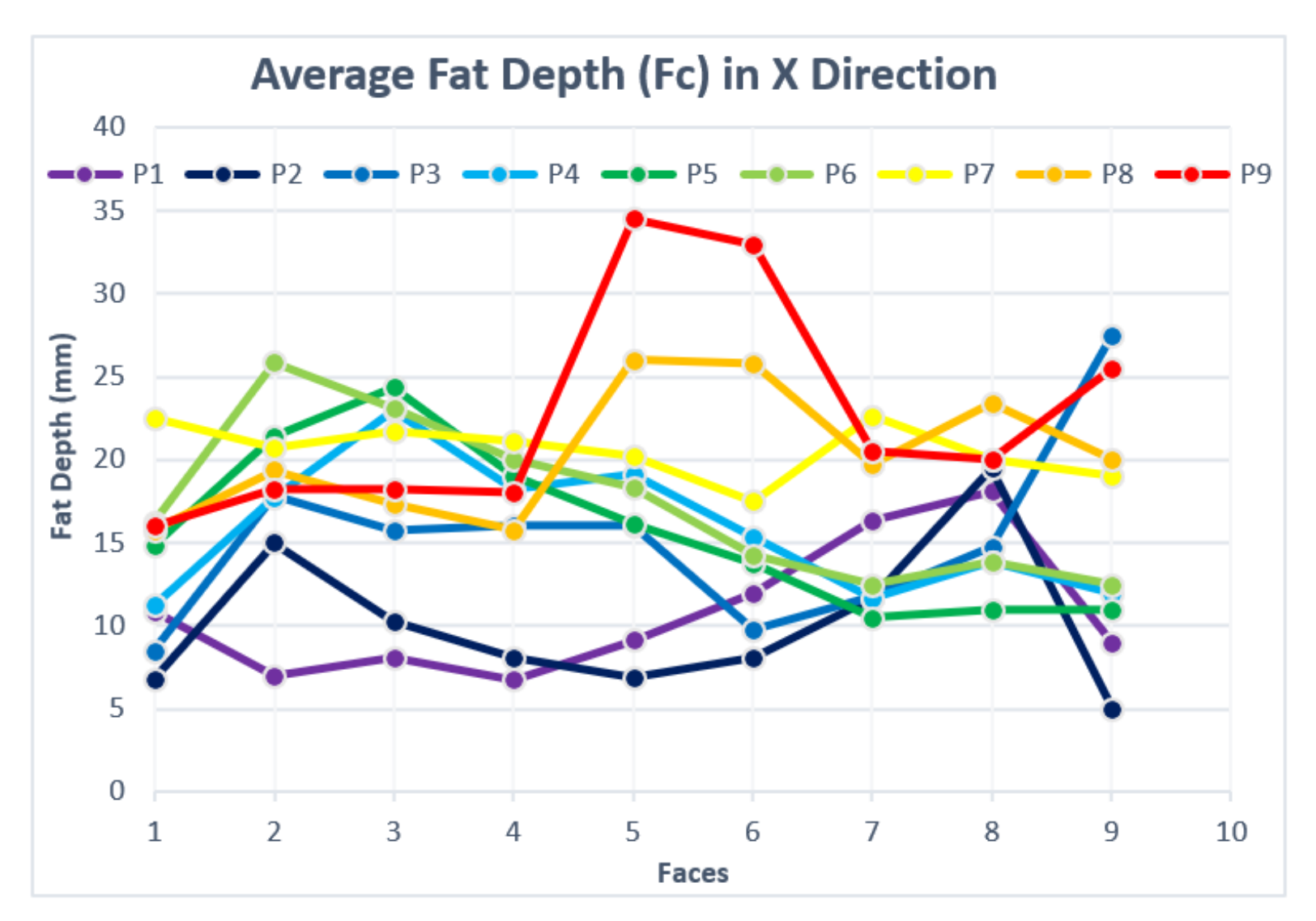


Figure B- 1: The average fat depth of the striploin dataset (Fc) illustrating the gradient across the length (Faces) in the 'X' direction.

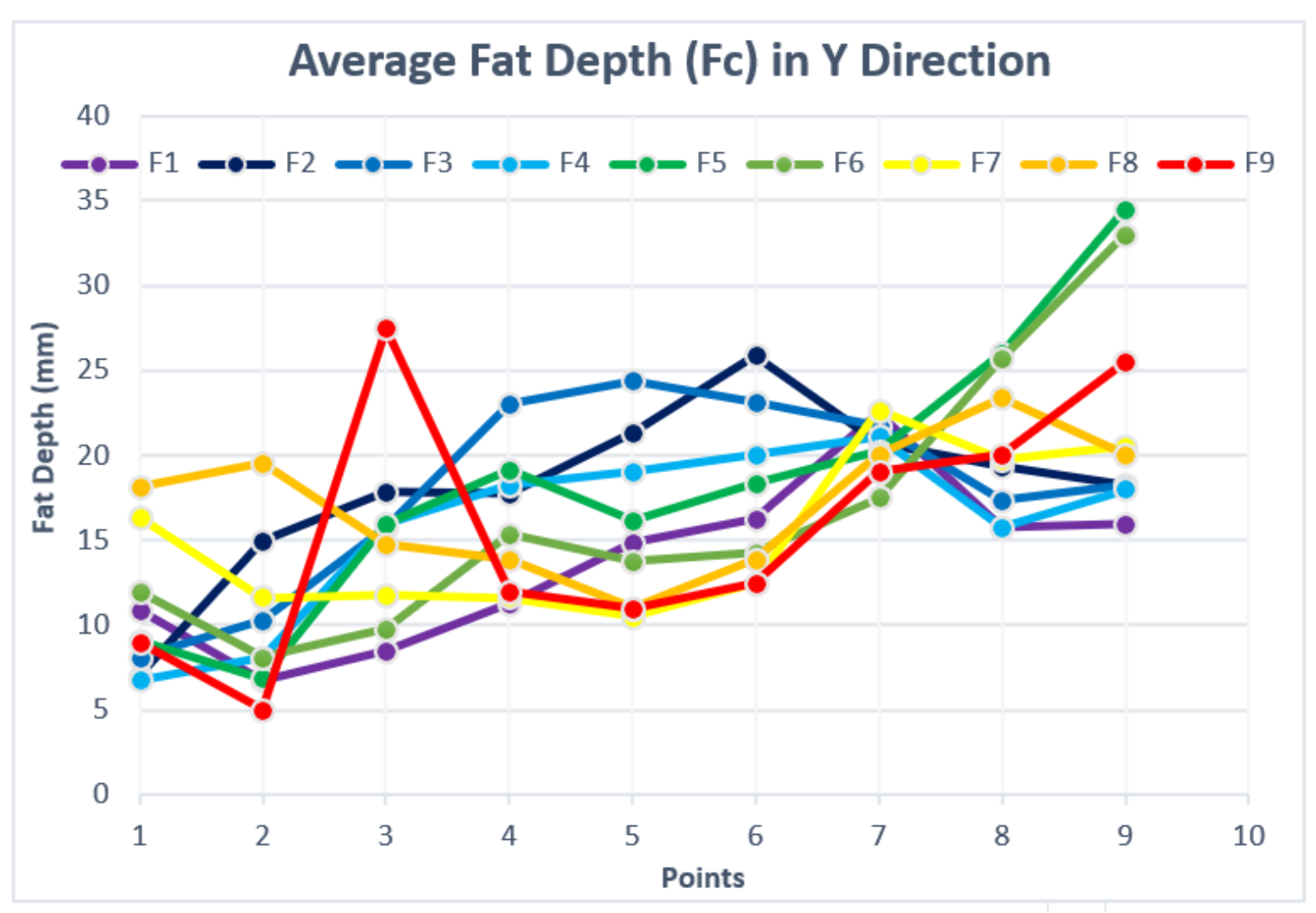


Figure B- 2: The average fat depth of the striploin dataset (Fc) illustrating the gradient across the width (points) in the 'Y' direction.

### **Appendix C: Computed-Tomography Error Dataset Measurements**

This appendix includes the manual and CT measurements for the striploin dataset (1R, 2R, 3L and 4L) used to calculate the error dataset used for results presented in Chapter 4. These are:

- Striploin 1R (see Table C- 1: Raw Data for Calculating Error Dataset (E = Ruler CT) for Striploin 1R)
- Striploin 2R (see Table C- 2: Raw Data for Calculating Error Dataset (E = Ruler CT) for Striploin 2R)
- Striploin 3L (see Table C- 3: Raw Data for Calculating Error Dataset (E = Ruler CT) for Striploin 3L)
- Striploin 4L (see Table C- 4: Raw Data for Calculating Error Dataset (E = Ruler CT) for Striploin 4L)

Table C- 1: Raw Data for Calculating Error Dataset (E = Ruler - CT) for Striploin 1R

Point	ŀ	Face 1 Face 2				ace 3			Face 4			Face 5			ace 6			ace 7			ace 8			
Polit	Ruler	СТ	Diff.	Ruler	СТ	Diff.	Ruler	СТ	Diff.	Ruler	СТ	Diff.	Ruler	СТ	Diff.	Ruler	СТ	Diff.	Ruler	СТ	Diff.	Ruler	СТ	Diff.
1	11.0	9.9	1.2	2.0	1.5	0.5	5.5	2.8	2.7	2.0	1.5	0.5	6.0	6.2	- 0.2	10.5	9.9	0.6	18.5	12.1	6.4	10.5	11.4	- 0.9
2	4.5	4.1	0.4	8.0	6.6	1.4	4.0	2.7	1.3	0.5	0.6	- 0.1	3.0	2.8	0.2	6.0	3.9	2.1	4.0	4.3	- 0.3	11.0	8.2	2.8
3	8.5	6.6	1.9	12.5	12.2	0.3	16.0	12.6	3.4	9.0	6.5	2.5	13.0	9.5	3.5	5.0	4.9	0.1	7.0	6.6	0.4	7.0	5.6	1.4
4	7.0	4.8	2.2	9.0	8.6	0.4	21.0	20.7	0.3	15.0	13.8	1.2	20.0	17.2	2.8	15.0	14.6	0.4	12.0	12.4	- 0.4	11.0	8.7	2.3
5	11.5	7.9	3.6	26.0	24.7	1.3	21.0	21.2	- 0.2	14.0	13.3	0.7	13.5	13.0	0.5	13.0	11.1	1.9	7.0	5.3	1.7	7.5	7.3	0.2
6	14.5	14.4	0.1	24.5	24.1	0.4	17.5	17.5	-	15.0	13.8	1.2	14.0	11.1	2.9	11.0	9.9	1.1	8.0	4.1	3.9	11.0	11.8	- 0.8
7	20.0	20.4	- 0.4	17.0	16.2	0.8	15.0	13.8	1.2	11.0	10.8	0.2	9.5	9.7	- 0.2	12.0	10.2	1.8	13.5	11.9	1.6	16.0	15.5	0.5
8	7.0	5.6	1.4	12.5	12.5	-	11.5	10.8	0.7	16.5	16.7	- 0.2	17.0	16.4	0.6	27.0	26.7	0.3	17.0	15.6	1.4	15.5	13.7	1.8
9	4.0	2.3	1.7	7.5	4.8	2.7	14.0	12.4	1.6	17.0	20.5	- 3.5	40.0	41.2	- 1.2	22.0	21.1	0.9	-	-	-	15.5	12.8	2.7

Table C- 2: Raw Data for Calculating Error Dataset (E = Ruler - CT) for Striploin 2R

Point	Face 1 Face 2				Face 3			Face 4		ı	Face 5			Face 6			Face 7			Face 8		ı	Face 9				
Polit	Ruler	СТ	Diff.	Ruler	ст	Diff.	Ruler	ст	Diff.	Ruler	ст	Diff.	Ruler	ст	Diff.	Ruler	ст	Diff.	Ruler	ст	Diff.	Ruler	СТ	Diff.	Ruler	ст	Diff.
1	10.0	7.5	2.5	10.0	9.4	0.6	12.0	11.7	0.3	10.0	8.0	2.0	12.0	9.7	2.3	12.0	8.4	3.6	12.0	9.6	2.4	29.0	21.9	7.1	9.0	7.2	1.8
2	5.0	3.6	1.4	13.0	10.2	2.8	9.0	7.7	1.3	8.0	6.0	2.0	8.5	7.4	1.1	9.0	6.6	2.4	13.0	11.2	1.8	24.0	22.6	1.4	5.0	5.2	- 0.2
3	8.0	7.1	0.9	12.5	13.0	- 0.5	14.0	11.2	2.8	13.5	10.4	3.1	10.5	8.8	1.7	4.0	2.8	1.2	7.5	5.4	2.1	15.0	13.5	1.5	27.5	21.1	6.4
4	8.5	7.2	1.3	13.5	11.8	1.7	25.0	22.6	2.4	17.5	16.5	1.0	15.5	13.3	2.2	14.0	12.1	1.9	8.0	6.2	1.8	13.0	10.7	2.3	12.0	10.8	1.2
5	9.0	7.1	1.9	16.5	16.7	- 0.2	26.5	24.4	2.1	19.0	14.8	4.2	14.5	12.1	2.4	15.5	15.2	0.3	9.0	7.7	1.3	9.0	6.7	2.3	11.0	7.4	3.6
6	15.0	11.9	3.1	27.0	28.7	- 1.7	30.0	28.4	1.6	22.0	15.8	6.2	17.0	13.5	3.5	13.5	10.7	2.8	11.0	9.9	1.1	11.0	7.7	3.3	12.5	8.7	3.8
7	24.0	25.4	- 1.4	26.0	25.6	0.4	25.0	22.6	2.4	18.0	13.0	5.0	15.0	13.0	2.0	14.5	11.8	2.7	16.5	15.8	0.7	18.0	18.6	- 0.6	19.0	17.2	1.8
8	16.0	13.4	2.6	29.0	28.5	0.5	18.0	16.4	1.6	15.0	11.0	4.0	25.0	22.6	2.4	32.0	35.2	- 3.2	20.0	18.3	1.7	24.0	21.2	2.8	20.0	19.3	0.7
9	28.0	27.8	0.2	29.0	28.1	0.9	22.5	16.6	5.9	19.0	18.3	0.7	29.0	28.5	0.5	44.0	48.5	- 4.5	20.5	17.6	2.9	24.5	23.8	0.7	25.5	28.5	- 3.0

Table C- 3: Raw Data for Calculating Error Dataset (E = Ruler - CT) for Striploin 3L

Point	Face 1			Face 2			Face 3			Face 4			Face 5			Face 6			Face 7			Face 8		
Politi	Ruler	ст	Diff.																					
1	17.0	16.1	0.9	15.0	12.2	2.8	11.0	9.1	1.9	11.0	8.1	2.9	14.5	11.2	3.3	18.0	16.6	1.4	23.0	21.8	1.2	21.0	15.6	5.4
2	16.5	16.8	- 0.3	29.0	22.1	6.9	19.5	16.5	3.0	18.0	16.4	1.6	8.0	5.6	2.4	10.5	9.5	1.0	21.5	20.2	1.3	32.0	28.6	3.4
3	17.5	19.3	- 1.8	30.5	28.1	2.4	21.0	19.3	1.7	25.0	23.9	1.1	22.5	23.7	- 1.2	14.5	12.6	1.9	15.5	13.1	2.4	20.5	18.7	1.8
4	29.5	23.8	5.7	31.5	30.0	1.5	23.0	21.1	1.9	24.5	21.9	2.6	20.0	18.0	2.0	13.5	11.4	2.1	13.5	10.6	2.9	17.5	14.4	3.1
5	29.0	27.9	1.1	25.0	21.2	3.8	24.0	20.7	3.3	22.0	19.6	2.4	17.5	16.0	1.5	11.0	9.8	1.2	11.0	10.5	0.5	13.5	10.9	2.6
6	23.5	20.6	2.9	18.0	15.5	2.5	18.0	15.1	2.9	20.0	18.3	1.7	24.0	20.2	3.8	17.0	17.7	- 0.7	15.5	14.1	1.4	12.5	10.1	2.4
7	25.0	22.5	2.5	15.0	14.2	0.8	20.0	15.2	4.8	38.5	34.8	3.7	22.5	21.9	0.6	22.5	21.6	0.9	40.5	38.4	2.1	20.0	18.4	1.6

Table C- 4: Raw Data for Calculating Error Dataset (E = Ruler - CT) for Striploin 4L

Point	Face 1			Face 2			Face 3			Face 4			Face 5			Face 6			Face 7			Face 8		
	Ruler	ст	Diff.	Ruler	ст	Diff.	Ruler	ст	Diff.	Ruler	ст	Diff.												
1	5.5	5.6	- 0.1	1.0	1.0	-	4.0	4.1	- 0.1	4.0	3.1	0.9	4.0	6.7	- 2.7	7.5	8.9	- 1.4	12.0	13.8	- 1.8	12.0	12.0	-
2	1.0	2.5	- 1.5	10.0	11.6	- 1.6	8.5	6.3	2.2	6.0	4.9	1.1	8.0	14.1	- 6.1	7.0	7.0	-	8.0	8.9	- 0.9	11.0	11.6	- 0.6
3	-	-	-	16.0	15.9	0.1	12.0	12.7	- 0.7	16.5	16.6	- 0.1	18.0	19.7	- 1.7	15.5	16.4	- 0.9	17.0	19.6	- 2.6	16.5	19.2	- 2.7
4	-	-	-	17.0	17.0	-	23.0	22.8	0.2	16.0	17.6	- 1.6	21.0	23.5	- 2.5	19.0	22.9	- 3.9	13.0	15.5	- 2.5	14.0	11.6	2.4
5	10.0	10.4	- 0.4	18.0	17.9	0.1	26.0	27.2	- 1.2	21.0	23.4	- 2.4	19.0	20.4	- 1.4	15.5	16.8	- 1.3	15.0	17.1	- 2.1	14.0	11.6	2.4
6	12.0	15.0	- 3.0	34.0	33.3	0.7	27.0	29.0	- 2.0	23.0	26.9	- 3.9	18.5	19.5	- 1.0	15.5	20.4	- 4.9	No F-L	No F-L	NA	21.0	22.8	- 1.8
7	21.0	20.3	0.7	25.0	31.7	- 6.7	27.0	24.6	2.4	17.0	19.4	- 2.4	34.0	36.6	- 2.6	No READ	NO READ	NA	20.0	21.8	- 1.8	26.0	27.1	- 1.1
8	20.0	16.9	3.1	18.0	20.5	- 2.5	20.0	21.3	- 1.3	-	-	-	31.0	33.9	- 2.9	22.0	19.7	2.3	21.0	22.6	- 1.6	27.0	27.8	- 0.8

#### **Appendix D: B-Mode Ultrasound Device Datasheets**

This appendix includes the datasheets of the ultrasound sensors evaluated in Chapter for this application.

### D.1: B-Mode Ultrasound: ReproScan Flexx

In the preliminary analysis of Chapter 5 in determining the feasibility of the ultrasound for the application this sensor was found inappropriate for use at its current configuration (probe head shape). The following links are useful for accessing more information on this device:

- Product Specifications: <a href="https://repro-scan.com/products/flexx/">https://repro-scan.com/products/flexx/</a>
- Product PDFs (downloadable): <a href="https://repro-scan.com/pdfs/">https://repro-scan.com/pdfs/</a>

### D.2: B-Mode Ultrasound System (Butterfly iQ+)

This B-Mode ultrasound was developed and evaluated as shown in Chapter 5. The following links are useful for accessing more information on this device:

- Product Specifications:
   <a href="https://support.butterflynetwork.com/hc/en-us/articles/16910421132187-System-Specifications">https://support.butterflynetwork.com/hc/en-us/articles/16910421132187-System-Specifications</a>
- User Manual:
   <a href="https://support.butterflynetwork.com/hc/en-">https://support.butterflynetwork.com/hc/en-</a>
   us/articles/16910421132187-System-Specifications